COMBINED FREE AND FORCED LAMINAR CONVECTION IN INCLINED WIDE RECTANGULAR CHANNELS HEATED FROM BELOW AND COOLED FROM ABOVE

A Thesis

Submitted to the Faculty of Engineering
University of Lagos

By

F. L. BELLO-OCHENDE

For the Degree of
Doctor of Philosophy

Faculty of Engineering
University of Lagos
Lagos, Nigeria.

DECEMBER 1980

ABSTRACT

The steady-state two-dimensional problem of combined free and forced laminar convection with upward flow in inclined rectangular channels heated from below and cooled from above, has been investigated by numerical, parameter perturbation and experimental methods. The results indicate that for air (Pr = 0.73), maximum heat transfer rates occur at the hotwall for inclinations between 30° and 60° to the horizontal. In addition, the perturbation analysis predicts the occurence of maximum bulk temperatures and minimum heat transfer rates at the cold wall for the same range of inclinations to the horizontal.

For the two cases of thermal boundary conditions considered, the maximum mean hot wall Nusselt numbers and the maximum bulk temperature from the perturbation analysis together with their corresponding optimum inclinations in radians, appear to obey the following power laws.

Case A: Constant surface temperatures

Numerical: $Nu_{mh} = 1.804(Ar)^{0.008}(\alpha_{OPT})^{0.029}; \left\{ \begin{array}{l} 0.050 \leq Ar \leq 0.500 \\ \frac{\pi}{6} \leq \alpha_{OPT} \leq \frac{\pi}{3} \end{array} \right\}$

Perturbation: $Nu_{BH} = 2.120(Ar)^{0.005}(\alpha_{OPT})^{-0.038} \left\{ \begin{array}{l} 0.0313 \leq Ar \leq 0.222 \\ \frac{\pi}{6} \leq \alpha_{OPT} \leq \frac{3\pi}{10} \end{array} \right\}$

$\theta_B = 0.504(Ar)^{-0.003}(\alpha_{OPT})^{0.175}$

Case B: Constant heat flux at the hot wall and arbitrarily-varying cold wall temperature.

Numerical: $Nu_{mh} = 3.520(Ar_m \alpha_{OPT}^2)^{0.006}; \left\{ \begin{array}{l} 0.025 \leq Ar_m \leq 0.100 \\ \frac{\pi}{6} \leq \alpha_{OPT} \leq \frac{11\pi}{24} \end{array} \right\}$

ACKNOWLEDGMENTS

TABLE OF CONTENTS

LIST OF TABLES

LIST OF FIGURES

FIGURE

NOMENCLATURE

$A,$ Dimensionless mean longitudinal temperature gradient, $\frac{d\Theta}{dx}$

$A^*,$ Dimensional longitudinal hot wall temperature gradient, $\frac{dT_h}{dX}$

$Ar,$ Archimedes number, $\frac{Gr}{Re^2}$

$b,$ Dimensional channel height

$f, C_f,$ Frictional Coefficient

$C_p,$ Specific heat of fluid at constant pressure

$Gr,$ Grashof number, $\frac{\beta g(T_h - T_c)b^3}{\nu^2}$

$Gr_m,$ Modified Grashof number, $\frac{\beta g A^* b^4}{\nu^2}$

$h,$ Heat transfer coefficient, enthalpy

$K_f,$ Thermal conductivity of fluid

$X_L,$ Channel length

$M, N,$ Divisions along the X-and Y-directions respectively

$Nu_x,$ Local Nusselt number

$P,$ Dimensional pressure

$p,$ Non-dimensional pressure

Pe Pecklet numbers, RePr

$Pe',$ Modified Peclet numer RePrA

$Pr,$ Prandtl number, $\frac{\nu}{\lambda}$

$Re,$ Reynolds number, $\frac{U_m b}{\nu}$

St_x,   Local Stanton number, $\dfrac{Nu_x}{RePr}$

T,   Dimensional temperature

U, V,   Dimensional Longitudinal and transverse velocities respectively.

u, v,   Non-dimensional longitudinal and transverse velocity components respectively.

X, Y,   Cartesian coordinate axes

x, y,   Non-dimensional distances

Δx, Δy Non-dimensional grid-sizes

GREEK SYMBOLS

α^o,   Angle of channel inclination to the horizontal

β,   Cubical coefficient of thermal expansion of fluid

γ^o,   Slope of inclined manometer

θ,   Non-dimensional temperature difference, $\dfrac{T - T_c}{T_h - T_c}$ or $\dfrac{T - T_\infty}{RePrA}$

ρ,   Fluid density

τ,   Shear stress

μ,   Dynamic viscosity of fluid

ν,   Kinematic viscosity of fluid, $\dfrac{K_f}{\rho C_p}$

ϕ,   Dummy variable

Ψ,   Dimensional Stream function,

ψ,   Non-dimensional Stream function $\dfrac{\Psi}{U_m b}$

ω',   Dimensional Vorticity

ω,   Non-dimensional vorticity, $\dfrac{\omega' b}{U_m}$

ε,   Epsilon, iteration convergence criterion $\Sigma(\phi^{k+1} - \phi^k)$

∇^2,   Laplacian operator in rectangular cartesian coordinates $\left(\dfrac{\partial^2}{\partial x^2} + \dfrac{\partial^2}{\partial y^2}\right)$

∇^4 Biharmonic operator, $\left(\dfrac{\partial^2}{\partial x^2} + \dfrac{\partial^2}{\partial y^2}\right)\left(\dfrac{\partial^2}{\partial x^2} + \dfrac{\partial^2}{\partial y^2}\right)$

SUBSCRIPTS

BH ,   Value based on wall/bulk temperature difference.

c,   Cold wall value

h,   hot wall value

m,   mean value

mh,   mean value at hot-wall

mc,   mean value at cold wall

OPT,   optimum value

SUPERSCRIPTS

k,   iteration counter

n_1, n_2, n_3, n_4,   exponents in three-dimensional power Laws.

INTRODUCTION

The analyses of flows with heat transfer in channels have been restricted mostly to fully developed regions. This is usually done to reduce the complexity of the mathematical model of the physical problem. The formulations usually start by considering three-dimensional through-flows bounded by a continuous rigid boundary subject to given thermal conditions. By making plausible assumptions which conserve the physics of the problem a set of governing equations are obtained. The analyses then proceed by considering remote sections from the inlet. At such sections the dependent space variables are assumed invariant with the predominant direction of flow. The latter assumption further simplifies the governing equations by reducing the problem to a two-dimensional one. Using an appropriate set of normalisation variables, the governing equations are reduced to non-dimensional forms, resulting in the emergence of known non-dimensional parameters. These equations are then solved by either a numerical scheme or any other suitable analytical method for the prescribed boundary conditions.

A numerical study of fully developed combined free and forced laminar convection in inclined rectangular channels under the thermal boundary conditions of axially uniform wall heat flux was reported by Ou et. al. [1]. The improved formulation used by these authors redefined the Reynolds and Rayleigh numbers in terms of the angle of inclination to the horizontal. Because of the introduction of these modified non-dimensional parameters, their formulation excludes the horizontal case as a limiting orientation. Cheng and Hwang [2] presented numerical

results for fully developed combined free and forced laminar convection in horizontal channels under the thermal boundary conditions of axially uniform wall heatflux and peripherally uniform wall temperature. Cheng and Hong [3] reported a numerical study using a combination of boundary vorticity and line iterative methods to determine free convection effects on fully developed laminar upward flow in inclined tubes with the angle of inclination appearing explicitly in their formulation. The work of Ozoe et. al. [4], showed the influence of inclination angle on heat transfer rates in inclined square channels heated isothermally from below and similarly cooled from above. The other pair of vertical bounding sides were kept under adiabatic conditions. All the above references were restricted to fully developed regimes where rigid boundaries were considered as a continuous streamline to which a single value may be ascribed.

The present analyses pertain to the problem of combined free and forced laminar convection in inclined rectangular channels heated from below and cooled from above. The rigid boundaries involved are two parallel streamlines whose values differ. Two approaches have been adopted: Numerical and Perturbation methods. In the numerical solutions no general assumptions of fully developed regimes were made. The numerical solutions include all regions of the flowfield. The perturbation analysis was based on pure forced convection solution. The two thermal boundary conditions of interest were:

Case A: Constant surface temperatures

Case B: Constant Heatflux at the hot surface and arbitrarily-varying cold surface temperatures.

In solving the present problem, the pressure gradient terms were eliminated by cross-differentiation and subtraction of the momentum equations. The resulting vorticity transport and energy equations were normalised following Mori and Uchida [5] for case A, and Ou et. al. [1] for case B.

The vorticity transport and energy equations were discretized following Deniss [6]. The numerical solution was carried out by using boundary vorticity method and the five-point Gauss-Seidel iterative procedure.

As a prelude to perturbation solution, it was established by dimensional analysis using 'vector-length' approach that the pertinent parameter for the power series expansion is the Archimedes number, $\frac{Gr}{Re^2}$. The perturbation analysis was carried out for case A only.

To test the adequacy or otherwise of the mathematical model, an experimental set-up was designed, constructed and run. It was found that both numerical predictions and experimental results agree especially in indicating the occurence of maximum heat transfer rates from the hot wall at inclinations between 30° and 60° to the horizontal.

At this stage it must be stated that no works on cases A and B are known to the author except that of Mori and Uchida [5] which approximates to case A. They investigated the phenomenon of forced convective heat transfer between horizontal flat plates whose surfaces were kept at constant temperatures; the top plate being cooled and the bottom one heated. However, their analysis was restricted to the fully developed regime and they evaluated the heat transfer rates by way of

entropy production technique. Therefore it has not been possible to compare rigorously the present work with existing ones.

The two-dimensional assumption made must be complied with in constructing the experimental apparatus. Since the aspect ratio determines whether or not the effects of the vertical bounding sides could be ignored, an aspect ratio of about 10 was chosen. To ensure the 2-D claim, the channel was calibrated at a station x = 121.92 cm from channel inlet for an isothermal flow. Cheng and Hwang [2] carried out extensive investigation on the effect of aspect ratio on the central core space variables for channels whose long sides are horizontal and the short ones vertical. It was reported by them that for aspect ratios greater than 5, the central core space variables are not affected by the presence of the short vertical bounding sides. The present experimental set-up satisfies the requirement for a two-dimensional flow.

CHAPTER ONE

MATHEMATICAL FORMULATION OF THE PROBLEM

In formulating the problem, it is assumed, a priori, that the channel aspect ratio is large, that is, its width is several times the magnitude of its height so that the lateral end effects are negligible when a longitudinal section, far-removed from the vertical bounding sides, is taken. For moderate temperature gradients the problem reduces to a two-dimensional one. The channel can therefore be regarded as an open domain bounded by two parallel surfaces kept at different temperatures.

When the temperature difference between the surfaces is appreciable, buoyancy forces are generated and the resulting secondary flow is superimposed on the pure forced convection. The mutual interaction of the hydrodynamic and thermal fields in an oriented gravitational field is investigated by making the following simplifying assumptions to reduce the mathematical complexity of the governing equations. Figure 1 represents, the physical model, coordinate system and numerical grid.

1.1   Basic assumptions:

(a)   The thermophysical properties are constant, except for the density variations with the temperature (Boussinesq Approx.).

(b)   The flow is upward, steady, laminar and incompressible.

(c)   The fluid is Newtonian and viscous dissipation is negligible.

(d)   There is no internal heat generation.
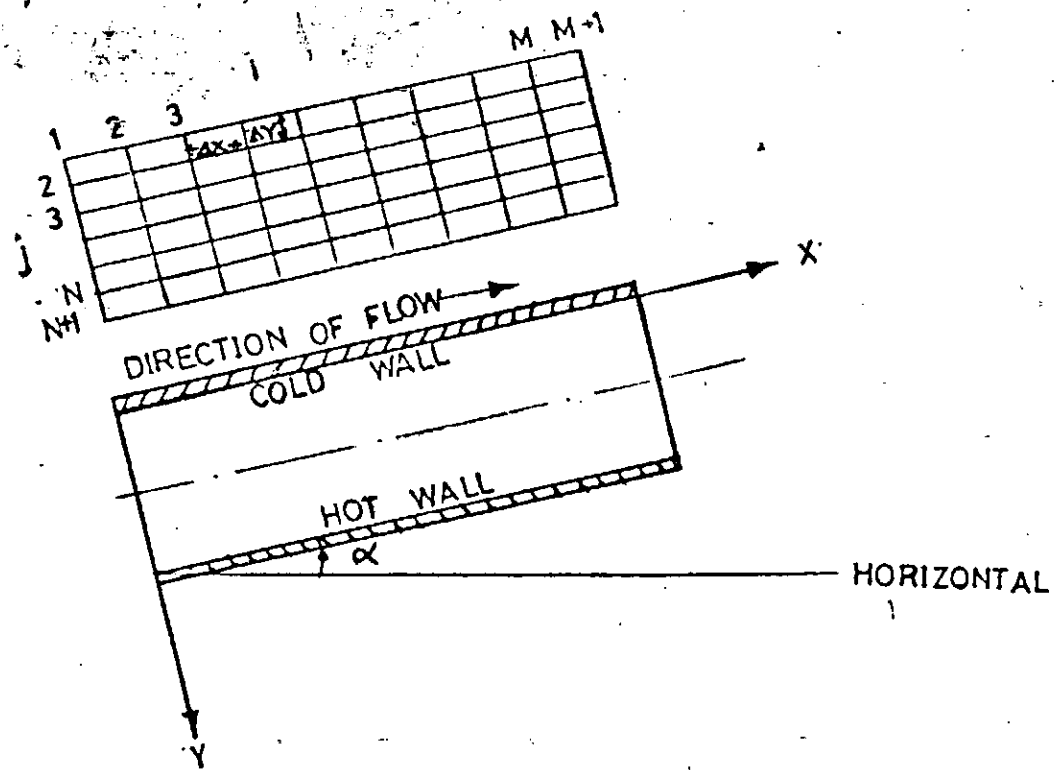
Fig.1.1.Physical Model, Coordinate System
and Numerical Grid.

1.2 Derivation of the governing equations

The continuity and energy equations are derived from the control volume analysis. However, the momentum equations, for the sake of brevity, have been deduced from the Navier-Stokes equations for a two-dimensional incompressible boundary layer flow.

1.21 Continuity equation
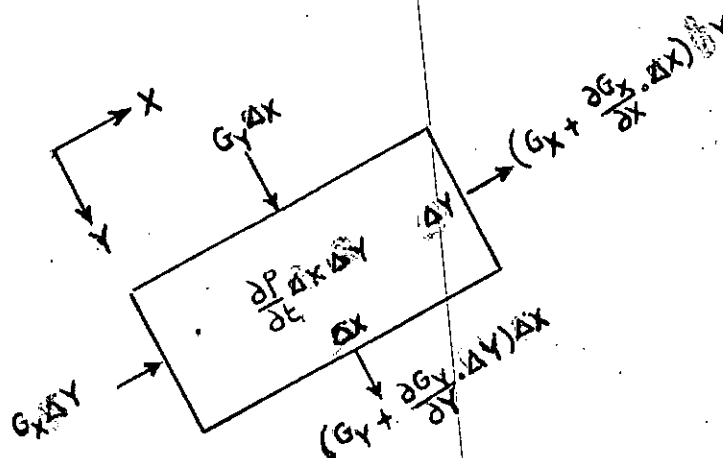
Fig. 1.1a control volume for development of continuity equation.

Consider a two-dimensional flow in the X-Y plane, out of which a control volume of infinitesimal dimensions has been cut. Let ΔX, ΔY be the X- and Y- dimensions respectively of the element. $\vec{G}$, represents the mass flux and G_X, G_Y represent the respective components of $\vec{G}$ in the X-and Y-directions, per unit length

With reference to the above figure,

Mass inflow into element $= G_Y \Delta X + G_X \Delta Y$

Mass outflow from element $= (G_X + \frac{\partial G_X}{\partial X} \cdot \Delta X) \Delta Y + (G_Y + \frac{\partial G_Y}{\partial Y} \cdot \Delta Y) \Delta X + 0[(\Delta X)^2 + (\Delta Y)^2]$

Rate of change of mass storage within the control volume
$= \frac{\partial \rho}{\partial t} \cdot \Delta X \Delta Y$

By the principle of mass conservation,

Mass inflow – mass outflow = Rate of change of mass storage within control volume

$$\therefore \quad G_Y \Delta X + G_X \Delta Y - \{(G_X + \frac{\partial G_X}{\partial X} \cdot \Delta X)\ \Delta Y + (G_Y + \frac{\partial G_Y}{\partial Y} \cdot \Delta Y)\Delta X\} = \frac{\partial \rho}{\partial t} \cdot \Delta X \Delta Y$$

Simplification yields

$$\frac{\partial G_X}{\partial X} + \frac{\partial G_Y}{\partial Y} + \frac{\partial \rho}{\partial t} = 0$$

For a steady-state flow, $\frac{\partial \rho}{\partial t} = 0$.

$$\therefore \quad \frac{\partial G_X}{\partial X} + \frac{\partial G_Y}{\partial Y} = 0$$

Substituting for $G_X = \rho_m U$ and $G_Y = \rho_m V$ then the above equation becomes

$$\frac{\partial}{\partial X}(\rho_m U) + \partial \frac{(\rho_m U)}{\partial Y} = 0$$

$$\therefore \quad U \frac{\partial \rho_m}{\partial X} + \rho_m \frac{\partial U}{\partial X} + V \frac{\partial \rho_m}{\partial Y} + \rho_m \frac{\partial V}{\partial Y} = 0$$

$$\therefore \quad \rho_m (\frac{\partial U}{\partial X} + \frac{\partial V}{\partial Y}) + (U \frac{\partial \rho_m}{\partial X} + V \frac{\partial \rho_m}{\partial Y}) = 0$$

Since the fluid is incompressible, $\frac{\partial \rho_m}{\partial X} = \frac{\partial \rho_m}{\partial Y} = 0$.

The continuity equation becomes,

$$\therefore \quad \frac{\partial U}{\partial X} + \frac{\partial V}{\partial Y} = 0 \quad \dots\dots\dots\dots\dots\dots\dots\dots\dots\dots(1.1)$$

1.22 Momentum Equation

In order to avoid the rather tedious derivation of the momentum equation from considerations of Newton's second Law of motion, it is proposed to deduce the relevant momentum equations from the general Navier-Stokes equations as cast in the compact tensorial notation in [7].

$$\rho_m \left(\frac{\partial V_i}{\partial t} + V_j \frac{\partial V_i}{\partial X_j} \right) = \vec{B}_i - \frac{\partial P}{\partial X_i} + \frac{\partial}{\partial X_j} \left\{ \mu \left(\frac{\partial V_i}{\partial X_j} + \frac{\partial V_j}{\partial X_i} \right. \right.$$

$$\left. \left. - \frac{2}{3} \sigma_{ij} \frac{\partial V_k}{\partial X_k} \right) \right\} \dots\dots\dots (1.2)$$

where σ_{ij}, is the kronecker delta

$$\text{and } \sigma_{ij} = 1 \quad \begin{cases} i = j \\ i \neq j \end{cases}$$
$$\phantom{\text{and } \sigma_{ij}} = 0$$

$(i, j, k = 1, 2, 3)$

V is the velocity vector and B, the body force per unit volume.

Since k is a dummy variable it can be replaced by j so that consideration for a two-dimensional case can be made.

Since the boundary layer flow is incompressible and steady, then $\dfrac{\partial V_i}{\partial t} = 0$.

In addition, $\dfrac{\partial V_k}{\partial X_k} = \dfrac{\partial V_j}{\partial X_j}$

Hence for the two-dimensional case, $i, j = 1, 2$

$$\therefore \frac{2}{3} \sigma_{ij} \frac{\partial V_j}{\partial X_j} = \frac{2}{3} \left[\sigma_{11} \frac{\partial V_1}{\partial X_1} + \sigma_{12} \frac{\partial V_2}{\partial X_2} + \sigma_{21} \frac{\partial V_1}{\partial X_1} + \sigma_{22} \frac{\partial V_2}{\partial X_2} \right]$$

But $\sigma_{ij} = \begin{array}{l} 1 \\ 0 \end{array} \quad \begin{cases} i = j \\ i \neq j \end{cases}$

$$\therefore \quad \sigma_{11} = \sigma_{22} = 1$$

$$\therefore \quad \sigma_{12} = \sigma_{21} = 0.$$

$$\therefore \quad \frac{2}{3} \sigma_{ij} \frac{\partial V_j}{\partial X_j} = \frac{2}{3} \left(\frac{\partial V_1}{\partial X_1} + \frac{\partial V_2}{\partial X_2} \right)$$

Since directions 1 and 2 can be associated with the coordinate axes of the rectangular cartesian coordinate system, the above equation can be written as

$$\frac{2}{3} \sigma_{ij} \frac{\partial V_j}{\partial X_j} = \frac{2}{3} \left(\frac{\partial U}{\partial X} + \frac{\partial V}{\partial Y} \right)$$

From the continuity equation (1.1),

$$\frac{2}{3} \sigma_{ij} \frac{\partial V_j}{\partial X_j} = 0. \quad \left(i, j = 1, 2. \right)$$

The general Navier-Stokes equation reduces to

$$\rho_m V_j \frac{\partial V_i}{\partial X_j} = \vec{B}_i - \frac{\partial P}{\partial X_i} + \frac{\partial}{\partial X_j} \left\{ \mu \left(\frac{\partial V_i}{\partial X_j} + \frac{\partial V_j}{\partial X_i} \right) \right\}$$

Expanding the right hand side for a constant viscosity fluid,

$$\rho_m V_j \frac{\partial V_i}{\partial X_j} = \vec{B}_i - \frac{\partial P}{\partial X_i} + \mu \left(\frac{\partial^2 V_i}{\partial X_j \partial X_j} + \frac{\partial^2 V_j}{\partial X_j \partial X_i} \right)$$

$$\therefore \quad \rho_m V_j \frac{\partial V_i}{\partial X_j} = \vec{B}_i - \frac{\partial P}{\partial X_i} + \mu \left\{ \frac{\partial^2 V_i}{\partial X_j \partial X_j} + \frac{\partial}{\partial X_i} \left(\frac{\partial V_j}{\partial X_j} \right) \right\} \quad (i,j = 1,2)$$

Again from considerations of continuity condition,

$$\frac{\partial V_j}{\partial X_j} = 0 \quad (j = 1, 2)$$

$$\therefore \rho_m \ V_j \ \frac{\partial V_i}{\partial X_j} = \vec{B}_i - \frac{\partial P}{\partial X_i} + \mu \frac{\partial^2 V_i}{\partial X_j \partial X_j} \quad (i,j = 1,2) \ \ldots\ldots\ldots\ldots(1.\ )$$

Noting that a repeated subscript indicates summation over the range of that subscript, the following equations result.

For i = 1, j = 1,2,

$$\rho_m (V_1 \frac{\partial V_1}{\partial X_1} + V_2 \frac{\partial V_1}{\partial X_2}) = B_1 - \frac{\partial P}{\partial X_1} + \mu(\frac{\partial^2 V_1}{\partial X_1^2} + \frac{\partial^2 V_1}{\partial X_2^2}) \ \ldots(1.4 $$

For i = 2, j = 1,2,

$$\rho_m (V_1 \frac{\partial V_2}{\partial X_1} + V_2 \frac{\partial V_2}{\partial X_2}) = B_2 - \frac{\partial P}{\partial X_2} + \mu(\frac{\partial^2 V_2}{\partial X_1^2} + \frac{\partial^2 V_2}{\partial X_2^2}) \ \ldots(1.5)$$

If V_1, B_1 and X_1 are the components of velocity, Body-force per unit volume and displacement in the X-directions respectively and V_2, B_2 and X_2 their corresponding components in the Y-direction, then the following substitutions can be made.

$$V_1 = U \ ; \quad V_2 = V$$
$$X_1 = X \ ; \quad X_2 = Y$$

Equations (1.4) and (1.5) become

$$\rho_m (\frac{U \partial U}{\partial X} + \frac{V \partial U}{\partial Y}) = B_X - \frac{\partial P}{\partial X} + \mu \nabla^2 U \ \ldots\ldots\ldots\ldots\ldots\ldots(1.4b)$$

$$\rho_m (\frac{U \partial V}{\partial X} + \frac{V \partial V}{\partial Y}) = B_Y - \frac{\partial P}{\partial Y} + \mu \nabla^2 V \ \ldots\ldots\ldots\ldots\ldots(1.5b)$$

Equations (1.4b) and (1.5b) represent the X-and Y-momentum equations respectively.

The body force in this case can be expressed as follows:

The density at any temperature, T, is related to the mean density by the Boussinesq approximation:

$$\rho_T = \rho_m (1-\beta\Delta T)$$

Body-force due to weight of element of mean density ρ_m is $\rho_m g\Delta X\Delta Y$ per unit length.

Body-force due to weight of element of mean density ρ_T is $\rho_T g\Delta X\Delta Y$ per unit length.

Buoyancy force = $\rho_m g\ \Delta X\Delta Y - \rho_T g\Delta X\Delta Y$

$$= g\Delta X\Delta Y\left[\rho_m - \rho_T\right]$$

From the Boussinesq approximation, $\rho_m - \rho_T = \rho_m\beta\Delta T$

∴ Buoyancy force $= \beta\rho_m g\Delta X\Delta Y\ \Delta T$

∴ Buoyancy force per unit volume $= \beta\rho_m g\Delta T$

$$\therefore\ \vec{B}_i = \beta\vec{g}_i\rho_m\Delta T$$

where $\vec{g}_i$ is the gravitational component in the i-direction.

Accordingly, $B_1 = B_X = \rho_m\beta g\cos\alpha\Delta T$

and $B_2 = B_Y = \rho_m\beta g\sin\alpha\ \Delta T$

The complete momentum equations are therefore

$$\frac{U\partial U}{\partial X} + \frac{V\partial U}{\partial Y} = -\frac{1}{\rho_m}\frac{\partial P}{\partial X} + \nu\nabla^2 U + g\beta\Delta T\sin\alpha \quad \ldots\ldots\ldots\ldots(1.6)$$

$$\frac{U\partial V}{\partial X} + \frac{V\partial V}{\partial Y} = -\frac{1}{\rho_m}\frac{\partial P}{\partial Y} + \nu\nabla^2 V - g\beta\Delta T\cos\alpha \quad \ldots\ldots\ldots\ldots(1.7)$$

1.23   Energy Equation
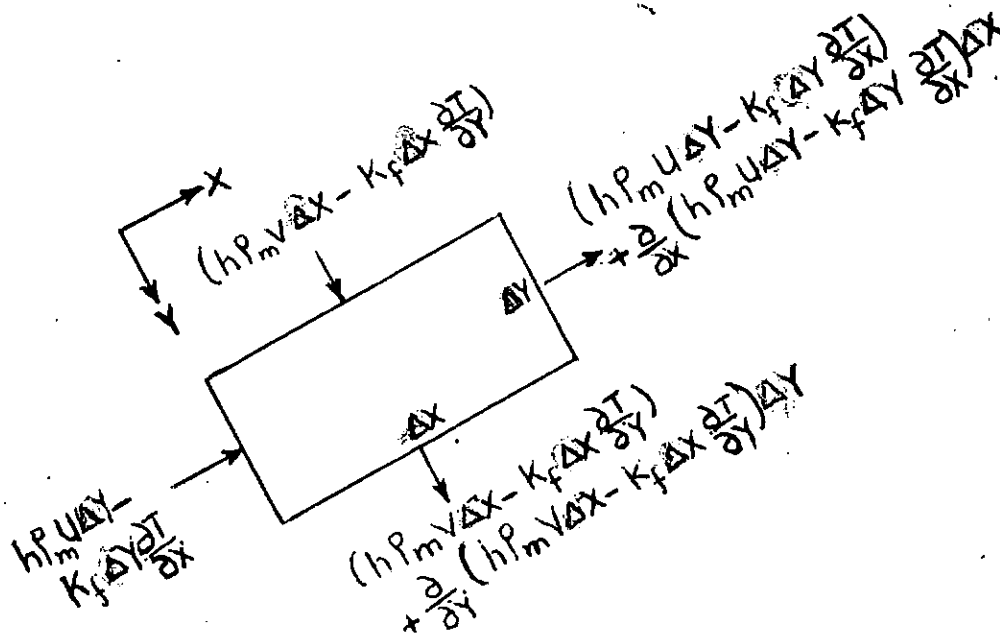
Fig. 1.1b Control volume for derivation of Energy differential equation

The control volume shows the various components of energy entering and leaving it.

Energy entering the control volume/length =

$$h\rho_m U\Delta Y - \kappa_f \Delta Y \frac{\partial T}{\partial X} + h\rho_m V\Delta X - \kappa_f \Delta X \frac{\partial T}{\partial Y}$$

Energy leaving the control volume /length =

$$h\rho_m U\Delta Y + \frac{\partial}{\partial X}(h\rho_m U\Delta Y)\Delta X - \kappa_f \Delta Y \frac{\partial T}{\partial X} + \frac{\partial}{\partial X}(-\kappa_f \Delta Y \frac{\partial T}{\partial X})\Delta X$$

$$+ h\rho_m V\Delta X + \frac{\partial}{\partial Y}(h\rho_m V\Delta X)\Delta Y$$

$$- \kappa_f \Delta X \frac{\partial T}{\partial Y} + \frac{\partial}{\partial Y}(-\kappa_f \Delta X \frac{\partial T}{\partial Y})\Delta Y$$

Considering thermal energy balance for the control volume,

$$h\rho_m U\Delta Y - \kappa_f \Delta Y \frac{\partial T}{\partial X} + h\rho_m V\Delta X - \kappa_f\Delta X \frac{\partial T}{\partial Y} = h\rho_m U\Delta Y + \frac{\partial}{\partial X}(h\rho_m U\Delta Y)\Delta X$$

$$-\kappa_f \Delta Y \frac{\partial T}{\partial X}$$

$$+ \frac{\partial}{\partial X}(-\kappa_f \Delta Y \frac{\partial T}{\partial X})\Delta X$$

$$+ h\rho_m V\Delta X + \frac{\partial}{\partial Y}(h\rho_m V\Delta X)\Delta Y$$

$$- \kappa_f \Delta X \frac{\partial T}{\partial Y} + \frac{\partial}{\partial Y}(-\kappa_f\Delta X \frac{\partial T}{\partial Y})\Delta Y$$

Simplification yields

$$\frac{\partial}{\partial X}(\kappa_f \frac{\partial T}{\partial X}) + \frac{\partial}{\partial Y}(\kappa_f \frac{\partial T}{\partial Y}) = \frac{\partial}{\partial Y}(h\rho_m V) + \frac{\partial}{\partial X}(h\rho_m U)$$

But $h = Cp\, T$. and since κ_f = constant, then

$$\kappa_f \frac{\partial^2 T}{\partial X^2} + \kappa_f \frac{\partial^2 T}{\partial Y^2} = \rho_m C_p \frac{\partial}{\partial X}(UT) + \rho_m C_p \frac{\partial}{\partial Y}(VT)$$

Expanding the right hand side yields

$$\kappa_f \nabla^2 T = \rho_m C_p \left[U \frac{\partial T}{\partial X} + T \frac{\partial U}{\partial X} + V \frac{\partial T}{\partial Y} + T \frac{\partial V}{\partial Y}\right]$$

$$\kappa_f \nabla^2 T = \rho_m C_p \left[(U \frac{\partial T}{\partial X} + U \frac{\partial T}{\partial Y}) + T(\frac{\partial U}{\partial X} + \frac{\partial V}{\partial Y})\right]$$

From the continuity condition, $\frac{\partial U}{\partial X} + \frac{\partial V}{\partial Y} = 0$.

$$\therefore \quad \kappa_f \nabla^2 T = \rho_m C_p (U \frac{\partial T}{\partial X} + V \frac{\partial T}{\partial Y})$$

Hence the Energy Transport equation is given by,

$$U \frac{\partial T}{\partial X} + V \frac{\partial T}{\partial Y} = \lambda \nabla^2 T \dots\dots\dots(1.8)$$

where $\lambda = \dfrac{\kappa_f}{\rho_m C_p}$, the thermal diffusivity.

1.3 Vorticity Transport Equation

Since the primary aim of this analysis is to present the heat transfer and flow characteristics, the pressure gradient terms in both momentum equations can be eliminated by cross-partial differentiation.

Differentiating equations (1.6) with respect to Y and (1.7) with respect to X and subtracting the results, gives,

$$\frac{\partial}{\partial Y}(U\frac{\partial U}{\partial X} + V\frac{\partial U}{\partial Y}) - \frac{\partial}{\partial X}(U\frac{\partial V}{\partial X} + V\frac{\partial V}{\partial Y}) = \nu(\frac{\partial}{\partial Y}\nabla^2 U - \frac{\partial}{\partial X}\nabla^2 V)$$

$$+ g\beta(\frac{\partial T}{\partial Y}\sin\alpha + \frac{\partial T}{\partial X}\cos\alpha)$$

$$\therefore \quad (\frac{\partial U}{\partial Y}\cdot\frac{\partial U}{\partial X} + U\frac{\partial^2 U}{\partial X\partial Y} + \frac{\partial V}{\partial Y}\cdot\frac{\partial U}{\partial Y} + V\frac{\partial^2 U}{\partial Y^2}) - (\frac{\partial U}{\partial X}\cdot\frac{\partial V}{\partial X} + U\frac{\partial^2 V}{\partial X^2}$$

$$+ \frac{\partial V}{\partial X}\cdot\frac{\partial V}{\partial Y} + V\frac{\partial^2 V}{\partial X\partial Y})$$

$$= \nu(\frac{\partial}{\partial Y}\nabla^2 U - \frac{\partial}{\partial X}\nabla^2 V)$$

$$+ g\beta(\frac{\partial T}{\partial Y}\sin\alpha + \frac{\partial T}{\partial X}\cos\alpha)$$

Collecting and regrouping terms, yield

$$V(\frac{\partial^2 U}{\partial Y^2} - \frac{\partial^2 V}{\partial X\partial Y}) + U(\frac{\partial^2 V}{\partial X\partial Y} - \frac{\partial^2 V}{\partial X^2}) + (\frac{\partial U}{\partial Y}\cdot\frac{\partial U}{\partial X} - \frac{\partial U}{\partial X}\cdot\frac{\partial V}{\partial X})$$

$$+ (\frac{\partial V}{\partial Y}\cdot\frac{\partial U}{\partial Y} - \frac{\partial V}{\partial X}\cdot\frac{\partial V}{\partial Y})$$

$$= \nu(\frac{\partial}{\partial Y}\nabla^2 U - \frac{\partial}{\partial X}\nabla^2 V) + g\beta(\frac{\partial T}{\partial Y}\sin\alpha + \frac{\partial T}{\partial X}\cos\alpha)$$

$$\therefore \quad V\frac{\partial}{\partial Y}\left(\frac{\partial U}{\partial Y}-\frac{\partial V}{\partial X}\right) + U\frac{\partial}{\partial X}\left(\frac{\partial U}{\partial Y}-\frac{\partial V}{\partial X}\right) + \left(\frac{\partial U}{\partial X}+\frac{\partial V}{\partial Y}\right)\cdot\left(\frac{\partial U}{\partial Y}-\frac{\partial V}{\partial X}\right)$$

$$= \nu\left(\frac{\partial}{\partial Y}\nabla^2 U - \frac{\partial}{\partial X}\nabla^2 V\right) + g\beta\left(\frac{\partial T}{\partial Y}\sin\alpha + \frac{\partial T}{\partial X}\cos\alpha\right)$$

Invoking the continuity condition, i.e. $\frac{\partial U}{\partial X}+\frac{\partial V}{\partial Y}=0$, yields

$$V\frac{\partial}{\partial Y}\left(\frac{\partial U}{\partial Y}-\frac{\partial V}{\partial X}\right) + U\frac{\partial}{\partial X}\left(\frac{\partial U}{\partial Y}-\frac{\partial V}{\partial X}\right) = -\nu\left(\frac{\partial}{\partial Y}\nabla^2 U-\frac{\partial}{\partial X}\nabla^2 V\right)+g\beta\left(\frac{\partial T}{\partial Y}\sin\alpha\right.$$

$$\left.+\frac{\partial T}{\partial X}\cos\alpha\right)$$

$$\therefore \quad V\frac{\partial}{\partial Y}\left(\frac{\partial U}{\partial Y}-\frac{\partial V}{\partial X}\right) + U\frac{\partial}{\partial X}\left(\frac{\partial U}{\partial Y}-\frac{\partial V}{\partial X}\right) = -\nu\left[\frac{\partial^3 U}{\partial X^2\partial Y}+\frac{\partial^3 U}{\partial Y^3}-\frac{\partial^3 V}{\partial X^3}-\frac{\partial^3 V}{\partial Y^2\partial X}\right]$$

$$+ g\beta\left(\frac{\partial T}{\partial Y}\sin\alpha + \frac{\partial T}{\partial X}\cos\alpha\right)$$

$$= \nu\left[\frac{\partial^2}{\partial X^2}\left(\frac{\partial U}{\partial Y}-\frac{\partial V}{\partial X}\right) + \frac{\partial^2}{\partial Y^2}\left(\frac{\partial U}{\partial Y}-\frac{\partial V}{\partial X}\right)\right]$$

$$+ g\beta\left(\frac{\partial T}{\partial Y}\sin\alpha + \frac{\partial T}{\partial X}\cos\alpha\right)$$

By definition the vorticity, $\omega' = \frac{\partial V}{\partial X}-\frac{\partial U}{\partial Y}$

Substituting this into the equation above yields

$$-V\frac{\partial\omega'}{\partial Y}-U\frac{\partial\omega'}{\partial X} = -\nu\left(\frac{\partial^2\omega'}{\partial X^2}+\frac{\partial^2\omega'}{\partial Y^2}\right) + g\beta\left(\frac{\partial T}{\partial Y}\sin\alpha + \frac{\partial T}{\partial X}\cos\alpha\right)$$

The vorticity Transport equation is therefore given by,

$$\therefore \quad U\frac{\partial\omega'}{\partial X} + V\frac{\partial\omega'}{\partial Y} = \nu\nabla^2\omega' - g\beta\left(\frac{\partial T}{\partial Y}\sin\alpha + \frac{\partial T}{\partial X}\cos\alpha\right) \quad \dots\dots\dots\dots\dots(1.9)$$

1.4 Boundary Conditions:

Two thermal boundary conditions have been considered in conjuction with the no-slip hydrodynamic conditions at the rigid boundaries.

These are:

1.41. Case A: Constant but unequal surface temperatures.

1.42. Case B: Constant Heatflux at the hot surface and arbitrarily-
varying cold surface temperature.

In both cases the input velocity and temperature at channel entrance are assumed uniform. At the channel exit the gradient, boundary condition $\partial\phi/\partial x = 0$ is imposed on the flow. The applicable mathematical representations of the boundary conditions will be given in the Analysis of Numerical methods.

1.5 Normalisation of Governing equations

The governing equations in their present form would be valid for a given system of units. For the equations to be valid in another system of units, various conversion factors must be introduced. In order to render the governing equations independent of any system of units, appropriate sets of normalising variables are introduced. The continuity and vorticity transport equations are considered first, followed by considerations of the two cases of thermal boundary conditions. The following substitutions have been made for the continuity and vorticity transport equations:

$$U = U_m u$$

$$V = U_m v$$

$$X = bx$$

$$Y = by$$

$$\omega = \frac{U_m \omega}{b}$$

For the energy equation the following substitutions are made for cases A & B

Case A: $\theta = \dfrac{T-T_c}{T_h-T_c}$, for constant but unequal surface temperature

Case B: $\theta = \dfrac{(T-T_{0})}{RePrA*b}$, Constant Heatflux at hot surface and, arbitrarily varying cold surface temperature

1.51 Continuity equation:

Substituting the above transformation coordinates into the primitive continuity equation (1.1) gives,

$$Um \frac{\partial u}{b\partial x} + Um \frac{\partial v}{b\partial y} = 0$$

$$\frac{Um}{b} \left(\frac{\partial u}{\partial x} + \frac{\partial v}{\partial y} \right) = 0$$

Since $\dfrac{Um}{b} \neq 0$, both sides can be divided by $\dfrac{Um}{b}$.

The non-dimensional form of the continuity equation is therefore,

$$\frac{\partial u}{\partial x} + \frac{\partial v}{\partial y} = 0 \quad \dots\dots\dots\dots\dots\dots\dots\dots\dots\dots\dots\dots\dots\dots\dots\dots(1.10a)$$

1.52 Vorticity Transport equation

Substituting the transformation coordinates into equation (1.9) gives

Case A.

$$\frac{(Um u)\partial \frac{(Um\omega)}{b}}{b\partial x} + \frac{(Um v)\partial \frac{(Um\omega)}{b}}{b\partial y} = -\nu\left[\frac{\partial^2 \frac{(Um\omega)}{b}}{b^2\partial x^2} + \frac{\partial^2 \frac{(Um\omega)}{b}}{b^2\partial y^2} \right]$$

$$- g\beta \frac{(T_h - T_c)}{b}\left[\frac{\partial \theta}{\partial y} \sin\alpha + \frac{\partial \theta}{\partial x} \cos\alpha \right]$$

$$\therefore \quad (\frac{U_m^2}{b^2})\{u\frac{\partial \omega}{\partial y} + v\frac{\partial \omega}{\partial y}\} = \frac{\nu U_m}{b^3} \nabla^2 \omega - \frac{g\beta(T_h-T_c)}{b} (\frac{\partial \theta}{\partial y} \sin\alpha + \frac{\partial \theta}{\partial x} \cos\alpha)$$

Dividing both sides by $\frac{U_m^2}{b^2}$ gives

$$\therefore \quad u\frac{\partial \omega}{\partial x} + v\frac{\partial \omega}{\partial y} = (\frac{\nu}{U_m b}) \nabla^2 \omega - \frac{g\beta b(T_h - T_c)}{U_m^2} (\frac{\partial \theta}{\partial y} \sin\alpha + \frac{\partial \theta}{\partial x} \cos\alpha)$$

Introducing $\rho_m \mu$ into the source term gives

$$u\frac{\partial \omega}{\partial x} + v\frac{\partial \omega}{\partial y} = \frac{1}{(\frac{U_m b}{\nu})} \nabla^2 \omega - \frac{g\beta\rho_m^2(T_h-T_c)b^3}{\frac{\rho_m^2 U_m^2 b^2}{\mu^2} \cdot \mu^2} (\frac{\partial \theta}{\partial y} \sin\alpha + \frac{\partial \theta}{\partial x} \cos\alpha)$$

$$= \frac{1}{(\frac{U_m b}{\nu})} \cdot \nabla^2 \omega - \frac{g\beta(T_h - T_c)b^3}{\nu^2 \cdot (\frac{U_m b}{\nu})^2} (\frac{\partial \theta}{\partial y} \sin\alpha + \frac{\partial \theta}{\partial x} \cos\alpha)$$

Recognising $\frac{U_m b}{\nu}$ as Re based on the channel height and $\frac{g\beta(T_h-T_c)b^3}{\nu^2}$

= Gr based on the temperature potential between the two surfaces,

then the vorticity transport equation in its dimensionless form is

$$u\frac{\partial \omega}{\partial x} + v\frac{\partial \omega}{\partial y} = \frac{1}{Re} \nabla^2 \omega - \frac{Gr}{Re^2} (\frac{\partial \theta}{\partial y} \sin\alpha + \frac{\partial \theta}{\partial x} \cos\alpha) \quad \ldots\ldots\ldots(1.10b)$$

where $\frac{Gr}{Re^2}$ = Ar, the Archimedes number.

Case B:

For the constant heatflux at the hot surface and arbitrarily-varying
cold surface temperature, the Grashof number is based on the dimen-
sional axial temperature gradient, $\overset{*}{A}$, along the hot surface.

Accordingly, the modified Grashof and Archimedes numbers are:

$$Gr_m = \frac{g\beta\tilde{\lambda}b^4}{\nu^2} , \quad Ar_m = \frac{Gr_m}{Re^2} .$$

1.58   Energy equation

Case A:

$$\theta = \frac{T - T_c}{T_h - T_c}$$

$$U_m u \frac{(T_h - T_c)}{b} \frac{\partial \theta}{\partial x} + U_m v \frac{(T_h - T_c)}{b} \frac{\partial \theta}{\partial y} = \frac{\lambda (T_h - T_c)}{b^2} \nabla^2\theta$$

$$\therefore \quad \frac{U_m}{b} (u \frac{\partial \theta}{\partial x} + v \frac{\partial \theta}{\partial y}) = \frac{\lambda}{b^2} \nabla^2\theta$$

$$\therefore \quad u \frac{\partial \theta}{\partial x} + v \frac{\partial \theta}{\partial y} = \frac{\lambda}{U_m b} \nabla^2\theta = \frac{(\frac{\lambda}{\nu})}{(\frac{U_m b}{\nu})} \nabla^2\theta .$$

By definition, $\frac{\lambda}{\nu} = \frac{1}{P_r}$ and $\frac{U_m b}{\nu} = Re$

The non-dimensional form of the energy equation is

$$\therefore \quad u \frac{\partial \theta}{\partial x} + v \frac{\partial \theta}{\partial y} = \frac{1}{RePr} \nabla^2\theta \quad \dots\dots\dots\dots\dots\dots\dots\dots\dots\dots\dots(1.10c)$$

Case B:

$$\theta = \frac{(T - T\infty)}{RePrA^*b} .$$

By a similar manipulation as done above, the final equation still
assumes the same form as (1.10c).

CHAPTER TWO

2.

ANALYSIS OF NUMERICAL METHOD - CASE A

The condition of no-slip imposed at the rigid boundaries requires very high velocity gradients to stagnate the flow at such boundaries. As a result of the high velocity gradients, vortices are generated at the rigid boundaries and are convected and dissipated in the fluid stream. The problem is therefore a boundary-value one and the success of the numerical computation depends on the correct determination of the boundary vorticities. Considering the fact that in some regions of the flow field the secondary effects may aid or oppose the forced flow, the method of Spalding and Greenspan $\begin{bmatrix} 6 \end{bmatrix}$ may be used in discretising the non-linear terms in the governing equations for constant coefficients. As usual the non-convective components in the equations are dis-cretized using the central-difference approximation.

The reason for the one-sided differences of the non-linear terms is to ensure that the matrix associated with the difference equations is diagonally-dominant. This is a necessary and suffi-cient condition for convergence of the Gauss-Seidel iterative procedure adopted. In order to further accelerate convergence, an optimum relaxation parameter is introduced into the Poisson equation of the stream function.

2.1 Discretization of the governing equations

Let ϕ be a dependent variable which can represent one of a large number of particular dependent variables. These include:

(a)   The fluid velocity components u, v

(b)   The vorticity, ω

(c)   The fluid temperature, θ

(d)   The Stream function, ψ

(e)   The dummy variable used in the convergence test for numerical solution

In general, $\phi_{i,j}$ represents the value of ϕ at a grid point (i,j) in the mesh system shown in figure1.1. The value of ϕ at any of the four neighbouring nodes to the grid- point (i,j) can also be represented by $\phi_{i+1,j}$, $\phi_{i-1,j}$, $\phi_{i,j+1}$, $\phi_{i,j-1}$. Since ϕ is a continuous space variable, its Taylor series expansion about any of the nodal points can be stated. Thus:

$$\phi_{i,j-1} = \phi_{i,j} + \sum_{n=1}^{\infty} \frac{(-1)^n (\Delta y)^n}{n!} \left. \frac{\partial^n \phi}{\partial y^n} \right|_{i,j} \quad \cdots\cdots\cdots\cdots\cdots(2.1)$$

$$\phi_{i,j+1} = \phi_{i,j} + \sum_{n=1}^{\infty} \frac{(\Delta y)^n}{n!} \left. \frac{\partial^n \phi}{\partial y^n} \right|_{i,j} \quad \cdots\cdots\cdots\cdots\cdots(2.2)$$

$$\phi_{i+1,j} = \phi_{i,j} + \sum_{n=1}^{\infty} \frac{(\Delta x)^n}{n!} \left. \frac{\partial^n \phi}{\partial x^n} \right|_{i,j} \quad \cdots\cdots\cdots\cdots\cdots(2.3)$$

$$\phi_{i-1,j} = \phi_{i,j} + \sum_{n=1}^{\infty} \frac{(-1)^n (\Delta x)^n}{n!} \left. \frac{\partial^n \phi}{\partial x^n} \right|_{i,j} \quad \cdots\cdots\cdots\cdots\cdots(2.4)$$

By truncating the above series, approximations to the first- and second-order partial derivatives of ϕ can be made.

2.1.1 Approximations to second-order partial derivatives

In order to find approximations to the second-order derivatives the infinite series expansions are carried out for up to $n = 3$.

For $\left.\dfrac{\partial^2 \phi}{\partial y^2}\right|_{i,j}$:

Equation (2.1) + (2.2) yields

$$\phi_{i,j-1} + \phi_{i,j+1} = 2\phi_{i,j} + \sum_{n=1}^{3}\frac{(-1)^n(\Delta y)^n}{n!}\left.\frac{\partial^n\phi}{\partial y^n}\right|_{i,j} + \sum_{n=1}^{3}\frac{(\Delta y)^n}{n!}\left.\frac{\partial^n\phi}{\partial y^n}\right|_{i,j} + 0(\Delta y)^{l}$$

Simplifying and solving for $\left.\dfrac{\partial^2 \phi}{\partial y^2}\right|_{i,j}$, produces

$$\left.\frac{\partial^2\phi}{\partial y^2}\right|_{i,j} = (\phi_{i,j+1} - 2\phi_{i,j} + \phi_{i,j-1})/(\Delta y)^2 + 0(\Delta y)^3 \ldots\ldots\ldots (2.5)$$

Similarly, from equations (2.3) and (2.4),

$$\left.\frac{\partial^2\phi}{\partial x^2}\right|_{i,j} = (\phi_{i+1,j} - 2\phi_{i,j} + \phi_{i-1,j})/(\Delta x)^2 \ldots\ldots\ldots\ldots\ldots\ldots (2.6)$$

2.1.2 Approximations to first partial derivatives

For $\left.\dfrac{\partial \phi}{\partial y}\right|_{i,j}$, either of equations (2.1) and (2.2) can be used depending on whether it is the backward or forward difference that is required. Only two terms of the expansions are considered in this case.

For the backward difference, equation (2.1) applies.

Thus $\left.\dfrac{\partial \phi}{\partial y}\right|_{i,j} = (\phi_{i,j} - \phi_{i,j-1})/\Delta y$ ....(2.7a)

Similarly, from equation (2.2) the forward difference is given by

$\left.\dfrac{\partial \phi}{\partial y}\right|_{i,j} = (\phi_{i,j+1} - \phi_{i,j})/\Delta y$ ....(2.7b)

Equations (2.7a) and (2.7b) can be combined to obtain a more general expression for $\left.\dfrac{\partial \phi}{\partial y}\right|_{i,j}$

Thus, $\left.\dfrac{\partial \phi}{\partial y}\right|_{i,j} = \{A_1 (\phi_{i,j+1} - \phi_{i,j}) + A_2 (\phi_{i,j} - \phi_{i,j-1})\}/\Delta y$ ...(2.8)

where A_1 and A_2 alternately assume values of 1 and 0 depending on the local flow direction. Following Spalding and Greenspan [6], when the local flow velocity is negative, the forward difference is used so that $A_1 = 1.0$ and $A_2 = 0$. for this case. However for a positive local velocity the backward difference is used and A_1 and A_2 exchange values accordingly.

Since the flow is forced, the local velocity in the general direction of forced flow is regarded as positive so that the backward difference relation used throughout the computation is

$\left.\dfrac{\partial \phi}{\partial x}\right|_{i,j} = (\phi_{i,j} - \phi_{i-1,j})/\Delta x$ ....(2.9)

2.2 Finite-difference Analogs of governing equations

At this stage, ϕ can be particularised for a chosen dependent variable.

2.2.1   Energy Equation: $\theta = \phi$.

$$\therefore \left. \frac{\partial^2\theta}{\partial x^2} \right|_{i,j} = (\theta_{i+1,j} - 2\theta_{i,j} + \theta_{i-1,j})/(\Delta x)^2$$

$$\left. \frac{\partial^2\theta}{\partial y^2} \right|_{i,j} \approx (\theta_{i,j+1} - 2\theta_{i,j} + \theta_{i,j-1})/(\Delta y)^2$$

$$\left. \frac{\partial\theta}{\partial y} \right|_{i,j} \approx \{A_1(\theta_{i,j+1} - \theta_{i,j}) + A_2(\theta_{i,j} - \theta_{i,j-1})\}/\Delta y$$

$$\left. \frac{\partial\theta}{\partial x} \right|_{i,j} \approx (\theta_{i,j} - \theta_{i-1,j})/\Delta x$$

Substituting these approximations into the energy equation
(1.10c) gives,

$$\frac{u_{i,j}}{\Delta x}(\theta_{i,j} - \theta_{i-1,j}) + \frac{v_{i,j}}{\Delta y}\{A_1(\theta_{i,j+1} - \theta_{i,j}) + A_2(\theta_{i,j} - \theta_{i,j-1})\}$$

$$= \frac{1}{RePr}\left\{\frac{(\theta_{i+1,j} - 2\theta_{i,j} + \theta_{i-1,j})}{(\Delta x)^2} + \frac{(\theta_{i,j+1} - 2\theta_{i,j} + \theta_{i,j+1})}{(\Delta y)^2}\right\} \quad (2.10)$$

Simplifying and solving for $\theta_{i,j}$ yields the
discretized form of the energy transport equation.

$$\theta_{i,j} = \cfrac{\left[\begin{array}{l} \dfrac{1}{RePr} \left\{ \dfrac{(\theta_{i,j+1} + \theta_{i,j-1})}{(\Delta y)^2} + \dfrac{(\theta_{i+1,j} + \theta_{i-1,j})}{(\Delta x)^2} \right\} \\[2mm] + (u_{i,j}\,\theta_{i-1,j})/\Delta x + \dfrac{v_{i,j}}{\Delta y}(A_2\,\theta_{i,j-1} - A_1\,\theta_{i,j+1}) \end{array} \right]}{\left[\dfrac{u_{i,j}}{\Delta x} + \dfrac{(A_2 - A_1)v_{i,j}}{\Delta y} + \dfrac{2}{RePr}\left\{\dfrac{1}{(\Delta x)^2} + \dfrac{1}{(\Delta y)^2}\right\} \right]} \qquad \ldots (2.11)$$

where $i = 2, 3, \ldots M$

$j = 2, 3, \ldots N$ and $\begin{array}{l} A_1 = +1.0 \\ A_2 = 0.0 \end{array} \Big\} v_{i,j} < 0; \begin{array}{l} A_1 = 0.0 \\ A_2 = 1.0 \end{array} \Big\} v_{i,j} > 0$

By a similar procedure as above, the vorticity transport and stream-function equations are obtained. The simplified results are stated below.

2.22 Vorticity Transport equation

$$\omega_{i,j} = \cfrac{\left[\begin{array}{l} \dfrac{1}{Re}\left\{ \dfrac{(\omega_{i,j+1} + \omega_{i,j-1})}{(\Delta y)^2} + \dfrac{(\omega_{i+1,j} + \omega_{i-1,j})}{(\Delta x)^2} \right\} \\[2mm] + (u_{i,j}\,\omega_{i-1,j})/\Delta x + v_{i,j}(A_3\,\omega_{i,j-1} - A_4\omega_{i,j+1})/\Delta y \\[2mm] - \dfrac{Gr}{Re^2}\Big[\{A_4(\theta_{i,j+1} - \theta_{i,j}) + A_3(\theta_{i,j} - \theta_{i,j-1})\} \dfrac{Sin\alpha}{\Delta y} \\[2mm] \qquad\qquad + (\theta_{i,j} - \theta_{i-1,j}) \dfrac{Cos\alpha}{\Delta x} \Big] \end{array} \right]}{\left[u_{i,j}/\Delta x + (A_3 - A_4)\dfrac{v_{i,j}}{\Delta y} + \dfrac{2}{Re}\left\{\dfrac{1}{(\Delta x)^2} + \dfrac{1}{(\Delta y)^2}\right\} \right]} \qquad \ldots (2.12)$$

where $i = 2, 3, \ldots M$ and $\begin{array}{l} A_3 = 0.0 \\ A_4 = 1.0 \end{array} \} v_{i,j} < 0;$ $\begin{array}{l} A_3 = 1.0 \\ A_4 = 0.0 \end{array} \} v_{i,j} > 0$

$j = 2, 3, \ldots N$

2.28 The Poisson Equation of the Streamfunction:

The streamfunction is obtained from the equation $\omega = - \nabla^2 \psi$.

$$\psi_{i,j} = \frac{\{\omega_{i,j} + \dfrac{(\psi_{i,j+1} + \psi_{i,j-1})}{(\Delta y)^2} + \dfrac{(\psi_{i+1,j} + \psi_{i-1,j})}{(\Delta x)^2}\}}{2\left[\dfrac{1}{(\Delta x)^2} + \dfrac{1}{(\Delta y)^2}\right]} \quad \ldots\ldots\ldots\ldots(2.13)$$

$i = 2, 3 \ldots M$
$j = 2, 3 \ldots N-1$

For relaxation purposes in order to accelerate convergence the optimum relaxation parameter, ω_0, which lies between 1 and 2, is introduced into equation (2.13) following Roache $\begin{bmatrix} 8 \end{bmatrix}$. Thus,

$$\psi_{i,j} = \psi_{i,j} + \frac{\omega_0}{(1+\beta_i^2)} \left[\psi_{i+1,j} + \psi_{i-1,j} + \beta_i^2 (\psi_{i,j+1} + \psi_{i,j-1}) - (\Delta x)^2 \omega_{i,j} - \right.$$

$$\left. 2(1+\beta_i^2)\psi_{i,j} \right] \ldots\ldots(2.14)$$

where ω_0, for a Dirichlet problem in a rectangular domain of uniform grid sizes Δx and Δy, is given by

$$\omega_0 = \frac{2(1 - \sqrt{1 - \xi})}{\xi} \quad \ldots\ldots\ldots\ldots\ldots\ldots\ldots\ldots\ldots\ldots\ldots\ldots\ldots\ldots(2.15a)$$

where $\xi = \left[\frac{Cos(\frac{\pi}{I-1}) + \beta_i^2 Cos (\frac{\pi}{J-1})}{1 + \beta_i^2} \right]^2 \quad \ldots\ldots\ldots\ldots\ldots\ldots\ldots\ldots(2.15b)$

and $\beta_i = \dfrac{\Delta x}{\Delta y}$, the mesh aspect Ratio; $J = N+1$; $I = M+1$

2.2.4 Near-boundary Conditions

Near the rigid boundaries where the flow is considerably retarded, the Stream function values do not differ appreciably from its boundary values. The near-boundary values are approximated as follows.

For the cold wall:(J=1). Considering two immediate nodal points to the cold wall, the Taylor series expansion for these points are:

$$\psi_{i,j+1} = \psi_{i,j} + \sum_{n=1}^{\infty} \frac{(\Delta y)^n}{n!} \frac{\partial^n \psi}{\partial y^n}\bigg|_{i,j} \quad \dots\dots\dots\dots\dots\dots\dots(2.16)$$

$$\psi_{i,j+2} = \psi_{i,j} + \sum_{n=1}^{\infty} \frac{(2\Delta y)^n}{n!} \frac{\partial^n \psi}{\partial y^n}\bigg|_{i,j} \quad \dots\dots\dots\dots\dots\dots\dots(2.17)$$

Considering only the first three terms of each expansion, each equation yields

$$\psi_{i,j+1} = \psi_{i,j} + \Delta y \left.\frac{\partial \psi}{\partial y}\right|_{i,j} + \frac{(\Delta y)^2}{2!} \left.\frac{\partial^2 \psi}{\partial y^2}\right|_{i,j} + O(\Delta y)^3 \quad \dots\dots(2.18a)$$

and

$$\psi_{i,j+2} = \psi_{i,j} + 2\Delta y \left.\frac{\partial \psi}{\partial y}\right|_{i,j} + 4\frac{(\Delta y)^2}{2!} \left.\frac{\partial^2 \psi}{\partial y^2}\right|_{i,j} + O(\Delta y)^3 \quad \dots\dots(2.18b)$$

For $j = 1$, (2.18a) and (2.18b) respectively become

$$\psi_{i,2} = \psi_{i,1} + \Delta y \left.\frac{\partial \psi}{\partial y}\right|_{i,1} + \frac{(\Delta y)^2}{2} \left.\frac{\partial^2 \psi}{\partial y^2}\right|_{i,1} + O(\Delta y)^3$$

$$\psi_{i,3} = \psi_{i,1} + 2\Delta y \left.\frac{\partial \psi}{\partial y}\right|_{i,1} + 4\frac{(\Delta y)^2}{2} \left.\frac{\partial^2 \psi}{\partial y^2}\right|_{i,1} + O(\Delta y)^3$$

Neglecting terms of $O(\Delta y)^3$ and eliminating $\left.\frac{\partial^2 \psi}{\partial y^2}\right|_{i,1}$ from both equations, yields

$$4\psi_{i,2} - \psi_{i,3} = 3\psi_{i,1} + 2\Delta y \left.\frac{\partial \psi}{\partial y}\right|_{i,1}$$

Since the point $(i,1)$ coincides with the wall, then the no-slip condition there demands that $\left.\frac{\partial \psi}{\partial y}\right|_{i,1} = 0$

Hence $4\psi_{i,2} - \psi_{i,3} = 3\psi_{i,1}$

The Streamfunction near the cold wall is approximated from

$$\therefore \quad \psi_{i,2} = (3\psi_{i,1} + \psi_{i,3})/4 \quad \dots\dots\dots\dots\dots\dots\dots(2.19)$$

$$i = 2, 3, 4, \dots N, N+1$$

<u>For the Hot wall $(J=N+1)$</u>. The following Taylor series expansions apply for the points near the hot wall

$$\psi_{i,j-1} = \psi_{i,j} + \sum_{n=1}^{\infty} \frac{(-1)^n (\Delta y)^n}{n!} \left.\frac{\partial^n \psi}{\partial y^n}\right|_{i,j} \quad \dots\dots\dots\dots\dots\dots(2.20)$$

$$\psi_{i,j-2} = \psi_{i,j} + \sum_{n=1}^{\infty} \frac{(-2)^n (\Delta y)^n}{n!} \left.\frac{\partial^n \psi}{\partial y^n}\right|_{i,j} \quad \dots\dots\dots\dots\dots\dots(2.21)$$

By a similar procedure as was done for the cold wall, the stream function near the hot wall is approximated from the finite-difference expression.

Thus,

$$\psi_{i,N} = (\psi_{i,N-1} + 3\psi_{i,N+1})/4 \quad \dots\dots\dots\dots\dots\dots(2.22)$$

$$i = 2, 3, 4, \dots N, N+1$$

2.2.5   <u>Velocity Components</u>

The velocity components are derived from the Cauchy-Riemann conditions $\quad u = \frac{\partial \psi}{\partial y}, \quad v = -\frac{\partial \psi}{\partial x}$.

The finite-difference representations are simply,

$$u_{i,j} = (\psi_{i,j+1} - \psi_{i,j-1})/2\Delta y \quad \dots\dots\dots\dots\dots\dots(2.23)$$

$$v_{i,j} = -(\psi_{i+1,j} - \psi_{i-1,j})/2\Delta x \quad \dots\dots\dots\dots\dots\dots(2.24)$$

where $i = 2, 3, \dots M$

$j = 2, 3, \dots N.$

2.3 Boundary Conditions

The normalised forms of the boundary conditions applicable are:

2.31 Thermal boundary conditions:

(a) $\left. \theta \right|_{\substack{x=0 \\ 0 < y < 1.0}} = \left. \theta \right|_{\substack{y=0 \\ 0 < x < x_L}} = \left. \frac{\partial\theta}{\partial x} \right|_{\substack{x = x_L \\ 0 < y < 1}} = 0 \quad \dots\dots\dots(2.25a)$

(b) $\left. \theta \right|_{\substack{y=1 \\ 0 < x < x_L}} = 1.0 \quad \dots\dots\dots\dots\dots\dots\dots\dots\dots\dots\dots\dots\dots\dots\dots(2.25b)$

2.32 Hydrodynamic boundary conditions:

(a) $\left. u \right|_{\substack{x=0 \\ 0 < y < 1.0}} = +1.0 \quad$ (uniform flow at entrance)

$\dots\dots\dots\dots\dots\dots\dots\dots\dots\dots\dots\dots\dots\dots\dots(2.26a)$

$\left. v \right|_{\substack{x=0 \\ 0 < y < 1.0}} = 0 \quad \dots\dots\dots\dots\dots\dots\dots\dots\dots\dots\dots\dots\dots\dots\dots(2.26b)$

(b)
$$u\bigg|_{\substack{y=0 \\ 0\leqslant x \leqslant x_L}} = v\bigg|_{\substack{y=0 \\ 0\leqslant x \leqslant x_L}} = \psi\bigg|_{\substack{y=0 \\ 0\leqslant x \leqslant x_L}} = 0 \quad \dots\dots(2.27)$$

But $\quad \omega\bigg|_{\substack{y=0 \\ 0\leqslant x \leqslant x_L}} \neq 0 \qquad$ (No-slip conditions)

(c)
$$u\bigg|_{\substack{y=1.0 \\ 0\leqslant x \leqslant x_L}} = v\bigg|_{\substack{y=1.0 \\ 0\leqslant x \leqslant x_L}} = 0 \qquad \dots\dots\dots\dots\dots\dots\dots\dots\dots\dots(2.28a)$$

$$\psi\bigg|_{\substack{y=1.0 \\ 0\leqslant x \leqslant x_L}} = 1.0 \qquad \dots\dots\dots\dots\dots\dots\dots\dots\dots\dots\dots(2.28b)$$

But $\omega\bigg|_{\substack{y=1 \\ 0\leqslant x \leqslant x_L}} \neq 0 \qquad$ (No-slip condition)

(d) The gradient boundary condition at the channel exit where the

flow is presumed not to vary with the channel length is given by

$$\frac{\partial \psi}{\partial y}\bigg|_{\substack{x=x_L \\ 0<y<1.0}} = \frac{\partial \omega}{\partial x}\bigg|_{\substack{x=x_L \\ 0<y<1}} = 0 \quad \dots\dots \ (2.29)$$

The discretised forms of the gradient boundary conditions are

$$\theta_{M+1,j} = \theta_{M,j} \quad \dots\dots\dots\dots\dots\dots\dots\dots\dots\dots\dots\dots (2.30a)$$

$$\omega_{M+1,j} = \omega_{M,j} \quad \dots\dots\dots\dots\dots\dots\dots\dots\dots\dots\dots\dots (2.30b)$$

$$\psi_{M+1,j} = \psi_{M,j} \quad \dots\dots\dots\dots\dots\dots\dots\dots\dots\dots\dots\dots (2.30c)$$

$$u_{M+1,j} = u_{M,j} \quad \dots\dots\dots\dots\dots\dots\dots\dots\dots\dots\dots\dots (2.30d)$$

where $j = 2, 3, \dots N$.

(e) Boundary Vorticity

The boundary vorticities at the rigid surfaces brought about by the stagnation of the flow can be evaluated from the definition of vorticity in terms of the velocity gradients.

In general for a two-dimensional flow,

$$\omega = \frac{\partial v}{\partial x} - \frac{\partial u}{\partial y}$$

At the wall, $\left.\omega\right|_{wall} = \left.\frac{\partial v}{\partial x}\right|_{wall} - \left.\frac{\partial u}{\partial y}\right|_{wall}$

Since the transverse component of velocity v is always zero at the wall, the contribution of $\left.\frac{\partial v}{\partial x}\right|_{wall}$ is obviously nil. The boundary vorticity is therefore determined solely by the normal gradient of the longitudinal velocity at the wall.

Thus, $\left.\omega\right|_{wall} = -\left.\dfrac{\partial u}{\partial y}\right|_{wall}$ ....(2.31)

Consideration will be given to the cold wall first.

(a) <u>Cold wall boundary vorticity</u>:

Considering u as a particularisation of the general dependent variable ϕ, the Taylor series expansions about the points $(j+1)$ and $(j+2)$ respectively give,

$$u_{i,j+1} = u_{i,j} + \sum_{n=1}^{\infty} \frac{(\Delta y)^n}{n!} \left.\frac{\partial^n u}{\partial y^n}\right|_{i,j} \quad ....(2.32a)$$

$$u_{i,j+2} = u_{i,j} + \sum_{n=1}^{\infty} \frac{(2\Delta y)^n}{n!} \left.\frac{\partial^n u}{\partial y^n}\right|_{i,j} \quad ....(2.32b)$$

If each series expansion is truncated after three terms, the equations respectively become,

$$u_{i,j+1} = u_{i,j} + \Delta y \left.\frac{\partial u}{\partial y}\right|_{i,j} + \frac{(\Delta y)^2}{2!} \left.\frac{\partial^2 u}{\partial y^2}\right|_{i,j} + 0\,(\Delta y)^3 \quad (2.33)$$

$$u_{i,j+2} = u_{i,j} + 2\Delta y \left.\frac{\partial u}{\partial y}\right|_{i,j} + 4\frac{(\Delta y)^2}{2!} \left.\frac{\partial^2 u}{\partial y^2}\right|_{i,j} + 0(\Delta y)^3 ..(2.33)$$

Neglecting terms of $0(\Delta y)^3$ and eliminating $\left.\dfrac{\partial^2 u}{\partial y^2}\right|_{i,j}$ from both equations, yields

$$4u_{i,j+1} - u_{i,j+2} = 3u_{i,j} + 2\Delta y \left.\frac{\partial u}{\partial y}\right|_{i,j}$$

Solving for $\left.\dfrac{\partial u}{\partial y}\right|_{i,j}$, gives

$$\left.\frac{\partial u}{\partial y}\right|_{i,j} = (4u_{i,j+1} - u_{i,j+2} - 3u_{i,j})/2\Delta y$$

At the cold wall, $j = 1$

$$\therefore \quad \left.\frac{\partial u}{\partial y}\right|_{i,1} = (4u_{i,2} - u_{i,3} - 3u_{i,1})2\Delta y.$$

invoking the no-slip condition at the walls, $u_{i,1} = 0$

$$\therefore \quad \left.\frac{\partial u}{\partial y}\right|_{i,1} = (4u_{i,2} - u_{i,3})/2\Delta y$$

The discretised form of the boundary vorticity for the cold wall is

$$\omega_{i,1} = - (4u_{i,2} - u_{i,3})/2\Delta y \quad \dots\dots\dots\dots\dots\dots\dots\dots\dots\dots\dots\dots(2.34)$$

where $i = 2, 3, \dots N, N+1$.

(b) Hot wall boundary vorticity:

The applicable Taylor series expansions are:

$$u_{i,j-1} = u_{i,j} + \sum_{n=1}^{\infty} \frac{(-1)^n(\Delta y)^n}{n!} \left.\frac{\partial^n u}{\partial y^n}\right|_{i,j} \quad \dots\dots\dots\dots\dots(2.35a)$$

$$u_{i,j-2} = u_{i,j} + \sum_{n=1}^{\infty} \frac{(-2)^n(\Delta y)^n}{n!} \left.\frac{\partial^n u}{\partial y^n}\right|_{i,j} \quad \dots\dots\dots\dots\dots(2.35b)$$

By a similar procedure as was done in (a), the finite-difference approximation for the hot-wall boundary vorticity at $j=N+1$ is given by

$$\omega_{i,N+1} = - (u_{i,N-1} - 4u_{i,N})/2\Delta y \quad \dots\dots\dots\dots\dots\dots\dots\dots\dots\dots\dots(2.36)$$

$$i = 2, 3, \dots N, N+1$$

2.4   Treatment of Numerical Singularity:

Since the physical model discontinues as.shown in figure
2.1a, at $x = 0$, $y = 0$ and $x = 0$, $y = 1.0$ there is no justification
to assume that the derivatives of some space variables are continuous
at these points. The streamfunction, velocity components and
temperature values present no problem since they have been specified.
However, the geometric singularity affects the vorticity only.
This is because while the other variables are specified by Dirichlet
conditions, the vorticity is specified by Neumann conditions based
on derivatives.
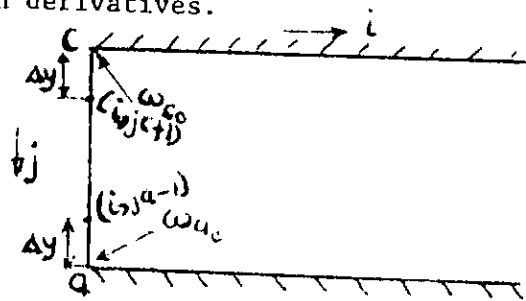
Fig. 2.1a. Notation for   Vorticity at Points of Singularity.

To evaluate the vorticities at c and a, the non-slip at wall
conditions can be applied. Only first-order formulations will be
considered for each point.

(i)   Point c:

The Taylor series expansion about $(i, jc+1)$ for the
stream function is given by

$$\psi_{i,jc+1} = \psi_{i,jc} + \frac{\partial \psi}{\partial y}\Big|_{i,jc} \Delta y + \frac{1}{2} \frac{\partial^2 \psi}{\partial y^2}\Big|_{i,jc} (\Delta y)^2 + O(\Delta y)^3 \ldots (2.36a)$$

For no-slip at wall, $\left.\dfrac{\partial \psi}{\partial y}\right|_{i,jc} = u_{i,jc} = 0$

$$\left.\frac{\partial^2 \psi}{\partial y^2}\right|_{i,jc} = \left.\frac{\partial u}{\partial y}\right|_{i,jc}$$

By definition, $\quad \omega_{i,jc} = \left.\dfrac{\partial v}{\partial x}\right|_{i,jc} - \left.\dfrac{\partial u}{\partial y}\right|_{i,jc}$

Since $v = 0$, always on the rigid boundaries, then

$$\left.\frac{\partial v}{\partial x}\right|_{i,jc} = 0.$$

Therefore $\quad \omega_{i,jc} = -\left.\dfrac{\partial u}{\partial y}\right|_{i,jc}$

i.e. $\quad \omega_{i,jc} = -\left.\dfrac{\partial^2 \psi}{\partial y^2}\right|_{i,jc}$

From equation (2.36a),

$$\left.\frac{\partial^2 \psi}{\partial y^2}\right|_{i,jc} = \frac{2(\psi_{i,jc+1} - \psi_{i,jc})}{(\Delta y)^2} + 0(\Delta y)$$

Neglecting terms of $0(\Delta y)$ gives

$$\omega_{co} = -\frac{2(\psi_{i,jc+1} - \psi_{i,jc})}{(\Delta y)^2} \quad \ldots (2.36c)$$

Point a.

The Taylor series expansion about point $(i, ja-1)$ is given by

$$\psi_{i,ja-1} = \psi_{i,ja} - \frac{\partial \psi}{\partial y}\bigg|_{i,ja} \Delta y + \frac{1}{2} \frac{\partial^2 \psi}{\partial y^2}\bigg|_{i,ja} (\Delta y)^2 + O(-\Delta y)^3 \ldots \quad (2.36d).$$

Following the procedure in the preceeding section for point c,

$$\omega_{a_0} = - \frac{2(\psi_{i,ja-1} - \psi_{i,ja})}{(\Delta y)^2} \qquad (2.36e)$$

2.4.1   Application in Numerical Scheme:

The significance of the points of singularity arises when the vorticities at these points enter into computations of vorticities at neighbouring points. Thus, when ω_c is used in a finite-difference equation about node $(ic, jc+1)$, just below c, then $\omega_c = \omega_{c_0}$ is used. When ω_a is used in a difference equation about the node $(ia, ja-1)$, just above a, then $\omega_a = \omega_{a_0}$ is considered.

2.5 Polynomial Temperature Profile:

In order to predict the heat transfer on a heated surface over which simultaneous developments of the thermal and hydrodynamic boundary layers occur, a suitable statement must be made as to the shape of the temperature profile in the boundary layer. Therefore, an expression with a number of free functions is chosen. These functions are determined such that the assumed profile satisfies a set of prescribed boundary conditions. Since a numerical method is being adopted, the temperatures at two immediate nodal points with another point coincident with the wall will be assumed given. Since the normal derivative of temperature at the wall is constant, then its second derivative at the wall may vanish. There are therefore four conditions to be satisfied. These are,

(a) The hot wall,

$$\theta\Big|_{x,1} = \theta_{i,N+1} \quad \dots\dots\dots\dots\dots\dots\dots\dots\dots(2.37a)$$

$$\theta\Big|_{x,1-\Delta y} = \theta_{i,N} \quad \dots\dots\dots\dots\dots\dots\dots\dots\dots(2.37b)$$

$$\theta\Big|_{x,1-2\Delta y} = \theta_{i,N-1} \quad \dots\dots\dots\dots\dots\dots\dots\dots\dots(2.37c)$$

$$\frac{\partial^2\theta}{\partial y^2}\Big|_{x,1} = 0 \quad \dots\dots\dots\dots\dots\dots\dots\dots\dots\dots(2.37d)$$

According to these four conditions, a polynomial of four functions will be used.

Thus

$$\theta = A'_o + A'_1 y + A'_2 y^2 + A'_3 y^3 \quad \ldots\ldots\ldots\ldots\ldots\ldots\ldots\ldots(2.33)$$

where A'_o, A'_1, A'_2 and A'_3 are constants which depend on the longitudinal distance x.

From (2.37a)

$$\theta_{i,N+1} = \theta\Big|_{x,1}$$

$$\therefore \quad \theta_{i,N+1} = A'_o + A'_1 + A'_2 + A'_3 \quad \ldots\ldots\ldots\ldots\ldots\ldots\ldots\ldots(2.39)$$

From (2.37b),

$$\theta_{i,N} = \theta\Big|_{x,(1-\Delta y)}$$

$$\therefore \quad \theta_{i,N} = A'_o + A'_1 (1-\Delta y) + A'_2 (1-\Delta y)^2 + A'_3 (1-\Delta y)^3 \quad \ldots(2.40)$$

From (2.37c)

$$\theta_{i,N-1} = 0\Big|_{x,(1-2\Delta y)}$$

$$\therefore \quad \theta_{i,N-1} = A'_o + A'_1 (1-2\Delta y) + (A'_2 (1-2\Delta y)^2 + A'_3 (1-2\Delta y)^3 \ldots(2.41)$$

From (2.37d),

$$\frac{\partial^2 \theta}{\partial y^2}\Big|_{x,1} = 0$$

Hence differentiating (2.38) twice and equating y=1 gives

$$\therefore \quad \frac{\partial^2 \theta}{\partial y^2}\Big|_{x,1} = 2A'_2 + 6A'_3 = 0 \quad \ldots\ldots\ldots\ldots\ldots\ldots\ldots\ldots(2.42)$$

$$\text{Also,} \quad \frac{\partial \theta}{\partial y}\Big|_{x,1} = A'_1 + 2A'_2 + 3A'_3 \quad \ldots\ldots\ldots\ldots\ldots\ldots\ldots\ldots\ldots(2.43)$$

Solving equations (2.39), (2.40), (2.41) and (2.42) simultaneously shows that

$$A_1' = \frac{(\theta_{i,N+1} - \theta_{i,N})}{\Delta y} - \frac{(\theta_{i,N-1} - 2\theta_{i,N} + \theta_{i,N+1})\left[(1-\Delta y)^2(2+\Delta y)-2\right]}{2\Delta y\left[(1-\Delta y)^2(2+\Delta y)-(1+\Delta y)(1-2\Delta y)^2 - 1\right]} \quad (2.44)$$

and

$$A_3' = \frac{(\theta_{i,N-1} - 2\theta_{i,N} + \theta_{i,N+1})}{2\left[(1-\Delta y)^2(2+\Delta y)-(1+\Delta y)(1-2\Delta y)^2 - 1\right]} \quad \dots\dots\dots\dots(2.45)$$

From (2.42) and (2.43) it is clear that

$$\left.\frac{\partial \theta}{\partial y}\right|_{x,1} = A_1' - 3A_3' \dots\dots\dots\dots\dots\dots\dots\dots\dots\dots\dots\dots\dots\dots(2.46)$$

Since it is the normal temperature gradient at the wall that is of interest, it is not necessary to engage in additional algebra to evaluate the constants A_o' and A_2'.

Substituting A_1' and A_3' into equation (2.45) yields

$$\left.\frac{\partial \theta}{\partial y}\right|_{x,1} = (\theta_{i,N-1} - 8\theta_{i,N} + 7\theta_{i,N+1})/(6\Delta y) \dots\dots\dots\dots\dots(2.47)$$

(b)   For the cold wall:

A similar expression as in (2.47) can be deduced for the temperature gradient at the cold wall

Thus,

$$\left.\frac{\partial \theta}{\partial y}\right|_{x,0} = (\theta_{i,3} - 8\theta_{i,2} + 7\theta_{i,1})/6\Delta y \dots\dots\dots\dots(2.48)$$

2.6   Evaluation of the local and mean heat-transfer and flow characteristics

2.6.1 Nusselt Number:

The ultimate aim of this work is to determine the heat transfer coefficient based on the characteristic linear dimension and the temperature difference between the hot and cold surfaces. Since the flow is laminar, it can be presumed that close to the wall, the mode of heat transfer is predominantly by conduction in the direction of higher/negative temperature gradient; that is, the y-direction. Therefore, by Fourier's Law of Heat conduction in one dimension,

$$q_x = -k_f \frac{\partial T}{\partial Y}\Big|_{wall} \quad \dots \dots \dots \dots \dots \dots \dots (2.48a)$$

But

$$q_x = h_x(T_h - T_c) \quad \dots \dots \dots \dots \dots \dots \dots (2.49)$$

Hence

$$h_x(T_h - T_c) = -k_f \frac{\partial T}{\partial Y}\Big|_{wall}$$

Introducing the normalising variables yields

$$h_x b = -k_f \frac{\partial \theta}{\partial y}\Big|_{wall}$$

$$\rightarrow \quad \frac{h_x b}{k_f} = -\frac{\partial \theta}{\partial y}\Big|_{wall}.$$

But by definition, $\dfrac{h_x b}{k_f} = Nu_x$.

Therefore, the local Nusselt number is simply,

$$Nu_x = -\frac{\partial \theta}{\partial y}\Big|_{wall} \quad \dots \dots \dots \dots \dots \dots (2.50)$$

The average or mean Nusselt number for a channel of x_L is given by

$$Nu_m = \frac{1}{x_L} \int_0^{x_L} Nu_x \, dx \dots\dots\dots\dots\dots\dots\dots\dots\dots\dots(2.51)$$

This mean value is obtained by the trapezoidal rule of integration.

2.6.2 Stanton Number

The local Nusselt number has been defined by

$$Nu_x = \frac{h_x b}{k_f}$$

This equation can be represented in a different way that allows an interesting comparison. The Stanton number is a non-dimensional conductance defined by

$$St_x = \frac{h_x}{\rho_m c_p U_m}.$$ That is, the ratio of energy conducted to that convected:

$$\therefore \quad St_x = \left(\frac{h_x b}{k_f}\right) . \quad \frac{k_f}{b \rho_m C_p U_m} . \quad \frac{\mu}{\mu} = \left(\frac{h_x b}{k_f}\right) . \quad \frac{1}{\left(\frac{\mu C_p}{k_f}\right) . \left(\rho_m \frac{U_m b}{\mu}\right)}$$

$$\therefore \quad St_x = Nu_x . \frac{1}{PrRe}$$

The local stanton number is therefore given by

$$St_x = \frac{Nu_x}{RePr}. \quad \dots\dots\dots\dots\dots\dots\dots\dots\dots\dots\dots\dots(2.52)$$

The mean Stanton number for a channel of length x_L is given by

$$St_m = \frac{1}{x_L} \int_0^{x_L} St_x \, dx. \quad \dots\dots\dots\dots\dots\dots\dots\dots\dots\dots(2.53)$$

An alternative expression for the mean Stanton Number is given by

$$St_m = \frac{Nu_m}{RePr}$$

It is therefore easy to note the similarity in the form of the corresponding friction coefficient, C_{fx}, for a given Nu_x, Pr.

2.7 General Computational Procedure

The finite-difference analogs of the governing equations are solved simultaneously using the Gauss-Seidel iterative procedure. The type of integration steps involve the following nested iterative processes.

1. θ, u, v, ψ, are initialised for all interior, inlet and oulet grid points. Using the initial values of u, the boundary vorticities at the rigid surfaces are computed from equations (2.34) and (2.35). Thereafter, the following quantities are evaluated in the order given using the most recently computed values of other quantities. However, it is important to note that the iteration process for each variable is carried to completion before proceeding to the next step.

2. θ at interior points from equation (2.11) and on the outflow boundary from equation (2.30a).

3. ω at interior points from equation (2.12) and on the outflow boundary from equation (2.30b)

4. ψ at interior points from equations (2.13), (2.19) and (2.22) and on the outflow boundary from equation (2.30c).

5. u, v, are finally computed for all interior points and outflow boundary from equations (2.23), (2.24) and (2.30d) respectively.

6. Using the most recently computed values of θ and u, the local and mean values of the Nusselt, Stanton numbers and friction factors are computed from equations (2.50), (2.51), (2.52), (2.53), (2.54) (2.55) respectively. In addition, the boundary vorticities are computed from (2.34) and (2.36).

7. The above steps, two through six, constitute a stage or cycle of the numerical computation. Starting from step two, the integration process is repeated using the last computed values of $\theta, \omega, \psi, u, v$ as fresh initial values, until convergence is achieved. The purpose of carrying the computation over several stages are to ensure that the computation is terminated when the fields cease to vary with stages and to study the behaviour of the vortex field in respect of numerical instability discussed in Chapter Four.

The iteration criterion used in the computation is given by

$$\varepsilon = \Sigma_{i,j} \left| \phi_{i,j}^{k+1} - \phi_{i,j}^{k} \right| < 10^{-3}$$

where k is the iteration counter and ϕ, a dummy variable.

and $i = 2, 3, \ldots M+1$

$j = 2, 3, \ldots N+1$

2.8   Discussion of Results

Since three independent parameters are involved in the present problem, a complete parametric study is not practical, hence only representative cases for air (Pr = 0.73) are given to illustrate the inclination angle or body-force orientation effects. Since the flow must be forced, the free convection is regarded as a perturbation superimposed on the forced flow. The parameter which represents the mutual interaction of the free and forced convection effects is $\frac{Gr}{Re^2}$, the Archimedes number. Individual effects of Gr and Re are discussed first and their combined effect on the heat transfer and flow parameters later.

Figure 2.1 shows the systematic development of dimensionless longitudinal velocity distribution across channel with its length for an isothermal system. Near the channel inlet, a square longitudinal velocity profile is obtained. However, for distances greater than $x_e = 0.04Re$, the entrance length, the flow is fully developed. The velocity profile is parabolic and symmetrical about the channel axis. Since the entrance length, x_e for $Re = 150$ is 6.0, then the flow is already fully developed at $x = 10.0$. It is observed that the maximum value of the longitudinal velocity at $x = 10.0$ is one and a half times the mean velocity, and agrees with theoretical fully developed flow predictions.

In order to compare the present numerical solution with those of previous workers, the centre-line velocity is plotted against the channel length for a Reynolds number of 150 based on the channel height. Figure 2.2 shows composite predictions of Runchal, Wang and Longwell and Schlichting in Runchal et al [9] and the present analysis. The agreement is satisfactory.

Figure 2.3 depicts the systematic development of the temperature profile across the channel along its length. In general, the temperature profile flattens out as the channel exit is approached.

Figure 2.4 indicates the influence of Reynolds number on the temperature distribution across the channel for a given Grashof number for the horizontal case. It is clear that as the Reynolds number increases, the local temperatures decrease accordingly. This reciprocal variation is anticipated since a decrease in the Reynolds number reduces the convected heat in the longitudinal direction but promotes increased heat transfer by molecular conduction in the transverse direction.

Figure 2.5 illustrates the effect of Grashof number on the temperature profiles for a given Reynolds number. As expected, increases in heating must naturally be accompanied by increased local temperatures.

Figures 2.6 and 2.7 represent respective influences of the
Reynolds and Grashof numbers on the velocity profiles. While
increases in the Grashof number generally enhance asymmetry of
the velocity profiles, increases in the Reynolds number tend to
destroy such asymmetries.

Figures 2.8 and 2.9 respectively show the influence of the
angle of inclination on the velocity and temperature profiles.
At the channel axis of symmetry, the local velocity is practically
insensitive to changes in inclination as it is also shown in
figure 2.8. A possible explanation could be that at this
point, the aiding and opposing effects of free convection counter-
balance each other. Near the hot plate the local velocity is higher
than it is near the cold plate. This is anticipated since energy is
added to the fluid near the hot plate and extracted near the cold
one. Figure 2.9 shows that the local temperatures increase generally
with increasing inclination.

Figure 2.10 shows the variation of the local Nusselt numbers
with channel length for a given Ar with the angle of inclina-
tion as a parameter. It is found that the local Nusselt number
decreases asymptotically to its fully developed value at the channel
exit. This is expected since the local temperature within
the channel increases with its length; hence the decrease in the
normal temperature gradient along the channel.

Using Ar as parameter, the variations of the mean Nusselt and Stanton numbers and friction factors with the channel orientations are presented in figures 2.11, 2.12 and 2.13 respectively. Of particular interest is the variation of the mean Nusselt number with the angle of inclination. A number of important observations can be made in figure 2.11. At $\alpha = 15^{o}$, the mean Nusselt number is the same for all non-vanishing Archimedes numbers. Between $\alpha = 30^{o}$ and $\alpha = 60^{o}$, there is a critical angle at which the mean Nusselt number is a maximum for a given Ar. This maximum varies proportionately with Ar while the corresponding critical angle increases with decreasing Ar. For a given Ar, this variation of the mean Nusselt number with α is similar to that obtained by Ozoe et al [4] for the variation of the mean Nusselt number with the angle of inclination for natural convection in a square channel heated isothermally from below and similarly cooled from above.

It is recognised that Archimedes number can vary in two ways; Re can be kept constant while Gr is varied and vice versa. Therefore the mean Nusselt number and the friction coefficient are each bound to vary in two ways. Figures 2.14 and 2.15 show the plots of Nu_m vs Ar and f_m Vs.Ar respectively for the two modes of variation of Ar for a number of channel orientations. A critical Archimedes number exists for a given inclination at which the mean Nusselt number assumes a single value. The same is true for the mean friction factor. In both cases, the critical Archimedes number $\approx$ 0.5 and remains so for all inclinations, but the unique values of Nu_m and f_m depend on the inclinations. This is a very significant finding since it assures us that at this critical

Archimedes number, there are single mean values of Nu and f associated with α. Since the results predict the existence of optimum inclinations for which maximum heat transfer occurs, it is of interest to derive correlation relations.

Although separation is predicted at the cold boundary, it is obvious that the value of Ar for which separation occurs depends on the inclination. No rigorous numerical compuation has been carried out in this respect. However, at the vertical position at which separation is most likely to set in, the maximum value of $Ar = 1.00$. A more rigorous determination will be presented in the perturbation analysis.

2.8.1 Derivation of Correlation Equation

The Numerical results for the mean Nusselt numbers at the hot wall predict the existence of optimum inclinations for the range of Archimedes numbers considered. That is

$0.050 \leqslant Ar \leqslant 0.50.$

It is also evident that the mean maximum Nusselt numbers vary with the optimum inclinations. Such a variation is tabulated below:

TABLE 2.1. MAXIMUM MEAN NUSSELT NUMBERS AT HOT WALL

Ar	Nu_{mH}	α_{OPT} (Optimum in radians)
0.050	1.7713	$\dfrac{\pi}{3}$
0.150	1.7813	$\dfrac{19\pi}{60}$
0.350	1.7850	$\dfrac{7\pi}{24}$
0.500	1.7880	$\dfrac{\pi}{4}$

It is possible to express the dependent variable Nu_{mH} in terms of the two other independent variables Ar and α_{opT} by the equation.

$$Nu_{mH} = C(Ar)^{n_1}(\alpha_{opT})^{n_2} \text{ where C is a constant and } n_1, n_2 \text{ are} \quad (2.58)$$

exponents to be determined.

Taking the logarithm of each side to base 10,

$$\log_{10} Nu_{mH} = \log_{10}C + n_1 \log_{10} Ar + n_2 \log_{10}\alpha_{opT} \quad \ldots (2.59)$$

If $\log_{10} Nu_{mH} = z$; $\log_{10}C = C_o$; $\log_{10} Ar = x$; $\log_{10} \alpha_{opT} = y$, then the above expression reduces to

$$z = C_o + n_1 x + n_2 y. \quad \ldots\ldots\ldots\ldots\ldots\ldots\ldots\ldots\ldots\ldots\ldots\ldots\ldots (2.60)$$

If z, x, y are the mutually orthogonal space coordinates, then (2.60) represents the equation of a surface which cuts the z-y plane such that $z = C_o$. The physical significance of this is that it represents i.e. $z = C_o$, the case of pure forced convection and this is approximately true for low Ar's.

In equation (2.60) the unknowns are three and three simultaneous equations are adequate to determine these constants. Considering Ar = 0.050, 0.150 and 0.500 the following set of simultaneous equations are obtained.

For Ar = 0.050

$$z = \log_{10} 1.7713 = 0.2480$$

$$x = \log_{10} 0.050 = -1.3010$$

$$y = \log_{10} \frac{\pi}{3} = 0.0200$$

The corresponding equation is

$$\boxed{0.2480 = C_o - 1.301n_1 + 0.020n_2} \quad \dots\dots\dots\dots\dots(2.61')$$

For Ar = 0.150

$$z = \log_{10} 1.7813 = 0.2510$$

$$y = \log_{10} \frac{19\pi}{60} = -0.0010$$

$$x = \log_{10} 0.150 = -0.8240$$

The corresponding equation is

$$\boxed{0.2510 = C_o - 0.8240n_1 - 0.001n_2} \quad \dots\dots\dots\dots\dots(2.62)$$

For Ar = 0.500

$$z = \log_{10} 1.7880 = 0.2520$$

$$y = \log_{10} \frac{\pi}{4} = -0.1040$$

$$x = \log_{10} 0.500 = -0.3010$$

The corresponding equation is

$$\boxed{0.2520 = C_o - 0.301n_1 - 0.104n_2} \quad \dots\dots\dots\dots\dots(2.63)$$

Solving (2.61), (2.62), (2.63) simultaneuously yields

$$n_1 \simeq 0.008$$

$$n_2 \simeq 0.029$$

and $C_o = 0.2570 \rightarrow C = 1.804$

The correlation therefore becomes

$$N_{u_{mH}} = 1.804 \ (Ar)^{0.008} \ (\alpha_{OPT})^{0.029} \qquad (2.64)$$

$$\text{for } 0.050 \leqslant Ar \leqslant 0.500$$

$$\frac{\pi}{6} \leqslant \alpha_{OPT} \leqslant \frac{\pi}{3}$$

For $Ar = 0.350$, the value of Nu_{mH} obtained using the above equation agrees with its value from numerical solution.

2.9 Conclusion

1. The mean hot wall Nusselt number is independent of non-zero Archimedes numbers when the angle of inclination to the horizontal is 15°.

2. For a given non-zero Archimedes number, the optimum inclination at which the mean heat transfer and flow coefficients are maximum, lies between 30° and 60°.

3. A unique solution to the thermal problem exists for a given inclination when $Ar = 0.50$.

4. The results of Ozoe et al [4] which they confirmed experimentally further suggests the validity of the present solution.
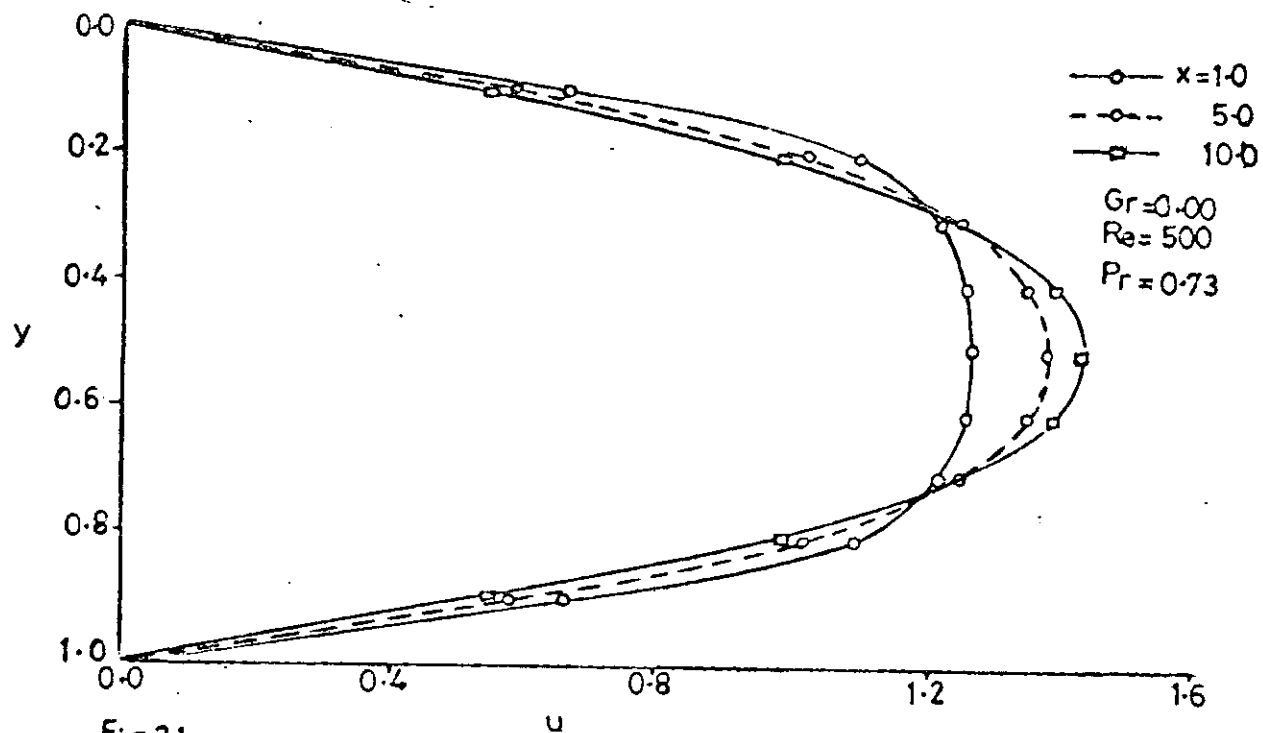
Fig 2.1. Predictions of dimensionless longitudinal Velocity distribution across channel at various locations along its length for Isothermal flow.
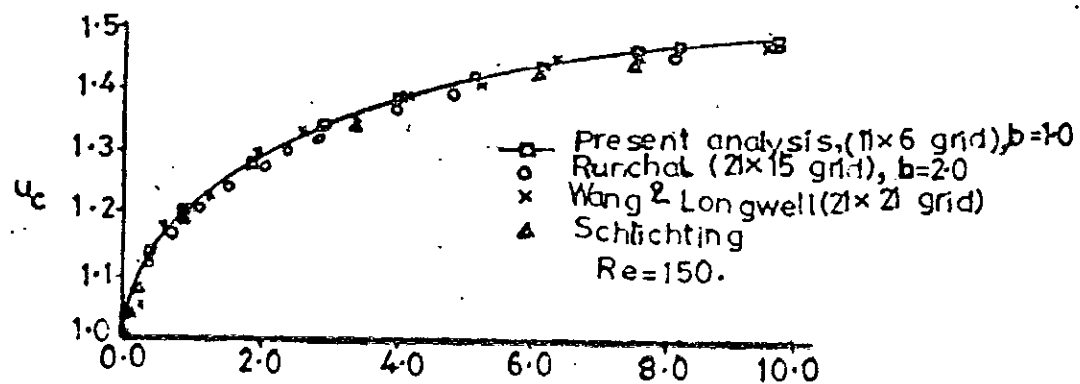
Fig·2-2· Comparison of predicted centreline
non-dimensional longitudinal velocity
of the channel for an Isothermal flow.
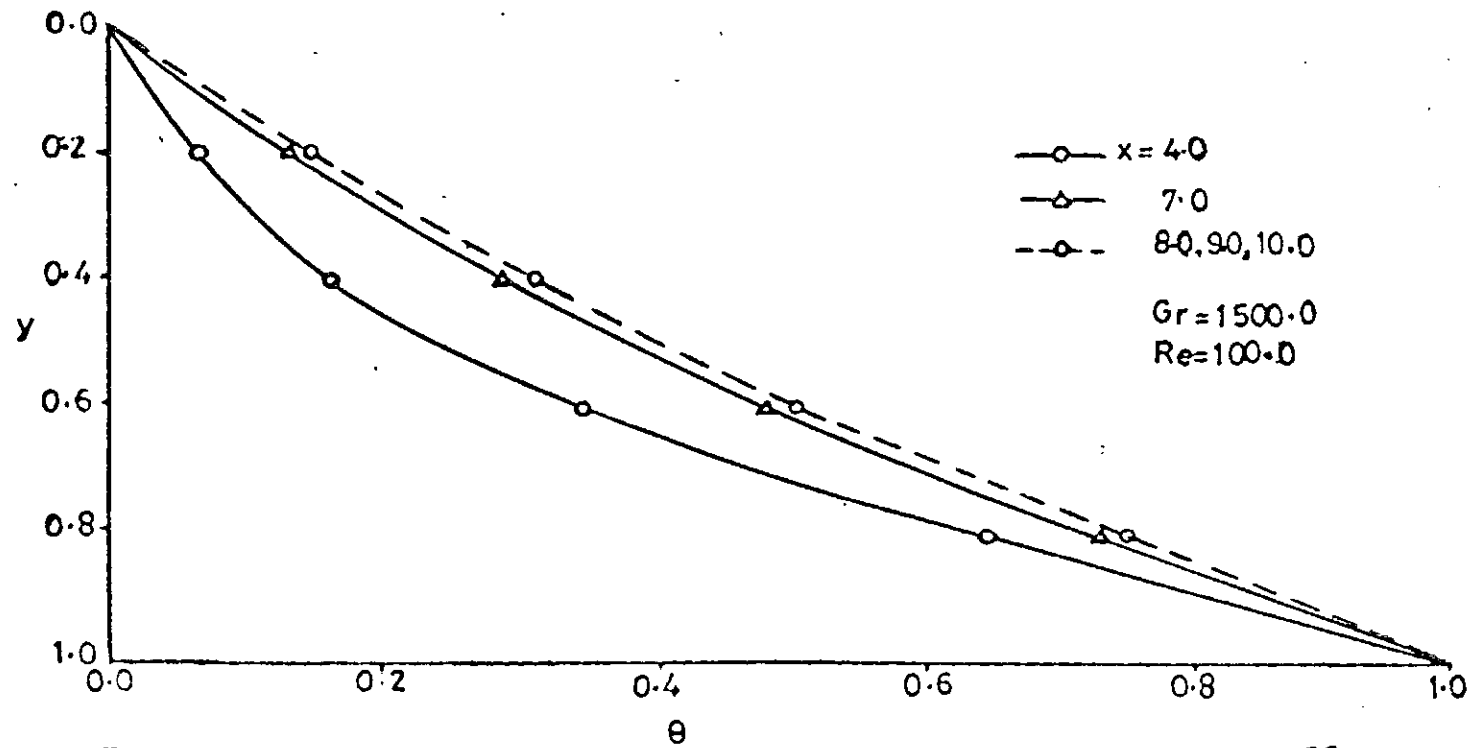
Fig. 2.3. Predictions of dimensionless temperature Profiles across channel at various locations along its length for Pr=0.73.
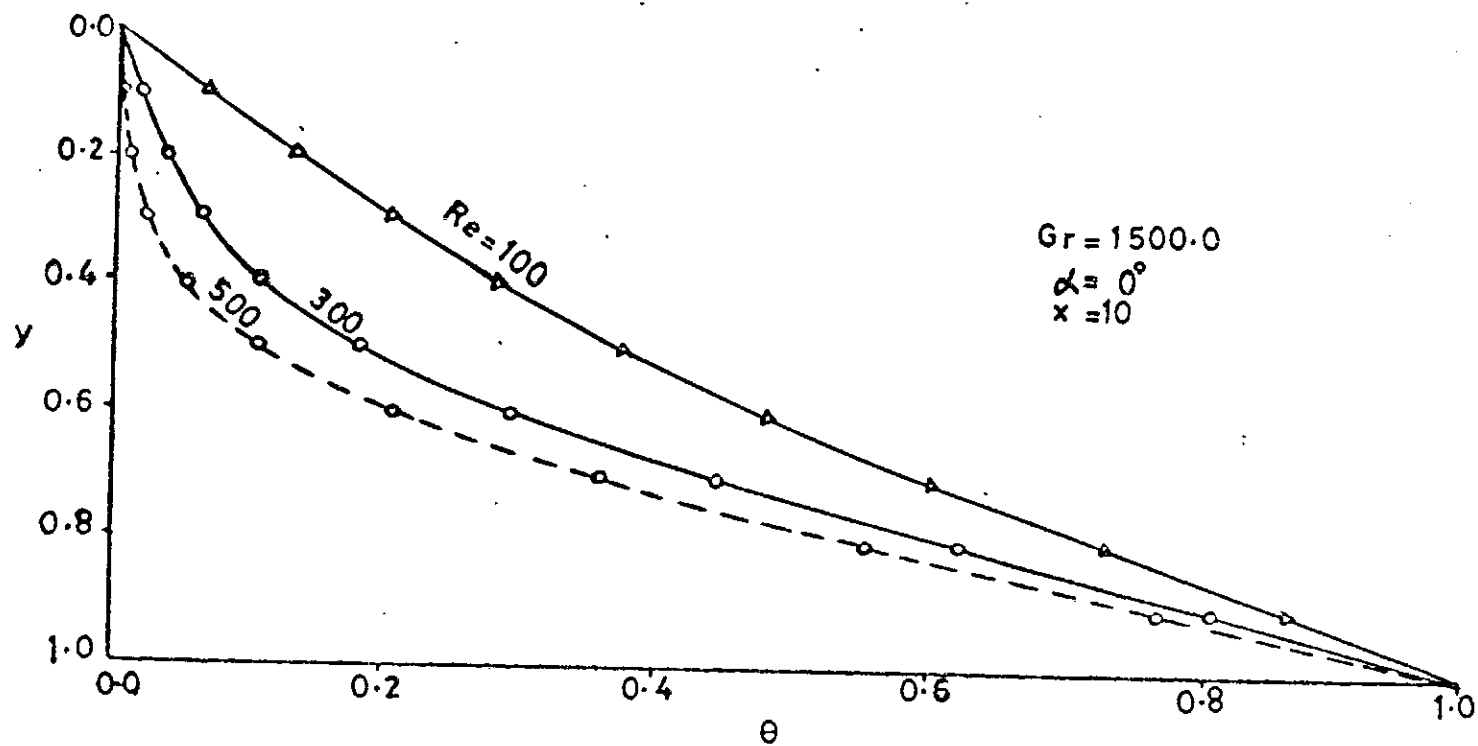
FIG. 2-4. Influence of Reynolds number on dimensionless temperature Profiles across channel for Pr = 0.73
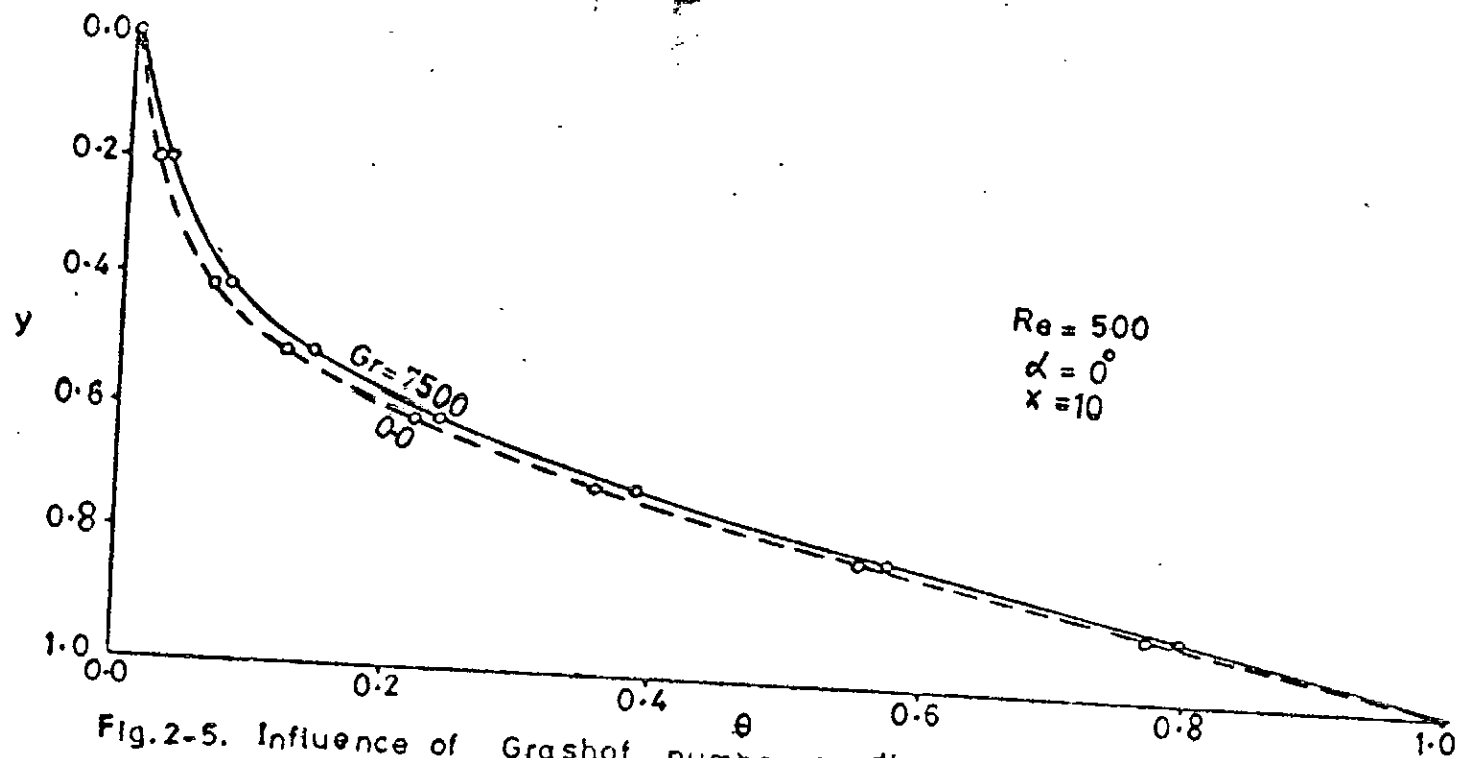
Fig. 2-5. Influence of Grashof number on dimensionless temperature Profile across channel for Pr= 0.73.
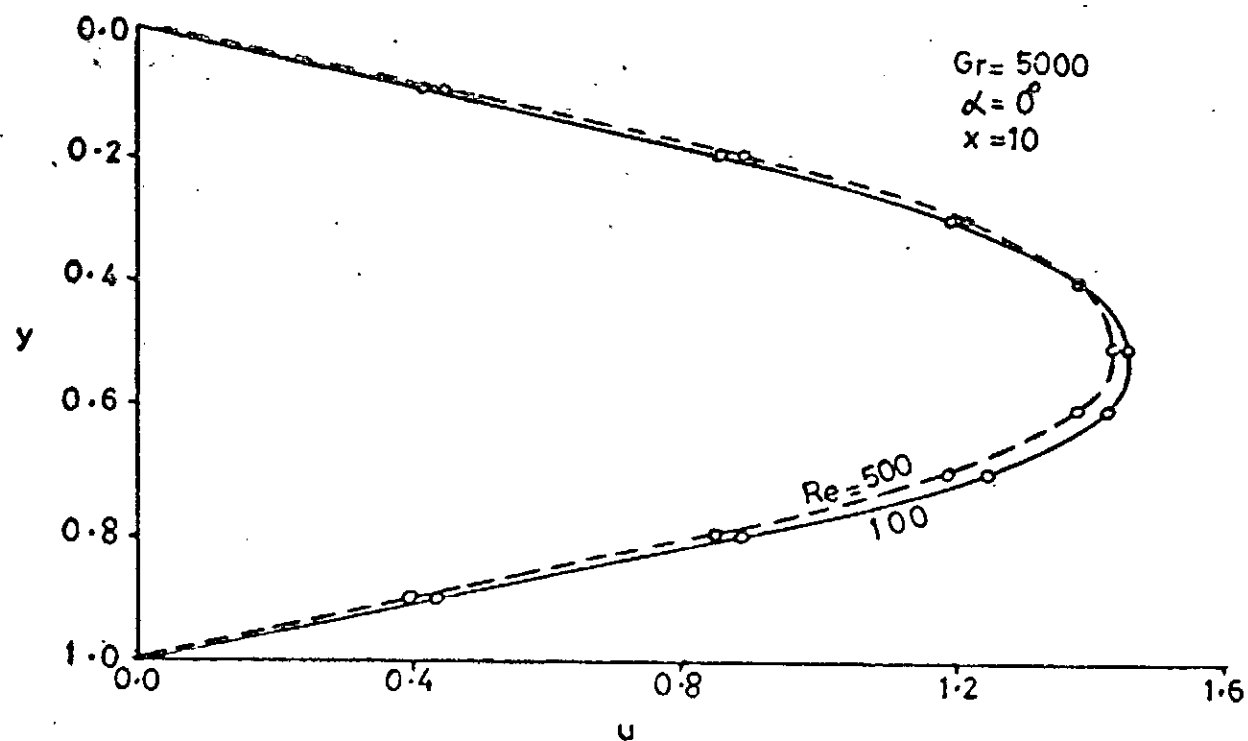
Fig. 2-6. Influence of Re on dimensionless longitudinal velocity
Profile across channel for $P_r = 0.73$.

Gr = 5000
$\alpha = 0$
x = 10

Re = 500
100
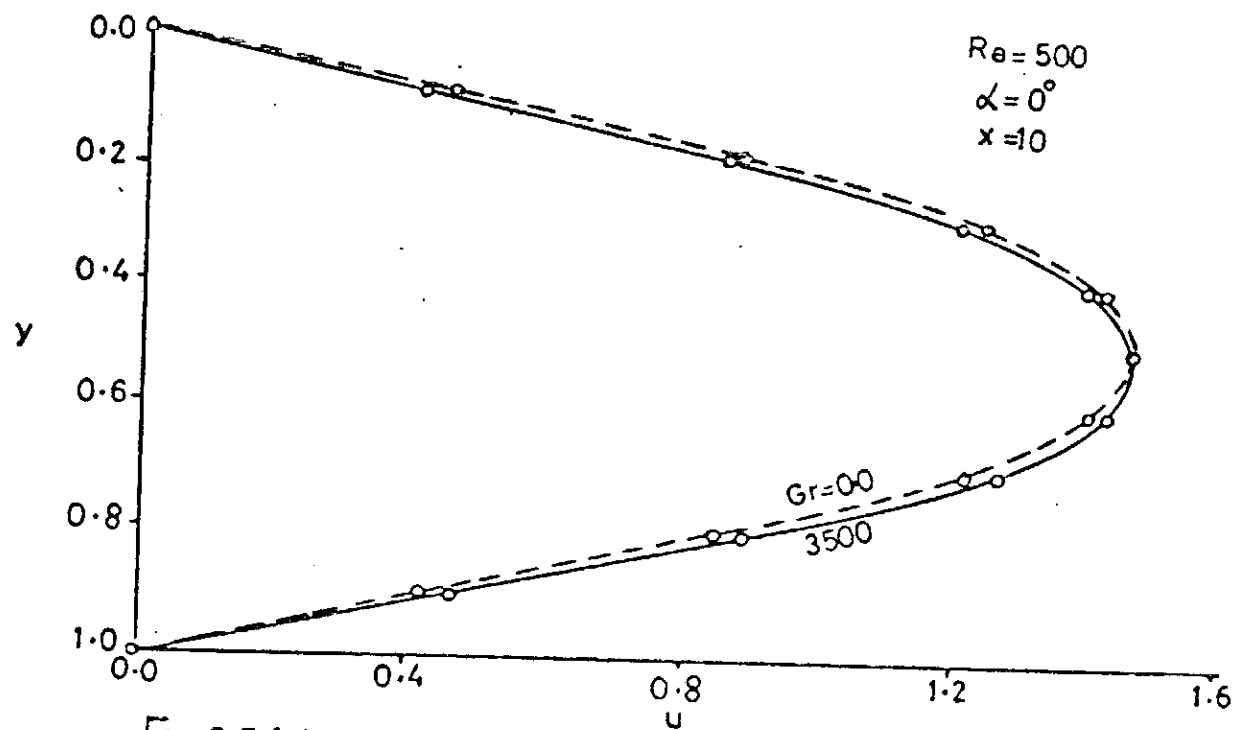
Fig.2-7. Influence of Gr on dimensionless longitudinal velocity Profile across channel for $Pr = 0.73$.
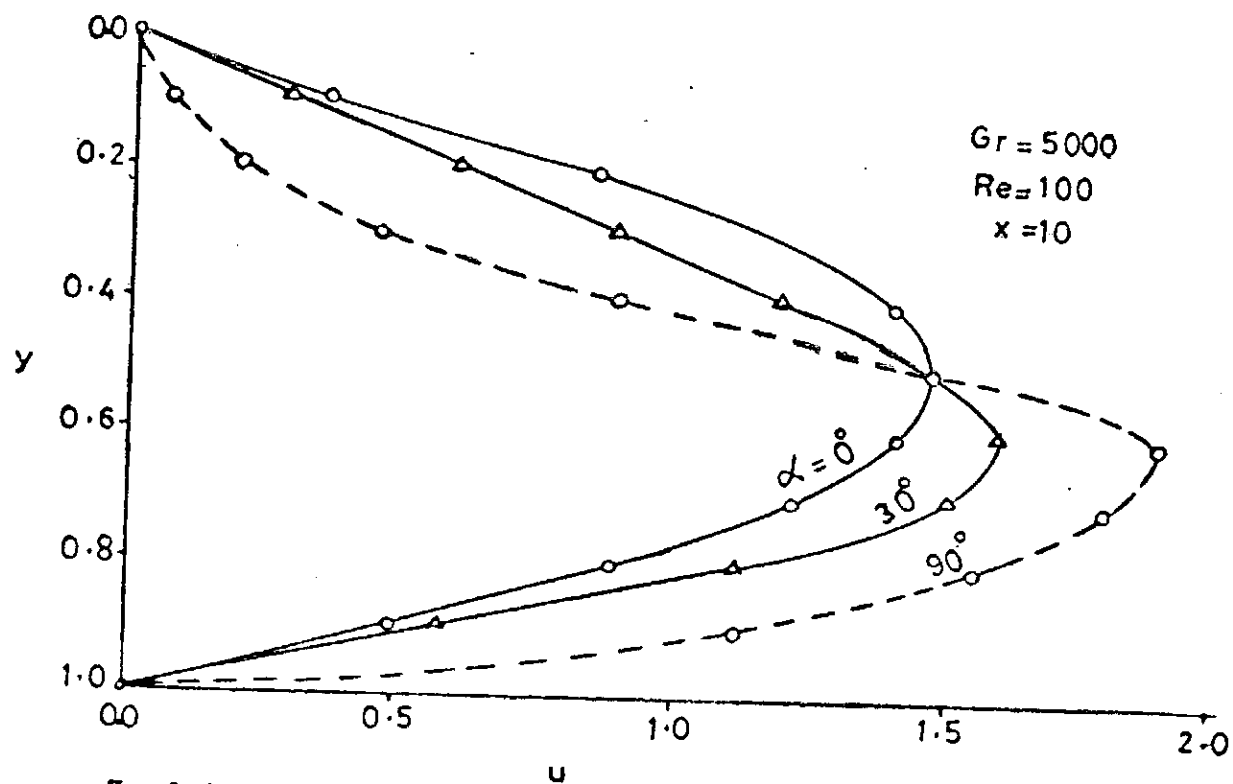
Fig. 2-8. Influence of channel orientation on dimensionless longitudinal velocity Profile for $Pr = 0.73$.
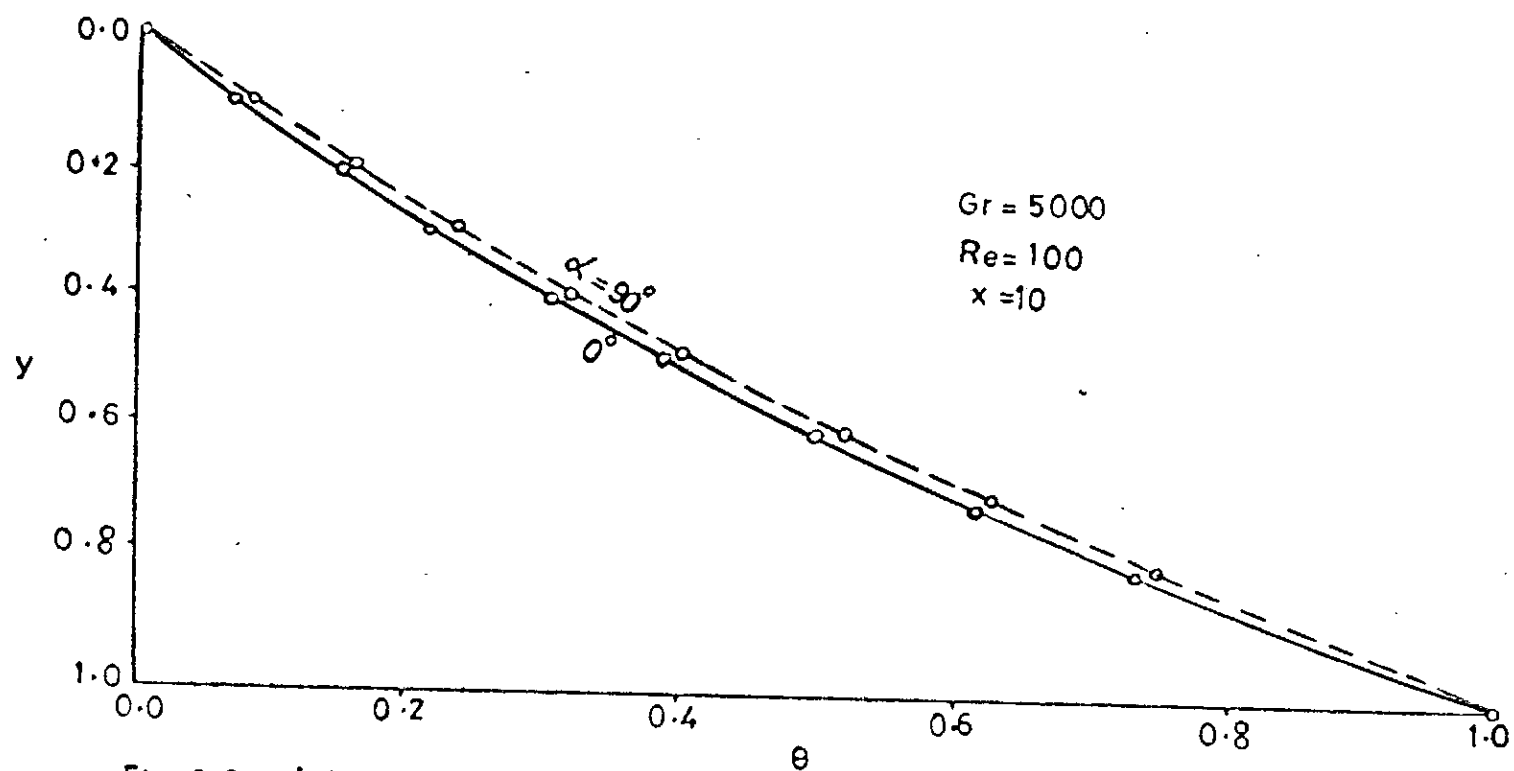
Fig. 2-9. Influence of channel orientation on dimensionless temperature Profile for Pr = 0.73.
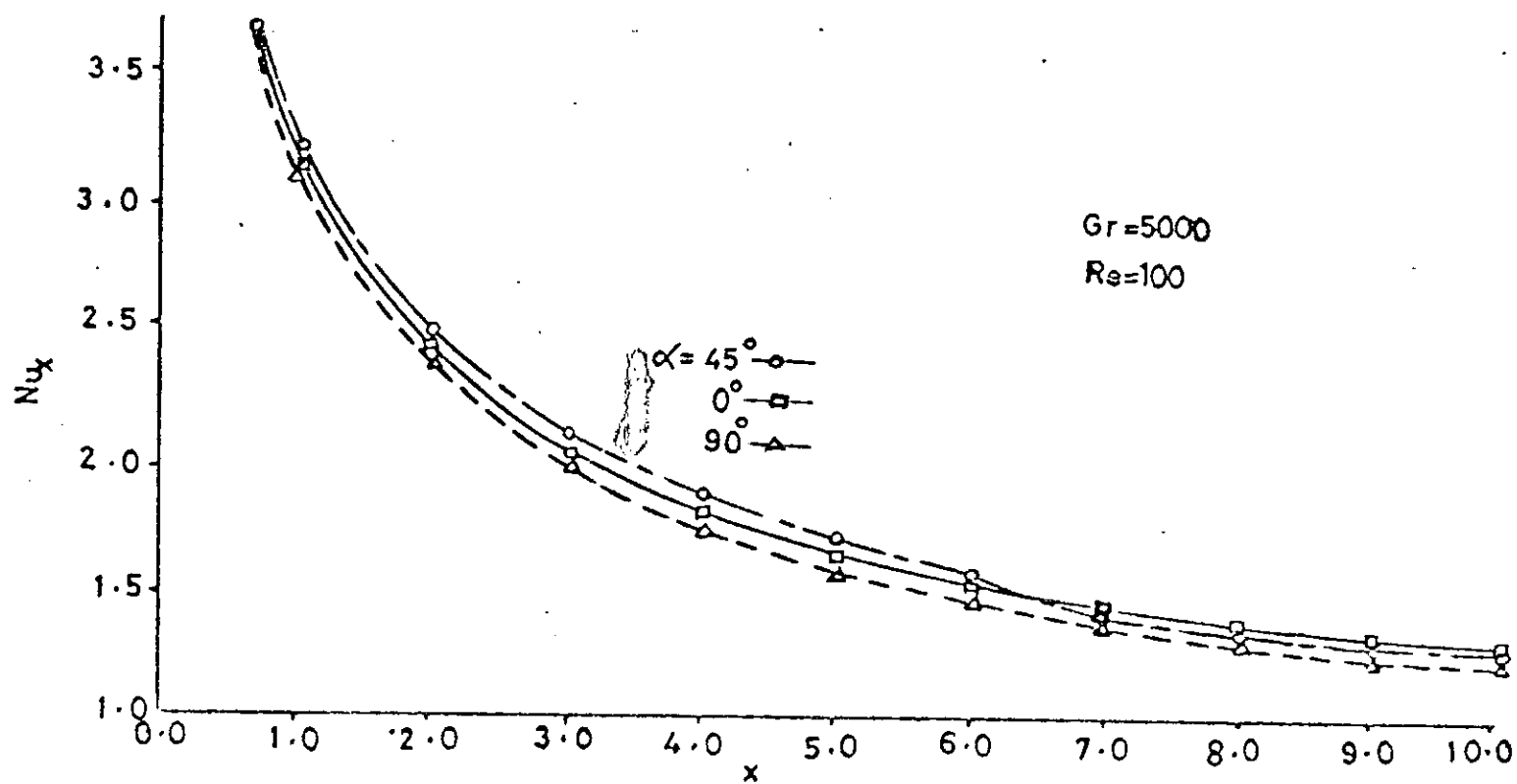
Fig.2-10. Variation of local Nussell number with dimensionless longitudinal distance for $Pr = 0.73$ and α as minor Parameter.
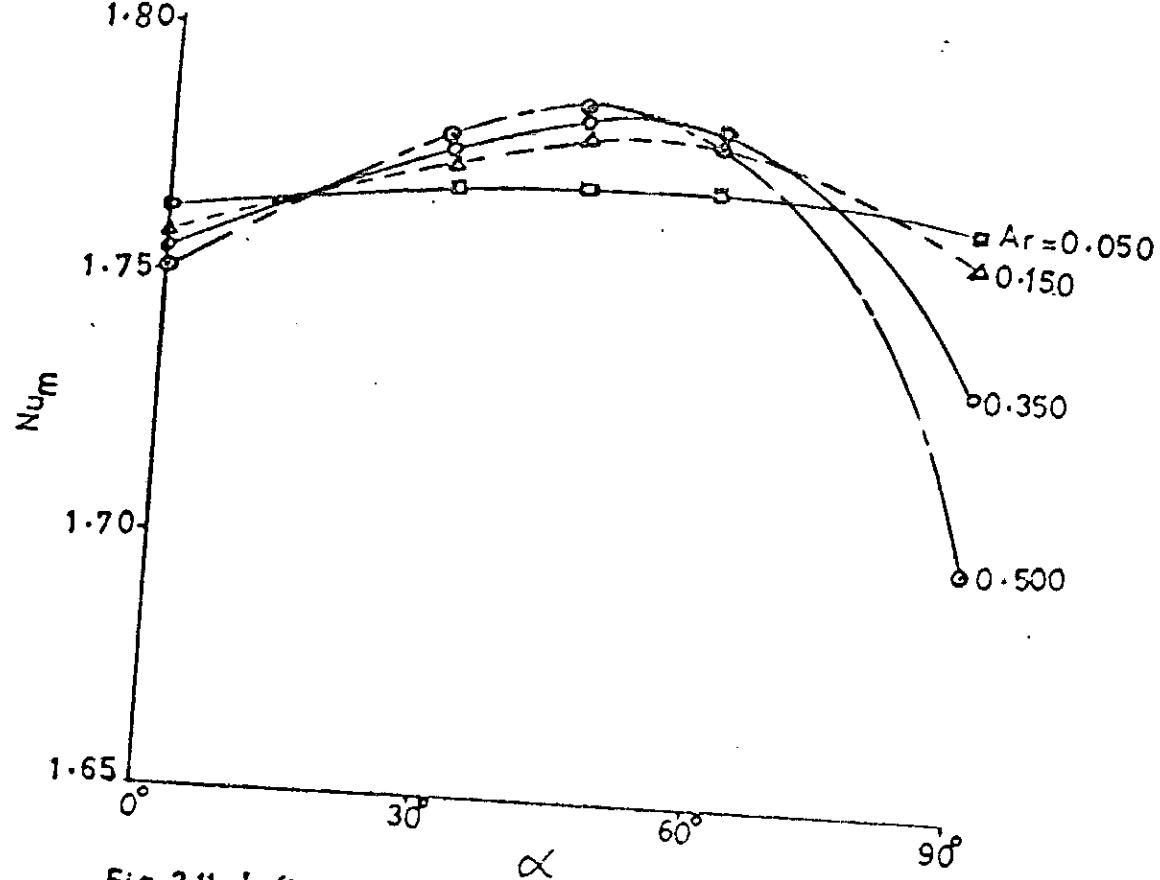
Fig. 2-11. Influence of channel orientation on the mean hot wall Nusselt number for Pr=0.73 with Ar as Parameter, (500 ≤ Gr ≤ 5000, Re=100).
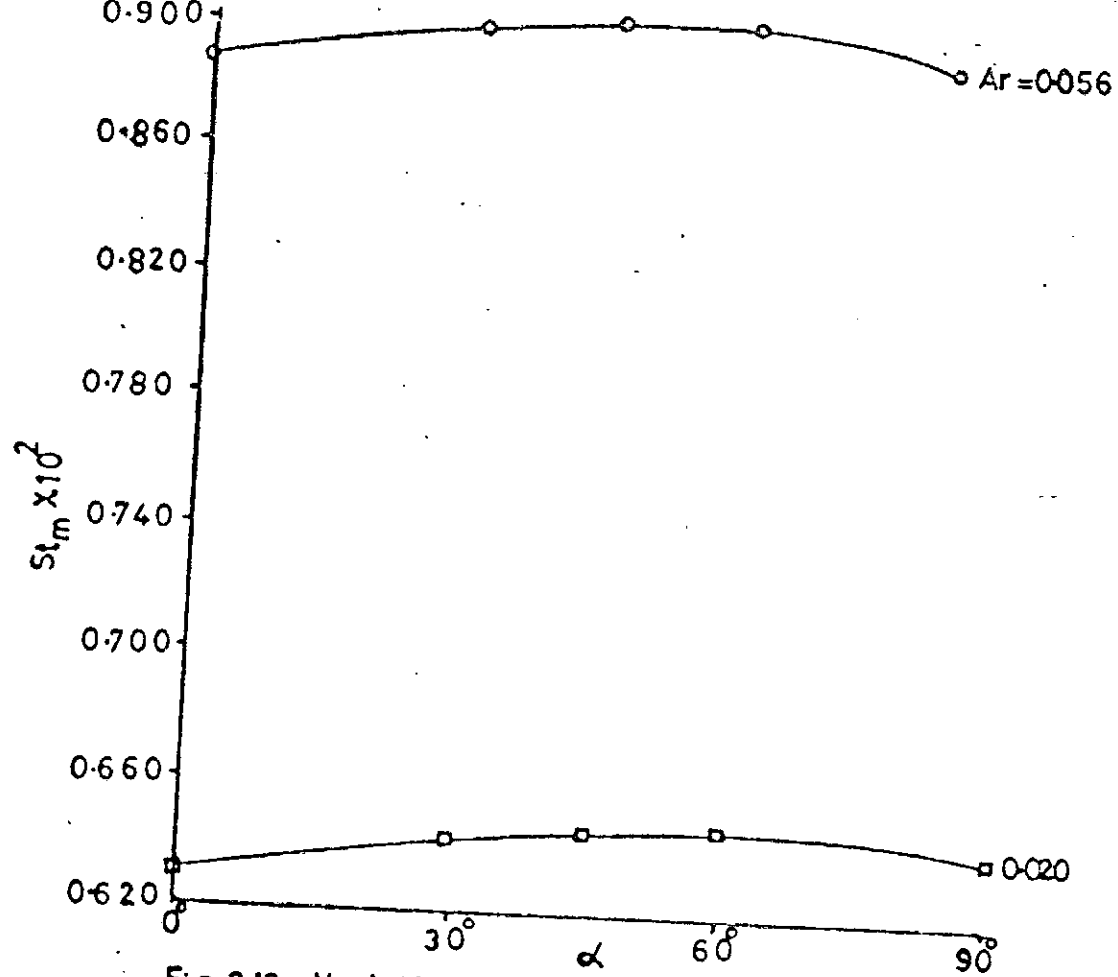
Fig. 2-12. Variation of the mean hotwall Stanton number with channel orientation for $Pr = 0.73$, ($Gr = 5000$, $300 \leqslant Re \leqslant 500$).
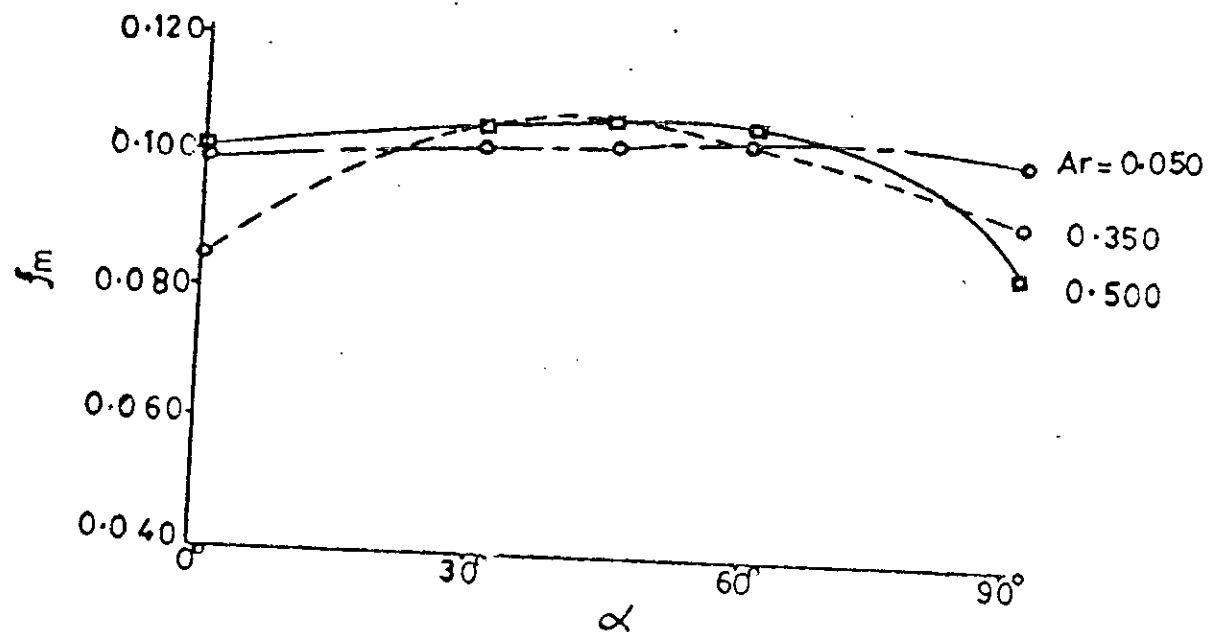
Fig. 2-13. Influence of channel orientation on the mean hotwall friction factor for $Pr = 0.73$ with Ar as Parameter $(500 \leqslant Gr \leqslant 5000; Re = 100)$.
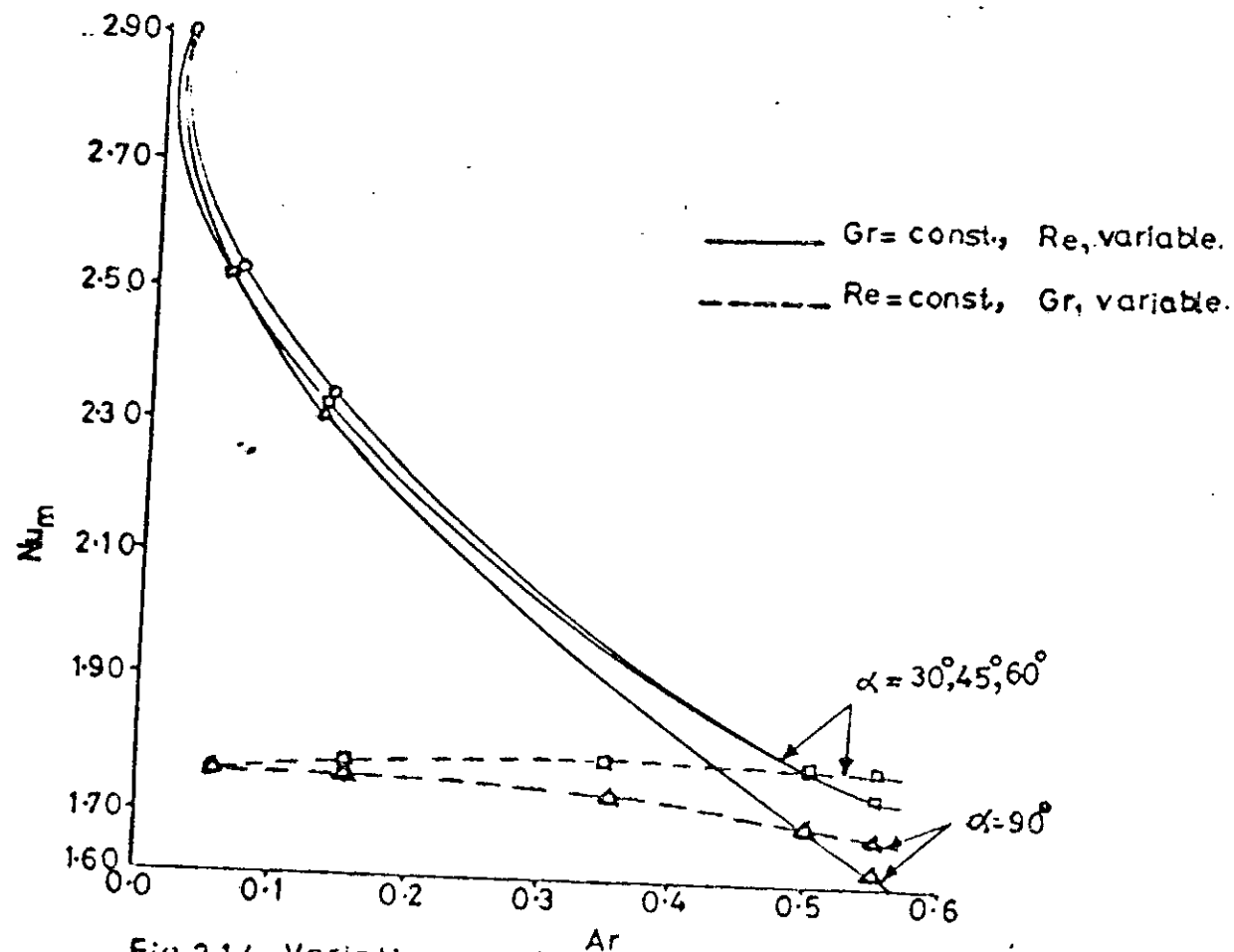
Fig. 2-14. Variation of the mean hotwall Nusselt number with Archimedes number for Pr= 0·73 and various inclinations, (0 ≤ Gr ≤ 6000 ; 100 ≤ Re ≤ 300).
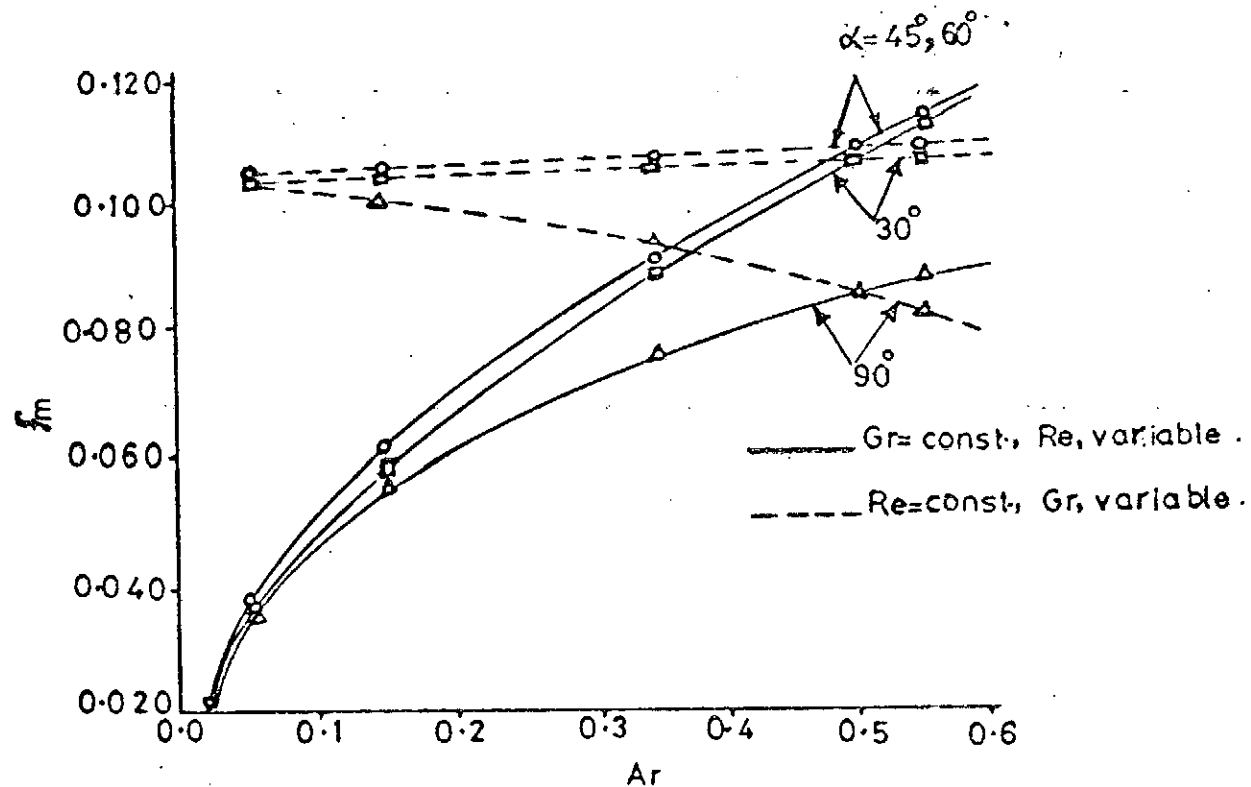
Fig. 2-15. Variation of the mean hotwall friction
factor with Archimedes number for Pr = 0·73
and various inclinations,
(0 ⩽ Gr ⩽ 6000 ; 100 ⩽ Re ⩽ 300).

CHAPTER THREE

3. ANALYSIS OF NUMERICAL METHOD - CASE B

3.1 Preliminary discussion:

The previous chapter was devoted to investigating constant but unequal surface temperature thermal boundary condition. In most engineering applications other wall-temperature variations are often of interest. For example in flat plate solar collectors, the source of heat is radiant energy. Technically, this constitutes a constant heatflux problem and the surface temperature variation along the hot plate is linear. For the cold plate, its surface temperature variation cannot be determined a priori since it depends on the prevailing ambient conditions on both sides of the plate. In particular, the ambient temperature of the adjoining cooling medium will depend on the method of cooling. If the cold plate is exposed to the atmosphere, the preferred mode of cooling is by free or natural convection. However, if this cooling medium is accelerated by an external force, the mode of cooling is obviously by forced convection. In a practical situation the cooling may be achieved by mixed convection. It is clear that whichever of the methods of cooling is adopted, the ambient temperature of the cooling medium plays a significant role in determining the surface temperature of the cold plate. In addition, the specification of this ambient temperature becomes crucial for the completeness of the thermal problem. Also, because of the variable surface temperatures, there is need to redefine the dimensionless temperature difference.

In this chapter, the dimensionless temperature difference has been defined in terms of the dimensional axial temperature gradient along the hot-wall. The reference temperature is the ambient temperature of the fluid at entrance to the channel. Because of the slow rate of convergence, the numerical computation has been carried out by Successive-Over-Relaxation (SOR) method. This is done by introducing the optimum relaxation factor, ω_o, into the poisson equation of the streamfunction to obtain equation (2.34).

The finite-difference analogs of the governing equations have the same form as those in chapter two. However, the thermal boundary conditions differ considerably, while the no-slip condition at the walls still holds.

3.2 Thermal boundary conditions

3.2.1 Cold wall:

The cold wall temperature at a given location can be predicted from considerations of the second normal derivative of the temperature at that point. As stated previously in chapter two,

$$\left.\frac{\partial^2 T}{\partial y^2}\right|_{y=0} = 0$$

Introducing the normalising coordinates, $\theta = \frac{T-T\omega}{RePrA*b}$ and $Y = $ by yields

$$\left.\frac{\partial^2 \theta}{\partial y^2}\right|_{y=0} = 0$$

The finite-difference representation is given by,

$$\frac{(\theta_\omega - 2\theta_{i,1} + \theta_{i,2})}{(\Delta x)^2} = 0$$

Simplification and solution for $\theta_{i,1}$ yields

$$\theta_{i,1} = (\theta_{i,2} + \theta_\infty)/2 , \dots\dots\dots\dots\dots\dots\dots\dots\dots\dots(3.1)$$

$$\text{where } i = 2, 3, \dots M, M+1$$

For computational convenience, the dimensionless ambient temperature θ_∞ is taken to be zero, the ambient temperature at channel inlet.

3.22 Hot-wall

The constant heatflux imposed on this wall implies a linear wall temperature variation in the longitudinal direction. This variation can be expressed as

$$T_{hw}(X) = T_\infty + \overset{*}{\Lambda}X + o(X^2) \dots\dots\dots\dots\dots\dots\dots(3.2)$$

Differentiating both sides with respect to X, gives,

$$\frac{d}{dx}\left[T_{hw}(X)\right] = \frac{d}{dx}\left[T_\infty + \overset{*}{\Lambda}X\right]$$

$$\therefore \quad \frac{d}{dx}\left[T_{hw}(X) - T_\infty\right] = \frac{d}{dx}(\overset{*}{\Lambda}X)$$

In the non-dimensional form,

$$RePr \frac{d}{dx}\left[\theta_{hw}(x)\ \overset{*}{\Lambda}b\right] = \frac{d}{dx}(\overset{*}{\Lambda}bx)$$

$$\therefore \quad \frac{d\theta_{hw}(x)}{dx} = 1/RePr \dots\dots\dots\dots\dots\dots\dots\dots\dots\dots\dots(3.3)$$

The discretised form of (3.3) is

$$(\theta_{i,N+1} - \theta_{i-1,N+1})/\Delta x = 1/RePr$$

$$\theta_{i,N+1} = \frac{\Delta x}{RePr} + \theta_{i-1,N+1} \dots\dots\dots\dots\dots\dots\dots\dots(3.4)$$

Having specified the thermal boundary conditions at the walls,
it is necessary to have a closer look at the outflow boundary conditions

3.3 Outflow boundary conditions

Since the wall temperatures vary continuously in the general
direction of flow, it is anticipated that continuous variations in
the velocity and temperature profiles may occur even at remote distances
from the channel entrance. The simple gradient boundary conditions at
exit in chapter two are not strictly applicable in this case. However,
at any grid point at remote distances from the entrance, the first
derivative of any space variable with respect to x has a constant value.
At this point, the second derivative of the space variable with respect
to x must therefore vanish. The following less restrictive computational
outflow boundary conditions have therefore been imposed.

$$\frac{\partial^2 \theta}{\partial x^2}\Big|_{M,j} = 0 \quad \dots\dots\dots(3.5a)$$

$$\frac{\partial^2 \omega}{\partial x^2}\Big|_{M,j} = 0 \quad \dots\dots\dots(3.5b)$$

$$\frac{\partial^2 \psi}{\partial x^2}\Big|_{M,j} = 0 \quad \dots\dots\dots(3.5c)$$

$$\frac{\partial^2 v}{\partial x^2}\Big|_{M,j} = 0 \quad \dots\dots\dots(3.5d)$$

where $j = 2, 3, \dots N$

The finite-difference equivalents of the above equations are;

(a) For Temperature:

$$\frac{\partial^2 \theta}{\partial x^2}\bigg|_{M,j} = \frac{(\theta_{M-1,j} - 2\theta_{M,j} + \theta_{M+1,j})}{\Delta x^2} = 0$$

Solving for $\theta_{M+1,j}$ gives

$$\theta_{M+1,j} = 2\theta_{M,j} - \theta_{M-1,j} \quad\dots\dots\dots\dots\dots\dots(3.6a)$$

By analogy,

(b) For vorticity:

$$\omega_{M+1,j} = 2\omega_{M,j} - \omega_{M-1,j} \quad\dots\dots\dots\dots\dots\dots(3.6b)$$

(c) Streamfunction:

$$\psi_{M+1,j} = 2\psi_{M,j} - \psi_{M-1,j} \quad\dots\dots\dots\dots\dots\dots(3.6c)$$

(d) Transverse velocity:

$$v_{M+1,j} = 2v_{M,j} - v_{M-1,j} \quad\dots\dots\dots\dots\dots\dots(3.6d)$$

where $j = 2, 3, \dots N$

3.4   Evaluation of heattransfer and flow parameters

3.4.1 Nusselt and Stanton numbers

It is sufficient to mention that a cubic polynomial in y for θ has been used, as in the previous chapter, to estimate the heat transfer. However, the local Nusselt number is based on the normal temperature gradient and the difference between the local wall temperature and the ambient. Hence the local Nusselt number can be represented by:

(a) For the cold wall:

$$Nu_{xc} = \frac{(70_{i,1} + \theta_{i,2} - 80_{i,3})}{6\Delta y(\theta_{i,1} - \theta_\infty)} \quad \dots\dots\dots\dots\dots \quad (3.7)$$

$$i = 2, 3 \dots M, M+1$$

The corresponding mean value is given by

$$Nu_{mc} = \frac{1}{x_L} \int_0^{x_L} Nu_{xc} dx \quad \dots\dots\dots\dots\dots\dots\dots (3.8)$$

(b) For the hotwall:

$$Nu_{xh} = \frac{(7\theta_{i,N+1} + \theta_{i,N-1} - 8\theta_{i,N})}{6\Delta y(\theta_{i,N+1} - \theta_\infty)} \quad \dots\dots\dots\dots(3.9)$$

$$\text{where } i = 2, 3 \dots M, M+1$$

$$\text{and } Nu_{mh} = \frac{1}{x_L} \int_0^{x_L} Nu_{xh} dx \quad \dots\dots\dots\dots\dots\dots(3.10)$$

The corresponding local and mean Stanton numbers for the cold and hot walls can be obtained from the following equations. Thus.

$$St_{xc} = \frac{Nu_{xc}}{RePr} \quad \dots\dots\dots\dots\dots\dots\dots\dots\dots(3.11a)$$

$$St_{mc} = \frac{1}{x_L} \int_0^{x_L} St_{xc} dx = \frac{Nu_{mc}}{RePr} \quad \dots\dots\dots(3.11b)$$

$$St_{xh} = \frac{Nu_{xh}}{RePr} \quad \dots\dots\dots\dots\dots\dots\dots\dots\dots(3.11c)$$

$$St_{mh} = \frac{Nu_{mh}}{RePr} \quad \dots\dots\dots\dots\dots\dots\dots\dots\dots(3.11d)$$

3.42 Friction Coefficients

The local friction coefficients are obtained from the relation

$$f_x = \frac{2}{Reu_{mx}^2} \left| \frac{\partial u}{\partial y} \right|_{wall} \quad \dots\dots\dots\dots\dots\dots(3.12)$$

The mean value is given by

$$f_m = \frac{1}{x_L} \int_0^{x_L} f_x dx \quad \dots\dots\dots\dots\dots\dots\dots(3.13)$$

3.5 General Computational Procedure

The iterative procedure is essentially the same as that of chapter two, except for a few additions. However, since the equations used in evaluating some boundary values differ considerably from those of chapter two, it is necessary to state the various steps in the computation.

(1) θ, u, v, ψ are initialised for all the interior, outlet grid points. Using the initial values of u, the boundary vorticities are computed from equations (2.34) and (2.36) of the previous chapter.

(2) θ is initialised at the cold boundary where the temperature variation is arbitrary. Using equations (2.12), and (3.6a) respectively, θ at interior points and outflow boundary are computed. When the temperature field has converged, the cold wall temperature is re-evaluated from equation (3.1).

(3) ω is computed for all interior points from equation (2.12) and on the outflow boundary from equation (3.6b).

(4) ψ at interior points are obtained from equations (2.14), (2.19) and (2.12) after computing the optimum relaxation factor ω_o from equations (2.15a) and (2.15b). The outflow boundary values are obtained from equation (3.6c).

(5) u, v are recomputed for all interior points from equations (2.13) and (2.14) and the outflow values of v from (3.6d).

(6) Using the most recently computed values of θ and u, the local

and mean values of the Nusselt, Stanton numbers and friction coefficients are computed from equations (3.7), (3.8), (3.9), (3.10), (3.11a), (3.11b) (3.11c), (3.11d), (3.12) and (3.13) respectively. In addition, the new boundary vorticities are computed from (2.34) and (2.36).

(7) Steps two through six are repeated until convergence is achieved for each variable. The computation is terminated thereafter.

3.6 Discussion of Results

Figure 3.1 shows the variation of the dimensionless hot-wall, cold-wall and mean temperatures with the channel length. The hot-wall temperature varies linearly with the longitudinal distance. The cold-wall temperature increases gradually with the channel length. As anticipated, the local mean temperatures lie between the hot-wall and cold-wall values. In general the local non-dimensional mean temperatures increases with the longitudinal distance.

Figure 3.2 depicts the temperature profiles across the channel at two different locations. Unlike the constant-surface-temperature solution, profiles do not originate and terminate at the same points. The longitudinal variation of the wall temperatures accounts for this.

On figure 3.3, the local cold-wall and hot-wall Nusselt numbers are plotted as functions of the longitudinal distance. For the hot-wall, the local Nusselt number decreases with channel length while that of the cold-wall (its absolute value) increases with channel length. This should not come as a surprise since the fluid temperature near the cold-wall is always higher than the cold-wall value at any axial location.

Figure 3.4 illustrates the variation of cold-wall and hot-wall Stanton numbers with the channel length. Their variations are similar to those of the respective Nusselt numbers from which they were evaluated. Figure 3.5 represents the variation of the local friction factors along the channel. Figures 3.6 and 3.7 show the influence of channel inclination and the modified Archimedes number respectively on the velocity profiles at remote distances from the channel inlet. Again, near the channel axis of symmetry, the velocity profiles are insensitive to both α and Ar_m. This could be attributed to the cancelling of the aiding and opposing effects of the free convection. The general lateral displacement of the velocity profile results from the unsymmetrical heating.

Figure 3.8 shows the influence of channel orientation on the mean hot-wall Nusselt number with the modified Archimedes number as the minor parameter. There exists optimum angles of inclination for which the mean hot-wall Nusselt numbers are maximum. For the range of modified Archimedes number considered, the maximum mean hot-wall Nusselt numbers and the optimum inclinations (in radians) are well correlated by a three-dimensional power law derived later. These optimum inclinations lie between 45° and 82.5^o.

Figure 3.9 shows the variation of the mean cold-wall Nusselt number with channel inclination. Optimum inclinations exist for which the absolute value of the mean cold-wall Nusselt numbers are maximum.

3.6.1 Correlation for the Mean hot-wall Nusselt numbers.

The results for the Mean Hot-wall Nusselt number show that optimum angles of inclination exist for which maximum Nusselt numbers are available.

Since it is the optimum angles of inclination that is of practical interest, its relationship with the maximum mean Nusselt number for the range of modified Archimedes numbers considered, can be expressed by a three dimensional power Law. This,

$$Nu_{mH} = C(Ar_m)^{n}1\,(\alpha_{OPT})^{n}2 \dots\dots\dots\dots\dots\dots\dots\dots\dots\dots\dots (3.26).$$

where α_{OPT} is the optimum inclination expressed in radians, n_1, n_2 are exponents; $C = const$.

Taking the logarithm of each side, we have

$$\log_{10} Nu_{mH} = \log_{10} C + n_1 \log_{10} Ar_m + n_2 \log_{10} \alpha_{OPT}$$

If $\quad \log_{10} Nu_{mH} = z$

$$\log_{10} C = C_o$$

$$\log_{10} Ar_m = x$$

$$\log_{10} \alpha_{OPT} = y$$

Then we have a linear equation of the form

$$z = C_o + n_1 x + n_2 y \dots\dots\dots\dots\dots\dots\dots\dots\dots\dots\dots (3.27)$$

(a) For $Ar_m = 0.025$

$$\alpha_{OPT} = \frac{7\pi}{24} = 52.5^{\circ}$$

$$Nu_{mH} = 3.444$$

$$\therefore \quad z = \log_{10} 3.444 = 0.5370$$

$$x = \log_{10} 0.025 = -1.602$$

$$y = \log_{10} \frac{7\pi}{24} = -0.036$$

The corresponding equation is

$$0.5370 = C_o - 1.602n_1 - 0.036n_2.$$

(b) For $Ar_m = 0.050$

$$\alpha_{OPT} = \frac{\pi}{4} = 45^o$$

$$Nu_{mH} = 3.456$$

$$\rightarrow \quad z = \log_{10} 3.456 = 0.5380$$

$$x = \log_{10} 0.050 = -1.301$$

$$y = \log_{10} \frac{\pi}{4} = -0.104$$

The corresponding equation is

$$0.5380 = C_o - 1.301n_1 - 0.104n_2 \quad \dots\dots\dots\dots\dots\dots\dots(3.29)$$

(c) For $Ar_m = 0.100$

$$\alpha_{OPT} = 82.5^o = \frac{11\pi}{24}$$

$$Nu_{mH} = 3.499$$

$$\rightarrow \quad z = \log_{10} 3.499 = 0.5430$$

$$x = \log_{10} 0.100 = -1.00$$

$$y = \log_{10} \frac{11\pi}{24} = +0.160$$

The corresponding equation is

$$0.5430 = C_o - 100n_1 + 0.160n_2 \quad \dots\dots\dots\dots\dots\dots(3.30)$$

The solution of the three simultaneous equations yields

$$n_1 = 0.006$$

$$n_2 = 0.012 \qquad \rightarrow \quad n_2 = 2n_1$$

$$C_o = 0.5471 \quad \rightarrow \quad \mathcal{C} = 3.520$$

Hence the three-dimensional correlation is

$$Nu_{mH} = 3.520 (Ar_m \, \alpha_{oPT}^2)^{0.006} \qquad \text{for } 0.025 < Ar_m < 0.100 \quad \dots(3.31)$$

$$\frac{\pi}{6} < \alpha_{oPT} < \frac{11\pi}{24}$$

Figures 3.10 and 3.11 depict respectively, the variation of the mean cold-wall and hot-wall Stanton numbers with the angle of inclination for a range of modified Ar_m. Figure 3.10 shows the existence of optimum inclinations for maximum (absolute value) mean cold-wall Stanton numbers to occur. Figure 3.11 exhibits an entirely different picture. For inclinations up to $30°$, the mean hot-wall Stanton numbers are independent of Ar_m and α. For inclinations less. than $30°$, St_{mh}, remains independent of small values of Ar_m and α. For $Ar_m = 0.100$, a significant increase in St_{mh} is shown for α greater than $30°$.

Figures 3.12 and 3.13 represent the respective variations of the mean hot-wall and cold-wall friction factors. In figure 3.12, optimum inclinations between $30°$ and $82.5°$ exist for maximum values of f_{mh} to occur. Figure 3.13 shows that in general f_{mc} decreases with α and Ar_m.

Again, this predicts separation at the cold-wall, especially near the vertical position. Although no rigorous attempt is made to define the criteria of separation for each inclination, the general tendency is that as the angle of inclination increases the critical Ar_m required for separation decreases. The minimum value of Ar_m occurs at the vertical position, its value being 0.500.

3.7 Applications

One application that readily comes to mind is in the design of flat-plate solar collectors where the hot plate is heated by solar energy and the heat generated is convected away by forced flow for various uses.

For instance, if air is the medium of convection, the heat convected can be used for drying grains. In view of the changing position of the sun, the orientation of such a heat transfer equipment with respect to the gravitational field becomes an important factor in predicting the position at which heat transfer is a maximum, if any.

3.8 Conclusions

Practically all conceivable channels are finite in extent so that fully developed regimes are hard to come by. The problem is therefore basically that of an entrance region and mean values of the heat transfer and flow parameters are more representative of actual results than those obtained for idealised fully developed regimes. In the light of the assumptions made to simplify the mathematical model, it can be concluded that optimum inclinations exist for which the heat transfer is maximum at the hot wall.
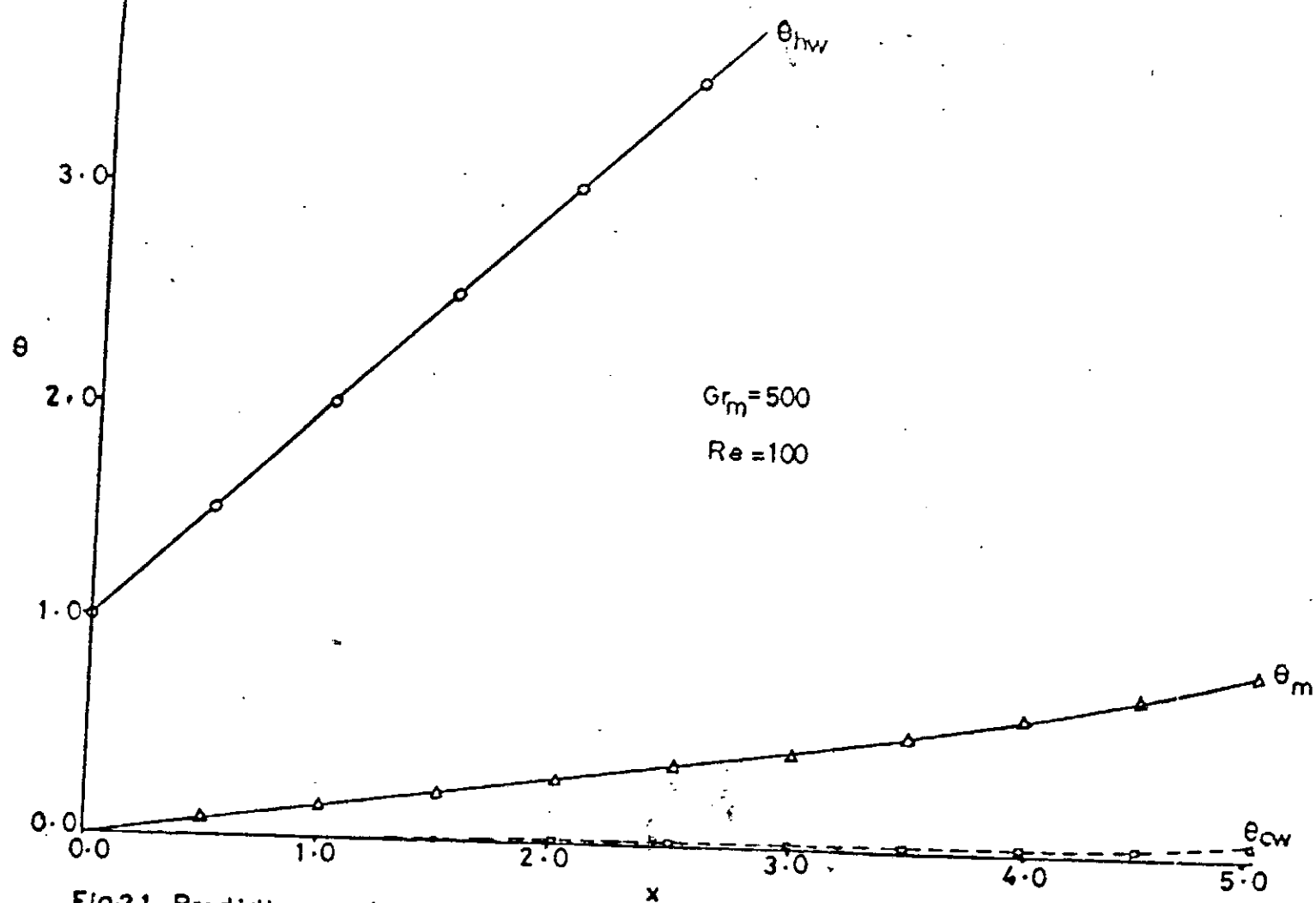
Fig·3·1· Predictions of dimensionless mean and wall temperature variations with channel length for $Pr = 0.73$ and $\alpha = 0°$
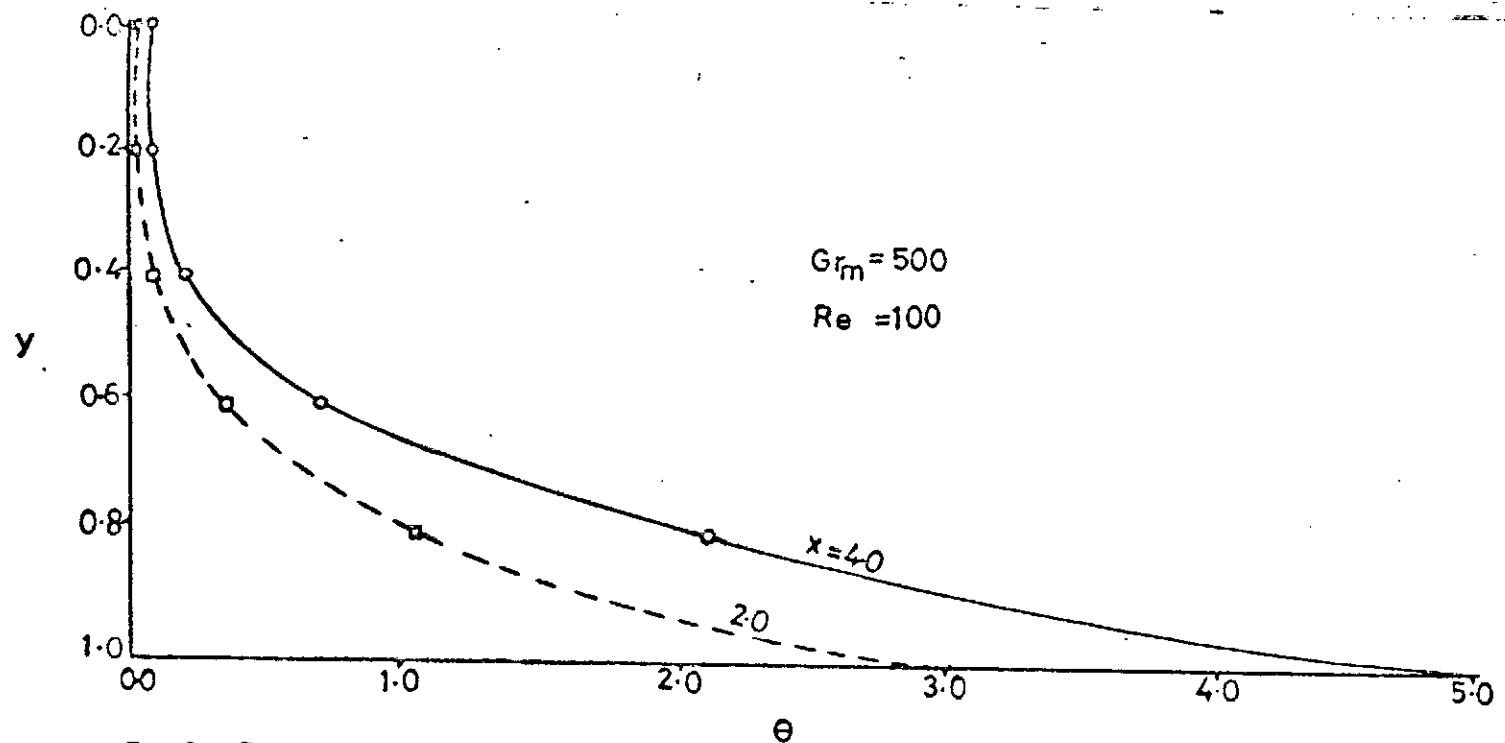
Fig. 3-2. Predictions of dimensionless temperature Profiles across channel at two locations along its length for $Pr = 0.73$ and $\alpha = 0°$.

In the figure: $Gr_m = 500$, $Re = 100$, with curves labeled $x = 40$ and 2.0.
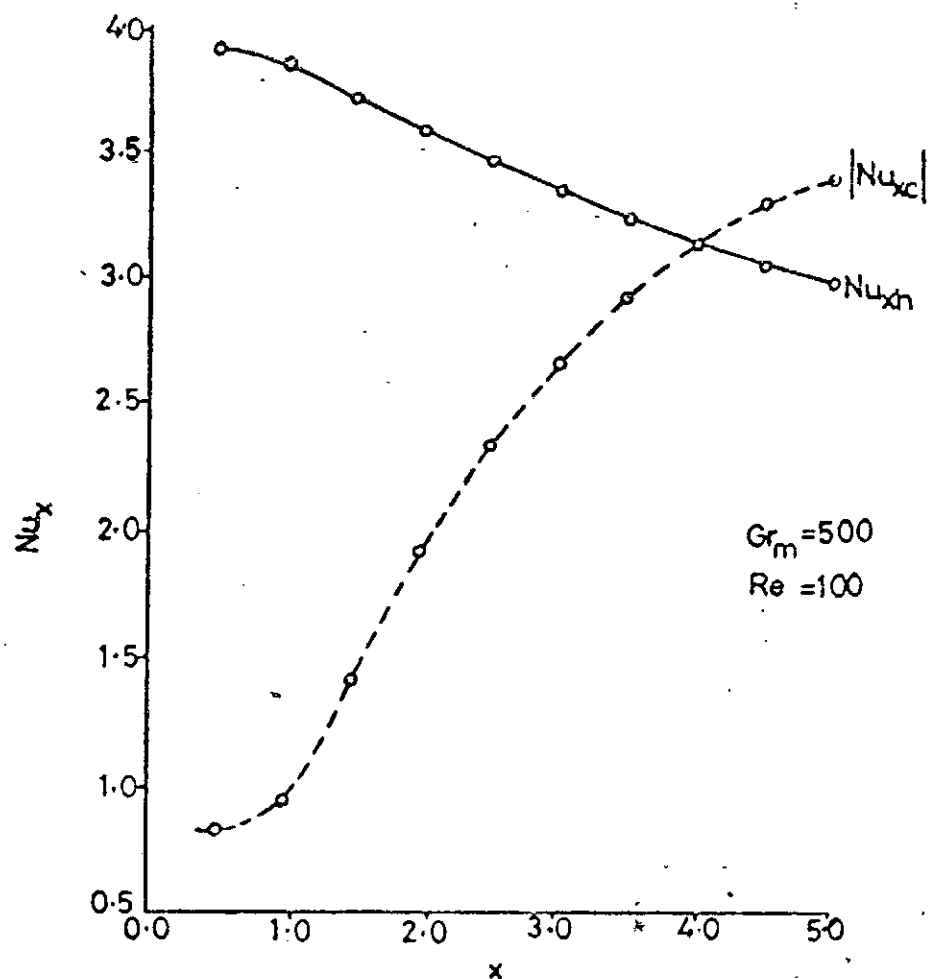
Fig. 3-3. Variation of local Nusselt numbers with channel length for Pr = 0.73 and $\alpha = 0$.
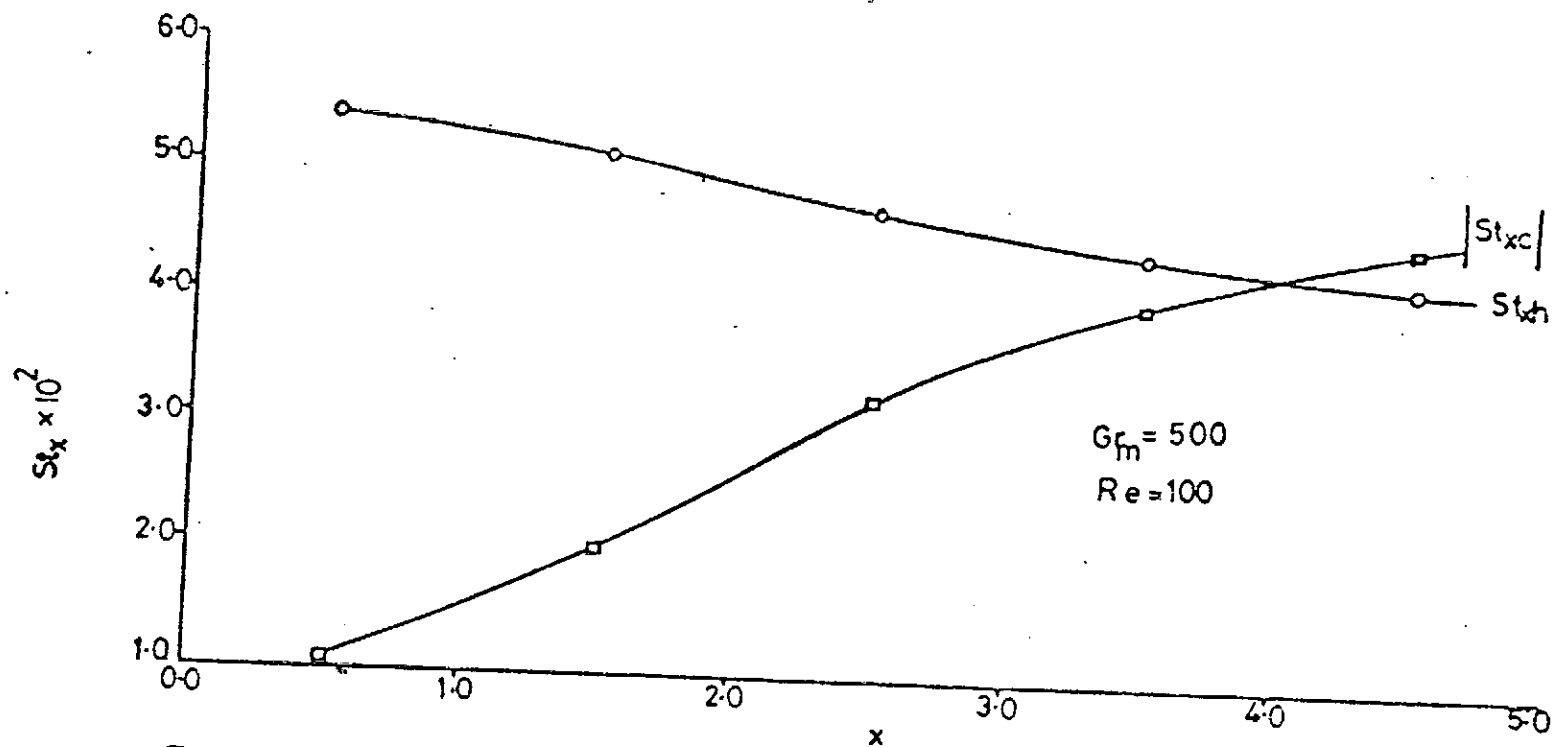
Fig.34. Variation of local Stanton numbers with channel length for $Pr = 0.73$ and $\alpha = 0°$.
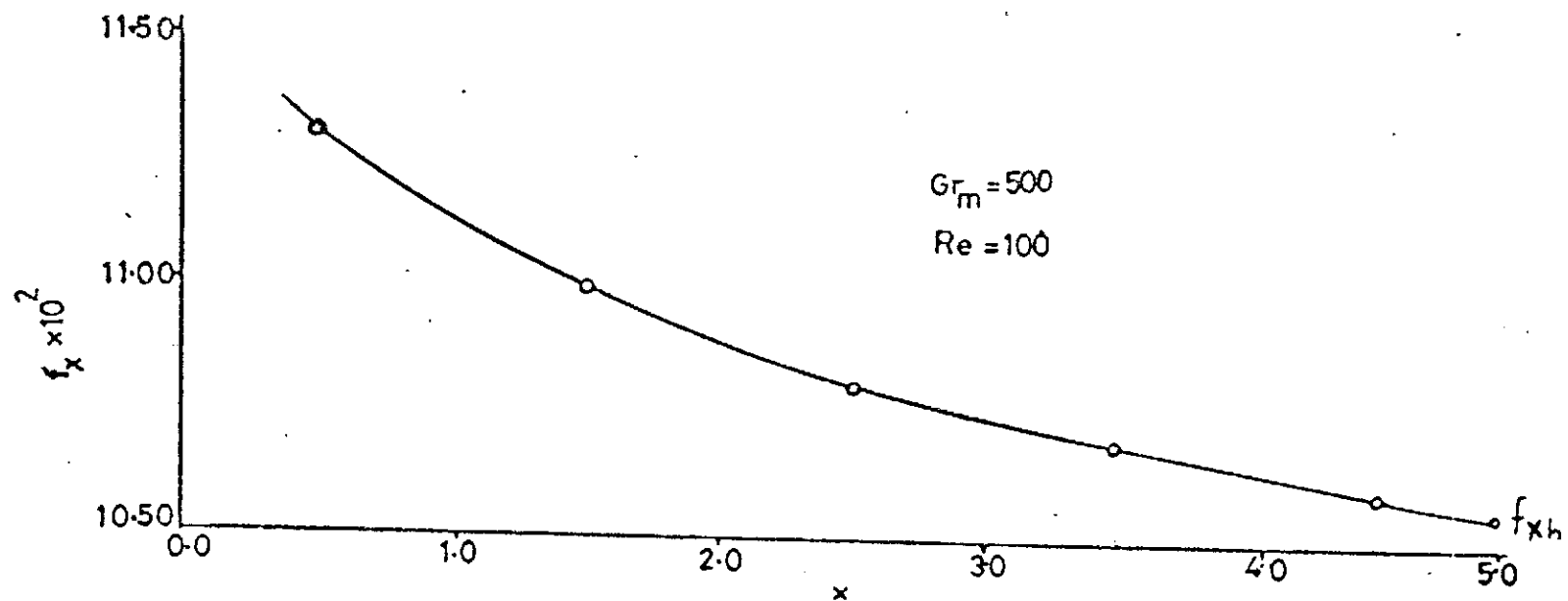
Fig.3-5. Variation of local friction factors with channel length for $Pr = 0.73$ and $\alpha = 0^\circ$.
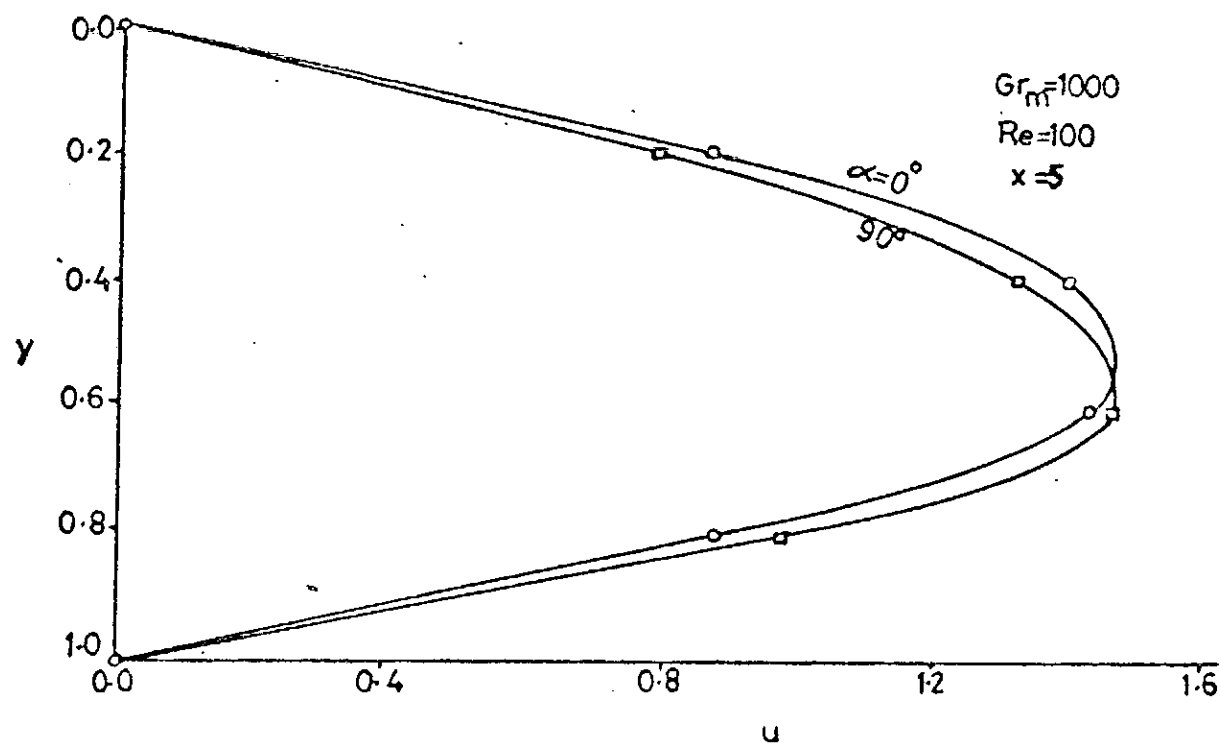
Fig 3-6. Influence of channel orientation on dimensionless longitudinal velocity distribution across channel for $Pr = 0.73$.

In the figure: $Gr_m = 1000$, $Re = 100$, $x = 5$, $\alpha = 0°$, $90°$.
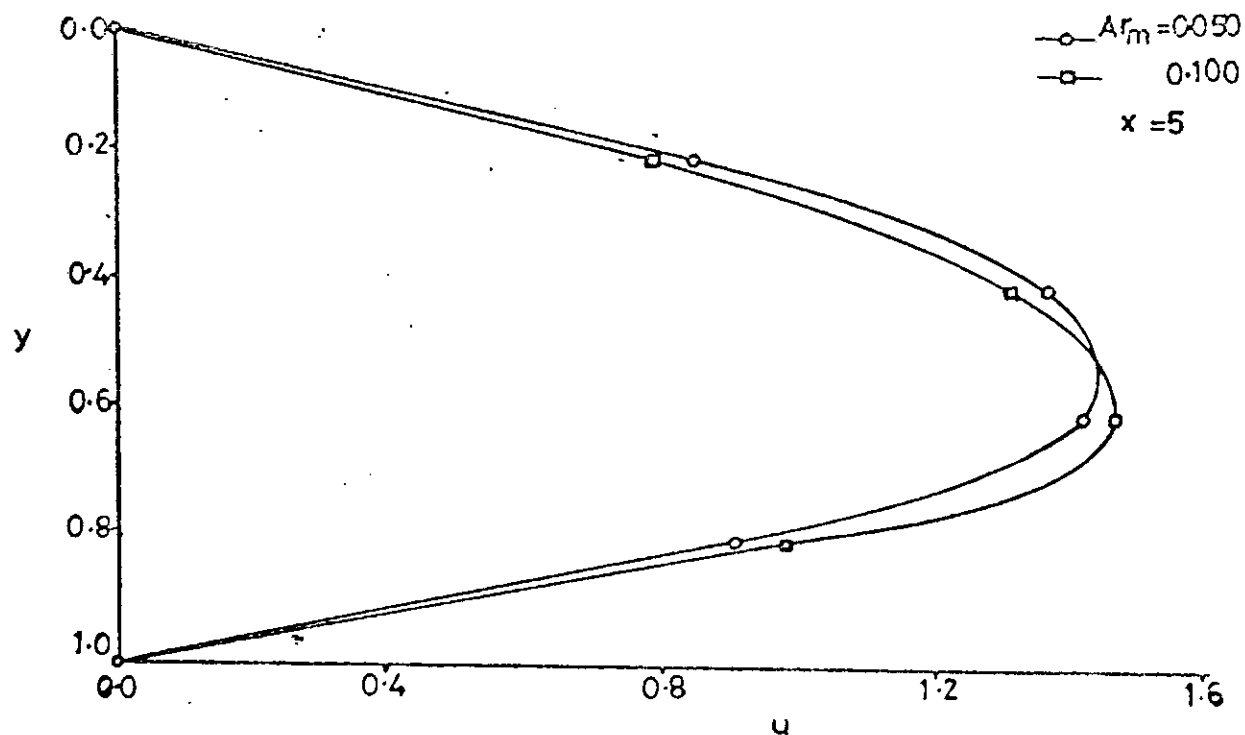
Fig. 3-7. Influence of modified Archimedes number on dimensionless longitudinal velocity distribution across channel for Pr=0.73 and $\alpha = 90°$, (Re =100; 500 ⩽ Grm ⩽ 1000).
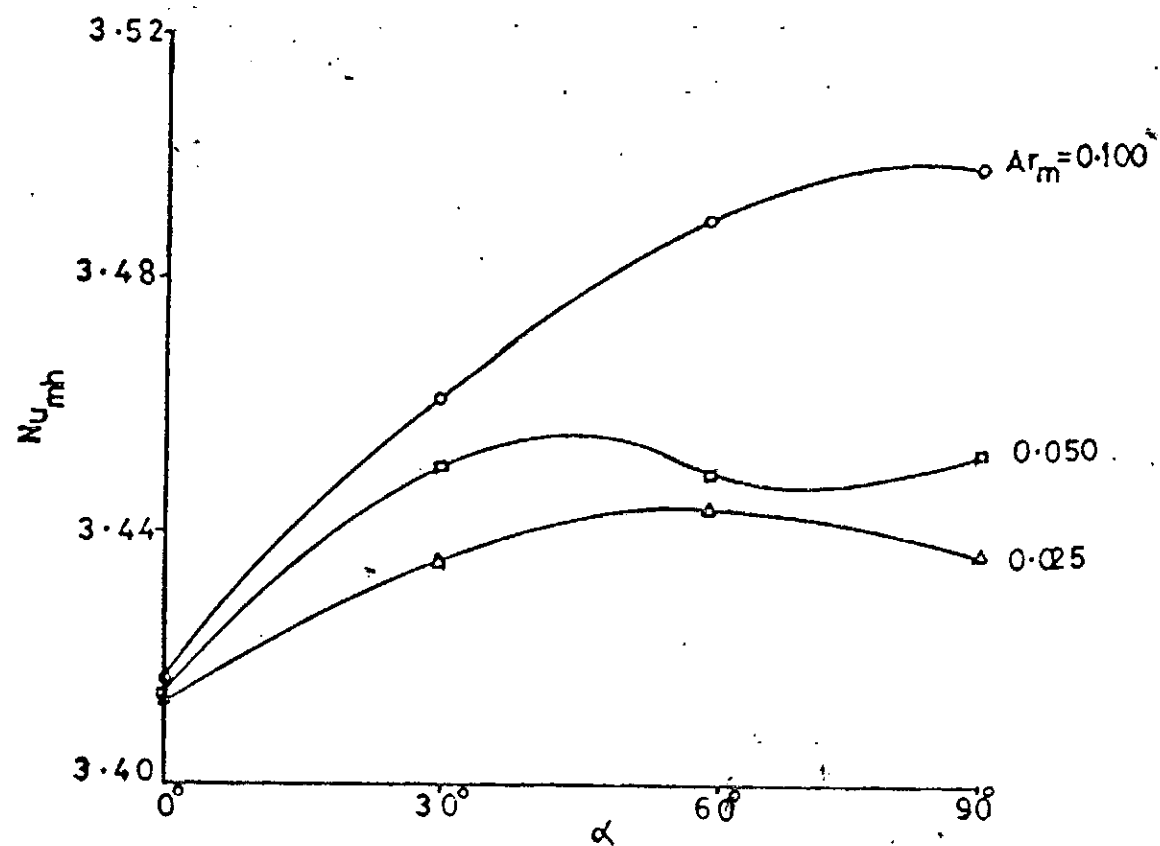
Fig.3-8. Influence of channel orientation on the mean hotwall Nusselt number for $Pr=0.73$ with Ar_m as Parameter, ($Re=100$; $250 \leqslant Gr_m \leqslant 1000$).
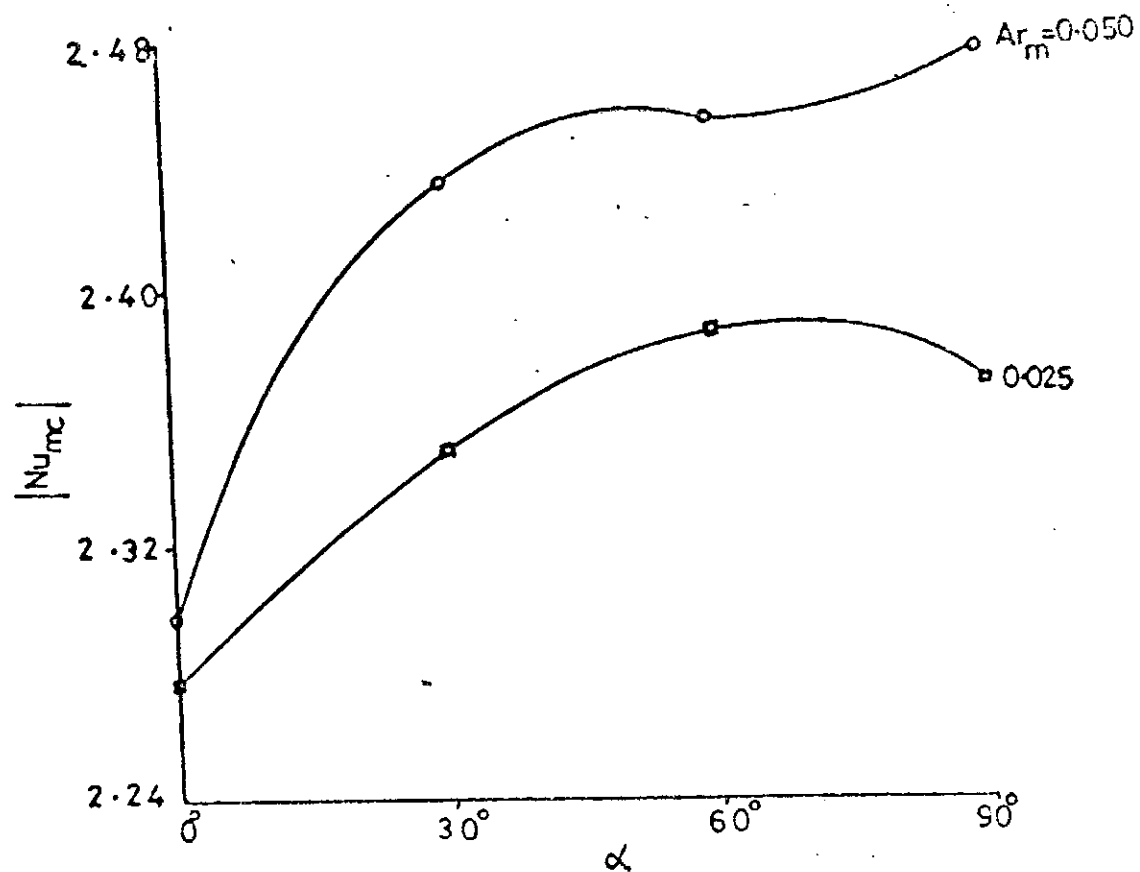
Fig. 3-9. Influence of channel orientation on the mean coldwall Nusselt number for $Pr = 0.73$ with Ar_m as Parameter, $(Re = 100; \ 250 \leqslant Gr_m \leqslant 500)$.
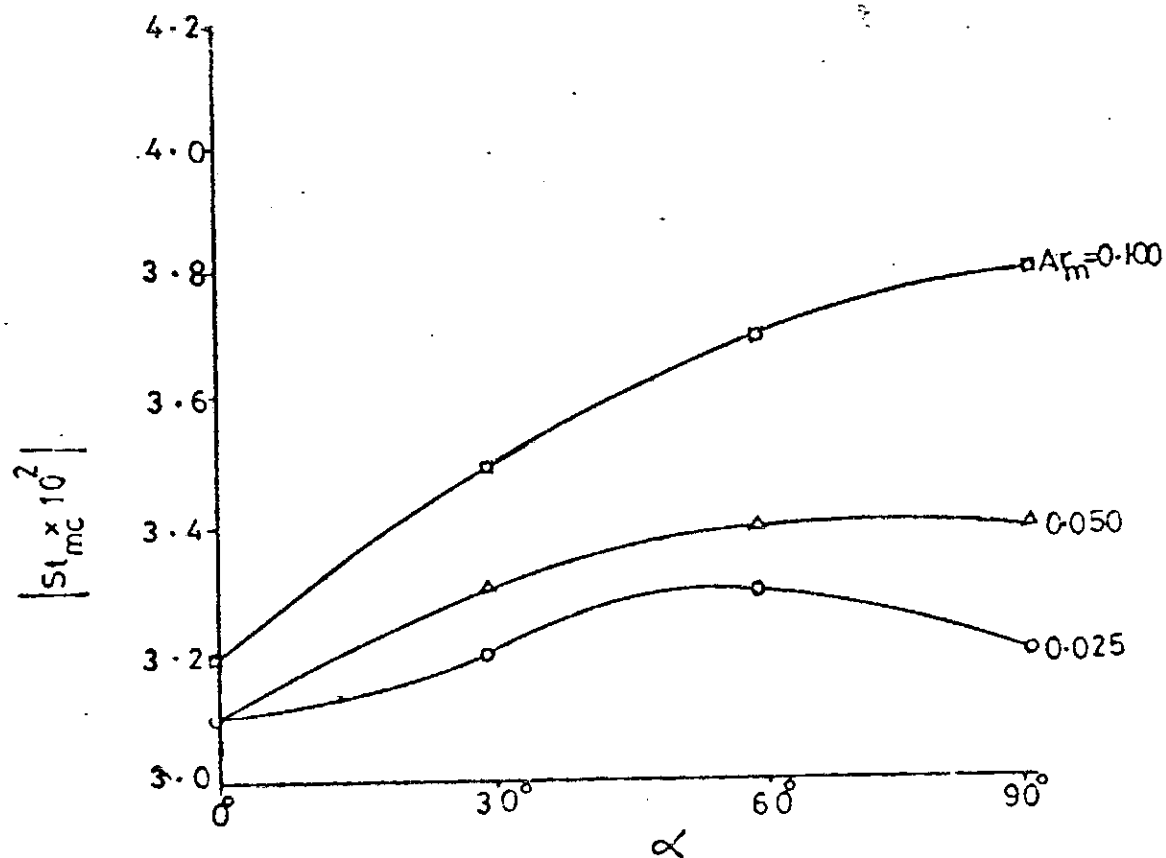
Fig. 3-10. Influence of channel orientation on the mean coldwall Stanton number for Pr=0.73 with Ar_m as parameter $(Re=100 ; 250 \leqslant Gr_m \leqslant 1000)$.
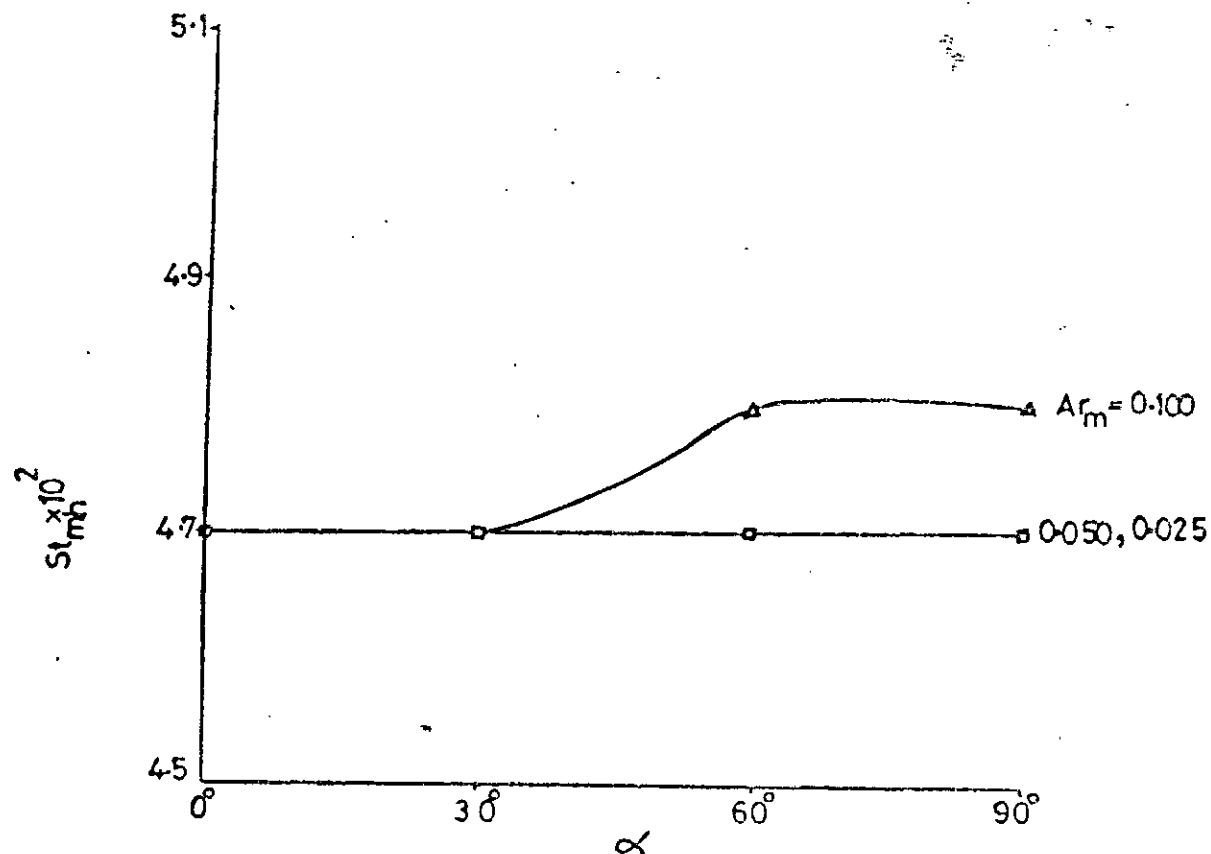
Fig. 3-11. Influence of channel orientation on the mean
hotwall Stanton number for $Pr = 0.73$ with
Ar_m as parameter, ($Re = 100$; $250 \leqslant Gr_m \leqslant 1000$)
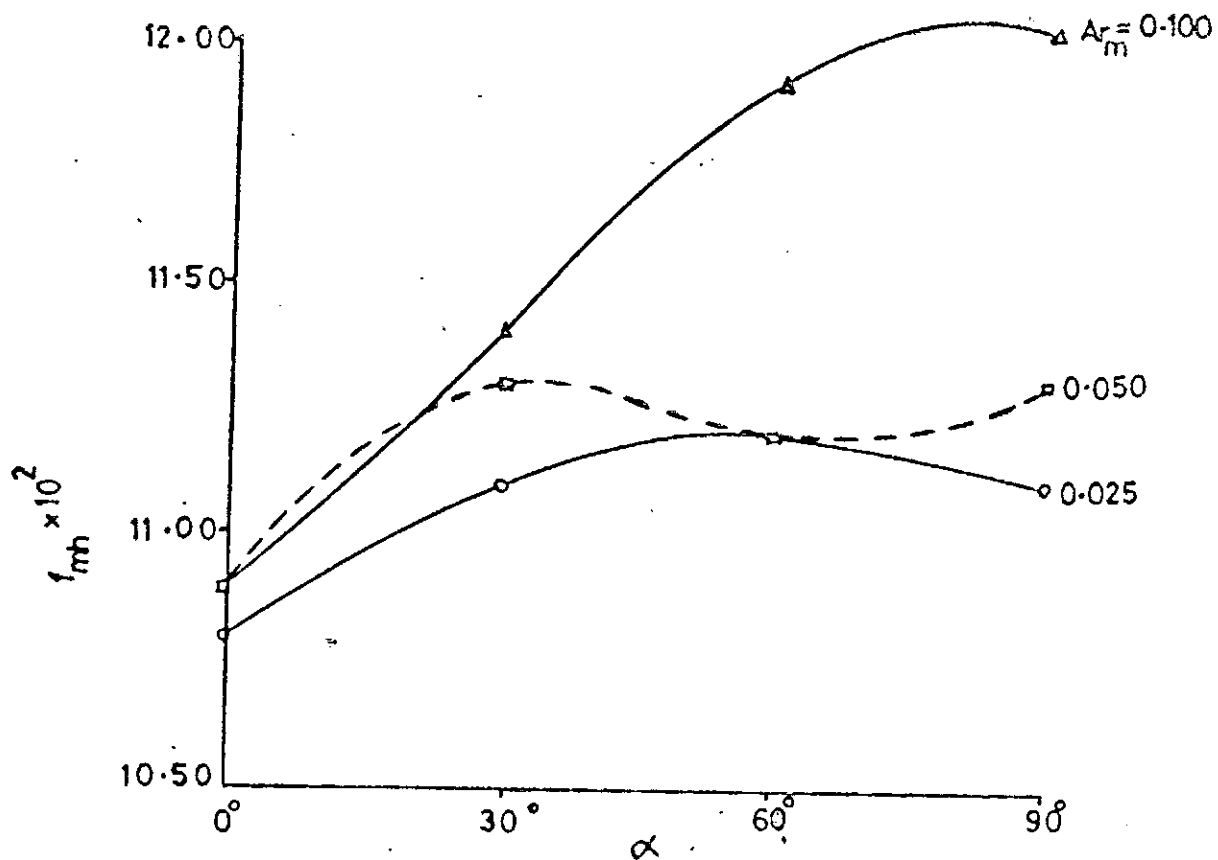
Fig. 3.12. Influence of channel orientation on the mean hotwall friction factor for Pr=0.73 with Ar_m as parameter, (Re=100, $250 \leqslant Gr_m \leqslant 1000$).
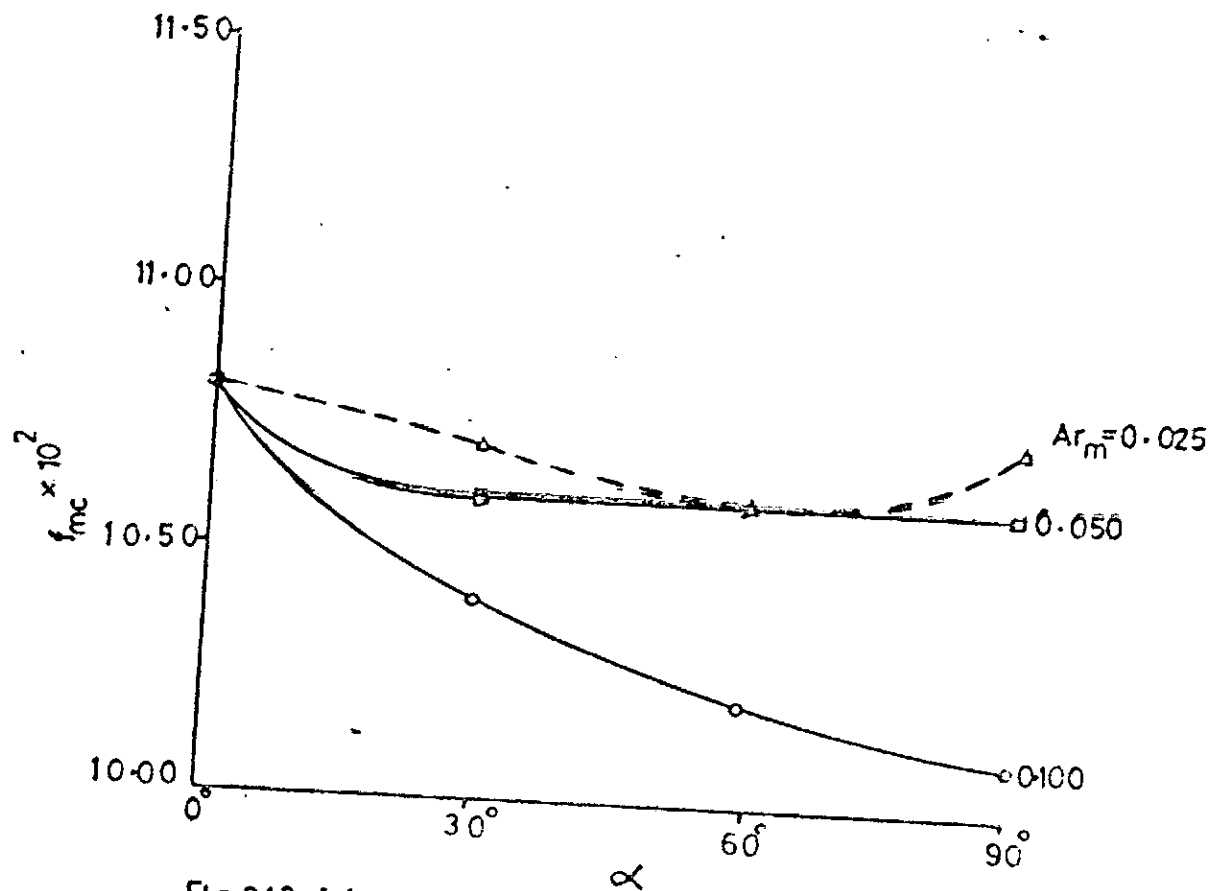
Fig.3-13. Influence of channel orientation on the mean cadwall friction factor* for $Pr=0.73$ with Ar_m as parameter, $(Re=100; 250 \leqslant Gr_m \leqslant 1000)$.

CHAPTER FOUR

4. STABILITY, CONVERGENCE AND ACCURACY OF NUMERICAL SCHEME

4.1 Preamble

To obtain a realistic simulation of a flow process from a computer, it must be supplied with a set of instructions (the computer programme) which embodies the implications of the conservation laws of mass, momentum and energy appropriate to a moving fluid. Since the laws governing the flux of mass, momentum energy are established for laminar flows, the predictions generated by the computer programme, with due care, may be as reliable as a physical experiment. Therefore, the question of stability, convergence and accuracy become crucial in obtaining a numerical scheme whose results are comparable with physical experiment.

4.2 Stability:

Stability is usually associated with the growth or decay of errors in numerical schemes. More generally, stability may be defined as the requirement of a bounded extent to which any component of the initial data can be amplified in the numerical procedure.

Two types of errors are associated with numerical schemes. They are:

(i)   Round-off errors,

(ii)   Discretisation or Truncation errors.

"Round-off" errors are due to the finite floating-point word length of electronic computers. Round-off errors are difficult to analyze because they introduce qualitative aberrant behaviour, e.g. floating-point addition and multiplication are cummulative, but not associative or distributive. The computer generally does not randomly round up or down as would be preferred.

"Truncation errors" refer to the errors incured by not retaining all terms in the infinite Taylor series expansions or equivalently by using finite grid-sizes Δx and Δy. These errors are usually of order (Δx), (Δy), $(\Delta x)^2$, $(\Delta y)^2$, etc. and can be reduced by decreasing the grid-sizes in a specified manner.

4.3 Convergence

A convergent finite-difference scheme is defined mathematically as one in which all values of the finite-difference solution approach that of the continuum differential equation as the finite-difference mesh sizes tend to zero. A necessary and sufficient condition for iteration convergence is that for the Gauss-Seidel iterative procedure used, the matrix of coefficients of the system of linear equations generated from the finite-difference scheme must be diagonally dominant [6]. It has been usual to approximate all derivatives of flow variables by central-difference formulae. More recently, Spalding (1967) and Greenspan (1968) suggested a method in which the first derivatives of flow variables are approximated by upwind or downwind differences depending on the local direction of flow at any given grid-point. Investigations carried out by researchers

showed that at large values of Reynolds number, the central-difference representation of first derivatives may fail to produce a matrix of coefficients that is diagonally dominant. Hence the solution diverges. However, the matrix associated with the equations obtained by approximating first derivatives by upwind and downwind differences, depending upon the local direction of flow, is diagonally dominant. It has been discussed in some detail by Runchal et. al. [9]. The disadvantage of this method is that the truncation error may be higher than that obtained when central-difference representations are used. The penalty is worth it.

Since convergence is intimately connected with grid-size it is useful to still investigate the phenomenon of "Wiggles" or "Spatial oscillations" which can induce divergence even after satisfying other conditions. "Wiggles" or spatial oscillations in a flow solution have been encountered in many works. In supersonic flow, they are usually associated with post-shock oscillations of methods using centered-space derivatives. Wiggles also arise in long-term incompressible flow calculations. Spatial oscillations manifest themselves in numerical solutions by alternating signs, - or +, of flow variables near rigid boundaries at various stages of numerical iteration. This pattern of behaviour makes it impossible to determine with confidence, the stage at which computation can be terminated. Some schools of thought have associated spatial oscillations with non-linearities or with

linear instabilities. Other schools of thought are of the view that wiggles are simply solutions of finite-difference equations. One fact is obvious: wiggles can indeed prevent iteration convergence, especially for the highly susceptible vortex field.

The condition required, from stability considerations, for wiggles not to occur for a 2-D through-flow problem is that $\frac{\Delta X}{\Delta Y} < \frac{1}{2} \frac{U\Delta Y}{\nu}$ [8] where $\frac{\Delta X}{\Delta Y}$ is the mesh aspect ratio and $\frac{U\Delta Y}{\nu}$ is the cell Reynods number.

The non-dimensional form of the inequality is $\frac{\Delta x}{\Delta y} < \frac{1}{2}$ Re uΔy. How this inequality affects the number of divisions in the X-and Y-directions needs further elaboration.

Thus, let, L = Non-dimensional channel length

$1.0 = $ Height of channel

$\Delta x = \frac{L}{M}$

$\Delta y = \frac{1}{N}$

Substituting these into the inequality yields, after simplification,

$$N^2 < \frac{\text{Re u M}}{2L}$$

For the entrance region, the channel length can be approximated by the relation L = 0.04Re. For demonstration purposes, suppose that the non-dimensional longitudinal local velocity, u = 0.20 near a rigid boundary.

Thus,

$$N^2 < \frac{\text{Re x 0.20 x M}}{2 \text{ x 0.04Re}}$$

$\therefore \quad N^2 < 2.5M$

Suppose M = 10

Then $N^2 < 25$, $\Rightarrow N < 5$.

It can readily be seen that to avoid spatial oscillations, the number of divisions, in this case, in the Y-direction must be less than half the number of divisions in the X-direction. Throughout the numerical analysis, this condition was rigidly adhered to.

To further accelerate convergence, an optimum relaxation factor ω_o was introduced into the equation of stream function following Roache [8].

4.4 Accuracy

The accuracy of a numerical solution cannot be considered in isolation; it must be considered along with convergence and stability criteria. It is possible for a numerical scheme to be stable and convergent but not necessarily to its true solution. An accurate solution is that which approximates to the continuum solution of the differential equation. This can usually be achieved by refining the grid-sizes. But this requires excessive computation time for convergence. It is not advisable to pursue this course for economic reasons. However, results obtained for several finite grid-sizes can be extrapolated to zero grid-size to offset discretisation errors as was done by Ozoe et. al. [4]. For analyses which involve low Reynolds numbers, excessive grid-refinement for channels with narrow openinings, is not necessary. For instance, for Re = 150 a grid-network of 11x6 for b = 1.0, the plots of centre-line velocity for an isothermal system compares favourably with that of Runchal et. al. [9] who used a grid-network of 21x15 for b = 2.0. as shown in figure 2.2.

In going from a grid-network of 11x6 to that of 22x8, the maximum deviation

in heat transfer and friction coefficients was about 10%. The penalty

paid for grid-refinement was excessive computation time and consequently

higher financial costs.

CHAPTER FIVE

5.   PARAMETER PERTURBATION ANALYSIS – CASE A

5.1   Preliminary discussion:

In reality, pure forced convective heat transfer seldom occurs since the density of ordinary fluids is dependent on temperature. In fact, mixed convection, that is, combined free and forced convection, is the most general type of phenomena. Thus, forced convection represents a limiting approach for vanishingly small heat transfer, and these solutions are valid approximately only within a very limited range of flow and heat transfer conditions. The solutions do not, in themselves, permit any estimate of the extent of range within which they are physically realistic. To assess the effectiveness of forced convection solutions experimental observations are necessary. However, for a two-dimensional problem, a computer simulation is just as good as an experiment.

One approach to investigating problems of convection in which the free and forced effects are comparable is to use the fully developed forced convection solution as a first approximation to both the velocity and temperature fields. The next approximation can be obtained from the buoyancy-driven secondary flow and a secondary temperature distribution due to the modified field of flow. This perturbation of the forced convection does allow for mutual interaction of the velocity and temperature fields; an essential feature of thermal convection.

A number of authors have adopted this approach by obtaining

solutions as power series in a chosen perturbation parameter. Faris and Viscanta [10] used $\frac{Gr}{Re^2}$, the Archimedes number, as their expansion parameter for flow in a horizontal tube. Iqbal and Stachiewcz [11] used the Rayleigh number for the case of constant heatflux boundary condition. Morton [12] used the product of the Rayleigh number and a modified Reynolds number as the expansion parameter for a uniformly heated horizontal pipe. The perturbation approach in general may converge for sufficiently small values of the expansion parameter when adequate terms of the power series are considered. However, on account of the labour involved in finding higher order terms, most works have been restricted to the second-order term. Therefore forced convection solution is bound to be in error. Hence perturbation solutions based on the fully developed forced convection solution, are in general, not strictly correct. However, the primary motivation is to improve on the understanding of the combined process and to extend the existing solutions to a wider range of conditions so that the analytical results may find direct physical application.

The present analytical study is based on the fully developed laminar forced convection in inclined rectangular channels heated isothermally from below and similarly cooled from above. From dimensional considerations with vector-length approach, it is established that the relevant expansion parameter for the power series is $\frac{Gr}{Re^2}$, the Archimedes number. Perturbation results are presented graphically for modified Peclet numbers, RePrA, ranging from 0.088 to 0.350. Numerical solutions are then compared with perturbation solutions for the case of

constant wall temperatures only. It has not been possible to obtain
the perturbation solutions for the case of constant heat flux at the hot
wall since the thermal boundary values are not specified.

5.2 Dimensional Analysis

In convective heat transfer problems, there are two approaches.
These are:

(a) The use of the theory of dimensional homogeneity to obtain
relations between relevant variables which affect the flow and
heat transfer.

(b) The isolation of an element of the boundary layer and its analysis
using the mass conservation concept (i.e. control of volume approach)
to obtain the governing equations.

Case (a) shall be considered. In doing so, consideration is given to;

(i) The traditional L, M, T, θ, as the fundamental system of units
without regard to the direction along which the characteristic
linear dimension, L, is measured.

(ii) The 'Vector Length' approach which considers the linear dimension,
L, as a vector resolvable in three mutually orthogonal directions
so that the fundamental system of units becomes L_X, L_Y, L_Z, M, T, θ.
Since the present analysis pertains to a two-dimensional flow, only
L_X, L_Y are considered relevant to the problem. The advantage
gained is an increase in the number of independent fundamental units
from four to five; the total number of physical quantities remaining
unchanged.

5.21 <u>Traditional Approach</u>: L, M, T, θ (fundamental units)

The heat transfer coefficient, h, per unit temperature difference is given by the functional relationship

$$h = f(U_m, \mu, K_f, C_p, \rho, \beta g, \theta, b, \alpha)$$

where each of the physical quantities in the bracket has the following dimensional representation.

$$U_m \; [=] \frac{L}{T}$$

$$\mu \quad [=] \frac{M}{LT}$$

$$K_f \; [=] \frac{ML}{\theta T^3}$$

$$C_p \; [=] \frac{L^2}{\theta T^2}$$

$$\rho \quad [=] \frac{M}{L^3}$$

$$\beta g \; [=] \frac{L}{\theta T^2}$$

$$\theta \quad [=] \theta$$

$$b \quad [=] L$$

$$h \quad [=] \frac{M}{\theta T^3}$$

$$\alpha \quad [=] \frac{L}{L}$$

If N is the total number of physical variables and n, the least number of independent fundamental units, then by Buckingham's π-theorem [13], the function $h = f(U_m, \mu, K_f, C_p, \rho, \beta g, \theta, b, \alpha)$ can be reduced to one involving (N-n) non-dimensional groups. Hence for the present case, there are six possible non-dimensional groups to replace the above

functional relationship. By cancellation method [14] the groups are:

(a) $\pi_1 \triangleq \rho \dfrac{U_m b}{\mu} \ [=] \ \dfrac{M}{L^3} \cdot \dfrac{L}{T} \cdot L \cdot \dfrac{LT}{M} \ [=] -$

where $\rho \dfrac{U_m b}{\mu}$ represents the Reynolds number for the forced flow.

$\therefore \ \pi_1 = Re$

(b) $\pi_2 \triangleq \dfrac{\beta g \theta b^3 \rho^2}{\mu^2} \ [=] \dfrac{L}{\theta T^2} \cdot \theta \cdot L^3 \cdot \dfrac{M^2}{L^6} \cdot \dfrac{L^2 T^2}{M^2} \ [=] -$

where $\dfrac{\beta g \theta b^3 \rho^2}{\mu^2}$ represents the Grashof number, Gr

$\therefore \ \pi_2 = Gr$

(c) $\pi_3 \triangleq \dfrac{\mu Cp}{K_f} \ [=] \ \dfrac{M}{LT} \cdot \dfrac{L^2}{\theta T^2} \cdot \dfrac{\theta T^3}{ML} \ [=] -$

where $\dfrac{\mu Cp}{K_f}$ represents the prandtl number, Pr, which is purely a property of the fluid.

$\therefore \ \pi_3 = Pr$

(d) $\pi_4 \triangleq \dfrac{hb}{K_f} \ [=] \ \dfrac{M}{\theta T^3} \cdot L \cdot \dfrac{\theta T^3}{ML} \ [=] -$

where π_4 represents the Nusselt number, Nu.

$\therefore \ \pi_4 = Nu.$

(e) $\pi_5 \triangleq \dfrac{U_m^2}{Cp\theta} \ [=] \ \dfrac{L^2}{T^2} \cdot \dfrac{\theta T^2}{L^2} \cdot \dfrac{1}{\theta} \ [=] -$

where π_5 represents the Eckert number, Ec. Since viscous dissipation is neglected in this analysis, Ec is only defined here to satisfy the requirements of Buckingham π-Theorem.

(f) $\pi_6 \overset{\Delta}{=} \alpha \; [=] \; \dfrac{L}{L} \; [=] -$

The fundamental relationship can be expressed thus:

$$Nu = f(Re, Gr, Pr, Ec, \alpha)$$

The above relationship merely states that heat transfer characteristic is a function of Re, Gr, Pr, Ec and α. The expression does not suggest the mode of combination of Re and Gr for a given fluid. If due consideration is given to the direction along which the characteristic linear dimension, L, is measured, the so-called non-dimensional groups may in fact be dimensional. By judicious combinations of these dimensional groups, a truely non-dimensional group may be obtained. This leads to the problem of dimensional analysis with vector length approach.

5.2.2 Dimensional Analysis – Vector Length Approach following Huntley [15]

Let L be the characteristic linear dimension whose resolutes in two orthogonal directions, X and Y, are L_X, L_Y respectively. If X is the direction of forced flow and U is the longitudinal velocity, then the shear stress τ_X is defined by

$$\tau_X = \mu \frac{\partial U}{\partial Y}, \text{ so that } \mu = \frac{\tau_X}{(\frac{\partial U}{\partial Y})}.$$

Hence, the dimensional representation of μ is given by

$$\mu [=] \frac{ML_X}{T^2} \cdot \frac{1}{L_X \cdot L_Y} \cdot \frac{L_Y}{L_X} \cdot T [=] \frac{M}{L_X T}$$

$$\therefore \; \mu [=] \frac{M}{L_X T}$$

Since the dominant mode of heat transfer near the walls is by molecular conduction, then from Fouriers Law of heat conduction in one dimension,

$$h\theta = K_f \left. \frac{\partial \theta}{\partial Y} \right|_{wall},$$

$$\therefore \quad K_f = \frac{h\theta}{\left(\frac{\partial \theta}{\partial Y} \right|_{wall})}$$

The dimensional representation of K_f is thus given by

$$K_f [=] \frac{M}{\theta T^3} \cdot \frac{\theta}{l} \cdot \frac{L_Y}{\theta} [=] \frac{ML_Y}{\theta T^3}$$

$$\therefore \quad K_f [=] \frac{ML_Y}{\theta T^3}$$

The relevant physical variables will therefore assume the following dimensions,

$$Um [=] \frac{L_x}{T}$$

$$\mu [=] \frac{M}{L_x T}$$

$$K_f [=] \frac{ML_Y}{\theta T^3}$$

$$C_p [=] \frac{L_x L_Y}{\theta T^2}$$

$$h [=] \frac{M}{\theta T^3}$$

$$\rho \; [=] \; \frac{M}{L_x \cdot L_y \cdot 1}, \; \text{for a two-dimensional problem.}$$

$$\beta g \; [=] \; \frac{L_x}{\theta T^2}$$

$$X \; [=] \; L_x$$

$$Y \; [=] \; L_y$$

$$\alpha \; [=] \; \frac{L_x}{L_y} \; \text{or} \; \frac{L_y}{L_x}$$

Again from Buckingham's π-theorem, the number of non-dimensional groups required is five, since the total number of physical variables is ten and the least number of independent fundamental units is five.

(a) $\pi_1 \triangleq \dfrac{\rho U_m X}{\mu} \; [=] \; \dfrac{M}{L_x \cdot L_y \cdot 1} \cdot \dfrac{L_x}{T} \cdot L_x \cdot \dfrac{L_x T}{M} \; [=] \; \dfrac{L_x^2}{L_y}$

where $\dfrac{\rho U X}{\mu}$ represents the Reynolds number based on X

$$\therefore \; \pi_1 = Re_x = \frac{L_x^2}{L_y} \quad \dots\dots\dots\dots\dots\dots\dots\dots\dots\dots\dots(5.1a)$$

(b) $\pi_2 \triangleq \dfrac{\beta g \theta X^3 \rho^2}{\mu^2} \; [=] \; \dfrac{L_x}{\theta T^2} \cdot \theta \cdot L_x^3 \cdot \dfrac{M^2}{L_x^2 \cdot L_y^2 \cdot 1} \cdot \dfrac{L_x^2 T^2}{M^2} \; [=] \; \dfrac{L_x^4}{L_y^2}$

where $\dfrac{\beta g \theta X^3 \rho^2}{\mu^2}$ represents the Grashof number based on X

$$\therefore \; \pi_2 = Gr_x \; [=] \; \frac{L_x^4}{L_y^2} \quad \dots\dots\dots\dots\dots\dots\dots\dots\dots\dots\dots(5.1b)$$

(c) $\pi_3^{'} \wedge \frac{\mu C_p}{K_f} \big[= \big] \frac{M}{L_x T} \cdot \frac{L_x L_Y}{\theta T^2} \cdot \frac{\theta T^3}{M L_Y} \big[= \big] -$

where $\frac{\mu C_p}{K_f}$ represents the prandtl number, Pr

$\therefore \quad \pi_3^{'} = Pr \quad \big[= \big] - \qquad \dots\dots\dots\dots\dots\dots\dots\dots\dots\dots(5.1c)$

(d) $\pi_4^{'} \wedge \frac{hX}{K_f} \big[= \big] \frac{M}{\theta T^3} \cdot L_x \cdot \frac{\theta T^3}{M L_Y} \big[= \big] \frac{L_x}{L_Y}$

where $\frac{hX}{K_f}$ represents the Nusselt number based on X

$\therefore \quad \pi_4^{'} = Nu_x \quad \big[= \big] \frac{L_x}{L_Y} \qquad \dots\dots\dots\dots\dots\dots\dots\dots\dots(5.1d)$

(e) $\pi_5^{'} \quad \alpha \quad \big[= \big] \frac{L_x}{L_Y} \text{ or } \frac{L_Y}{L_x}.$

An examination of equations (5.1a), (5.1b) shows clearly that
the Reynolds and Grashof numbers are in fact dimensional! By
combining these two dimensional groups, a dimensionless group relevant
to the problem being considered can be obtained. Since the problem
is one of mixed convective phenomenon where the flow must be forced,
$Re_x \neq 0$, then there is only one out of two possible combinations of
Gr_x and Re_x, since Gr_x can possibly vanish. From equations (5.1a)
and (5.1b) the relevant non-dimensional group is given by

$\frac{Gr_x}{Re_x^2} \big[= \big] \frac{L_x^4}{L_x^2} \cdot \frac{L_Y^2}{L_x^4} \big[= \big] -$

$\therefore \quad \frac{Gr_x}{Re_x^2} \big[= \big] -$

where $\dfrac{Gr_X}{Re_X^2}$ represents the Archimedes number, Ar.

Hence the functional relationship, $\bar{h} = f(U, \mu, K_f, C_p, \rho, \beta_g, \theta, b, \alpha)$ can be expressed in the non-dimensional form as:

$$Nu \left(\frac{L_Y}{L_X}\right) = f(Pr, Ar, \alpha) \tag{5.1e}$$

Equation (5.1e) shows that the Nusselt number is a function of X, Pr, Ar and α when evaluated at the walls. The Prandtl number evaluated using 'Vector-Length' approach shows that it is dimensionless. This implies that the Prandtl number is independent of the flow geometry and therefore it is purely a fluid property as stated earlier. Since Gr, Re are the governing parameters for a given fluid, the ratio, $\dfrac{Gr}{Re^2}$ is used as the expansion parameter for the power series.

5.3 Theoretical Analysis

5.3.1 Formulation of the Problem

Consider the configuration depicted in figure1, inclined at an angle α° to the horizontal, heated isothermally from below and similarly cooled from above. Let a steady pure fully developed forced flow parallel to the axis pass through the channel. As a result of the established temperature gradient across the channel, buoyancy forces are generated and superimposed on the pure forced convection. Since the temperature field is not fully developed, a general longitudinal temperature gradient results. Far from the entrance region, the longitudinal temperature gradient within the fluid becomes constant. This analysis is confined to this region where both free and forced convection effects are present.

5.3.2 The Governing Equations

The non-dimensionalised governing equations culled from Chapter One are recast here for reference. For case A thermal boundary condition, the equations are:

(a) Energy Transport:

$$\frac{u\partial\theta}{\partial x} + \frac{v\partial\theta}{\partial y} = \frac{1}{RePr} \nabla^2\theta$$

(b) Vorticity Transport:

$$\frac{u\partial\omega}{\partial x} + \frac{v\partial\omega}{\partial y} = \frac{1}{Re}\nabla^2\omega - \frac{Gr}{Re^2}(\frac{\partial\theta}{\partial y}\sin\alpha + \frac{\partial\theta}{\partial x}\cos\alpha)$$

Introducing the dimensionless stream function ψ defined by,

$u = \frac{\partial\psi}{\partial y}$, $v = -\frac{\partial\psi}{\partial x}$, into the governing equations yields the following forms of the energy and vorticity transport equations:

$$\frac{\partial\psi}{\partial y}\cdot\frac{\partial\theta}{\partial x} - \frac{\partial\psi}{\partial x}\cdot\frac{\partial\theta}{\partial y} = \frac{1}{RePr} \nabla^2\theta \tag{5.2a}$$

$$(\frac{\partial\psi}{\partial y}\cdot\frac{\partial}{\partial x} - \frac{\partial\psi}{\partial x}\cdot\frac{\partial}{\partial y})\nabla^2\psi = \frac{1}{Re}\nabla^4\psi + \frac{Gr}{Re^2}(\frac{\partial\theta}{\partial y}\sin\alpha + \frac{\partial\theta}{\partial x}\cos\alpha) \tag{5.2b}$$

Numerical solutions indicate that the dimensioness transverse velocity component, $\frac{\partial\psi}{\partial x}$, is of order 10^{-6} while the longitudinal counterpart, $\frac{\partial\psi}{\partial y}$, is of order 1 for a fully developed flow. Therefore, $\frac{\partial\psi}{\partial x}$ may be neglected in this case so that the flow approximates to a parallel one. The left hand side of equation (5.2b) then becomes a function of y only. Equation (5.2b) would be valid only if the right hand side is independent of x. This condition is clearly satisfied if the dimensionless temperature

is given by

$$\theta = Ax + Y(y) \tag{5.2c}$$

The form of equation (5.2c) is commonly used as the asympotic solution to the energy equation [ref. 16]. For this problem it implies that $\frac{\partial \theta}{\partial x} = A$, constant.

The governing equations (5.2b) and (5.2a) respectively become,

$$\frac{1}{Re} \nabla^4 \psi = - Ar(\frac{\partial \theta}{\partial y} \sin\alpha + A \cos\alpha) \tag{5.2d}$$

and $$\frac{\partial \psi}{\partial y} = \frac{1}{ARePr} \nabla^2 \theta \tag{5.2e}$$

The boundary conditions that must be satisfied are:

B.C. 1: $$\psi\Big|_{y=0} = \theta\Big|_{y=0} = 0$$

$$\psi\Big|_{y=1} = \theta\Big|_{y=1} = 1,0$$

B.C. 2: $$\frac{\partial \psi}{\partial y}\Big|_{y=0} = \frac{\partial \psi}{\partial y}\Big|_{y=1} = 0 \quad \text{(no-slip condition at the rigid boundaries)}$$

5.4 Perturbation Series

In order to obtain the solutions for the dependent variables, ψ, θ in equations (5.2d) and (5.2e), these unknowns are expanded in power series of Ar

$$\psi = \sum_{n=0}^{\infty} (Ar)^n \psi_n \tag{5.3}$$

$$\theta = \sum_{n=0}^{\infty} (Ar)^n \theta_n \tag{5.4}$$

The postulated forms from (5.3) and (5.4) are introduced into equations (5.2d) and (5.2e) to yield

$$\frac{1}{Re} \nabla^4 \left[\sum_{n=o}^{\infty} (Ar)^n \psi_n \right] = -Ar \left[\frac{\partial}{\partial y} (\sum_{n=o}^{\infty} (Ar)^n \theta_n) Sin\alpha + ACos\alpha \right] \tag{5.5}$$

$$\frac{\partial}{\partial y} (\sum_{n=o}^{\infty} (Ar)^n \psi_n) = \frac{1}{ARePr} \nabla^2 \left[\sum_{n=o}^{\infty} (Ar)^n \theta_n \right] \tag{5.6}$$

For values of $Ar < 1.0$, a few terms of the series expansion will be adequate for convergence. The resulting terms are reordered with respect to powers of Ar. From the requirement that the differential expressions which multiply each exponent of Ar must vanish singly, a cascade of differential equations are obtained.

5.4.1 Equations of Zero order

$$\nabla^4 \psi_0 = 0 \quad \ldots\ldots\ldots\ldots\ldots\ldots\ldots\ldots\ldots\ldots\ldots\ldots\ldots (5.7a)$$

$$\frac{\partial \psi_0}{\partial y} = \frac{1}{ARePr} \nabla^2 \theta_0 \quad \ldots\ldots\ldots\ldots\ldots\ldots\ldots\ldots\ldots (5.7b)$$

These are the equations describing the steady basic flow. The applicable boundary conditions are

$$\psi_0 \bigg|_{y=0} = \theta_0 \bigg|_{y=0} = \frac{\partial \psi_0}{\partial y} \bigg|_{y=0} = \frac{\partial \psi_0}{\partial y} \bigg|_{y=1} = 0$$

$$\psi_0 \bigg|_{y=1.0} = \theta_0 \bigg|_{y=1.0} = 1.0$$

5.4.2 Equations of First order

$$\frac{1}{Re} \nabla^4 \psi_1 = - \left(\frac{\partial \theta_0}{\partial y} \sin\alpha + A \cos\alpha \right) \quad \ldots\ldots\ldots\ldots (5.8a)$$

$$\frac{\partial \psi_1}{\partial y} = \frac{1}{ARePr} \nabla^2 \theta_1 \quad \ldots\ldots\ldots\ldots\ldots\ldots\ldots\ldots\ldots (5.8b)$$

The boundary conditions are prescribed such that ψ_1 and θ_1 have zero contributions to the fixed boundary values.

$$\therefore \quad \psi_1 \Big|_{y=0} = \psi_1 \Big|_{y=1.0} = \theta_1 \Big|_{y=0} = \theta_1 \Big|_{y=1.0} = 0;$$

$$\frac{\partial \psi_1}{\partial y} \Big|_{y=0} = \frac{\partial \psi_1}{\partial y} \Big|_{y=1.0} = 0.$$

5.4.3 Equations of the second order

$$\frac{1}{Re} \nabla^4 \psi_2 = - \frac{\partial \theta_1}{\partial y} \, Sin\alpha \quad \dots\dots\dots\dots\dots\dots\dots\dots\dots (5.9a)$$

$$\frac{\partial \psi_2}{\partial y} = \frac{1}{ARePr} \nabla^2 \theta_2 \quad \dots\dots\dots\dots\dots\dots\dots\dots\dots (5.9b)$$

The appropriate boundary conditions are

$$\psi_2 \Big|_{y=0} = \psi_2 \Big|_{y=1.0} = \theta_2 \Big|_{y=0} = \theta_2 \Big|_{y=1.0} = 0$$

$$\frac{\partial \psi_2}{\partial y} \Big|_{y=0} = \frac{\partial \psi_2}{\partial y} \Big|_{y=1.0} = 0.$$

5.4.4 Equations of third order

$$\frac{1}{Re} \nabla^4 \psi_3 = - \frac{\partial \theta_2}{\partial y} \, Sin\alpha \quad \dots\dots\dots\dots\dots\dots\dots\dots\dots (5.10a)$$

$$\frac{\partial \psi_3}{\partial y} = \frac{1}{ARePr} \nabla^2 \theta_3 \qquad\qquad (5.10b)$$

Boundary conditions

$$\psi_3 \bigg|_{y=0} = \psi_3 \bigg|_{y=1.0} = 0$$

$$\theta_3 \bigg|_{y=0} = \theta_3 \bigg|_{y=1} = 0$$

$$\frac{\partial \psi_3}{\partial y} \bigg|_{y=0} = \frac{\partial \psi_3}{\partial y} \bigg|_{y=1} = 0$$

5.5 Results and Discussions

It will be shown in appendix A7 that for a valid solution, the condition, $0 < RePrA < 2$, must be satisfied. Results have been presented graphically for representative values of the modified Peclet number, $RePrA$, ranging from 0.088 to 0.350.

Figures 5.1 and 5.2 show the influence of Ar and α respectively on the temperature profiles across the channel. Significant distortions of these profiles near the hot wall are clearly indicated. The reasons for these indentations of the temperature profiles are not far-fetched as they can be attributed to the onset of longitudinal vortex rolls. These cause the flow to degenerate from a two-dimensional phenomenon to that of three-dimensions. Since the present analysis is treated strictly as a two-dimensional phenomenon, low values of modified Peclet numbers have been used.

Figures 5.3 and 5.4 show the effects of Ar and α respectively on the velocity profiles. These are clearly in agreement with the predictions of Gill and Del Casal $\lceil 16 \rfloor$. In either case, at the proximity of the geometrical axis of symmetry, the velocity profiles remain largely uninfluenced by Ar and α. A possible explanation is that the aiding and opposing effects of the free convection annihilate each other. The general lateral displacement of the velocity profiles is due to asymmetrical heating.

To further investigate the nature of the perturbations, the temperature and velocity fields are decomposed into their components. That is, the zeroth, first, and second-order effects. Figure 5.5 illustrates the first and second-order perturbations on the basic temperature field. It is observed that the first-order perturbation tends to increase the local temperatures near the cold plate. This perturbation has no perceptible effect in the central region of the channel. Near the hot plate, the first and second-order perturbations, generally tend to decrease the local temperatures. The resultant temperature field is obtained by combining the basic field with its ordered perturbations.

Figure 5.6 shows the first and second-order perturbations on the basic velocity field. These perturbations appear as sinusoids with the centre of the channel as a node. While the first-order perturbation produces noticeable effects near the hot and cold walls, the second-order effect produces minute reciprocal changes in the basic velocity field.

The first-order perturbation increases the local velocity near the hot wall and reduces it near the cold one. Again, at the channel axis of symmetry, the first-order effect does not influence the local velocity. On the other hand the second-order effect collapses in the central region of the channel. The vector sum of basic and perturbation velocity fields gives the resultant unsymmetrical' profile across the channel.

This analysis has previously investigated the individual effects of Ar and α on the resultant fields. In actual fact, it is these perturbations which are being influenced. To demonstrate these effects, only the first-order perturbations are considered for the velocity field. In figure 5.7, the influence of Ar on the first-order velocity perturbation is shown for the horizontal case. In general, the magnitude of the perturbation is directly proportional to Ar.

Figure 5.8 shows the variation of the first-order velocity perturbation with the channel inclination for a given Ar. Again, the magnitude of this perturbation is directly proportional to α. However, this perturbation appears to be more sensitive to changes in α than those of Ar.

Figures 5.9 and 5.10 show the variation of friction factors with the channel inclination for a range of Ar. In general, the cold wall friction factors increase proportionately with Ar but decrease with α. This predicts separation at the cold wall. Though separation is not within the scope of this analysis, an attempt has been made to determine the condition for its occurence. However, at the hot

wall, the friction factor increases proportionately with both Ar and α so that there is no likelihood of separation occuring there.

Figure 5.11 illustrates the variation of the computed critical Ar_c with channel inclination for separation to occur at the cold wall for a given Ar. Though this critical Ar for separation decreases as α increases, it is always much greater than the input Ar. Therefore the curves represent the upper limits of Ar for a given inclination.

The dimensionless bulk temperature variation with the channel inclination is depicted in figure 5.12 for various Archimedes numbers. As anticipated, the bulk temperature increases proportionately with Ar for a given inclination. For the range of Ar considered, optimum angles of inclination exist for which the bulk temperatures are maximum. These optimum inclinations, (α_{OPT}) are proportional to Ar; and in conjuction with the bulk temperature, θ_B, obey the following power Law already stated in the abstract.

In figure 5.13 the mean hot wall Nusselt numbers are plotted against the angle of inclination with Ar as the minor parameter. These plots reveal that optimum angles of inclination exist for which the mean hot-wall Nusselt numbers attain their maximum values. These maximum values, and the corresponding optimum inclinations (α_{OPT} in radians) are well correlated by the three-dimensional power Law also stated in the abstract for the range of Ar considered. These optimum inclinations lie between 30° and 60° for both θ_B and Nu_{BH}.

Figure 5.14 shows the variation of the mean hot wall Stanton number with channel inclination for various Ar. Since these Stanton

numbers are derived from the Nusselt and Peclet numbers it is not necessary to obtain a correlation equation for them and their optimum inclinations which again lie between 30^0 and 60^0.

Figures 5.15 and 5.16 are cold wall equivalents of the figures 5.13 and 5.14 respectively. In particular figure 5.15 portrays a very important variation. For the same range of optimum inclinations, minimum cold-wall mean Nusselt numbers are predicted. The significance of this variation is that it leads to a very important conclusion about the net heat convected. Although the heat transported to the fluid is maximum for α_{OPT} between 30^0 and 60^0, the heat lost to the cold wall is minimum. It follows therefore that the net heat convected axially must be maximum since it is proportional to the numerical difference between the hot and cold wall Nusselt numbers.

5.6 <u>Comparison of Perturbation and Steady-state Numerical solutions</u>

The parameter perturbation and the steady-state numerical analysis are solutions to the same thermal problem. Therefore it is interesting to know how well the solutions agree. In order to provide plausible basis of comparison the following conditions must be met.

1. The heat transfer and flow parameters must be evaluated in the region of fully developed regime.

2. These parameters must be evaluated by the same method.

3. Since the perturbation analysis is valid for small values of Archimedes number, only such values should be considered in the numerical solution.

The perturbation analysis was patterned along conditions 1 and 3.

The heat transfer parameter was then evaluated on the basis of the Bulk/wall temperature difference. The following discussion pertains to the steady-state numerical solution with regards to the three conditions.

With respect to the first condition, the channel exit approximates the region of fully developed flow. The second condition requires that the mean local Nusselt number at the channel exit be based on the bulk/wall temperature difference as was done for the perturbation solution. It will be recalled that a third degree polynomial temperature profile was fitted near the wall. By consideration of the relevant thermal boundary conditions the normal temperature gradient at the wall was deduced. From Fourier's Law of heat conduction in one-dimension, it was established that the dimensionless form of this temperature gradient at the wall represented the local Nusselt number. Since the velocity field was presumed fully developed, the local non-dimensional bulk temperature was computed. To obtain the corresponding local mean Nusselt Number based on the bulk/wall temperature difference, a sample calculation, for $\alpha = 30^O$ and $Ar = 0.050$, follows.

$Gr = 500; \quad Re = 100$

The local Nusselt number at channel exit, $Nu_L = \left.\dfrac{\partial \theta}{\partial y}\right|_{y=1.0} = 1.2910$

Dimensionless local bulk temperature, $\theta_B = \dfrac{\int_0^1 u\theta dy}{\int_0^1 u dy} = 0.387$

Dimensionless wall temperature, $\theta_{hw} = 1.00$

∴ Dimensionless bulk/wall temperature difference

$$= (\theta_{hw} - \theta_B) = 0.613$$

∴ Local mean Nusselt number at channel exit,

$$Nu_{BH} = \frac{\frac{\partial \theta}{\partial y}\Big|_{y=1.0}}{(\theta_{hw} - \theta_B)} = \frac{1.291}{0.613} = 2.106$$

The corresponding Stanton number $St_{BH} = \dfrac{Nu_{BH}}{RePr}$

$$= \frac{2.106}{100 \times 0.73}$$

$$= 0.0288$$

From the results of the numerical solution, the dimensionless mean velocity, v_{mean}, at the section considered is given by

$$v_{mean} = \frac{\int_0^1 u\,dy}{\int_0^1 dy}$$

$$v_{mean} = 0.913$$

Using equation (4.34), for Re = 100,

$$C_{f_{BH}} = 0.1290.$$

The following table illustrates the perturbation and Numerical results for the Nusselt, Stanton numbers and friction coefficients for Re = 100, Gr = 500 and Ar = 0.050.

TABLE 5.1. COMPARISON OF PERTURBATION AND NUMERICAL RESULTS

α	Mean Nusselt Number, Nu_{BH}		Mean Stanton number, St_{BH}		Mean Friction Factors, f_{BH}	
	Numerical	Perturbation	Numerical	Perturbation	Numerical	Perturbation
0°	2.080	2.024	0.0285	0.0277	0.1240	0.1200
30°	2.106	2.038	0.0288	0.0279	0.1290	0.1242
45°	2.107	2.043	0.0288	0.0280	0.1319	0.1260
60°	2.114	2.047	0.0289	0.0280	0.1333	0.1280
90°	2.118	2.051	0.0290	0.0281	0.1320	0.1280

Figures 5.17 and 5.18 depict respectively, the variation of the Nusselt number and friction factors with α for Nu_{BH} and f_{BH}. However, because of the choice of scale, the disparity between the solutions has been graphically exaggerated. From the tabulated values, for any given α, the results differ by about 5% for the Nusselt numbers, 4% for St_{BH} and f_{BH}.

5.7 Computation of Physical quantities (Dimensional)

In order to realise the physical magnitudes of the space variables involved, it is proper to translate the dimensionless variables into their dimensional equivalents. This will be done for air whose physical properties at an ambient temperature of 35^oC are:

$$\text{Kinematic viscosity,} \quad \nu = 0.165 \text{ cm}^2/\text{s}$$

$$\text{Thermal conductivity,} \quad k_f = 0.233 \text{ cal/cm-hr}^\circ\text{C}$$

$$\text{Coefficient of cubical Exp.,} \beta = 3.25 \times 10^{-3}/^\circ\text{K}$$

$$\text{Density,} \quad \rho = 1.14 \text{ kg/m}^3$$

$$\text{The acceleration due to gravity,} \quad g = 980 \text{ cm/s}^2$$

Let the height of channel be $b = 6.0$ cm.

Mean velocity

For Reynolds number of 100, the mean velocity at channel inlet is given by

$$Um = \frac{Re\nu}{b}$$

$$= \frac{100 \times 0.165 \frac{cm^2}{s}}{6.0 \text{ cm}} = 2.75 \text{cm/s.}$$

(a) For the numerical scheme, the mean velocity at channel exit

$$= 0.913 Um = 2.51 \text{cm/s.}$$

(b) For the Perturbation analysis, the mean velocity at section

considered $= Um. = 2.75$cm/s.

Hence the forced convection solution is in error by 0.24cm/s.

Mean Temperature

For a Grashof number of 5000, the maximum temperature difference is obtained from $Gr = \dfrac{g(T_h - T_c)b^3}{\nu^2}$

$$\therefore \quad T_h - T_c = \frac{Gr. \nu^2}{\beta g b^3}$$

$$= \frac{5000 \times (0.165)^2 \frac{cm^4}{s^2}}{3.25 \times 10^{-3}/^\circ\text{C} \times 980 \frac{cm}{s^2} \times 2.16 cm^3 \times 10^2}$$

Simplification yields

$$T_h - T_c = 0.197 °C$$

$$\therefore \quad T_h = 35.197 °C.$$

The dimensionless mean temperature θ_m, is defined by

$$\theta_m = \frac{T_m - T_c}{T_h - T_c}$$

Solving for T_m gives

$$T_m = T_c + \theta_m (T_h - T_c)$$

Since θ_m varies with α, consideration may be given to $\alpha = 30°$

(a) For the Numerical scheme,

$$\theta_m \Big|_{\alpha=30°} = 0.4650$$

$$\rightarrow T_m \Big|_{\alpha=30°} = T_c + (0.4650 \times 0.197) = 35.092 °C$$

(b) For the Perturbation analysis,

$$\theta_m \Big|_{\alpha=30°} = 0.5113$$

$$\therefore \quad T_m \Big|_{\alpha=30°} = T_c + (0.5113 \times 0.197)$$

$$= \underline{35.107 °C}$$

From the above rough figures it is clear that the forced convection solution is inadequate even for small rates of heating of slow flows.

5.8 Conclusions

The results of the present analytical study have been presented graphically. Many restrictive assumptions which were made in the formulation and solution of the problem, render the results obtained somewhat qualitative. The results obtained can therefore be considered as a first approximation to the solution of the physical problem. However, these conclusions can be made.

1. The perturbation analysis proves conclusively that the maximum heat transfer occurs when the angle of inclination lies between 30° and 60°. This behavioral pattern of heat transfer with inclination compares favourably with the results of Iqbal and Stachiewicz [11] who used the Rayleigh number as their expansion parameter for a constant heat flux problem for Pr = 0.73 for tubes.

2. The existence of optimum inclinations between 30° and 60° for which the heat transfer to the cold wall is minimum, lends strong support to the first conclusion.

3. A rigorous comparision between the present analysis and the numerical solution for Case A, shows that the former is at variance with the latter by about 5% for the heat transfer and flow parameters computed.

4. The perturbation method when properly employed could be a useful tool in solving the governing partial differential equations which describe mixed convective phenomenon.
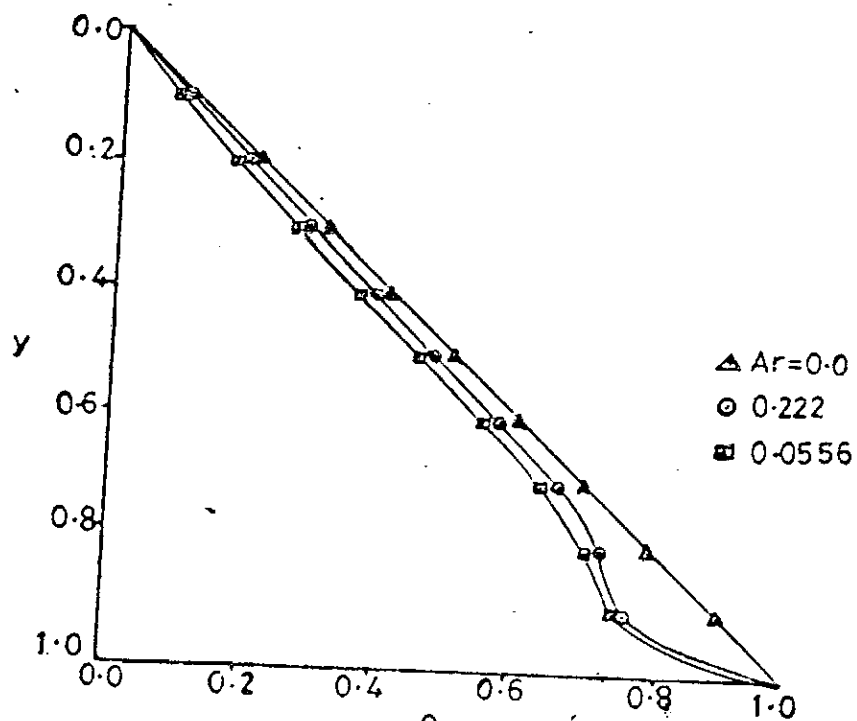
Fig·5·1· Influence of Archimedes number.
on dimensionless temperature
distribution across channel
for Pr=0·73 and α=60°,
(0 <Gr≤5000 ;150≤Re≤300).
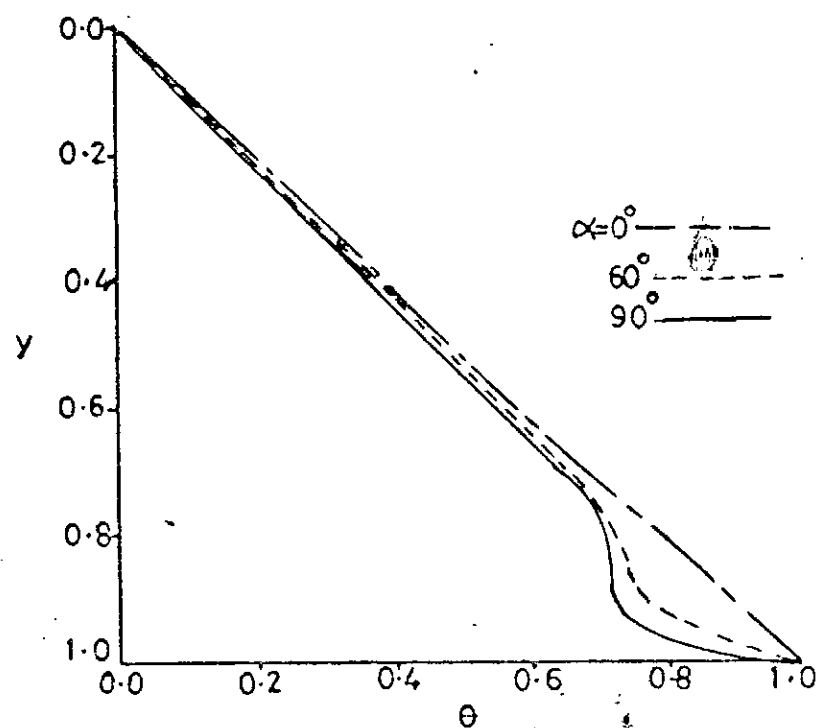
Fig. 5-2. Influence of channel orientation on dimensionless temperature profile across channel for $Pr=0.73$ and $Ar=0.222$, ($Gr=5000$; $Re=150$).
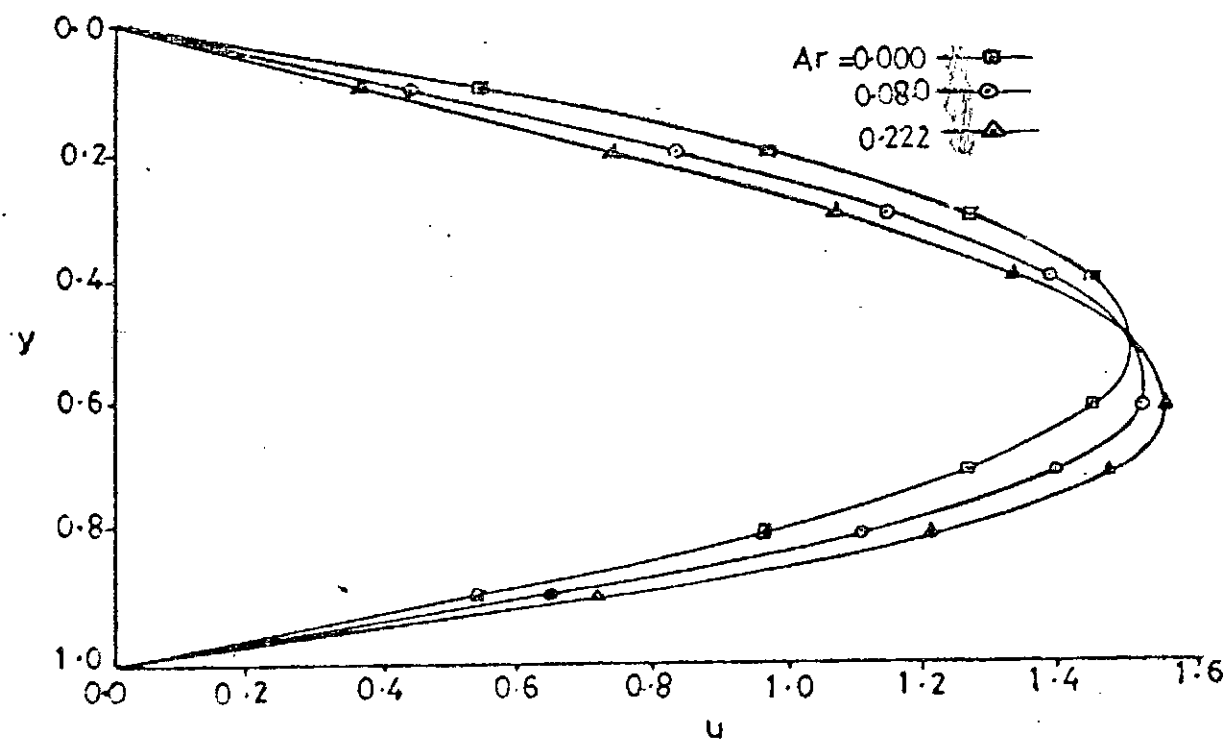
Fig. 5-3. Influence of Archimedes number on dimensionless longitudinal velocity profile across channel for Pr=0·73 and $\alpha = 60°$ ($0 \leqslant Gr \leqslant 5000$; $150 \leqslant Re \leqslant 250$).
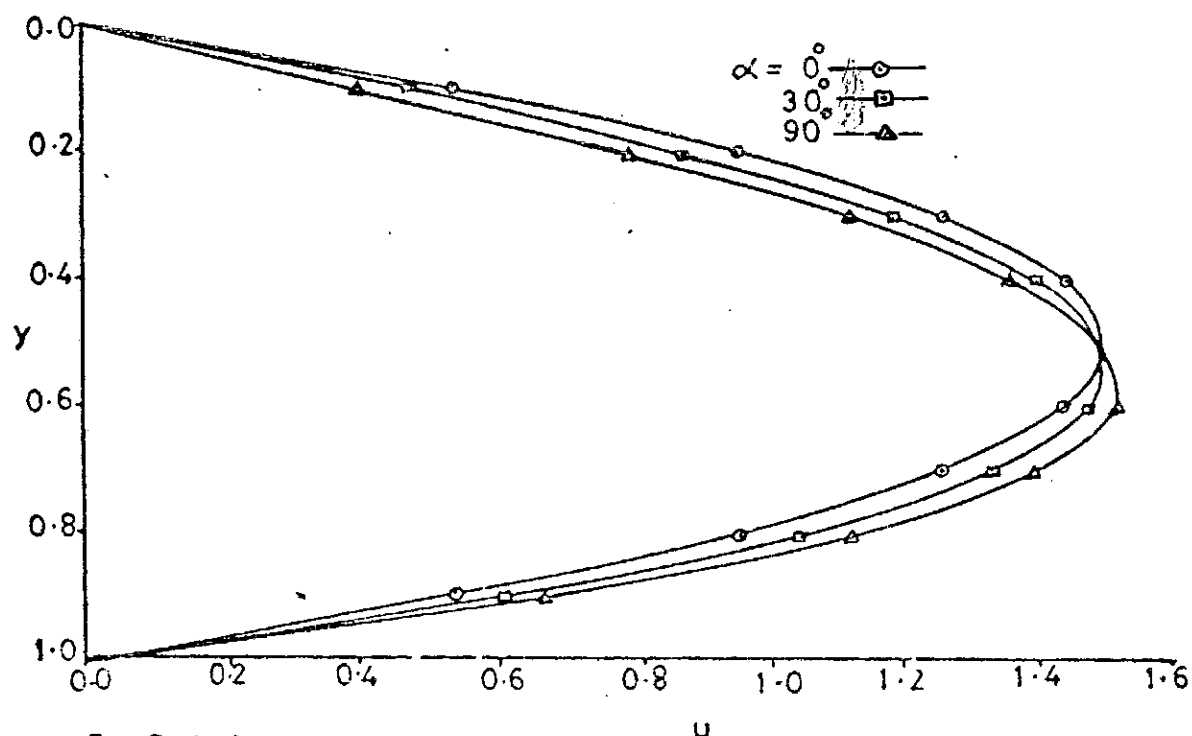
Fig. 5-4 Influence of channel orientation on dimensionless longitudinal velocity Profile across channel for Pr = 0.73 and Ar = 0.080, (Gr = 5000 ; Re = 250).
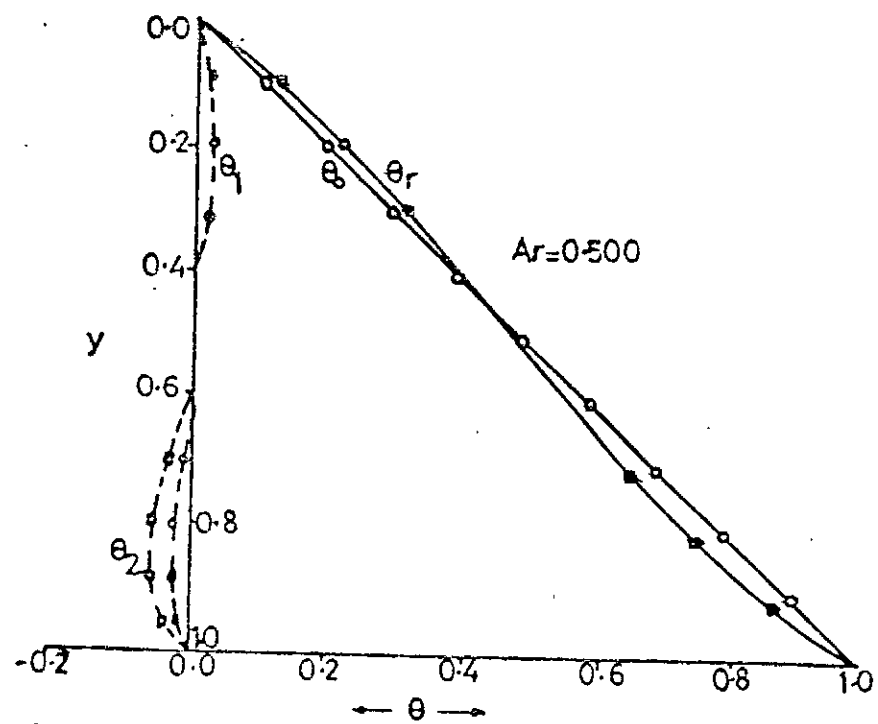
Fig 5-5. Solutions for θ_0, θ_1, θ_2 and the resultant temperature, θ_r for Gr=5000; Re=100; Pr=0.73, $\alpha=0°$.
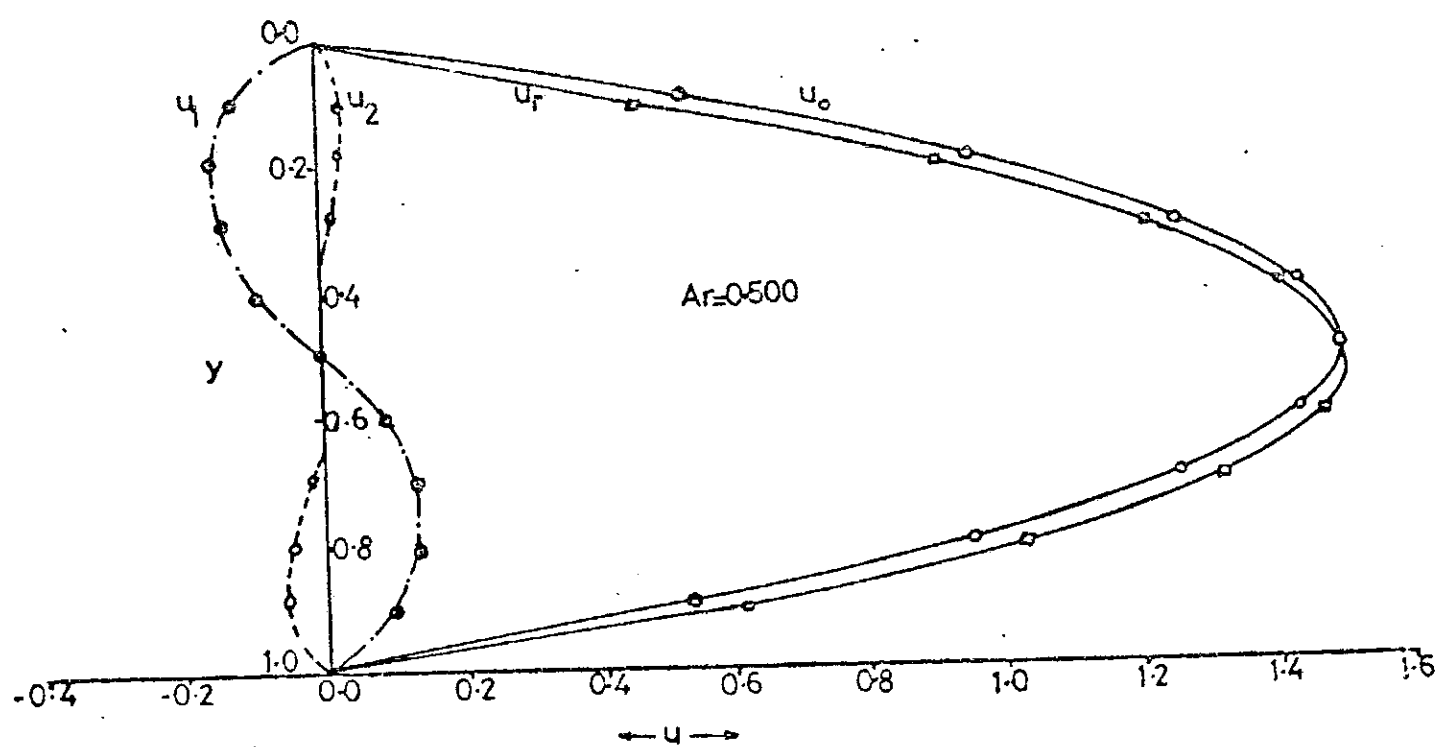
Fig.5-6. Solutions for $u_0; u_1; u_2$ and the resultant velocity, u_r for $Pr = 0.73$; $Gr = 5000$; $Re = 100$ and $\alpha = 0$.
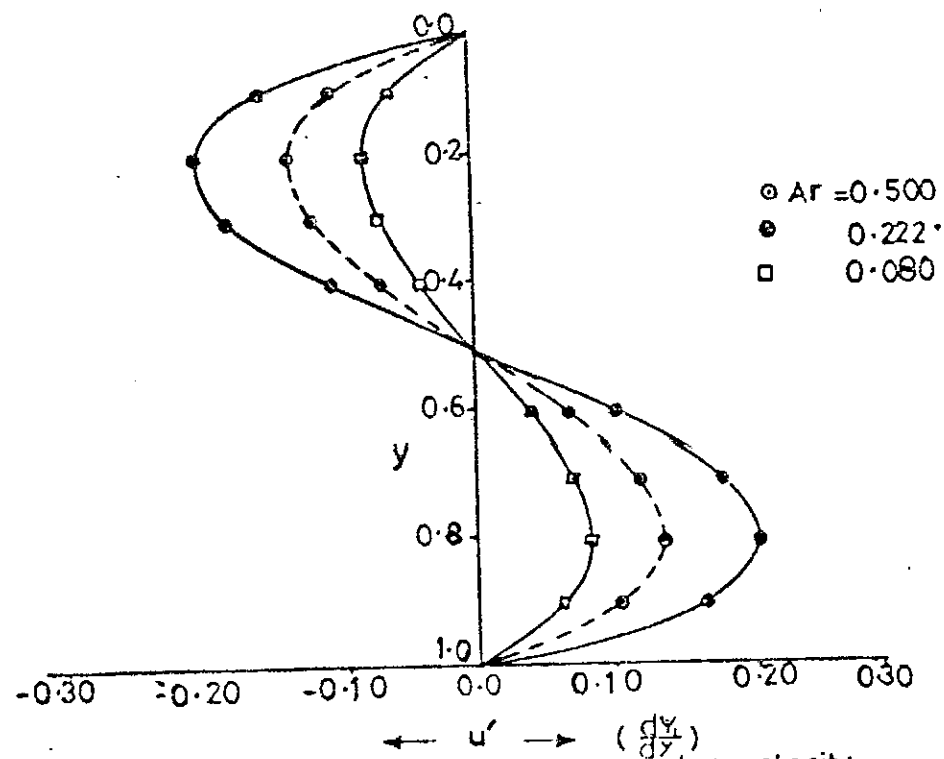
Fig.5-7. Influence of Ar on the first-order velocity
Perturbation for Pr=0 73, $\alpha=0°$,
(Gr=5000; 100≤Re ≤250).
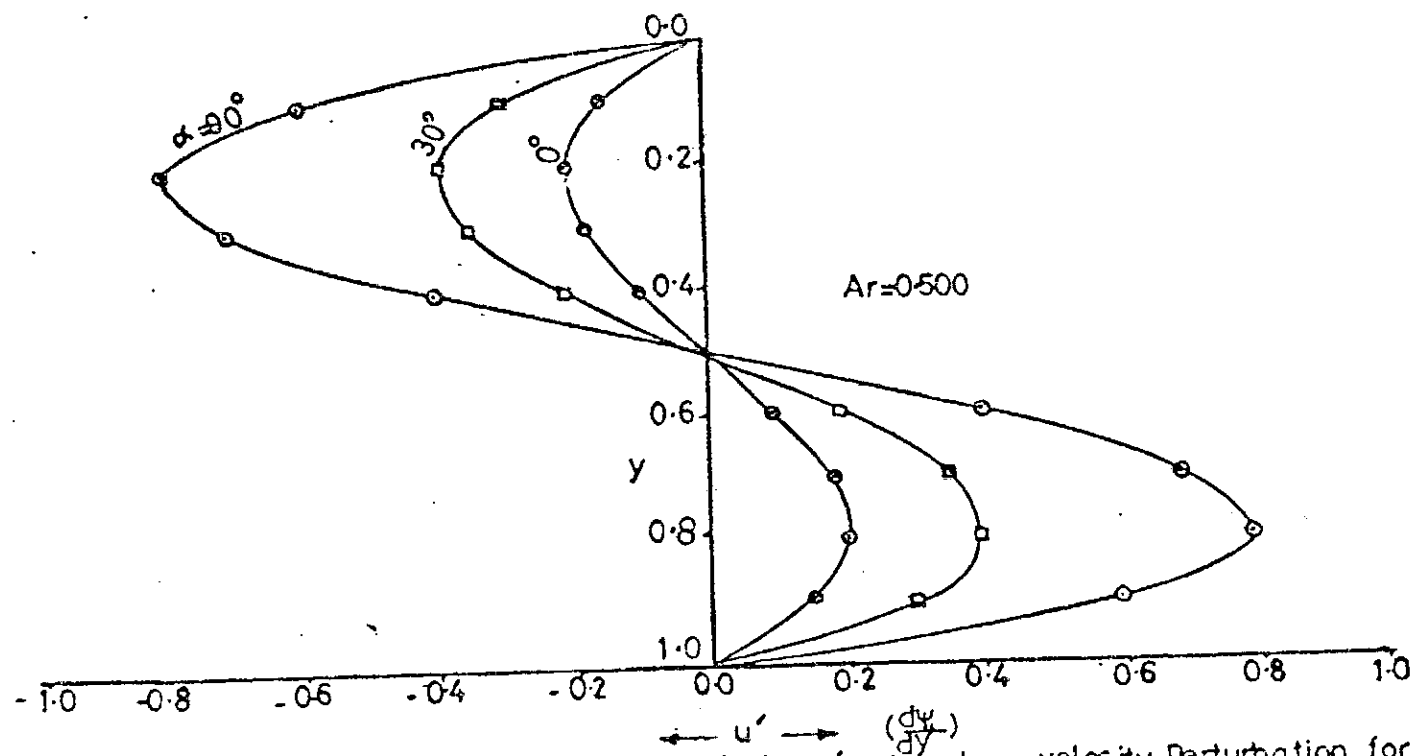
Fig. 5-8. Influence of channel orientation on the first-order velocity Perturbation for Pr=0.73, Gr=5000 and Re=100.
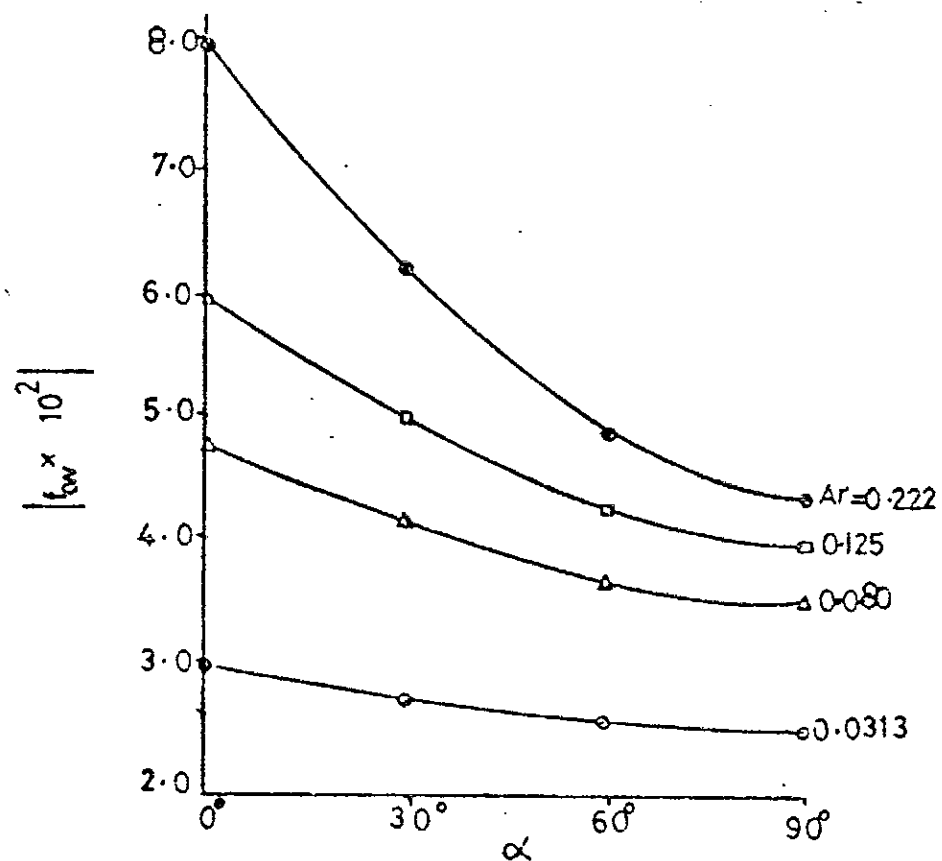
Fig 5-9. Influence of channel orientation on the coldwall friction factor for Pr=0.73 with Ar as Parameter, (Gr=5000 ; 150 ≤ Re ≤ 400).
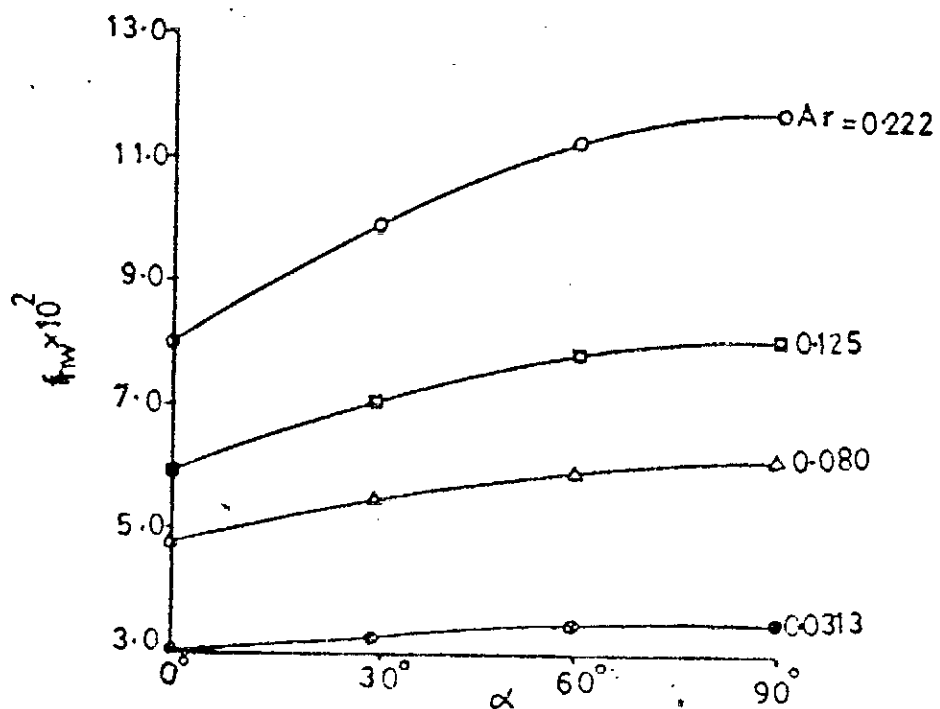
Fig. 5-10. Effect of channel orientation on the hotwall friction factor for Pr = 0.73 with Ar as Parameter. (Gr = 5000, 150 ≤ Re ≤ 400).
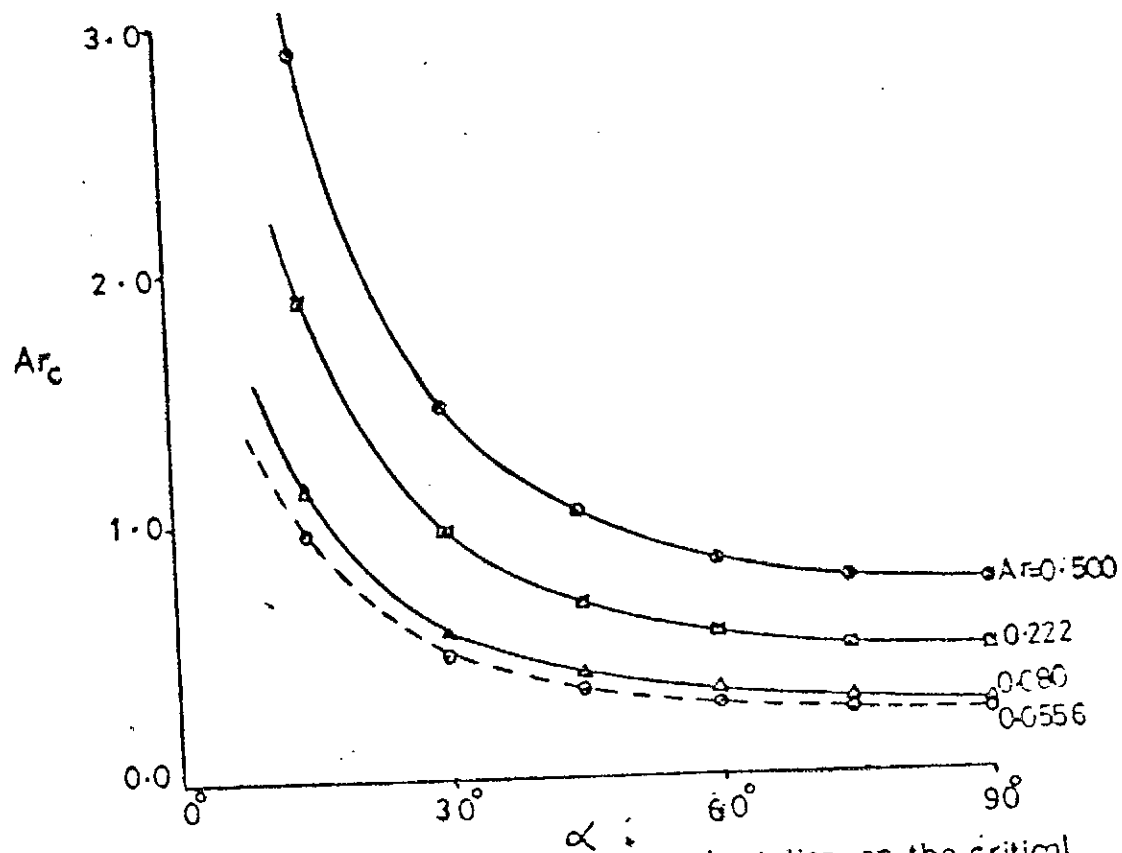
Fig. 5-11. Influence of channel orientation on the critical Archimedes number (Ar_C) required for separation to occur at the coldwall for $Pr = 0.73$ with Ar as parameter, ($Gr = 5000$; $100 \leqslant Re \leqslant 300$).
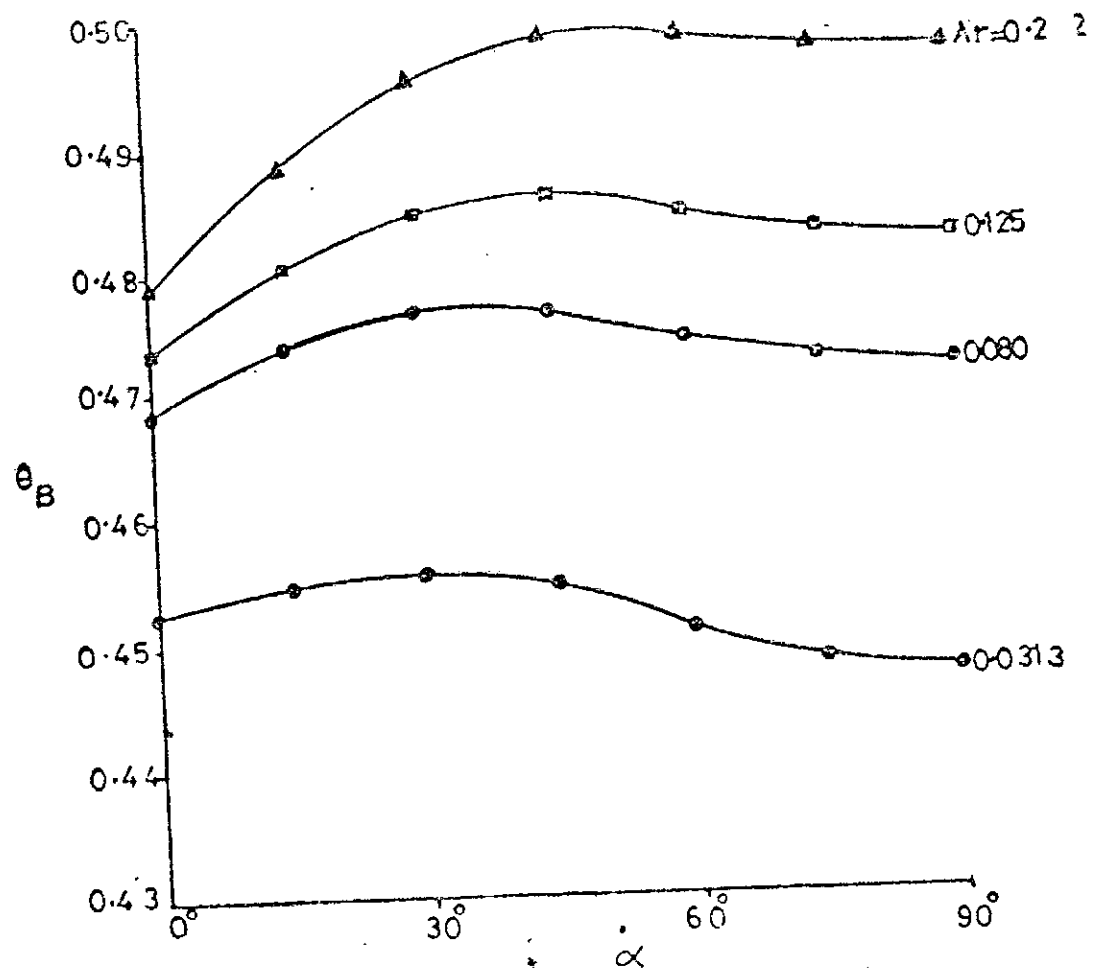
Fig. 5·12· Variation of non-dimensional bulk
temperature with channel orientation
for various Ar and Pr= 0·73,
(Gr=5000 ; 150 ≤ Re ⟨400).
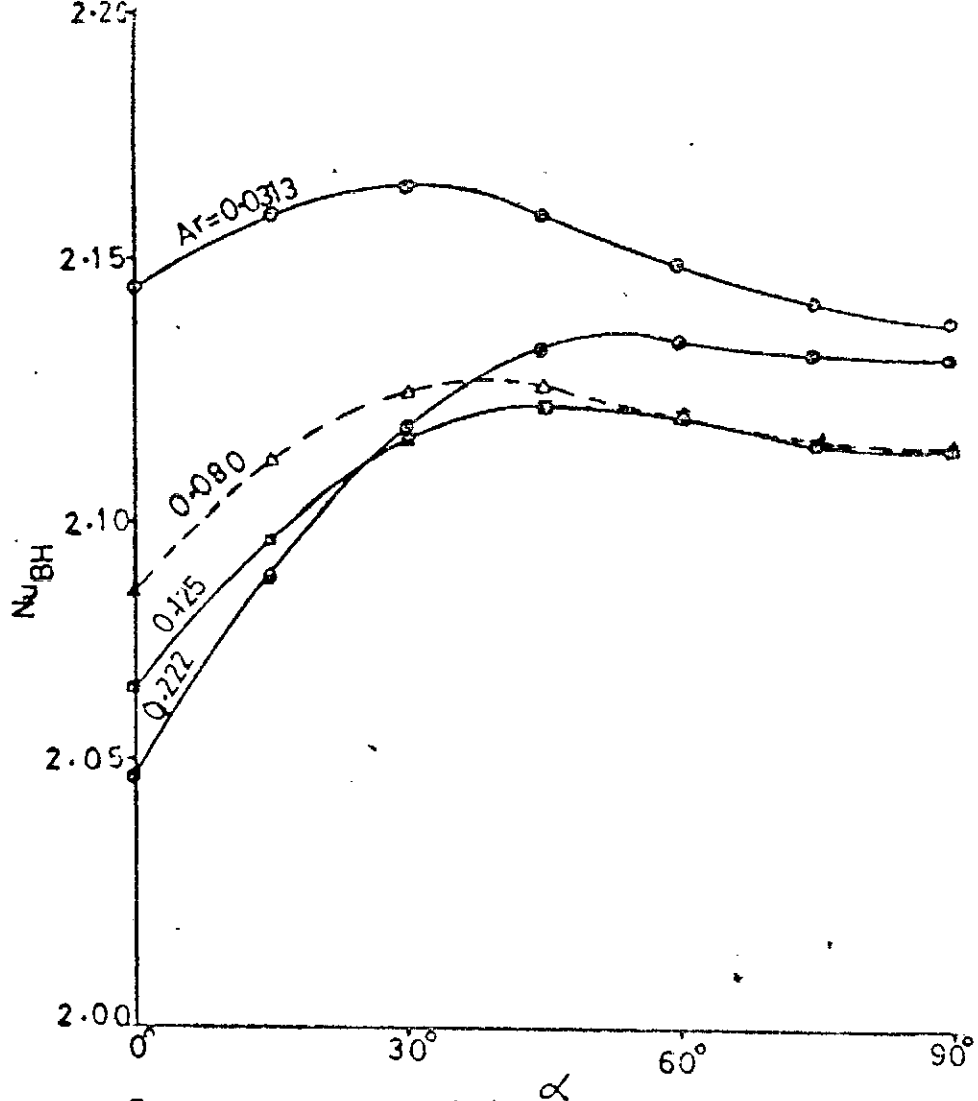
Fig. 5-13. Influence of channel orientation on the mean hotwall Nusselt number for various Ar and Pr=0.73, (Gr=5000; 150 ≤ Re ≤ 400).
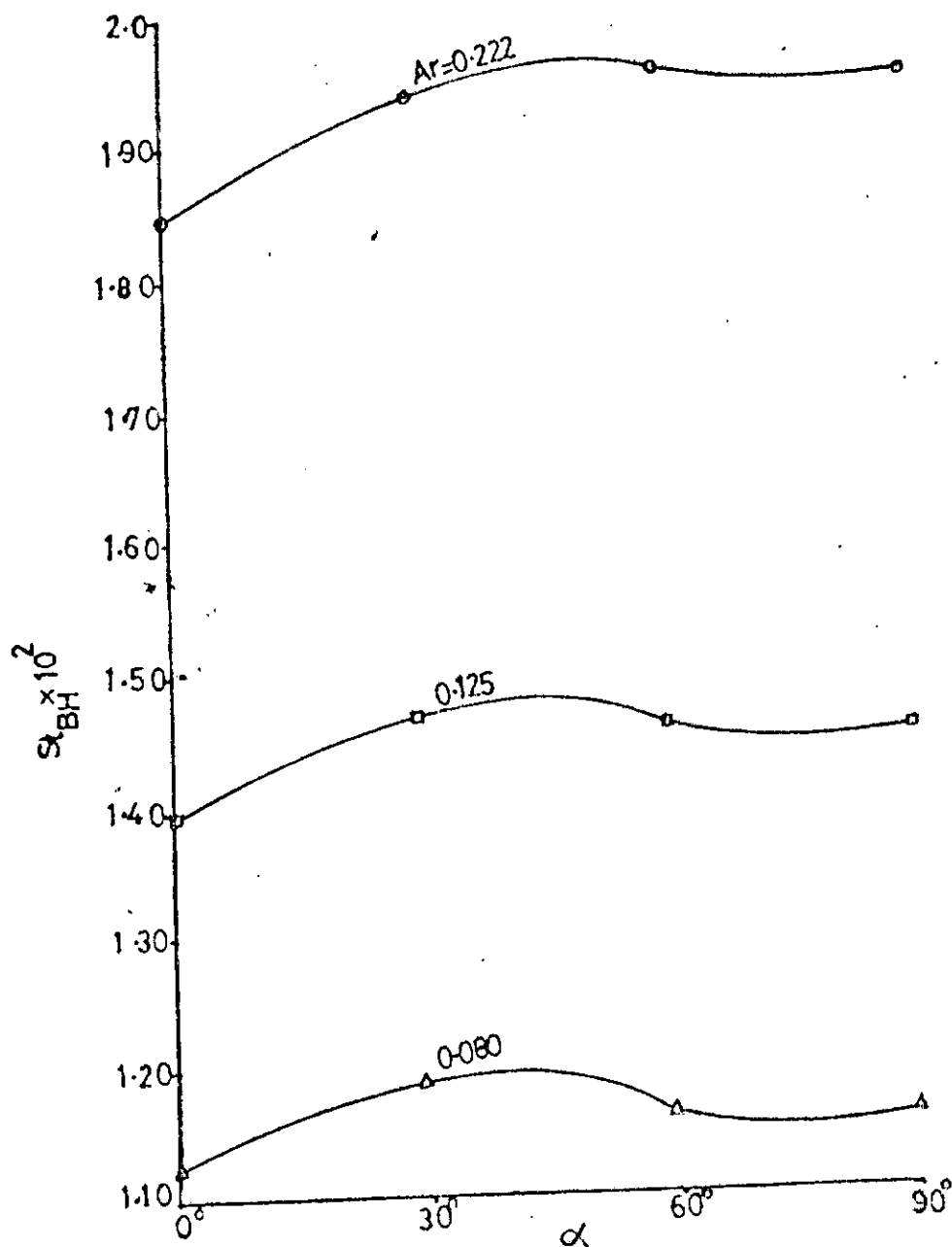
Fig.5.14. Variation of the mean hotwall Stanton number with channel orientation for various Ar and Pr=0.73, (Gr=5000; 150⩽Re⩽250).
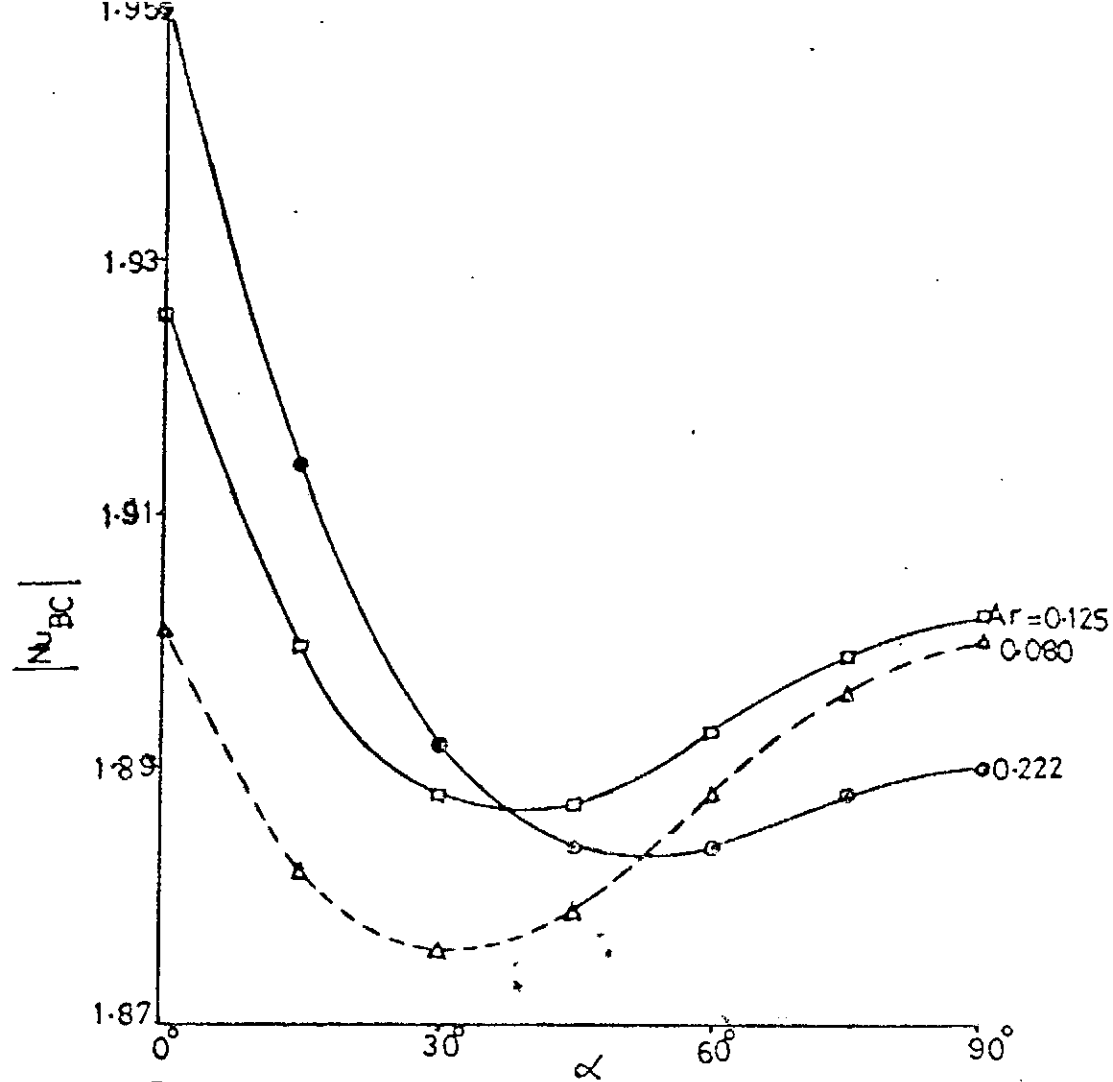
Fig. 5.15. Influence of channel orientation on the mean
coldwall Nusselt number for various Ar and
Pr = 0.73; (Gr=5000; 150 ≤ Re ≤ 250).
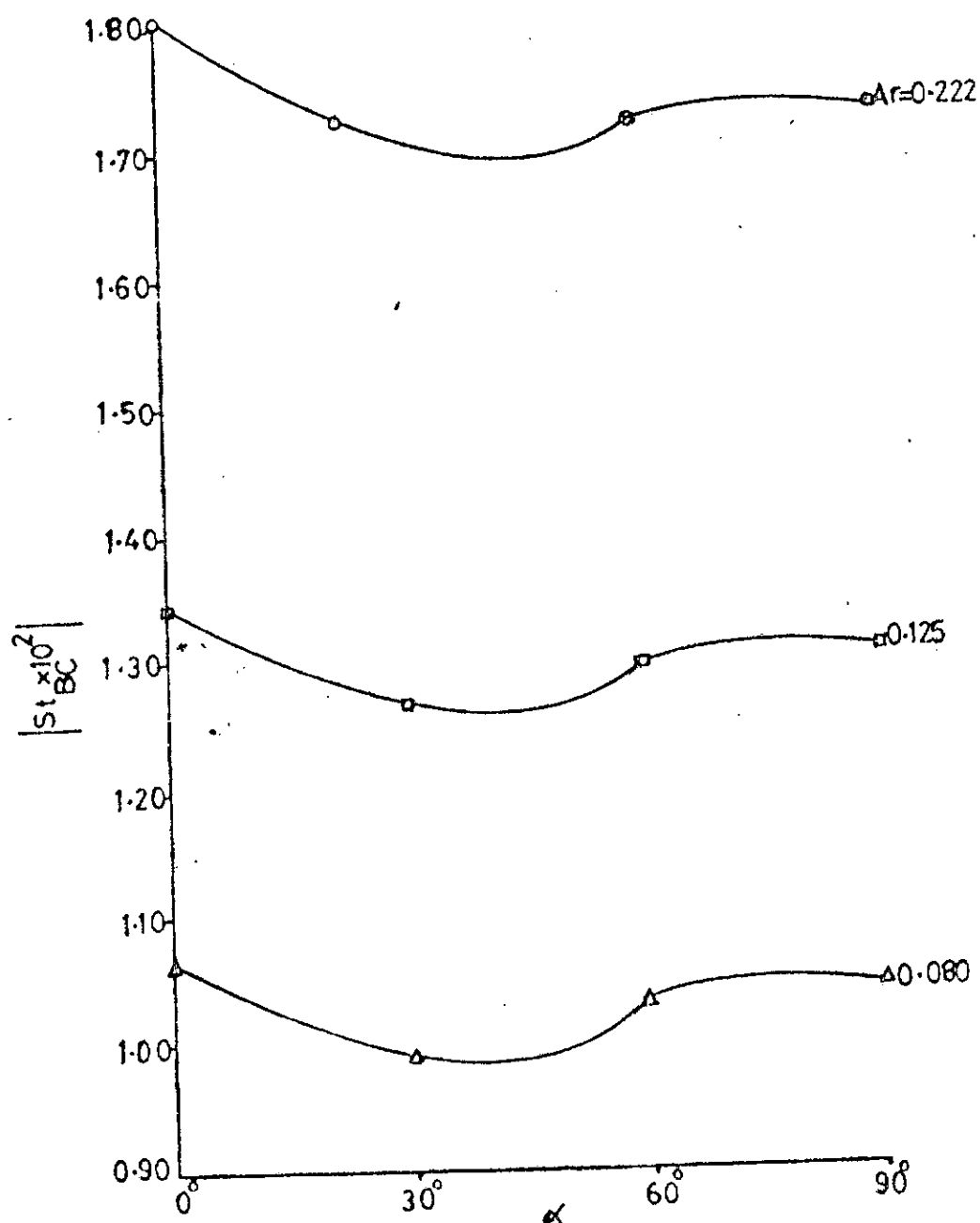
Fig. 5-16. Variation of the mean coldwall Stanton number with channel orientation for various Ar and Pr=0.73, (Gr=5000 ; 150 < Re ≤ 250)
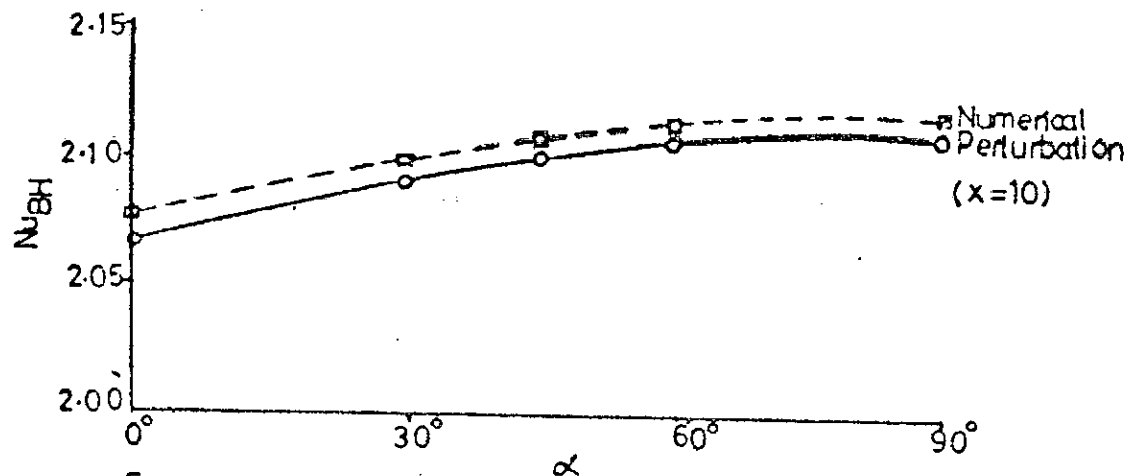
Fig.5-17. Comparison of numerical and Perturbation solutions for constant but unequal surface temperatures for $Gr=500$, $Re=100$, $Pr=0.73$. $(Ar=0.050)$
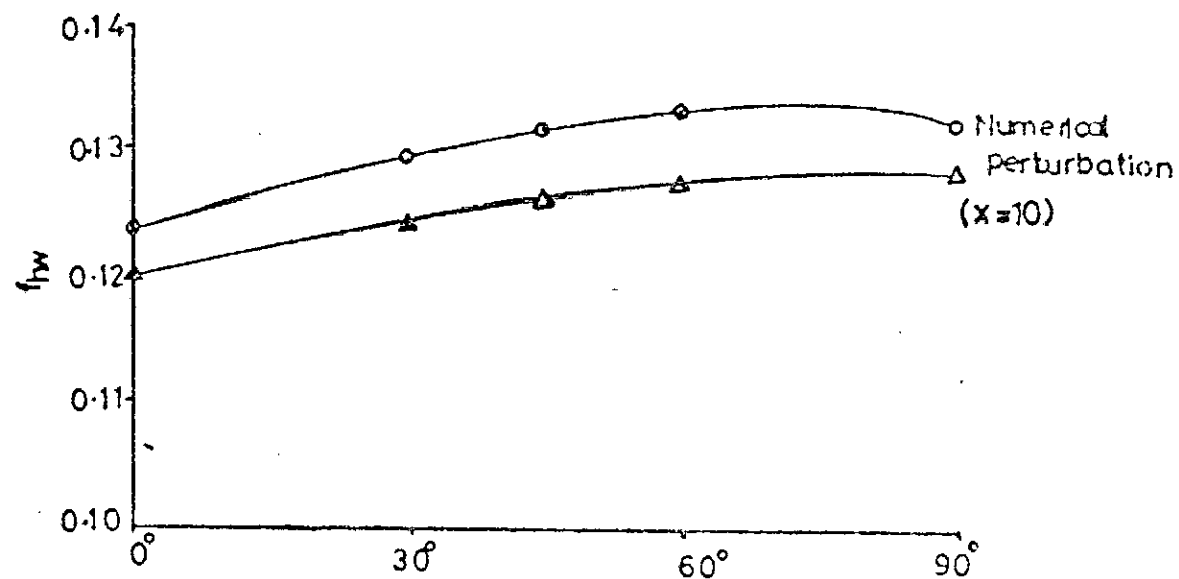
Fig. 5-18. Variation of hotwall friction factor with channel orientation for, Gr=500, Re=100, Pr=0.73 (Ar=0.050)

CHAPTER SIX

6.   EXPERIMENTAL   INVESTIGATIONS

6.1   Aim:

The purpose of the experiment is to compare experimental and predicted numerical results for the constant heatflux at the hot surface.

6.2   Experimental Set-up:

The set-up comprised various units which performed distinctive roles. The description, design and construction of each unit are presented as follows.

6.2.1 Intake Unit

The function of this unit was to draw stagnant atmospheric air and propell it down the channel. The intake unit consisted of a 38.10 cm. dia. axial blow fan mounted on a square iron framework. This was welded onto the square end of the intake duct made of galvanized steel sheet 0.16 cm. thick. The duct construction was such that the top and bottom faces sloped symmetrically about the longitudinal axis towards each other in the flow direction. The included angle of 20° between these faces was selected in accordance with the requirements of optimum flow in ducts of rectangular cross-section (Ref. 17). The top and bottom faces also flared out in the flow direction, thus increasing their respective widths from 38.10 cm. at fan end to 121.92 cm. at channel inlet.
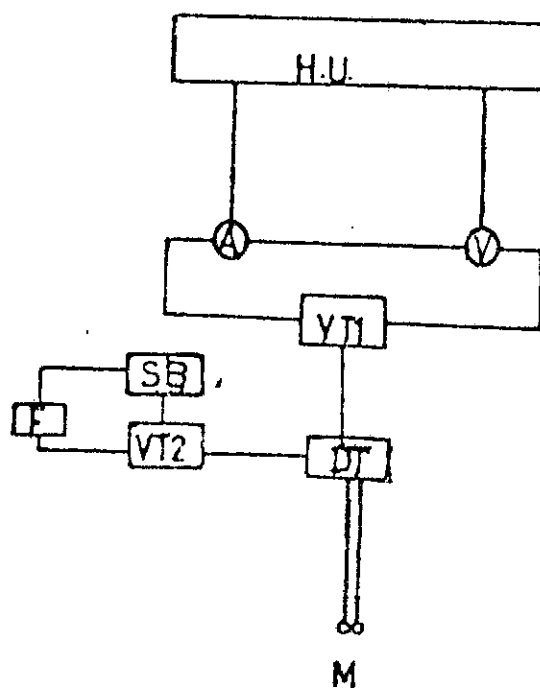
Fig.6-1. Electrical circuit diagram

H.U. : Heating Unit

V. : Voltmeter

VT1. : Variable Transformer for H.U.
DT. : Distribution Terminal
SB. : Switch Box
F. : Fan
VT 2. : Variable Transformer for F. (DISA 55D42)
A. : Ammeter
M. : Mains
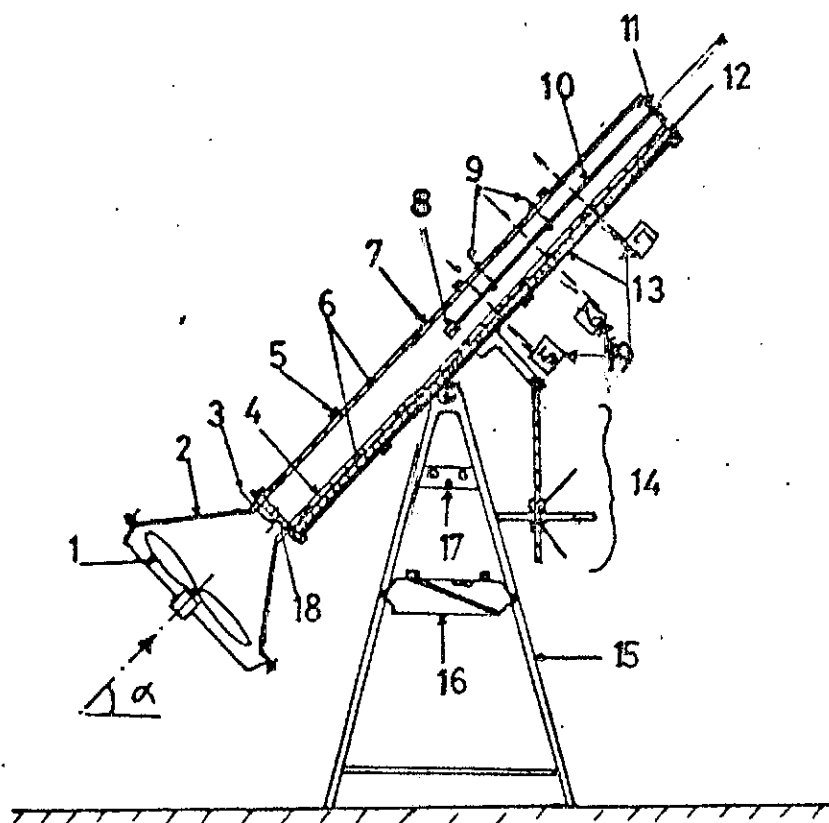
Fig.6-2 Schematic representation of assembled apparatu

1. Fan
2. Intake duct
3. Pitot tube
4. Aluminium sheet
5. Stiffener
6. Thermocouple locations
7. Perspex sheet
8. Probe
9. Traverse arms
10. Probe carrier
11. Carrier bracket

12. Heating unit
13. Insulation
14. Adjustment mechanism
15. Triangular stand
16. Inclined manometer
17. Thermocouple multi-pole
    switch board.
18. Wire gauz
19. Test Stations

The lateral plates of the intake duct were appropriately cut and bent at the top and bottom edges so that each side plate laped externally, the bottom and top edges of the top and bottom plates. The side plates were then rivetted and welded onto the bottom and top plates to ensure proper sealing. To prevent the resulting trapezoidal intake duct from distortion, it was flanged at the channel inlet with iron properly positioned so that it could be bolted onto the channel frame. Since the flow emanating from the fan may spiral in the longitudinal direction a fine wire gauz mounted on a 12.0 cm x 121.92 cm wooden frame was sandwiched between the channel and intake duct. The wire gauz dispersed the flow entering the channel.

6.2.2 Channel Frame.

The channel frame was made of two equally dimensioned rectangular metal frames 1.2312m x 2.4624m. These two frames were placed one directly above the other and were appropriately oriented so that the cold and hot plates could be mounted conveniently without falling off laterally. The two rectangular frames were then connected by 0.127m flat iron bars welded at each of the four corners. The resulting channel frame then appeared as a rectangular parallelopiped. Further rigidity was provided by means of welded-on extra spacers.

6.2.3 Top and Side Plates

The two vertical side and top plates were made of transparent perspex sheets 6.00 mm. thick. The side plates measured 0.12m x 2.462m. They were firmly secured to the channel frame by means of bolts and

nuts. The top plate, because of its flexibility, was provided with
transverse stiffeners at three longitudinal positions to guarantee
a flat surface.

6.2.4 Heating Unit

It consisted of the following parts:

(a) Heated Surface:

The hot surface was an electrically, indirectly heated
aluminium sheet 6.00mm thick, 1.2312m wide and 2.4624 m
long. This sheet was provided with a hole slightly offset
from each corner. Along the longitudinal mid-section, nine
equi-spaced 0.16mm dia. x 3.00 mm deep holes were drilled
for thermocouple insertions.

(b) The Electrical Heater:

The electrical heater was an aggregation of eight
smaller units measuring approximately 30.48cm x 30.48cm.
The heating element was Nichrome 3 wire. In constructing
the heater, it was desired that only one side of the high-
temperature resisting asbestos be wound to conserve
Nichrome wire and to reduce the overall resistance for the
unit. The resistance of each unit was about 124.0Ω. If
these resistances were connected in series a total of
about 992.0Ω would result. From Ohms Law, for an imposed
voltage of 240.0V, the current produced would be 0.24A.
From Joules Law of electrical heating, the heat produced
would be small for this case. Since the medium of heat

transport within the channel was air, the need to use quite high heat rates was obvious as the thermal conductivity of air is very low. Two possibilities existed for procuring higher heat rates. One was to step-up the voltage and the other was to reduce the effective resistance in the circuit. The latter possibility was chosen. The eight satellite heating units were connected in parallel so that the net resistance in the circuit became approximately 16.0Ω.

The eight satellite heating units were sandwiched between asbestos sheets and placed on the lower rectangular frame. Nine equidistant holes are made along the mid-plane for thermocouple wires to pass through after the Aluminium sheet had been placed on the heating unit. To improve proper thermal contact and check the movement of the Aluminium sheet it was bolted down at the four corners. Figure 6.1 shows the electrical circuits.

6.2.5 Support Unit:

This consisted of two reinforced triangular stands each carrying a ball bearing at its apex. Two short metal pipes each 6.0cm long were placed transversely and welded onto the two long sides of the lower rectangular frame. These pipes were placed closer to and equidistant from the fan end. This ensured that there was adequate ground clearance when the assembled unit was inclined at large angles to the horizontal. An iron rod 1.905 cm. diameter, with its ends reduced in diameter over different lengths, passed through the

pipes. The reduced projecting ends passed through the eye of the ball bearings on the apex of the triangular stands. Since the system was free to swing about the horizontal transverse axis, it was necessary to devise a means of checking the rotation.

6.2.6 Adjustment Mechanism:

This mechanism was primarily used to check the rotation of the system about the transverse axis and to select a desired channel inclination to the horizontal. The mechanism consists of a long iron rod threaded all through. One end of the rod was flattened and a hole centrally punched to accommodate freely, a partially threaded bolt. An iron bracket was bolted onto the centre of a cross-member on the underside of the heating unit. The protruding arm of this bracket was provided with a hole and connected to the punched end of the threaded rod by means of the loose-fitting partially threaded bolt and a nut. To check the lateral movement of the dangling rod, a horizontal guide made of T-shaped iron bars was provided. The T-bars were gapped so that their separation was greater than the diameter of the threaded rod. One end of the T-bars was welded onto an L-bar which in turn was bolted at both ends to approximately the mid-section of a pair of opposite sides of the triangular stands. The threaded rod was provided with two nuts which carry extension arms to facilitate easy turning. In operation, the nuts were situated at opposite sides of the guide; one below, the other above. Metal washers were provided. By turning the nuts using the extension arms in the appropriate directions the

channel can be made to assume any desired inclination. Once this was achieved the channel was held in position by turning the nuts in opposite directions until they bored tightly on the horizontal guide. The assembled diagram of the experimental apparatus is shown in figure 6.2 with the various units clearly identified.

6.2.7 Measuring Devices:

The measuring devices consist of the following: the voltmeter and ammeter for measuring voltage and current respectively. These had a reading accuracy of $\pm 0.5\%$. The temperature measuring devices included the thermocouple potentiometer for measuring surface temperatures and the Wallac Thermo-Anemometer which measured both velocity and temperatures of the fluid. Copper-constantan thermo-couple wires were used at nine equidistant positions along the hot wall and five along the cold wall. The copper wires were soldered onto a bank of terminals of multipole electrical switches mounted on a cardboard, while the constantan wires were soldered onto the appropriate terminals of the opposite bank. By turning the switch to a chosen position the temperatures on the surfaces were obtained. The reading accuracy of the thermocouple potentiometer was $\pm 0.05^{o}C$.

The anemometer probe was mounted on 2.0m long iron rod and it is oriented in such a way that it faced the flow directly. Before using the anemometer which was graduated both in m/s air-speed and ^{o}C air temperature, the zero-error was noted for air velocity.

The angle of inclination to the horizontal was obtained by means of a protractor and a simple pendulum. The pressure drop at the

channel inlet and hence the inlet air speed was obtained by means

of a boundary layer probe and an inclined manometer.

6.3   Experimental Runs:

The channel was first calibrated for air speed at inlet using

the boundary layer probe installed at the inlet and connected by

means of flexible tubing to an inclined manometer. The initial

manometer reading was noted. For a known variable transformer

(DISA 55 D42) setting, the new manometer reading is noted. The

procedure is repeated for other transformer settings. Using potential

flow theory and Bernoulli's equation, the corresponding velocity at

inlet can be estimated. Plots of Pressure drop and intake velocity

vs. Variable Transformer (DISA 55 D42) setting in m/s air speed are

obtained. Hence for very low settings of the transformer it was

possible to obtain by extrapolation the inlet velocity and pressure

drop from figure 6.3.

For a given fan speed and voltage, the system was allowed to run

until steady state was achieved. To ascertain this, surface tempe-

rature readings at chosen locations were taken at intervals of 15

minutes until no appreciable changes occur. It was found that 2 to

3 hrs elapsed before steady state was achieved. For each angle of

inclination, starting from 0° to 75° at intervals of 15°, three

experimental stations 5,6,7, were considered. At each station,

velocities and temperatures at specific points across the channel,

were measured using the thermo-anemometer. Three experimental runs

were made. For some practical reasons , it was not possible to

conduct the experiment for inclinations greater than 75°. Also,

it was not possible to use currents higher than 12.50A. This

limitation was imposed by the maximum current load of 13.0A which

the fuses could safely accommodate.

6.4 Analysis of Experimental Data

A common method of obtaining derivatives from experimental data

is to fit an analytical function with free parameters to the mesh-

point values, and then to analytically differentiate the function.

By so doing it is possible to obtain the finite-difference expressions

for the required derivatives. This procedure which was adopted

in the numerical scheme will be used in estimating the local heat

transfer and friction coefficients. The merit of this method is

that it provides an acceptable basis for comparing experimental

results with numerical predictions.

Sample computations of relevant non-dimensional parameters

such as the Reynolds, Grashof numbers, etc., are given in appendix B.

6.5 Discussion of Results

The experimental and predicted numerical results are displayed

both in graphical and tabular forms for the purpose of comparison.

Figure 6.4 represents a calibration of the channel to show the

spatial distribution of longitudinal velocity over the cross sectional

area at $x = 121.92$ cm for no heating. Clearly, for a given y-coordinate

the variation of the local longitudinal velocity with z is negligible.

Hence the assumption of a two-dimensional flow is justified.

From the recorded pressure drop, the mean inlet velocity to the channel is computed from potential flow theory. It is clear from figure 6.3 that it is relatively easy to read-off velocity values for a given pressure drop. Since the transformer settings for the three runs are known, their corresponding air-speeds at channel inlet can be obtained. These mean velocities are used in estimating the input Reynolds number. The modified Grashof number is estimated from the average longitudinal temperature gradient along the hot wall.

Fig. 6.5 depicts typical non-dimensional longitudinal velocity distribution across channel for a given station, inclination and set of non-dimensional parameters. It is observed that near the cold wall the predicted local velocities are smaller than those measured. Since the temperature potential between the cold and hot walls is significant, radiant heat exchange between the walls comes into play. Part of the radiant heat absorbed by the cold wall is invariably transferred to the cold fluid my mechanism molecular conduction, thus increasing its local velocity. This could account for the disparity in the results since numerical prediction did not take cognisance of radiation effects in its mathematical formulation. Near the hotwall the predicted local velocities are higher than those measured. However, both curves show that the local velocities near the cold wall are generally lower than those close to the hot wall - a situation anticipated.

Fig. 6.6 shows typical non-dimensional temperature profiles across channel for the same station and set of parameters used in preceding paragraph. It is clear from these graphs that numerical predictions indicate lower local temperatures than those measured except near the hot wall. The reasons aduced in the preceding paragraph to explain possible causes of higher measured local velocities near the cold plate, are also applicable here. It is interesting to note that in consonance with numerical results in chapter three, the cold wall temperature at the station considered is greater than the ambient temperature.

Figs. 6.7, 6.8 and 6.9 are plots to show the variations of predicted numerical experimental mean hot wall Nusselt numbers with channel inclination for three Power input runs. In fig. 6.7, the numerical predictions are higher than the experimental values for all inclinations, except the horizontal position. Here, the Nusselt numbers are very close. There appears to be maximum Nusselt numbers for the experimental results and numerical predictions when the inclination angle is about 30°. For inclinations greater than 45°, the Nusselt numbers for both results appear to be insensitive to changes in inclination. In figure 6.8 the experimental Nusselt numbers exceed the predicted numerical values for inclinations between 0° and 25.5°. Thereafter the predicted numerical values are higher than the experimental ones. For both curves, maximum Nusselt numbers occur between 30° and 60°. Fig. 6.9 exhibits the same pattern of variation with inclination as does fig. 6.8, except

that in the former, the difference between the experimental and predicted numerical results are more pronounced between 0° and 25.5^o. Again maximum Nusselt numbers occur for inclinations between 30° and 60°. A thorough scrutiny of figures 6.8 and 6.9 shows that the disparity between the experimental and theoretical results increases as the Archimedes number decreases, for inclinations between 0° and 25.5^o. The implication is that as the pure forced convection component becomes strong, the impact of free convection is minimized for this range of inclination considered. At inclinations less than 7.5^o the experimental curves turn upwards. This could be due to possible changes in the mode of circulation, a phenomenon predicted numerically.

Figs. 6.10, 6.11 and 6.12 show the impact of channel orientation on the mean friction coefficient and Stanton numbers at the hot wall. For purposes of comparison, the friction factors and the Stanton numbers have been plotted on the same graph using the same scale.

The experimental and predicted numerical friction factors exhibit peak values at roughly 15°. The probable cause is the change in mode of circulation as stated earlier. In fig. 6.10, the predicted numerical friction factors exceeded the experimental values for inclinations from 0° to 60°. Thereafter, experimental values are higher than the predicted numerical ones. The experimental and predicted numerical Stanton numbers are very close though the latter values are higher. Both results show that maximum Stanton numbers exist for inclinations between 30° and 45° to the horizontal.

In fig. 6.11, the experimental friction factors are less than
the numerical predictions for inclinations between 0° and 27°.
For inclinations greater than 27°, experimental results are higher
than the predicted numerical ones. However, the friction factors
in both cases show lack of appreciable sensitivity to changes in
inclination. As   expected, the Stanton numbers show similar
trends in variation with channel orientation as do the Nusselt
numbers in fig. 6.8.

In fig. 6.12, the predicted numerical friction factors are
higher than their experimental counterparts for most inclinations.
Again, the response of the Stanton numbers to changes in inclination
is similar to that of the preceding paragraph. It is generally
observed in the results that the Stanton number is approximately
half the friction factor.

6.6 Conclusion

Experimental results and numerical predictions for the mean
heat transfer and friction coefficients at the hot wall have been
compared graphically for a range of modified Archimedes numbers.
Both results strongly suggest that the heat transfer rate goes
through   maxima at inclinations between 30° and 60° to the hori-
zontal for the range of Archimedes numbers considered.

As the degree of inclination decreases below 7.5^O, multiple,
stable states are apparently possible. At 0° a stable mode is
eventually obtained. Thus the heat transfer rate was observed

both experimentally and theoretically to pass through a minimum when the angle of inclination is about 7.5°. For the range of inclinations at which maximum heat transfer occurs numerical and experimental predictions differ by 4.61% – 11.37%. Bearing in mind the various sources of experimental errors to be discussed later and numerical errors (Truncation or discretization and round-off) the discrepancy between the two results are tolerable. Therefore it can be concluded that the experimental and numerical predictions are reasonably in agreement.
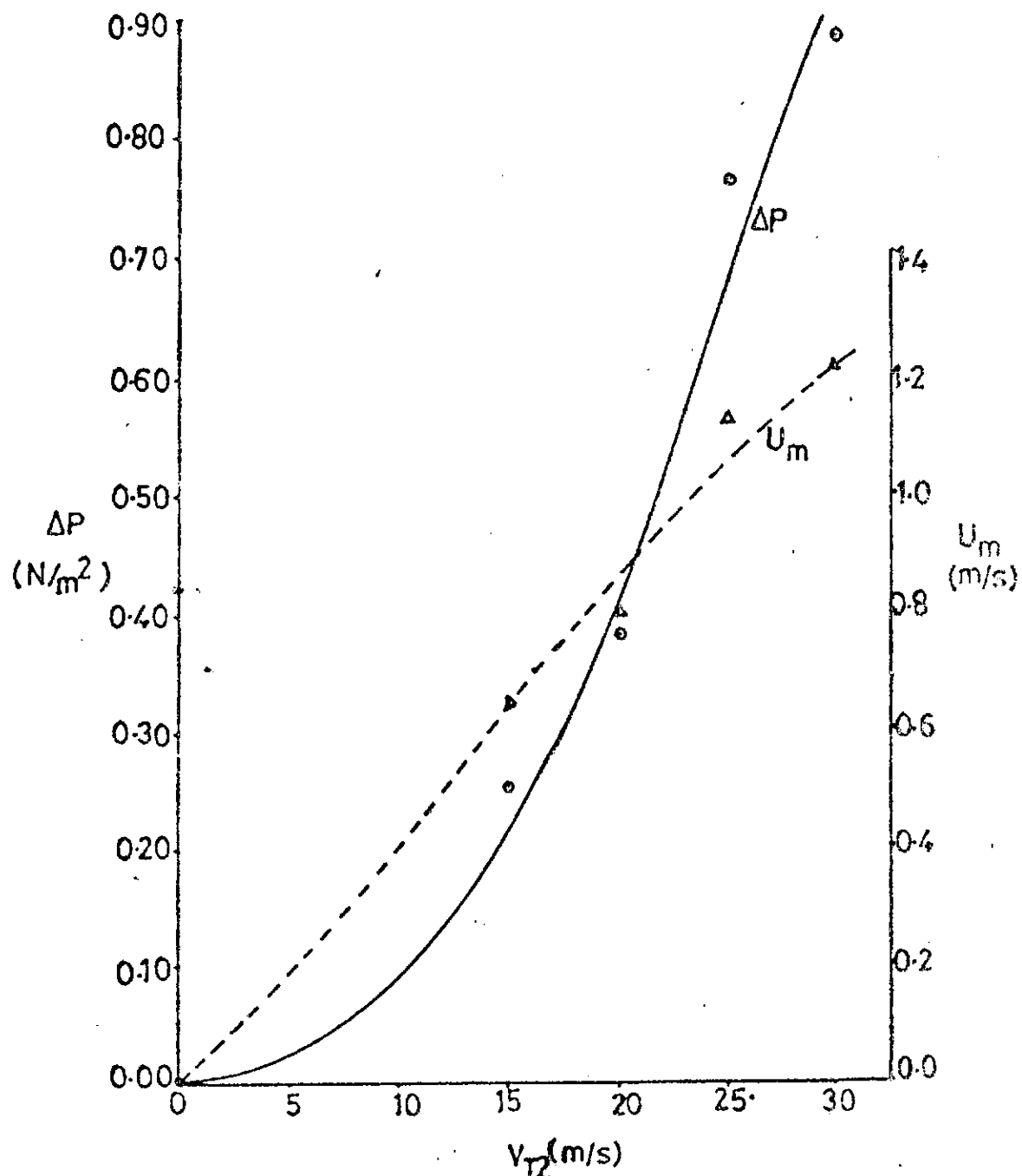
Fig 6-3 Pressure drop across channel inlet and mean inlet air-velocity Vs. Variable Transf. (DISA 55D42) Setting.
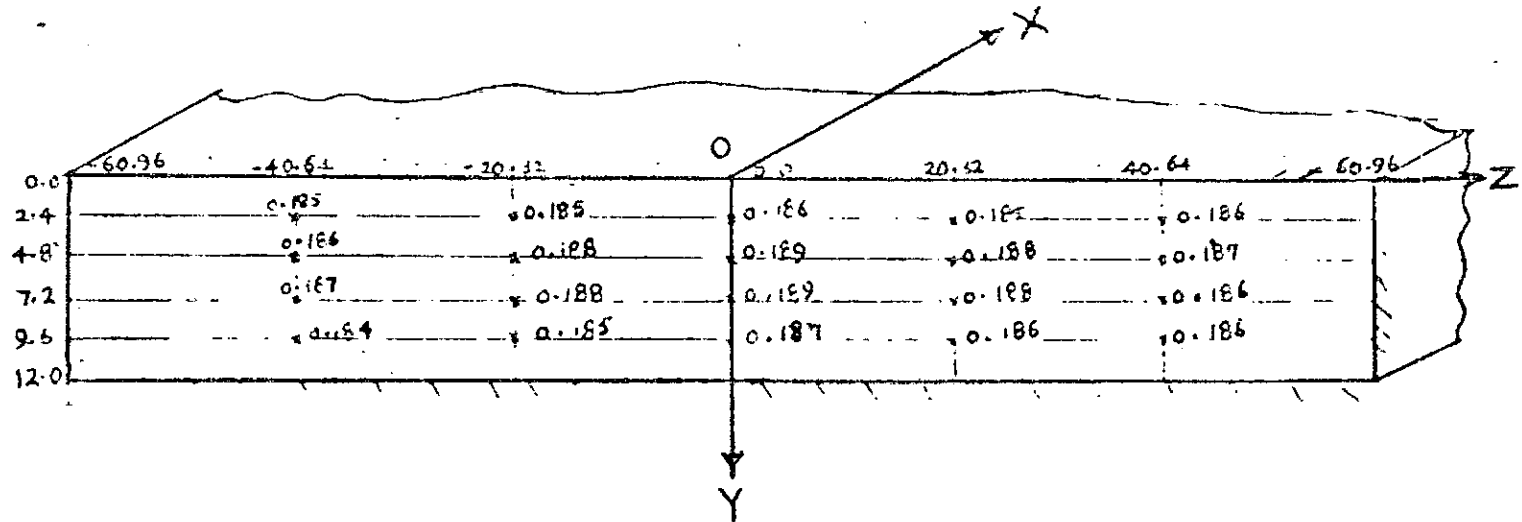
Fig. 6.4. Calibration of channel at X= 121.92 cm.
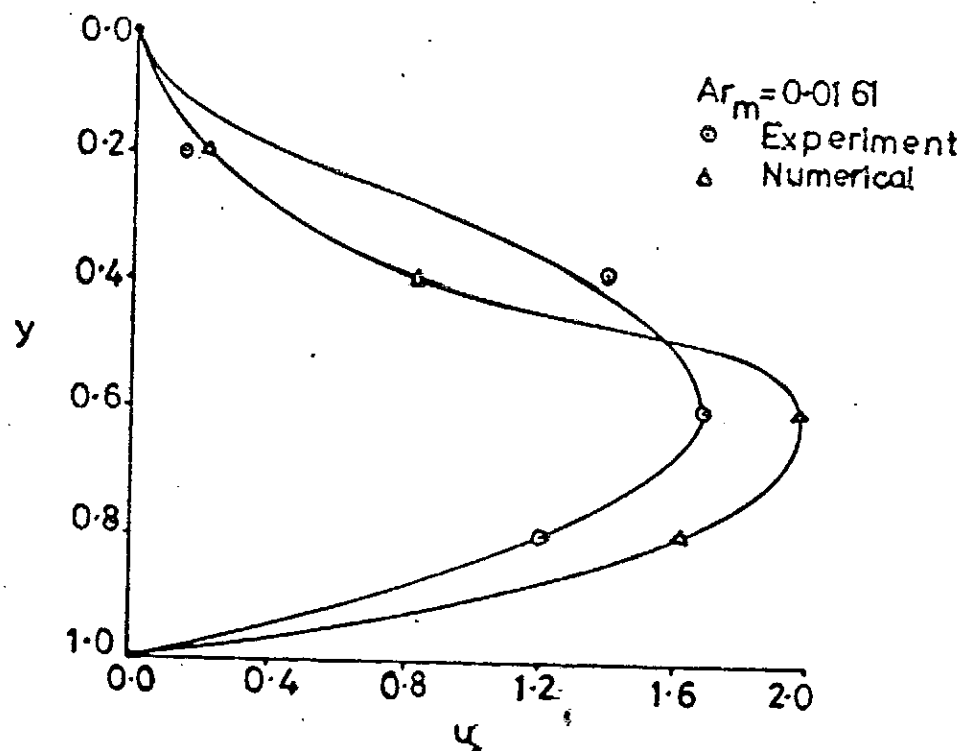
Fig. 6-5. Dimensionless longitudinal
velocity distribution across
channel at a typical station
for $\alpha = 30^\circ$; $Pr = 0.704$; $Gr_m = 28547.90$,
$Re = 1331.76$.
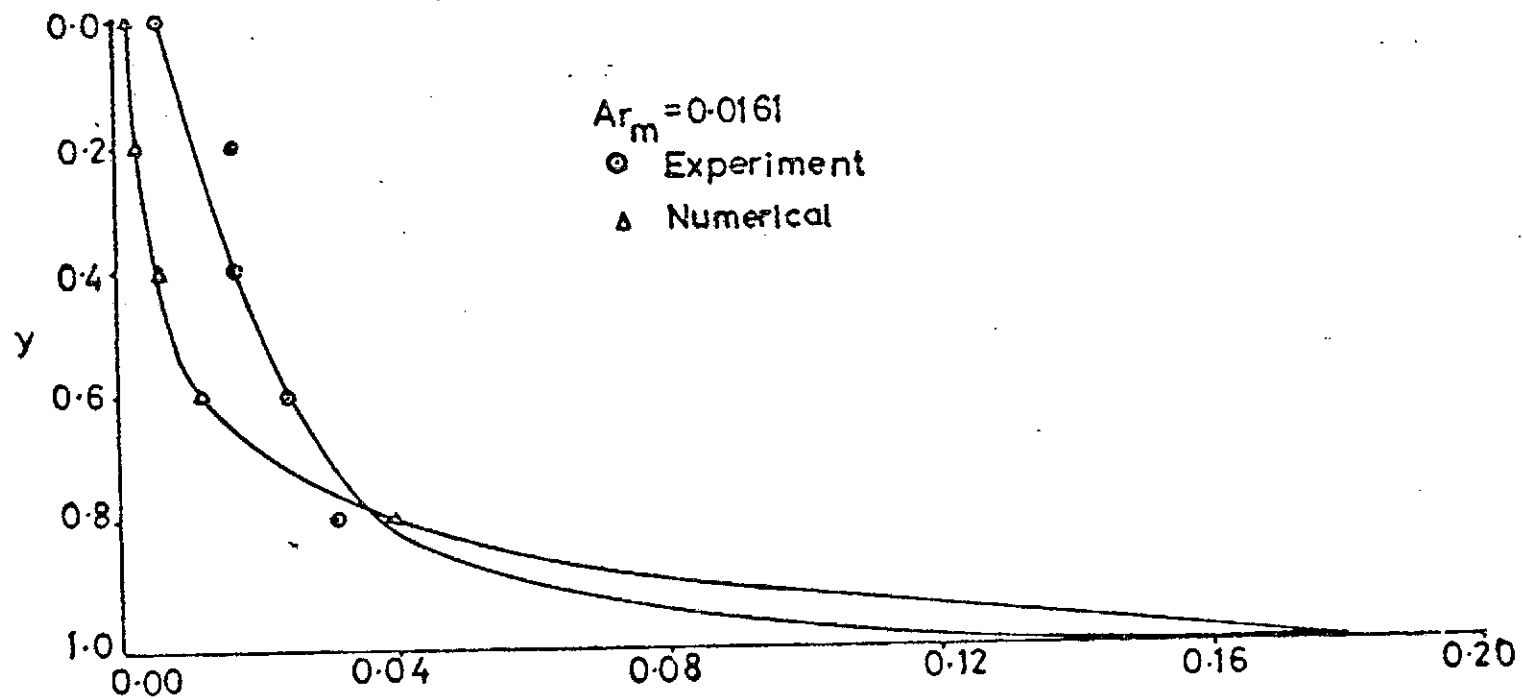
Fig.6-6 . Dimensionless temperature distribution across channel at a typical station for $\alpha = 30°$; Pr= 0.704; Gr_m= 2854790; Re =1331.76.
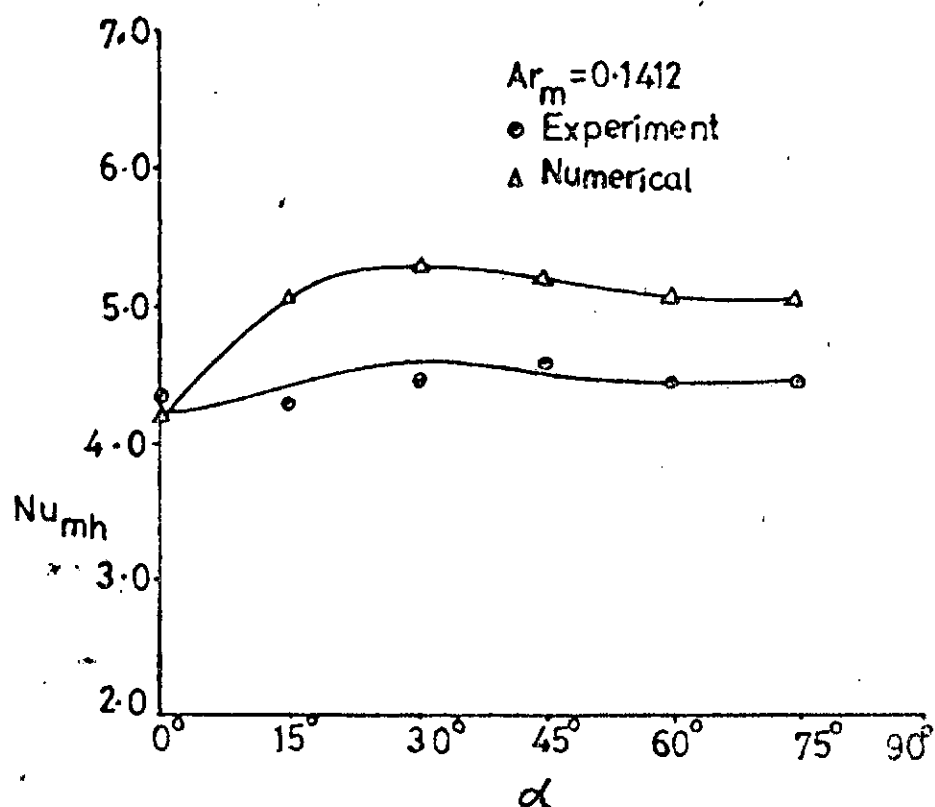
Fig. 6-7. Variation of mean hotwall Nusselt numbers with channel inclination for Re = 454·98 ; Gr_m = 29221·90 and Pr = 0·704 .
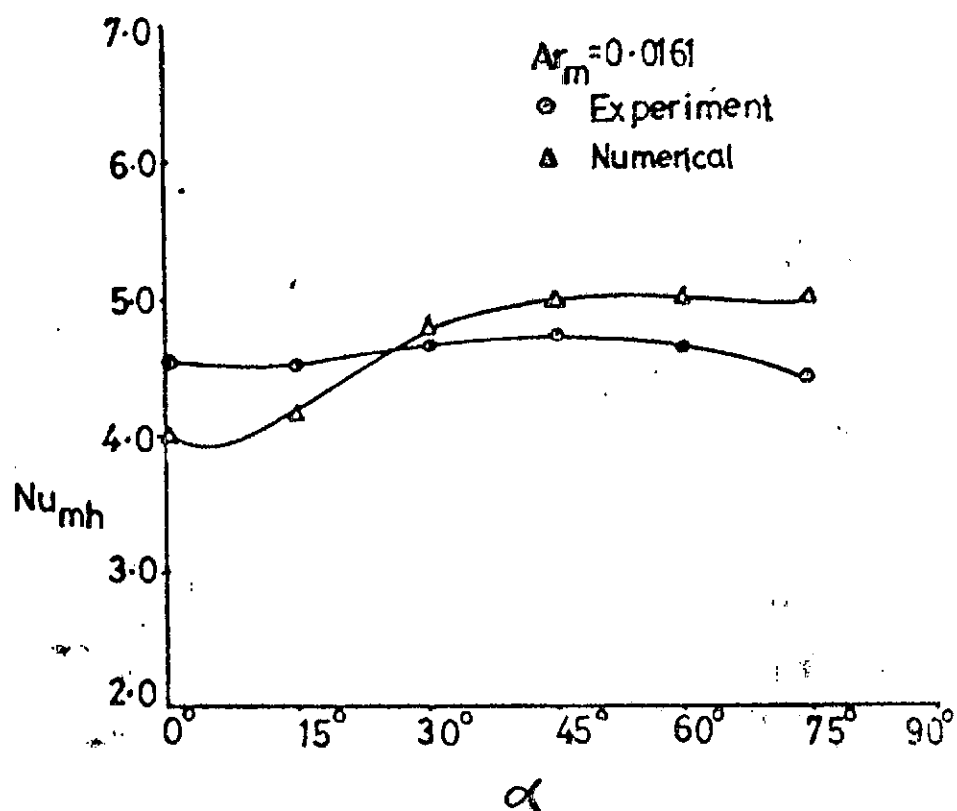
Fig.6-8. Variation of mean hotwall Nusselt numbers with channel inclination for Re = 1331·76 ; Gr_m = 28547·90 and Pr = 0·704 .
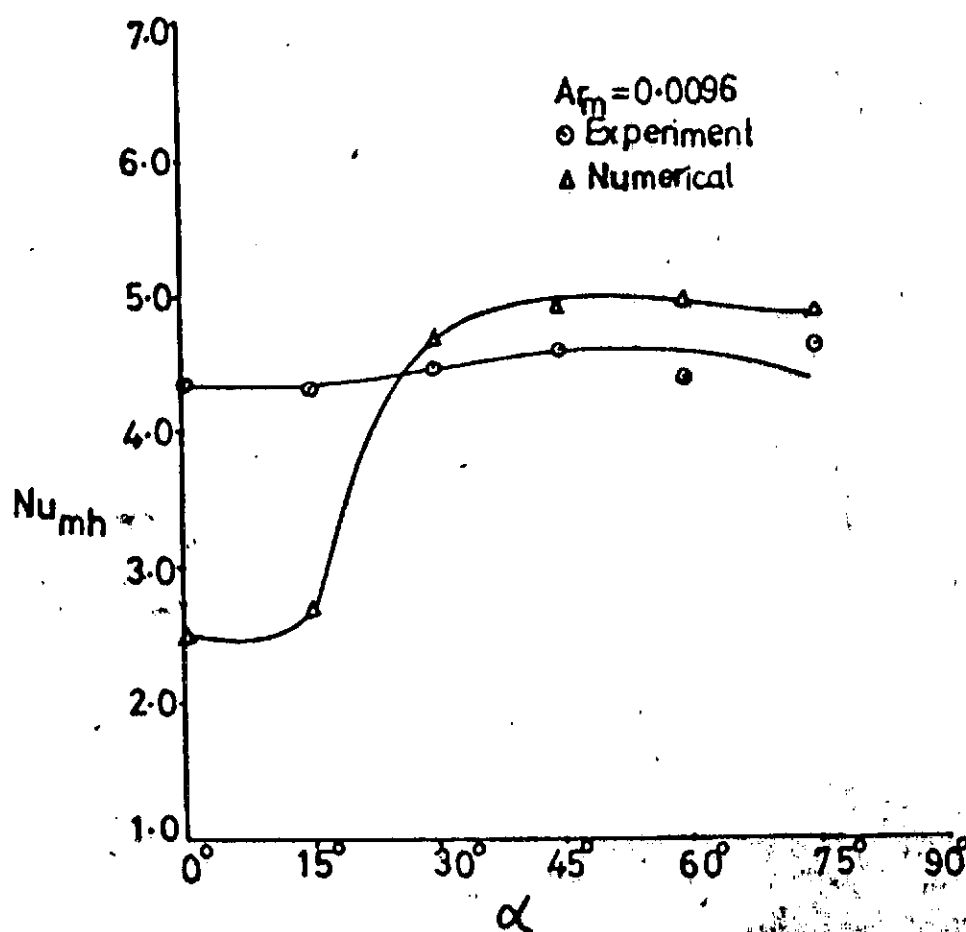
Fig. 6-9. Variation of mean hotwall Nusselt numbers with channel inclination for $Re = 2728 \cdot 82$; $Gr_m = 7171010$ and $Pr = 0.704$.
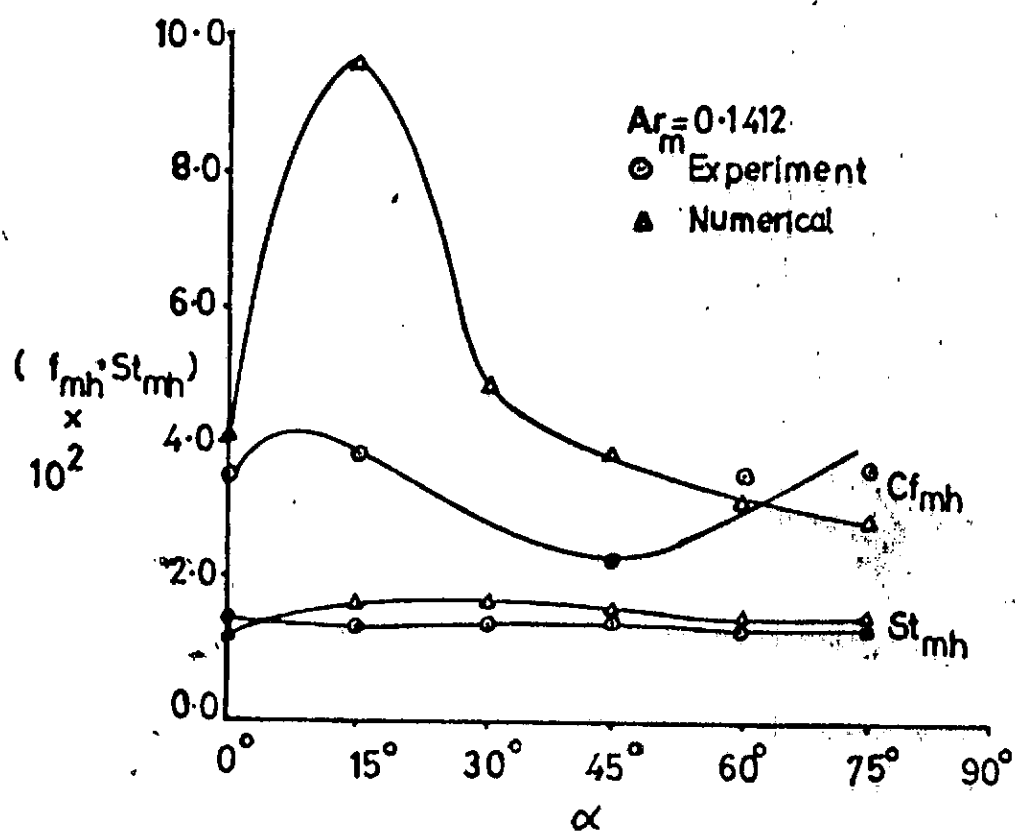
Fig.6-10. Variation of mean hotwall friction factors and Stanton numbers with channel orientation for Re = 454·98; Gr_m = 29221·90 and Pr = 0·704.
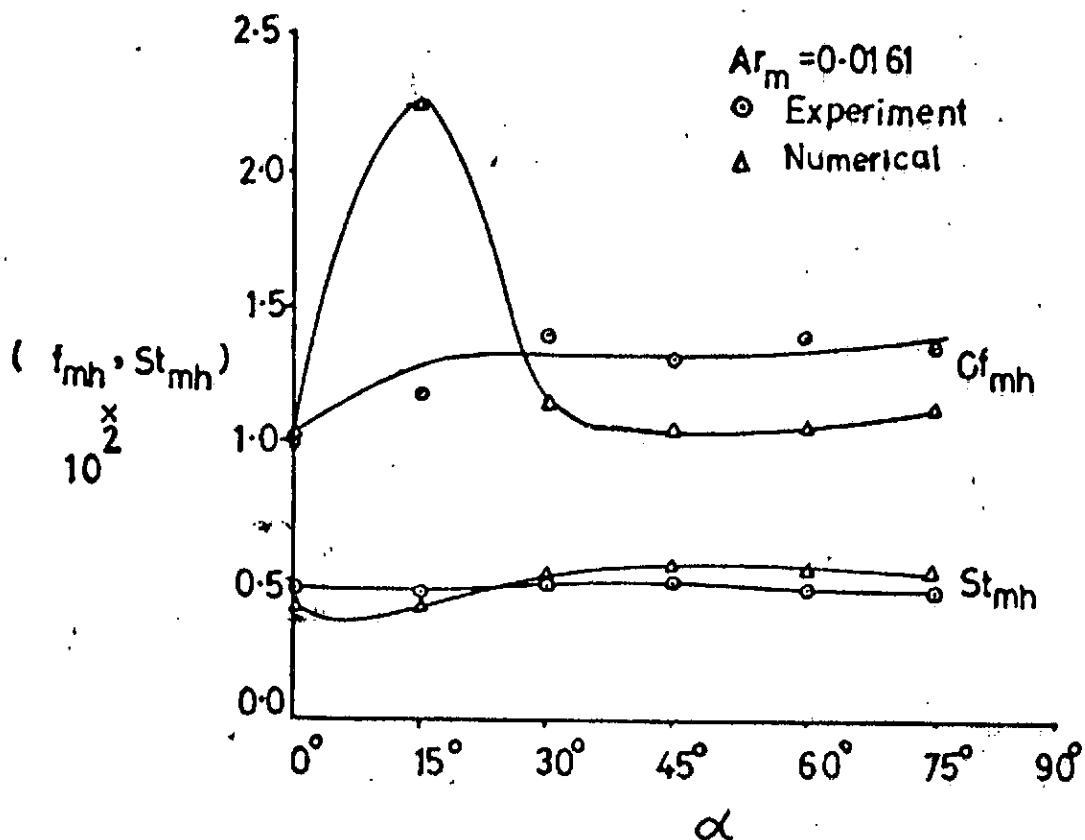
Fig. 6-11. Variation of mean hotwall friction factors and Stanton numbers with channel orientation for Re =1331·76, Gr_m= 28547·90 and Pr =0·704.
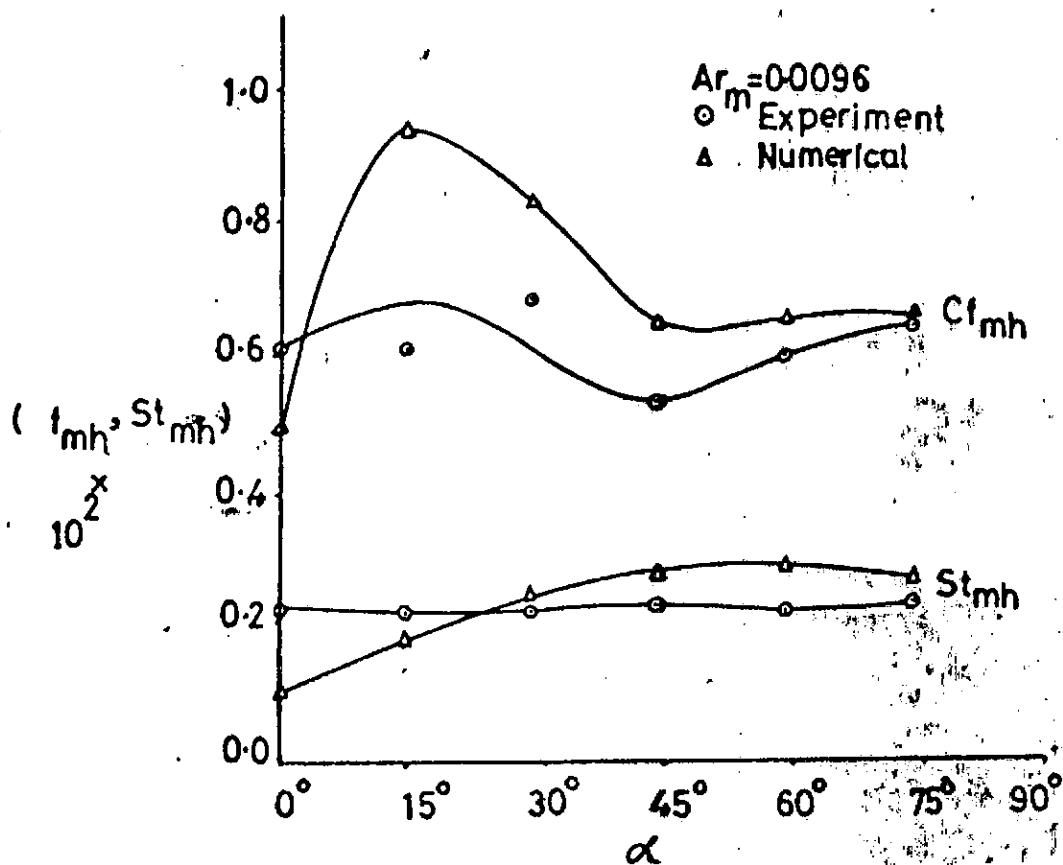
Fig.6-12. Variation of mean hotwall friction factors and Stanton numbers with channel orientation for Re=2728·82, Gr_m=71710·10 and Pr =0·704

CHAPTER SEVEN

7. SOURCES AND ESTIMATION OF EXPERIMENTAL ERRORS

7.1 Sources of Errors

Although exact errors cannot be evaluated, classification of errors provides a useful means of dealing with them.

7.1.1 Systematic Errors

These originate from faulty apparatus or instruments, their calibration, experimental conditions and personal equation. These errors are usually biased and often cumulative. Possible causes are: wrong calibration of instruments, change in external conditions such as the atmospheric temperature and pressure affecting the operation of the instruments. Constant errors which belong to this category influence measurement of a particular variable by the same amount in the same direction. This class of errors are determinate and can always be rectified.

7.1.2 Random Errors:

These are usually unbiased. They are therefore less serious than the biased errors since their equal chances of being positive or negative tend to counter balance one another. Random errors consist of two types: reading and repeatability errors. The first are direct consequences of limited reading accuracy of the various instruments. These errors are inherent in the instruments and are unavoidable unless more precise measuring devices are used. This class of errors pertain to this experiment since it was only possible

to read the graduations of the temperature and velocity measuring instrument to
a half of the smallest graduation.

The repeatability errors originate from fluctuating conditions and
minute disturbances. Examples are changes in the A.C. supply frequency
affecting input voltage and fan speed, and deteriorating conditions of
dry cells used in the potentiometer. Disturbance errors are due to the
physical pressence of measuring units within the flow region. The
measuring devices include the probe and probe carrier assembly which
interfere with the flow.

7.2 Estimation of Heat Losses

The heat loss can be estimated by considering the various modes
by which thermal energy is transported, these are conduction, convection
and radiation.

7.2.1 Conduction Heat Losses

These occur through the perspex sheets, asbestos insulations and
metal structures which carry the heating unit. Heat loss through metal
structures and insulated thermocouple wires are considered negligible.
Using the data for the second experimental run, the heat loss through
the asbestos and perspex are estimated below using Fourier's Law of heat
conduction.

(a)   For Top Perspex:

Length, L_p = 2.4384 m

Breadth, B_p = 1.2192 m

Thickness, t_p = 0.006 m

Thermal Conductivity, k_p = 48.9×10^{-3} $W/_m{}^oK$

Estimated Temperature diff., $\Delta T_p = (30 - 29.2) = 0.8°K$

From Fourier's Law, $Q_{P_T} = \left| k_p \dfrac{\Delta T_p}{t_p} L_p B_p \right|$

Substituting the above data and evaluating, yields

$Q_{P_T} = 19.3839 \times 10^{-3}$ KW

This represents 1.21% of the total input.

(b) **For Two Vertical Side Perspex Sheets:**

$L_p = 2.4384$ m

$B_p = 0.12$ m

$t_p = 0.006$ m

$\Delta T_p = 0.8°k$

$\therefore Q_{Ps} = 2 \left| k_p \dfrac{\Delta T_p}{t_p} L_p B_p \right|$

$Q_{Ps} = 3.8763 \times 10^{-3}$ KW

This represents 0.242% of Total Input.

(c) **For Asbestos Sheets (3 layers)**

$L_a = 2.4384$ m

$B_a = 1.2192$ m

$t_a = 0.006$ m

$k_a = 110.5 \times 10^{-3}$ W$/_{m}°K$

$\Delta T_a = (53.11 - 52.0)\ °R$

$$Q_a = \left| k_a \frac{\Delta T_a}{t_a} \cdot L_a B_a \right|$$

$$Q_a = 0.112 \text{ KW}$$

This represents 7.03% of the total input.

7.2.2 Heat losses by convection:

Convection heat losses from the asbestos and perspex sheets which are exposed to the atmosphere can be estimated using established empirical relations. These depend on the mode of thermal convection, configuration and geometry. Since the atmospheric air is not accelerated the mode of heat loss is by natural convection. From the heat transfer data book [18], the following relations for the surface heat transfer coefficient, h, holds for air. Thus for:

Horizontal plate, heated surface facing up: $h = 2.49(\Delta T)^{0.25}$ ... (7.1)

Horizontal plate, heated surface facing down: $h = 1.31(\Delta T)^{0.25}$ ... (7.2)

Vertical plate for height H<0.3m: $h = 1.37(\frac{\Delta T}{H})^{0.25}$ ... (7.3)

where $\Delta T = T_w - T_\infty$

H = channel Height.

Again, using the data for the second Power Input Run, the above relations will be applied to the relevant surface.

(a) Cold Top Perspex sheet

Geometry: Rectangular plate

Configuration: Horizontal plate, heated surface facing up.

Hence equation (7.1) applies.

From the previous dimensions, the area can be computed directly.

$$\Delta T = (30.0 - 29.2) = 0.8^{\circ}K$$

$$\therefore \quad h_p = 2.49 \, (0.8)^{0.25} \, W_{/m}2 \, ^{\circ}K$$

$$Q_p = (2.49(0.8)^{0.2} \, W_{/m}2 \, ^{\circ}K) \times 0.8^{\circ}K \times 1.219 \times 2.438m^2$$

$$= 0.0056 \, KW$$

This accounts for 0.35% of the total input.

(b) <u>The two side Perspex sheets</u>

    Geometry: Rectangular plate

Configuration: Vertical plate for height H < 0.3m.

Hence equation (7.3) is applicable

$$H = 0.12m$$

$$\Delta T = 0.8^{\circ}K$$

$$\therefore \quad L_p = 1.37 \left(\frac{\Delta T}{H}\right)^{0.25} \, W_{/m^2 \, ^{\circ}k}$$

$$= 1.76 \, W/m^2$$

For the two plates

$$Q_p = 2 \times 1.76 \, W_{/m}2 \times 0.12 \times 2.4384 \, m^2$$

$$\therefore \quad Q_p = 0.01024 \, KW$$

This accounts for 0.64% of the total input.

(c) <u>Bottom plates (Asbestos)</u>

    Geometry: Rectangular plates

Configuration: Horizontal plate, heated surface
                                facing down.

Hence, equation (7.2) applies

$$L_a = 2.4384m$$

$$B_a = 1.2192m.$$

$$\Delta T = (52.0 - 29.2)^\circ K = 22.8^\circ K$$

$$\therefore \quad h_a = 1.31(22.8)^{0.25} \; W_{/m^2 {}^\circ K} \times 22.8^\circ K \times 2.4384 \times 1.2192m^2$$

$$\therefore \quad Q_a = 0.194028 \; KW$$

This represents 11.4% of total input.

7.2.3 Radiation Heat Loss

In engineering applications of radiation, it is common to have a gaseous medium separating solid bodies. This gaseous medium which is often air may be assumed to have neither absorptivity nor reflectivity; that is its transmissivity is unity. This was the case in the experimental set-up. However, since the basic ingredient, high temperature potential between surfaces, that promotes radiant heat transport is present, it is worthwhile to consider the effect of radiation. When two surfaces exchange heat by radiation mechanism, the net amount of heat transported in the direction of smaller surface temperature is a function of the disposition or geometric arrangement of the areas concerned. The disposition is usually specified by the configuration factor. Rectangular planes are considered in the present problem. Two dispositions are relevant.

(a) Disposition 1: Perpendicular Rectangles

Radiation heat transport between finite perpendicular

rectangles with a common edge occurs between the hot plate
and each of the vertical bounding sides. From Heat and Mass
transfer data book [18], the hemispherical emissivity, ϵ,
of a grey body $= 0.725$

Configuration factor, F_{1-2} $\qquad = \qquad 0.047$

Average temp. of hot surface, T_1 $\quad = \qquad 53.11^{\circ}C$

Average temp. of vertical surface $T_2 = \qquad 30.0^{\circ}C$

Area A_1, of hot surface $\qquad = \qquad (1.2192 \times 2.4384)m^2$

Stefan - Boltzmann constant, σ $\qquad = \qquad 5.7 \times 10^{-8} W_{/m}2 \, ^{\circ}K^4$

Thus Net heat exchange, Q_{1-2} $\qquad = \qquad 2A_1 \, \epsilon F_{1-2}(T_1^4 - T_2^4)W$

Since the side plates are transparent only part of the net
incident radiation is absorbed and this is αQ_{1-2}. Assuming the
highest value of $\underset{\text{absorptivity}}{\alpha} = 0.97$ for real materials, then the net heat
absorbed is given by

$$Q_{1-2} = 2 A_1 \, \epsilon F_{1-2} \sigma \alpha (T_1^4 - T_2^4)W$$

$$= 2 \times 2.4384 \times 1.2192 \times 0.725 \times 0.047 \times 5.7 \times 10^{-8}$$
$$\times 0.97(53.11^4 - 30.10^4)$$

Simplication yields $Q_{1-2} = 0.0080W$

This represents 0.0005% of the total input.

Disposition 2: Parallel Rectangles.

With reference to the hot surface, the relevant data are:

Normal emissivity, $\epsilon_n = 0.760$

Configuration factor, $F_{1-3} = 0.90499$

$$T_1 \quad = \quad 53.11^{\circ}C$$

$$T_3 \quad = \quad 30.0^{\circ}C$$

$$A_1 \quad = \quad 1.2192 \times 2.4384 \ m^2$$

$$\therefore \ Q_{1-3} \quad = \quad 2A_1 \ \varepsilon_n F_{1-3} \sigma\alpha(T_1^{\ 4} - T_3^{\ 4})W$$

$$= \quad 2\times1.2192\times2.4384\times0.760\times0.90499\times5.7\times10^{-8}\times6.97$$

$$(53.11^4 - 30.0^4)W$$

Simplication yields $Q_{1-3} \quad = \quad 0.1616 \ W$

This accounts for 0.0101% of the total input.

7.3   Summary

From the on-going analysis of errors, it is clear that most of the losses incurred are through the asbestors. The least heat loss is through radiation. Hopefully these losses account for the disparity between predicted numerical results and the experimental ones.

TABLE 6.1

CALIBRATION OF CHANNEL FOR AN ISOTHERMAL FLOW

AIR VELOCITIES AT STATION, 5 'X =   121.92 cm

Y(cm) / Z(cm)	2.40	4.80	7.20	9.60
-60.96	u(m/s) 0.000	u(m/s) 0.000	u(m/s) 0.000	u(m/s) 0.000
-40.64	0.185	0.186	0.187	0.184
-20.32	0.185	0.188	0.188	0.185
0.00	0.186	0.189	0.189	0.187
+20.32	0.185	0.188	0.188	0.186
+40.64	0.186	0.187	0.186	0.186
+60.96	0.000	0.000	0.000	0.000

TABLE 6.2

Experimental Determination of Inlet Airspeed

Initial Inclined manometer reading, $h_o \approx 3.40$ mm H_2O

Inclination angle of manometer, $\gamma = 15^o$

Air density $\rho = 1.18$ kg/m^3

Variable Transformer Setting (DISA 55D42) (m/s)	Inclined manometer Reading h_1 mm H_2O	Pressure Drop across channel (N/m^2) $\Delta P = \rho g(h_o-h)\sin\gamma$	Actual Inlet Airspeed $u_\infty = 1.3\sqrt{\Delta P}$ m/s
0.0	3.40	0.000	0.000
15.0	3.30	0.254	0.655
20.0	3.25	0.381	0.802
25.0	3.10	0.762	1.135
30	3.05	0.889	1.226

EXPERIMENTAL AND NUMERICAL RESULTS FOR FIRST POWER INPUT RUN

Input current	=	7.55A
Input Voltage	=	120.8V
Input Power	=	0.91204KW
Input mean Air velocity, U_m	=	0.064 m/s
Ambient Air temperature, T_∞	=	27.5 ^{o}C
Channel height, b	=	0.12m
Channel Aspect Ratio, AR	=	10.0

TABLE 6.3 MEASURED WALL TEMPERATURES FOR FIRST POWER INPUT RUN

STATIONS ALONG CHANNEL	HOT WALL		COLD WALL	
	T_h(^{o}C)	$\theta_h = \dfrac{T_h - T_\infty}{RePrA^*b}$	T_c(^{o}C)	$\theta_c = \dfrac{T_c - T_\infty}{RePrA^*b}$
1	48.0	0.43361	30.0	0.05288
2	50.0	0.47592		
3	50.0	0.47592	30.0	0.05288
4	48.0	0.43361		
5	50.0	0.47592	30.0	0.05288
6	48.0	0.43361		
7	49.0	0.45477	30.0	0.05288
8	50.0	0.47592		
9	52.0	0.51822	30.0	0.05288

Estimated mean longitudinal Hotwall temperature gradient, $A^* = 1.230 ^o$Km

Operative fluid properties (for air):
$\nu = 1.688 \times 10^{-5}$ m^2/s
$K_f = 2.722 \times 10^{-5}$ KW/m^{o}K
$\beta = 3.3277 \times 10^{-3}$/^{o}K

Computed dimensionless parameters:
Re $= 454.98$
$Gr_m = 29221.90$
Pr $= 0.704$
$Ar_m = 0.1412$

TABLE 6.4-6.9: EXPERIMENTAL RESULTS AND NUMERICAL PREDICTIONS FOR VELOCITIES AND TEMPERATURES AT SELECTED STATIONS FOR FIRST POWER INPUT RUN AT VARIOUS INCLINATIONS TO THE HORIZONTAL

TABLE 6.4

$(\alpha = 0^\circ)$

Y (cm)	STATIONS											
	5				6				7			
	EXP. VALUES		NUMERICAL PREDICTIONS		EXP. VALUES		NUMERICAL PREDICTIONS		EXP. VALUES		NUMERICAL PREDICTIONS	
	LONG. VEL. (m/s)	TEMPT. (°C)	LONG. VEL. (m/s)	TEMP. (°C)	LONG. VEL. (m/s)	TEMP. (°C)	LONG. VEL. (m/s)	TEMP. (°C)	LONG. VEL. (m/s)	TEMP. (°C)	LONG. VEL. (m/s)	TEMP. (°C)
0.0	0.000	30.0	0.000	29.02	0.0	30.0	0.000	29.02	0.000	30.0	0.000	29.02
2.4	0.067	32.0	0.040	30.54	0.067	32.0	0.036	30.54	0.065	32.0	0.025	30.54
4.8	0.070	32.0	0.084	35.42	0.073	32.0	0.081	34.29	0.070	31.8	0.069	33.07
7.2	0.170	32.0	0.103	39.20	0.175	32.0	0.106	36.05	0.172	32.0	0.114	34.72
9.6	0.170	33.0	0.066	43.44	0.173	33.0	0.070	42.35	0.165	32.5	0.085	40.52
12.0	0.000	50.0	0.000	50.0	0.0	48.0	0.000	48.0	0.000	49.0	0.000	49.00

TABLE 6.5

$(\alpha = 15^{O})$

Y (cm)	STATIONS											
	5				6				7			
	EXP. VALUES		NUMERICAL PREDICTIONS		EXP. VALUES		NUMERICAL PREDICTIONS		EXP. VALUES		NUMERICAL PREDICTIONS	
	LONG. VEL. (m/s)	TEMPT. (^{O}C)	LONG. VEL. (m/s)	TEMP. (^{O}C)	LONG. VEL. (m/s)	TEMP. (oC)	LONG. VEL. (m/s)	TEMP. (^{O}C)	LONG. VEL. (m/s)	TEMP. (^{O}C)	LONG. VEL. (m/s)	TEMP. (^{O}C)
0.0	0.000	30.0	0.000	29.26	0.000	30.0	0.000	29.26	0.000	30.00	0.000	28.83
2.4	0.065	31.0	0.180	31.02	0.065	31.0	0.167	31.00	0.073	32.0	0.137	30.17
4.8	0.070	31.0	0.120	35.70	0.070	31.0	0.090	34.32	0.075	31.5	0.069	32.22
7.2	0.175	31.50	0.259	40.25	0.170	31.5	0.254	36.13	0.173	32.0	0.231	34.00
9.6	0.167	33.0	0.325	42.87	0.175	33.5	0.292	41.38	0.163	33.0	0.263	38.26
12.0	0.000	50.0	0.000	50.0	0.0	48.0	0.000	48.0	0.000	49.0	0.000	49.0

TABLE 6.6

$$(\alpha = 30^{O})$$

Y (cm)	STATIONS											
	5				6				7			
	EXP. VALUES		NUMERICAL PREDICTIONS		EXP. VALUES		NUMERICAL PREDICTIONS		EXP. VALUES		NUMERICAL PREDICTIONS	
	LONG. VEL. (m/s)	TEMPT. (°C)	LONG. VEL. (m/s)	TEMP. (°C)	LONG. VEL. (m/s)	TEMP. (°C)	LONG. VEL. (m/s)	TEMP. (°C)	LONG. VEL. (m/s)	TEMP. (°C)	LONG. VEL. (m/s)	TEMP. (°C)
0.0	0.000	30.0	0.000	28.9	0.000	30.0	0.000	28.29	0.000	30.0	0.000	28.14
2.4	0.070	30.5	0.250	29.08	0.065	30.5	0.248	29.06	0.070	30.5	0.222	28.79
4.8	0.170	30.80	0.147	31.19	0.170	30.8	0.157	30.07	0.170	30.5	0.144	29.94
7.2	0.270	31.0	0.318	32.48	0.270	31.2	0.314	32.10	0.270	31.5	0.292	31.12
9.6	0.170	32.5	0.369	37.31	0.175	32.5	0.379	37.24	0.167	32.5	0.359	36.61
12.0	0.000	50.0	0.000	50.0	0.000	48.0	0.000	48.0	0.000	49.0	0.000	49.0

TABLE 6.7

$(x = 45^{\circ})$

Y (cm)	STATIONS											
	5				6				7			
	EXP. VALUES		NUMERICAL PREDICTIONS		EXP. VALUES		NUMERICAL PREDICTIONS		EXP. VALUES		NUMERICAL PREDICTIONS	
	LONG. VEL. (m/s)	TEMPT. (°C)	LONG. EL. (m/s)	TEMP. (°C)	LONG. VEL. (m/s)	TEMP. (°C)	LONG. VEL. (m/s)	TEMP. (°C)	LONG. VEL. (m/s)	TEMP. (°C)	LONG. VEL. (m/s)	TEMP. (°C)
0.0	0.000	30.0	0.000	27.56	0.000	30.0	0.000	27.56	0.000	30.0	0.000	27.56
2.4	0.070	31.0	0.110	27.64	0.070	31.0	0.130	27.64	0.073	32.0	0.151	27.64
4.8	0.170	30.5	0.049	28.31	0.170	30.5	0.061	28.31	0.175	31.0	0.072	28.73
7.2	0.205	31.8	0.211	28.99	0.210	30.5	0.227	28.92	0.232	31.0	0.244	28.95
9.6	0.173	32.0	0.236	32.31	0.170	32.0	0.254	32.59	0.175	32.0	0.270	32.59
12.0	0.000	50.0	0.000	50.0	0.000	48.0	0.000	48.0	0.000	49.0	0.000	49.0

TABLE 6.8

$$(\alpha = 60^{\circ})$$

Y (cm)	STATIONS											
	5				6				7			
	EXP. VALUES		NUMERICAL PREDICTIONS		EXP. VALUES		NUMERICAL PREDICTIONS		EXP. VALUES		NUMERICAL PREDICTIONS	
	LONG. VEL. (m/s)	TEMPT. (°C)	LONG. VEL. (m/s)	TEMP. (°C)	LONG. VEL. (m/s)	TEMP. (°C)	LONG. VEL. (m/s)	TEMP. (°C)	LONG. VEL. (m/s)	TEMP. (°C)	LONG. VEL. (m/s)	TEMP. (°C)
0.0	0.000	30.0	0.000	28.50	0.000	30.0	0.000	28.50	0.000	30.0	0.000	28.50
2.4	0.070	31.0	0.076	28.51	0.067	30.5	0.095	28.51	0.063	31.0	0.126	28.51
4.8	0.073	30.5	0.020	28.52	0.075	30.2	0.030	28.52	0.070	31.0	0.046	28.52
7.2	0.175	30.5	0.187	29.10	0.220	30.5	0.201	29.10	0.169	31.0	0.227	29.03
9.6	0.174	32.0	0.199	31.49	0.175	32.0	0.213	31.76	0.175	33.0	0.237	31.88
12.0	0.000	50.0	0.000	50.0	0.000	48.0	0.000	48.0	0.000	49.0	0.000	49.0

TABLE 6.9

(α = 75°)

Y (cm)	STATIONS											
	5				6				7			
	EXP. VALUES		NUMERICAL PREDICTIONS		EXP. VALUES		NUMERICAL PREDICTIONS		EXP. VALUES		NUMERICAL PREDICTIONS	
	LONG. VEL. (m/s)	TEMPT. (°C)	LONG. EL. (m/s)	TEMP. (°C)	LONG. VEL. (m/s)	TEMP. (°C)	LONG. VEL. (m/s)	TEMP. (°C)	LONG. VEL. (m/s)	TEMP. (°C)	LONG. VEL. (m/s)	TEMP. (°C)
0.0	0.000	30.0	0.000	27.50	0.000	30.0	0.000	27.50	0.000	30.0	0.000	27.50
2.4	0.065	31.0	0.074	27.51	0.070	30.5	0.089	27.52	0.070	31.0	0.121	27.52
4.8	0.073	30.5	0.011	27.56	0.075	30.5	0.019	27.56	0.073	31.0	0.042	27.54
7.2	0.165	30.8	0.187	27.77	0.170	31.0	0.198	27.78	0.170	31.5	0.224	27.76
9.6	0.175	32.0	0.190	29.55	0.175	32.0	0.202	29.60	0.180	33.0	0.226	29.97
12.0	0.000	50.0	0.000	50.0	0.000	48.0	0.000	48.0	0.000	49.0	0.000	49.0

TABLE 6.10 Exp. Local Heat Transfer and Friction Coefficients For First Power Input Run

α (Degrees)	STATIONS								
	5			6			7		
	Nu_h	$f_h \times 10^2$	$St_h \times 10^2$	Nu_h	$f_h \times 10^2$	$St_h \times 10^2$	Nu_h	$f_h \times 10^2$	$St_h \times 10^2$
0	4.370	2.911	1.364	4.228	3.827	1.320	4.457	3.852	1.391
15	4.352	3.811	1.359	4.245	1.070	1.263	4.302	5.232	1.343
30	4.481	1.559	1.399	4.358	1.560	1.361	4.438	3.313	1.386
45	4.659	2.242	1.455	4.492	2.150	1.402	4.574	2.742	1.428
60	4.611	3.780	1.440	4.492	2.955	1.402	4.264	4.104	1.331
75	4.622	4.127	1.489	4.512	3.881	1.409	4.283	3.119	1.337

TABLE 6.11 COMPARISON OF EXPERIMENTAL RESULTS AND NUMERICAL PREDICTIONS OF THE MEAN HOT WALL HEAT TRANSFER AND FRICTION COEFFICIENTS FOR FIRST POWER INPUT RUN

α (Degrees)	EXPERIMENTAL VALUES			NUMERICAL PREDICTIONS		
	Nh_{mh}	$f_{mh} \times 10^2$	$St_{mh} \times 10^2$	Nu_{mh}	$f_{mh} \times 10^2$	$St_{mh} \times 10^2$
0	4.352	3.530	1.358	4.213	4.120	1.320
15	4.293	3.811	1.322	5.171	9.680	1.610
30	4.426	1.560	1.382	5.233	4.910	1.630
45	4.576	2.380	1.428	5.163	3.910	1.610
60	4.456	3.614	1.391	5.084	3.210	1.590
75	4.472	3.709	1.412	5.070	2.950	1.580

EXPERIMENTAL AND NUMERICAL RESULTS FOR SECOND POWER INPUT RUN

Input current	=	10.00A
Input voltage	=	160.0V
Input Power	=	1.600KW
Input Mean Air Velocity, U_m	=	0.189 m/s
Ambient Air temperature, T_∞	=	29.2°C
Channel height, b	=	0.12m.
Channel Aspect Ratio, AR	=	10.0

TABLE 6.12 MEASURED WALL TEMPERATURES FOR SECOND POWER INPUT RUN

STATIONS ALONG CHANNEL	HOT WALL		COLD WALL	
	T_h (°C)	$\theta_h = \dfrac{T_h - T_\infty}{RePrA^*b}$	T_c (°C)	$\theta_c = \dfrac{T_c - T_\infty}{RePrA^*b}$
1	52.0	0.16475	30.0	0.00578
2	53.0	0.17198		
3	54.0	0.17920	30.0	0.00578
4	51.0	0.15753	30.0	0.00578
5	54.0	0.17920	30.0	0.00578
6	52.0	0.16475		
7	53.0	0.17198	30.0	0.00578
8	54.0	0.17920		
9	55.0	0.18643	30.0	0.00578

Estimated mean longitudinal hot wall temperature gradient, $A^* = 1.230$ °K/m

Operative fluid properties (for air):
- $\nu = 1.703 \times 10^{-5}$ m²/s
- $K_f = 2.733 \times 10^{-5}$ KW/m°K
- $\beta = 3.3090 \times 10^{-3}$/°K

Computed dimensionless parameters:
- $Re = 1331.76$
- $Gr_m = 28547.90$
- $Pr = 0.704$
- $Ar_m = 0.0161$

TABLE 6.13-6-18: EXPERIMENTAL RESULTS AND NUMERICAL PREDICTIONS FOR VELOCITIES AND TEMPERATURES AT SELECTED STATIONS FOR SECOND POWER INPUT RUN AT VARIOUS INCLINATIONS TO THE HORIZONTAL

TABLE 6.13

$(\alpha = 0^\circ)$

	STATIONS											
	5				6				7			
Y (cm)	EXP. VALUES		NUMERICAL PREDICTIONS		EXP. VALUES		NUMERICAL PREDICTIONS		EXP. VALUES		NUMERICAL PREDICTIONS	
	LONG. VEL. (m/s)	TEMPT. (°C)	LONG. EL. (m/s)	TEMP. (°C)	LONG. VEL. (m/s)	TEMP. (°C)	LONG. VEL. (m/s)	TEMP. (°C)	LONG. VEL. (m/s)	TEMP. (°C)	LONG. VEL. (m/s)	TEMP. (°C)
0.0	0.000	30.0	0.000	29.72	0.000	30.0	0.000	29.75	0.000	30.0	0.000	29.78
2.4	0.120	31.0	0.160	30.25	0.120	31.5	0.153	30.31	0.115	32.5	0.148	30.37
4.8	0.210	31.0	0.253	33.40	0.210	32.0	0.249	32.91	0.278	32.5	0.246	33.21
7.2	0.405	31.5	0.267	37.33	0.400	33.5	0.273	36.26	0.415	33.0	0.277	36.00
9.6	0.210	33.0	0.180	42.76	0.210	35.0	0.185	42.14	0.310	34.5	0.189	43.30
12.0	0.000	54.0	0.000	54.0	0.000	52.0	0.000	52.0	0.000	53.0	0.000	53.0

TABLE   6.14

$(\alpha = 15°)$

Y (cm)	STATIONS											
	5				6				7			
	EXP. VALUES		NUMERICAL PREDICTIONS		EXP. VALUES		NUMERICAL PREDICTIONS		EXP. VALUES		NUMERICAL PREDICTIONS	
	LONG. VEL. (m/s)	TEMPT. (°C)	LONG. EL. (m/s)	TEMP. (°C)	LONG. VEL. (m/s)	TEMP. (°C)	LONG. VEL. (m/s)	TEMP. (°C)	LONG. VEL. (m/s)	TEMP. (°C)	LONG. VEL. (m/s)	TEMP. (°C)
0.0	0.000	30.0	0.000	29.88	0.000	30.0	0.000	29.51	0.000	30.0	0.000	29.62
2.4	0.073	31.50	0.048	30.56	0.120	32.0	0.012	29.81	0.073	31.5	0.039	30.44
4.8	0.310	32.0	0.145	32.90	0.210	32.0	0.135	32.59	0.310	32.0	0.140	31.86
7.2	0.355	32.0	0.345	37.14	0.400	32.0	0.354	36.49	0.355	32.0	0.352	35.21
9.6	0.265	34.0	0.315	43.62	0.221	34.5	0.328	42.93	0.265	34.0	0.323	41.81
12.0	0.000	54.0	0.000	54.00	0.000	52.0	0.000	52.0	0.000	53.0	0.000	53.0

TABLE 6.15

$(\alpha = 30^{\circ})$

Y (cm)	STATIONS											
	5				6				7			
	EXP. VALUES		NUMERICAL PREDICTIONS		EXP. VALUES		NUMERICAL PREDICTIONS		EXP. VALUES		NUMERICAL PREDICTIONS	
	LONG. VEL. (m/s)	TEMPT. (°C)	LONG. EL. (m/s)	TEMP. (°C)	LONG. VEL. (m/s)	TEMP. (°C)	LONG. VEL. (m/s)	TEMP. (°C)	LONG. VEL. (m/s)	TEMP. (°C)	LONG. VEL. (m/s)	TEMP. (°C)
0.0	0.000	30.0	0.000	29.38	0.000	30.0	0.000	29.38	0.000	30.0	0.000	29.36
2.4	0.025	31.5	0.038	29.55	0.120	31.5	0.031	29.55	0.120	32.0	0.021	29.52
4.8	0.265	31.5	0.156	30.04	0.215	32.0	0.150	29.93	0.215	31.5	0.144	29.70
7.2	0.320	32.0	0.358	30.79	0.310	32.0	0.363	30.79	0.310	31.5	0.371	30.63
9.6	0.228	33.5	0.307	34.60	0.237	34.0	0.314	34.94	0.262	33.5	0.324	34.98
12.0	0.000	54.0	0.000	54.0	0.000	52.0	0.000	52.0	0.000	53.0	0.000	53.0

TABLE 6.16

$(\alpha = 45^{\circ})$

Y (cm)	S T A T I O N S											
	5				6				7			
	EXP. VALUES		NUMERICAL PREDICTIONS		EXP. VALUES		NUMERICAL PREDICTIONS		EXP. VALUES		NUMERICAL PREDICTIONS	
	LONG. VEL. (m/s)	TEMPT. (°C)	LONG. EL. (m/s)	TEMP. (°C)	LONG. VEL. (m/s)	TEMP. (°C)	LONG. VEL. (m/s)	TEMP. (°C)	LONG. VEL. (m/s)	TEMP. (°C)	LONG. VEL. (m/s)	TEMP. (°C)
0.0	0.000	30.0	0.000	29.22	0.000	30.0	0.000	29.22	0.000	30.0	30.000	29.22
2.4	0.142	31.0	0.038	29.24	0.072	31.5	0.010	29.24	0.025	32.0	0.024	29.24
4.8	0.172	31.0	0.174	29.43	0.120	31.5	0.160	29.35	0.215	31.5	0.138	29.29
7.2	0.310	31.5	0.362	29.71	0.315	32.0	0.385	29.73	0.310	32.0	0.411	29.69
9.6	0.262	33.0	0.289	32.19	0.147	34.0	0.310	32.49	0.262	33.5	0.340	32.65
12.0	0.000	54.0	0.000	54.0	0.000	52.0	0.000	52.0	0.000	53.0	0.000	53.0

TABLE 6.17

$(\alpha = 60^{\circ})$

Y (cm)	STATIONS											
	5				6				7			
	EXP. VALUES		NUMERICAL PREDICTIONS		EXP. VALUES		NUMERICAL PREDICTIONS		EXP. VALUES		NUMERICAL PREDICTIONS	
	LONG. VEL. (m/s)	TEMPT. (°C)	LONG. EL. (m/s)	TEMP. (°C)	LONG. VEL. (m/s)	TEMP. (°C)	LONG. VEL. (m/s)	TEMP. (°C)	LONG. VEL. (m/s)	TEMP. (°C)	LONG. VEL. (m/s)	TEMP. (°C)
0.0	0.000	30.0	0.000	29.20	0.000	30.0	0.000	29.20	0.000	30.0	0.000	29.20
2.4	0.072	30.8	0.032	29.20	0.072	31.0	0.013	29.21	0.072	31.5	0.026	29.21
4.8	0.117	31.0	0.170	29.24	0.310	30.8	0.161	29.24	0.310	31.0	0.139	29.24
7.2	0.357	31.5	0.367	29.37	0.405	32.0	0.383	29.39	0.405	31.5	0.414	29.39
9.6	0.310	33.0	0.294	31.08	0.215	34.5	0.308	31.34	0.310	34.0	0.340	31.53
12.0	0.000	54.0	0.000	54.0	0.000	52.0	0.000	52.0	0.000	53.0	0.000	53.0

TABLE 6.18

$(\alpha = 75^{\circ})$

Y (cm)	STATIONS											
	5				6				7			
	EXP. VALUES		NUMERICAL PREDICTIONS		EXP. VALUES		NUMERICAL PREDICTIONS		EXP. VALUES		NUMERICAL PREDICTIONS	
	LONG. VEL. (m/s)	TEMPT. (°C)	LONG. EL. (m/s)	TEMP. (°C)	LONG. VEL. (m/s)	TEMP. (°C)	LONG. VEL. (m/s)	TEMP. (°C)	LONG. VEL. (m/s)	TEMP. (°C)	LONG. VEL. (m/s)	TEMP. (°C)
0.0	0.000	30.0	0.000	29.20	0.000	30.0	0.000	29.20	0.000	30.0	0.000	29.21
2.4	0.072	30.5	0.014	29.20	0.072	31.5	0.000	29.20	0.125	30.5	0.033	29.21
4.8	0.225	30.0	0.166	29.21	0.215	30.0	0.159	29.20	0.239	31.0	0.139	29.27
7.2	0.255	31.0	0.383	29.25	0.310	31.5	0.393	29.49	0.225	32.5	0.420	29.28
9.6	0.215	33.5	0.303	30.47	0.215	35.0	0.313	30.71	0.210	34.50	0.353	30.90
12.0	0.000	54.0	0.000	54.0	0.000	52.0	0.000	52.0	0.000	53.0	0.000	53.0

TABLE 6.19 Exp. Local Heat Transfer and Friction Coefficients For Second Power Input Run

α (Degrees)	STATIONS								
	5			6			7		
	Nu_h	$f_h \times 10^2$	$St_h \times 10^2$	Nu_h	$f_h \times 10^2$	$St_h \times 10^2$	Nu_h	$f_h \times 10^2$	$St_h \times 10^2$
0	4.889	0.864	0.521	4.295	0.879	0.458	4.482	1.385	0.478
15	4.637	1.319	0.495	4.386	0.955	0.468	4.587	1.319	0.489
30	4.772	1.326	0.509	4.532	1.358	0.483	4.709	1.527	0.502
45	4.889	1.564	0.521	4.532	0.784	0.483	4.727	1.706	0.504
60	4.889	1.936	0.521	4.386	0.852	0.468	4.569	1.429	0.487
75	4.738	1.481	0.505	4.221	1.272	0.450	4.464	1.445	0.476

TABLE 6.20 COMPARISON OF EXPERIMENTAL RESULTS AND NUMERICAL
PREDICTIONS OF THE MEAN HOT WALL HEAT TRANSFER
AND FRICTION COEFFICIENTS FOR SECOND POWER INPUT RUN

α	EXPERIMENTAL VALUES			NUMERICAL PREDICTIONS		
(Degrees)	Nh_{mh}	$f_{mh} X\ 10^2$	$St_{mh} X\ 10^2$	Nu_{mh}	$f_{mh} X 10^2$	$St_{mh} X 10^2$
0	4.555	1.043	0.486	4.000	1.047	0.430
15	4.537	1.198	0.484	4.140	2.307	0.440
30	4.671	1.404	0.498	4.796	1.147	0.510
45	4.716	1.351	0.503	4.944	1.053	0.530
60	4.615	1.406	0.492	5.008	1.090	0.530
75	4.474	1.399	0.477	5.045	1.140	0.540

EXPERIMENTAL RESULTS FOR THIRD POWER INPUT RUN

Input current	=	12.50A
Input Voltage	=	200.0V
Input Power	=	2.500KW
Input mean Air Velocity, U_m	=	0.400 m/s
Ambient Air temperature, T_∞	=	27.5°C
Channel height, b	=	0.12 m
Channel Aspect Ratio AR	=	10.0

TABLE 6.21 MEASURED WALL TEMPERATURES FOR THIRD POWER INPUT RUN

STATIONS ALONG CHANNEL	HOT WALL		COLD WALL	
	T_h (°C)	$\theta_h = \dfrac{T_h - T_\infty}{RePrA^*b}$	T_c (°C)	$\theta_c = \dfrac{T_c - T_\infty}{RePrA^*b}$
1	62.0	0.04548	31.0	0.00461
2	66.0	0.05075		
3	65.0	0.04943	31.0	0.00461
4	69.0	0.05471		
5	62.0	0.04548	31.0	0.00461
6	69.0	0.05471		
7	70.0	0.05603	31.0	0.00461
8	69.0	0.05471		
9	70.0	0.05603	31.0	0.00461

Estimated mean Longitudinal Hot wall temperature gradient, $A^* = 3.281$ °K/m

Operative fluid properties (for air):
$\nu = 1.759 \times 10^{-5}$ m^2/s
$K_f = 2.778 \times 10^{-5}$ KW/m°K
$\beta = 3.3277 \times 10^{-3}$/°K

Computed dimensioness parameters:
$Re = 2728.82$
$Gr_m = 71710.10$
$Pr = 0.704$
$Ar_m = 0.0096$

TABLES 6-22-6-27: EXPERIMENTAL RESULTS AND NUMERICAL PREDICTIONS FOR VELOCITIES AND TEMPERATURES AT SELECTED STATIONS FOR THIRD POWER INPUT RUN AT VARIOUS INCLINATIONS TO THE HORIZONTAL

TABLE 6.22

$(\alpha = 0^{\circ})$

Y (cm)	STATIONS											
	5				6				7			
	EXP. VALUES		NUMERICAL PREDICTIONS		EXP. VALUES		NUMERICAL PREDICTIONS		EXP. VALUES		NUMERICAL PREDICTIONS	
	LONG. VEL. (m/s)	TEMPT. (°C)	LONG. EL. (m/s)	TEMP. (°C)	LONG. VEL. (m/s)	TEMP. (°C)	LONG. VEL. (m/s)	TEMP. (°C)	LONG. VEL. (m/s)	TEMP. (°C)	LONG. VEL. (m/s)	TEMP. (°C)
0.0	0.000	31.0	0.000	28.18	0.000	31.0	0.000	28.04	0.000	31.0	0.000	28.37
2.4	0.500	33.2	0.344	28.87	0.310	33.5	0.341	29.94	0.310	33.5	0.341	29.24
4.8	0.500	34.0	0.525	34.42	0.405	33.5	0.526	34.01	0.500	34.0	0.527	35.14
7.2	0.500	34.5	0.558	44.06	0.595	34.0	0.562	42.77	0.690	34.2	0.562	44.70
9.6	0.500	37.5	0.389	49.60	0.405	37.0	0.388	50.06	0.500	36.5	0.388	55.22
12.0	0.000	62.0	0.000	62.0	0.000	69.0	0.000	69.0	0.000	70.00	0.000	70.0

TABLE 6.23

$(\alpha = 15°)$

Y (cm)	STATIONS											
	5				6				7			
	EXP. VALUES		NUMERICAL PREDICTIONS		EXP. VALUES		NUMERICAL PREDICTIONS		EXP. VALUES		NUMERICAL PREDICTIONS	
	LONG. VEL. (m/s)	TEMPT. (°C)	LONG. VEL. (m/s)	TEMP. (°C)	LONG. VEL. (m/s)	TEMP. (°C)	LONG. VEL. (m/s)	TEMP. (°C)	LONG. VEL. (m/s)	TEMP. (°C)	LONG. VEL. (m/s)	TEMP. (°C)
0.0	0.000	31.0	0.000	27.84	0.000	31.0	0.000	27.77	0.000	31.0	0.000	28.11
2.4	0.400	33.0	0.325	28.18	0.310	33.0	0.333	28.04	0.310	33.0	0.299	28.72
4.8	0.690	33.0	0.509	29.19	0.595	33.0	0.512	28.90	0.690	33.0	0.484	30.15
7.2	0.795	33.5	0.573	31.89	0.690	33.5	0.566	31.54	0.500	34.5	0.590	33.61
9.6	0.595	37.0	0.410	40.09	0.500	37.0	0.405	40.05	0.500	37.5	0.441	42.81
12.0	0.000	62.0	0.000	62.0	0.000	69.0	0.000	69.0	0.000	70.0	0.000	70.0

TABLE 6.24

$(\alpha = 30^{\circ})$

Y (cm)	STATIONS											
	5				6				7			
	EXP. VALUES		NUMERICAL PREDICTIONS		EXP. VALUES		NUMERICAL PREDICTIONS		EXP. VALUES		NUMERICAL PREDICTIONS	
	LONG. VEL. (m/s)	TEMPT. (°C)	LONG. VEL. (m/s)	TEMP. (°C)	LONG. VEL. (m/s)	TEMP. (°C)	LONG. VEL. (m/s)	TEMP. (°C)	LONG. VEL. (m/s)	TEMP. (°C)	LONG. VEL. (m/s)	TEMP. (°C)
0.0	0.000	31.0	0.000	27.54	0.000	31.0	0.000	27.54	0.000	31.0	0.000	27.55
2.4	0.595	32.5	0.224	27.57	0.400	33.0	0.141	27.57	0.405	33.0	0.187	27.61
4.8	0.690	33.0	0.457	27.74	0.595	33.0	0.435	27.64	0.690	32.8	0.402	28.16
7.2	0.790	33.0	0.654	28.26	0.780	34.0	0.690	28.21	0.785	33.5	0.681	28.72
9.6	0.690	36.0	0.487	32.10	0.690	36.5	0.520	32.33	0.690	36.0	0.527	33.73
12.0	0.000	62.0	0.000	62.0	0.000	69.0	0.000	69.0	0.000	70.0	0.000	70.0

TABLE 6.25

$$(\alpha = 45^{o})$$

Y (cm)	STATIONS											
	5				6				7			
	EXP. VALUES		NUMERICAL PREDICTIONS		EXP. VALUES		NUMERICAL PREDICTIONS		EXP. VALUES		NUMERICAL PREDICTIONS	
	LONG. VEL. (m/s)	TEMPT. (°C)	LONG. EL. (m/s)	TEMP. (°C)	LONG. VEL. (m/s)	TEMP. (°C)	LONG. VEL. (m/s)	TEMP. (°C)	LONG. VEL. (m/s)	TEMP. (°C)	LONG. VEL. (m/s)	TEMP. (°C)
0.0	0.000	31.0	0.000	27.50	0.000	31.0	0.000	27.50	0.000	31.0	0.000	27.50
2.4	0.595	32.0	0.078	27.51	0.410	32.0	0.037	27.51	0.595	32.0	0.060	27.50
4.8	0.785	32.0	0.381	27.50	0.595	32.0	0.355	27.52	0.690	32.5	0.355	27.51
7.2	0.870	32.0	0.772	27.70	0.880	33.0	0.804	27.70	0.785	33.0	0.783	27.70
9.6	0.595	35.5	0.600	29.99	0.595	36.0	0.636	30.22	0.595	34.0	0.630	31.07
12.0	0.000	62.0	0.000	62.00	0.000	69.0	0.000	69.0	0.000	70.0	0.000	70.0

TABLE 6.26.

$(\alpha = 60°)$

Y (cm)	STATIONS											
	5				6				7			
	EXP. VALUES		NUMERICAL PREDICTIONS		EXP. VALUES		NUMERICAL PREDICTIONS		EXP. VALUES		NUMERICAL PREDICTIONS	
	LONG. VEL. (m/s)	TEMPT. (°C)	LONG. VEL. (m/s)	TEMP. (°C)	LONG. VEL. (m/s)	TEMP. (°C)	LONG. VEL. (m/s)	TEMP. (°C)	LONG. VEL. (m/s)	TEMP. (°C)	LONG. VEL. (m/s)	TEMP. (°C)
0.0	0.000	31.0	0.000	27.50	0.000	31.0	0.000	27.50	0.000	31.0	0.000	27.50
2.4	0.405	32.0	0.041	27.50	0.405	32.0	0.010	27.50	0.405	32.0	0.010	27.50
4.8	0.690	31.5	0.359	27.52	0.595	31.8	0.329	27.52	0.600	32.2	0.329	27.51
7.2	0.880	33.0	0.802	27.58	0.785	32.5	0.841	27.60	0.690	33.0	0.831	27.67
9.6	0.690	38.0	0.630	29.16	0.500	37.0	0.674	29.37	0.595	34.5	0.671	29.96
12.0	0.000	62.0	0.000	62.0	0.000	69.0	0.000	69.0	0.000	70.0	0.000	70.0

TABLE 6.27

$(\alpha = 75°)$

Y (cm)	STATIONS											
	5				6				7			
	EXP. VALUES		NUMERICAL PREDICTIONS		EXP. VALUES		NUMERICAL PREDICTIONS		EXP. VALUES		NUMERICAL PREDICTIONS	
	LONG. VEL. (m/s)	TEMPT. (°C)	LONG. EL. (m/s)	TEMP. (°C)	LONG. VEL. (m/s)	TEMP. (°C)	LONG. VEL. (m/s)	TEMP. (°C)	LONG. VEL. (m/s)	TEMP. (°C)	LONG. VEL. (m/s)	TEMP. (°C)
0.0	0.000	31.0	0.000	27.50	0.000	31.0	0.000	27.50	0.000	31.0	0.000	27.50
2.4	0.310	31.0	0.010	27.52	0.405	31.2	0.056	27.52	0.210	31.5	0.010	27.52
4.8	0.500	31.2	0.330	27.53	0.595	31.2	0.299	27.53	0.500	31.8	0.297	27.53
7.2	0.592	31.5	0.837	27.55	0.690	32.0	0.880	27.55	0.595	32.0	0.874	27.59
9.6	0.500	34.5	0.691	28.86	0.500	36.0	0.716	29.05	0.500	34.5	0.716	29.45
12.0	0.000	62.0	0.000	62.0	0.000	69.0	0.000	69.0	0.000	70.0	0.000	70.0

TABLE 6.28 Exp. Local Heat Transfer and Friction Coefficients for Third Power Input Run

α (Degrees)	STATIONS								
	5			6			7		
	Nu_h	$f_h \times 10^2$	$St_h \times 10^2$	Nu_h	$f_h \times 10^2$	$St_h \times 10^2$	Nu_h	$f_h \times 10^2$	$St_h \times 10^2$
0	4,070	0.687	0.211	4,438	0.548	0.230	4,553	0.600	0.236
15	4.143	0.586	0.215	4,428	0.573	0.229	4,402	0.687	0.228
30	4,324	0.653	0.224	4,518	0.736	0.235	4,618	0.704	0.240
45	4,396	0.486	0.228	4,578	0.554	0.238	4,922	0.548	0.255
60	3,937	0.646	0.204	4,408	0.487	0.229	4,843	0.676	0.251
75	4,577	0.676	0.238	4,558	0.548	0.548	0,237	4,824	0.250

TABLE 6.29 COMPARISON OF EXPERIMENTAL RESULTS AND NUMERICAL PREDICTIONS OF THE MEAN HOT WALL HEAT TRANSFER AND FRICTION COEFFICIENTS FOR / THIRD POWER INPUT RUN

α	EXPERIMENTAL VALUES			NUMERICAL PREDICTIONS		
(Degrees)	Nh_{mh}	$f_{mh} \times 10^2$	$St_{mh} \times 10^2$	Nu_{mh}	$f_{mh} \times 10^2$	$St_{mh} \times 10^2$
0	4.354	0.612	0.226	2.460	0.480	0.130
15	4.324	0.615	0.224	2.685	0.940	0.140
30	4.487	0.698	0.233	4.716	0.830	0.240
45	4.632	0.529	0.240	4.932	0.640	0.260
60	4.396	0.603	0.228	4.932	0.660	0.260
75	4.653	0.646	0.242	4.916	0.660	0.260

REFERENCES

1. Ou, J.W., Cheng, K.C. and Lin, R.C. (1975). "Combined Free and Forced Laminar Convection in Inclined Rectangular Channels." *International Journal of Heat and Mass Transfer, 19, 277-283.*

2. Cheng, K.C. and Hwang, G.J. (1969). "Numerical Solution for Combined Free and Forced Laminar Convection in Horizontal Rectangular Channels." *Journal of Heat Transfer, 59-66.*

3. Cheng, K.C. and Hong, S.W. (1972). "Effect of Tube Inclination on Laminar Convection In Uniformly Heated Tubes for Flatplate Solar Collectors." *Solar Energy, 13, 363-371.*

4. Ozoe, H.; Sayama, H. and Churchill, S.W. (1973). "Natural Convection in Inclined Square Channel." *International Journal of Heat and Mass Transfer, 17, 401-406.*

5. Mori, Y. and Uchida, Y. (1966). "Forced Convective Heat Transfer Between Horizontal Flat Plates." *International Journal of Heat and Mass Transfer, 9, 803-817.*

6. Deniss, S.C.R. (1972). "The Numerical Solution of the Vorticity Transport Equation." *Proceedings of the Third International Confererence on Numerical Methods in Fluid Mechanics, number 19, II, 120-129.*

7. Schlichting, H. (1968). Boundary-Layer Theory, 58.

8. Roache, PJ. (1972). Computational Fluid Dynamics, 117-118.

9. Runchal, A.K., Spalding, D.B., Wolfstein, M., Pun, W.M. and Gosman, A.D. (1969). Heat and Mass Transfer in recirculating flows.

10. Faris, G.N. and Viscanta, R. (1969). "An Analysis of Laminar Combined Forced and Free Convection Heat Transfer in a horizontal Tube." *International Journal of Heat and Mass Transfer, 12, 1295-1309.*

11. Iqbal, M. and Stachiewicz, J.W. (1966). "Influence of Tube Orientation on combined Free and Forced Laminar Convection Heat Transfer." *Journal of Heat Transfer, 100-116.*

12. Morton, B.R. (1958). "Laminar Convection in Uniformly Heated Horizontal Pipes at Low Rayleigh numbers." *Quarterly Journal of Mechanics and Applied Mathematics, Part 4, XII, 411-420.*

13. Hughes, W.F. and Brighton, J.A. (1967). Theory and Problems of Fluid Dynamics, 62-63, McGraw-Hill Book Company, NY.

14. Reynolds, A.J. (1972). Thermofluid Dynamics, 369-370, Wiley - Interscience.

15. Huntley, H.E. (1967). Dimensional Analysis, 84-98, Dover Publications, NY.

16. Gill, W.M. and Casal, E.D. (1962). "A Theoretical Investigation of Natural Convection Effects in Forced Horizontal Flows." *A. I. Ch. Journal, No. 4, 8, 513-518.*

17. Jorgensen, R. Fan Engineering, 114.

18. Kothandaraman, C.P. and Subramanyan, S. (1975). Heat and Mass Trnasfer Data Book, 97 and 74-76, Wiley E.stern Private Limited, New Delhi.

APPENDIX A

SOLUTIONS OF THE ZEROTH, FIRST-AND SECOND-ORDER PERTURBATION EQUATIONS

It is important to note that ψ_o cannot be zero, as would have been the case if it were defined purely by secondary flows. In this case, it is a consequence of pure forced convection upon which the perturbation equation rests.

A1. Solutions for Zeroth-order Equations

From equation (5.7a),

$$\nabla^4 \psi_o = 0$$

Expanding the LHS gives,

$$\frac{\partial^4 \psi_o}{\partial x^4} + \frac{2\partial^4 \psi_o}{\partial y^2 \partial x^2} + \frac{\partial^4 \psi_o}{\partial y^4} = 0.$$

Since ψ_o is a function of y only,

$$\frac{\partial^2}{\partial x^2} \left(\frac{\partial^2 \psi_o}{\partial y^2} \right) = 0$$

The partial differential equation can then be replaced by the total derivatives.

$$\therefore \quad \frac{d^4 \psi_o}{dy^4} = 0.$$

Integrating, we have

$$\frac{d^3 \psi_0}{dy^3} = C_1$$

$$\therefore \quad \frac{d^2 \psi_0}{dy^2} = C_1 y + C_2$$

$$\therefore \quad \frac{d \psi_0}{dy} = \frac{C_1 y^2}{2} + C_2 y + C_3 \quad \dots\dots\dots\dots\dots(A.1a)$$

$$\therefore \quad \psi_0 = \frac{C_1 y^3}{6} + \frac{C_2 y^2}{2} + C_3 y + C_4 \quad \dots\dots\dots\dots\dots(A.1b)$$

where C_1, C_2, C_3, C_4 are integration constants to be determined from the boundary conditions.

For no-slip conditions (Neumann B.C.) using eqn (A.1a)

$$\frac{d\psi_0}{dy}\Big|_{y=0} = 0, \quad \rightarrow \quad C_3 = 0.$$

$$\frac{d\psi_0}{dy}\Big|_{y=1} = 0, \quad \rightarrow \quad 0 = \frac{C_1}{2} + C_2,$$

$$\text{i.e} \quad C_1 = -2C_2 \quad \dots\dots\dots\dots(A.2)$$

From the Dirichlet Boundary Conditions, using equation (A.1b)

$$\psi_0\Big|_0 = 0, \quad \rightarrow \quad C_4 = 0.$$

$$\psi_0 \Big|_{y=1} = 1, \rightarrow 1 = \frac{C_1}{6} + \frac{C_2}{2} \quad \dots\dots\dots\dots\dots\dots\dots\dots\dots\dots(A.3)$$

If we substitute (A2) into (A.3) we obtain

$$1 = -2\frac{C_2}{6} + \frac{C_2}{2}$$

$$1 = C_2(\tfrac{1}{2} - \tfrac{1}{3}) = \frac{C_2}{6}$$

i.e. $\underline{\underline{C_2 = 6}}$ and $\underline{\underline{C_1 = -12}}$

Substituting C_1, C_2, C_3, C_4 back into eqn (A.1b) we have

$$\psi_0 = -2y^3 + 3y^2$$

$$\rightarrow \psi_0 = 3y^2 - 2y^3 \quad \dots\dots\dots\dots\dots\dots\dots\dots\dots\dots\dots(A.4.)$$

This is a solution describing pure forced convection.

From (A.4), $\dfrac{\partial \psi_0}{\partial y} = 6y - 6y^2 = 6y(1-y)$

i.e. $u_0 = 6y(1-y)$

Substituting $\dfrac{\partial \psi_0}{\partial y}$ into equation (4.7b) gives,

$$6Ay(1-y) = \frac{1}{RePr}\left(\frac{\partial^2 \theta_0}{\partial x^2} + \frac{\partial^2 \theta_0}{\partial y^2}\right)$$

Since $\dfrac{\partial \theta_0}{\partial x} = A$, $\rightarrow \dfrac{\partial^2 \theta_0}{\partial x^2} = 0$.

$$\therefore \quad \frac{1}{RePr} \quad \frac{\partial^2 \theta_O}{\partial y^2} = 6A(y-y^2)$$

Replacing $\frac{\partial^2 \theta_O}{\partial y^2}$ by $\frac{d^2 \theta_O}{dy^2}$, the above equation can be integrated directly.

$$\therefore \quad \frac{1}{RePr} \quad \frac{d^2 \theta_O}{dy^2} = 6A(y-y^2)$$

$$\therefore \quad \frac{1}{RePr} \quad \frac{d\theta_O}{dy} = 6A(\frac{y^2}{2} - \frac{y^3}{3}) + D_1$$

$$\frac{1}{RePr} \quad \theta_O = 6A(\frac{y^3}{6} - \frac{y^4}{12}) + D_1 y + D_2 \quad \dots\dots\dots(A.5)$$

where D_1 and D_2 are constants of integration.
From the Boundary Conditions,

$$\theta_O \Big|_{y=0} = 0, \rightarrow D_2 = 0$$

$$\theta_O \Big|_{y=1} = 1, \rightarrow \frac{1}{RePr} = 6A(\frac{1}{6} - \frac{1}{12}) + D_1$$

$$= \frac{A}{2} + D_1$$

$$\rightarrow \quad D_1 = (\frac{1}{RePr} - \frac{A}{2})$$

Substituting for D_1 and D_2 in (A.5) gives,

$$\frac{\theta_O}{RePr} = 6A(\frac{y^3}{6} - \frac{y^4}{12}) + (\frac{1}{RePr} - \frac{A}{2})y$$

$$\rightarrow \quad \theta_O = 6RePrA(\frac{y^3}{6} - \frac{y^4}{12}) + y - \frac{RePrA\ y}{2} = RePrA(y^3 - \frac{y^4}{2} - \frac{y}{2}) + y$$

$$\theta_O = y - \frac{RePr}{2} A(y - 2y^3 + y^4) \quad \dots\dots\dots\dots\dots\dots\dots\dots(A.6)$$

A2   Solution for First-order Equations

Substitute ψ_O and θ_O into equations (5.8a) and (5.8b) respectively to solve for ψ_1 and θ_1.

$$\frac{1}{Re} \nabla^4 \psi_1 = -\left[\frac{\partial \theta_O}{\partial y} Sin\alpha + A\ Cos\alpha\right]$$

$$\therefore \quad \frac{1}{Re} \nabla^4 \psi_1 = -\left[\{1 - \frac{RePrA}{2}(1 - 6y^2 + 4y^3)\}Sin\alpha + A\ Cos\alpha\right]$$

$$\rightarrow \quad \frac{d^4\psi_1}{dy^4} = Re\left[\{1 - \frac{RePrA}{2}(1 - 6y^2 + 4y^3)\}Sin\alpha + A\ Cos\alpha\right]$$

$$\frac{d^3\psi_1}{dy^3} = -Re\left[\{y - \frac{RePrA}{2}(y - 2y^3 + y^4)\}Sin\alpha + A\ yCos\alpha\right] + k_1$$

$$\frac{d^2\psi_1}{dy^2} = -Re\left[\{\frac{y^2}{2} - \frac{RePrA}{2}(\frac{y^2}{2} - \frac{y^4}{2} + \frac{y^5}{5})\}Sin\alpha + \frac{A\ y^2}{2}Cos\alpha\right] + k_1 y + k_2$$

$$\frac{d\psi_1}{dy} = -Re\left[\{\frac{y^3}{6} - \frac{RePRA}{2}(\frac{y^3}{6} - \frac{y^5}{10} + \frac{y^6}{30})\}Sin\alpha + \frac{A\ y^3}{6}Cos\alpha\right]$$
$$+ \frac{k_1 y^2}{2} + k_2 y + k_3 \quad \dots\dots(A.7a)$$

$$\psi_1 = -\mathrm{Re}\left[\left\{\frac{y^4}{24} - \frac{\mathrm{RePrA}}{2}\left(\frac{y^4}{24} + \frac{y^6}{60} - \frac{y^7}{210}\right)\right\}\mathrm{Sin}\alpha + \frac{Ay^4}{24}\mathrm{Cos}\alpha\right]$$

$$+ \frac{k_1 y^3}{6} + \frac{k_2 y^2}{2} + k_3 y + k_4 \qquad (A.7b)$$

where k_1, k_2, k_3, k_4 are constants of integration.

For no-slip conditions at the rigid boundaries, using eqn (A.7a), gives

$$\frac{d\psi_1}{dy}\bigg|_{y=0} = 0, \quad \rightarrow \quad k_3 = 0$$

$$\frac{d\psi_1}{dy}\bigg|_{y=1} = 0, \quad \rightarrow \quad 0 = -\mathrm{Re}\left[\left\{\frac{1}{6} - \frac{\mathrm{RePrA}}{2}\left(\frac{1}{6} - \frac{1}{10} + \frac{1}{30}\right)\right\}\mathrm{Sin}\alpha + \frac{A}{6}\mathrm{Cos}\alpha\right]$$

$$\frac{k_1}{2} + k_2 = -\mathrm{Re}\left[\left\{\frac{1}{6} - \frac{\mathrm{RePrA}}{20}\right\}\mathrm{Sin}\alpha + \frac{A}{6}\mathrm{Cos}\alpha\right]\frac{k_1}{2} + k_2 \qquad (A.8a)$$

From the Dirichlet Boundary Conditions, using equation $(5.7b)$, yields

$$\psi_1\bigg|_{y=0} = 0, \rightarrow k_4 = 0.$$

$$\psi_1\bigg|_{y=1} = 0, \rightarrow \quad 0 = -\mathrm{Re}\left[\left\{\frac{1}{24} - \frac{\mathrm{RePrA}}{2}\left(\frac{1}{24} - \frac{1}{60} + \frac{1}{210}\right)\right\}\mathrm{Sin}\alpha + \frac{A}{24}\mathrm{Cos}\alpha\right]$$

$$+ \frac{k_1}{6} + \frac{k_2}{2}$$

$$\text{i.e } 0 = -\mathrm{Re}\left[\left\{\frac{1}{24} - \frac{25\mathrm{RePrA}}{1680}\right\}\mathrm{Sin}\alpha + \frac{A}{24}\mathrm{Cos}\alpha\right] + \frac{k_1}{6} + \frac{k_2}{2}$$

$$\rightarrow \quad 0 = -Re\left[\{\frac{1}{12} - \frac{25RePrA}{840}\}Sin\alpha + \frac{A}{12}Cos\alpha\right] + \frac{k_1}{3} + k_2 \quad \ldots\ldots(A.8b)$$

Subtracting equation (A.8b) from equation (A.8a) yields

$$0 = -Re\left[\{\frac{1}{12} - \frac{17RePrA}{840}\}Sin\alpha + \frac{A}{12}Cos\alpha\right] + \frac{k_1}{6}$$

Transposing, gives

$$\frac{k_1}{6} = \frac{Re}{840}\left[(70-17\,RePrA)Sin\alpha + 70ACos\alpha\right]$$

$$\rightarrow \quad k_1 = \frac{Re}{140}\left[(70-17RePrA)Sin\alpha + 70ACos\alpha\right]$$

$$\rightarrow \quad \frac{k_1}{2} = \frac{Re}{280}\left[(70-17RePrA)Sin\alpha + 70ACos\alpha\right]$$

Substituting into equation (A.8a), produces

$$0 = \frac{Re}{60}\left[(10-3RePrA)Sin\alpha + 10ACos\alpha\right] + \frac{Re}{280}\left[(70-17RePrA)Sin\alpha\right.$$

$$\left. + 70ACos\alpha\right] + k_2$$

$$\therefore \quad k_2 = \frac{14Re}{840}\left[(10-3RePrA)Sin\alpha + 10ACos\alpha\right] - \frac{3Re}{840}\left[(70-17RePrA)Sin\alpha\right.$$

$$\left. + 70ACos\alpha\right]$$

$$= \frac{Re}{840}\left[(140-42RePrA-210 + 51RePrA)Sin\alpha + 140ACos\alpha - 210ACos\alpha\right]$$

$$= \frac{Re}{840}\left[(-70 + 9RePrA)Sin\alpha - 70ACos\alpha\right]$$

$$\rightarrow k_2 = \frac{Re}{840}\left[(9RePrA - 70)Sin\alpha - 70ACos\alpha\right]\dots\dots\dots\dots(A.9)$$

Having determined the constants k_1, k_2, k_3, k_4, substitute these into equation (A.7b) to obtain the expression for ψ_1

$$\therefore \quad \psi_1 = -Re\left[\{\frac{y^4}{24} - \frac{RePrA}{2}(\frac{y^4}{24} - \frac{y^6}{60} + \frac{y^7}{210})\}Sin\alpha + \frac{Ay^4}{24}Cos\alpha\right]$$

$$+ \frac{Re}{840}\left[(70-17RePrA)Sin\alpha + 70ACos\alpha\right]y^3 + \frac{Re}{1680}\left[(9RePrA-70)Sin\alpha-70ACos\alpha\right]y$$

$$\psi_1 = -\frac{Re}{1680}\left[\{70y^4-RePrA(35y^4-14y^6+4y^7)\}Sin\alpha + 70Ay^4Cos\alpha\right]$$

$$+ \frac{Re}{1680}\left[(140-34RePrA)Sin\alpha+140ACos\alpha\right]y^3 + \frac{Re}{1680}\left[(9RePrA-70)Sin\alpha - 70ACos\alpha\right]y^2$$

$$\rightarrow \psi_1 = \frac{Re}{1680}\left[\{(9RePrA-70)y^2+(140-34RePrA)y^3-70y^4+RePrA(35y^4-14y^6+4y^7)\}Sin\alpha -70A(y^2-2y^3+y^4)Cos\alpha\right]$$

$$\psi_1 = \frac{Re}{1680}\left[\{(9RePrA-70)y^2+(140-34RePrA)y^3-70y^4+RePrA(35y^4-14y^6+4y^7)\}Sin\alpha \right.$$
$$\left. - 70A(y^2-2y^3+y^4)Cos\alpha \right] \quad (A.10)$$

Consider equation(5.8b) given by;

$$A\frac{\partial \psi_1}{\partial y} = \frac{1}{RePr}\nabla^2\theta_1$$

$$\rightarrow \quad \frac{1}{RePr}\frac{d^2\theta_1}{dy^2} = \frac{ReA}{1680}\left[\{(18RePrA-140)y+(420-102RePrA)y^2-280y^3+RePrA(140y^3 \right.$$
$$\left. -84y^5+28y^6)\}Sin\alpha-70A(2y-6y^2+4y^3)Cos\alpha \right]$$

Integrating,

$$\frac{1}{RePrA}\frac{d\theta_1}{dy} = \frac{Re}{1680}\left[\{9RePrA-70)y^2+(140-34RePrA)y^3-70y^4+RePrA(35y^4 \right.$$
$$\left. -14y^6+4y^7)\}Sin\alpha -70A(y^2-2y^3+y^4)Cos\alpha \right]+G_1$$

$$\therefore \frac{1}{RePrA}\theta_1 = \frac{Re}{1680}\left[\{(9RePrA-70)\frac{y^3}{3}+(140-34RePrA)\frac{y^4}{4}-14y^5+RePrA(7y^5 \right.$$
$$\left. -2y^7+\frac{y^8}{2})\}Sin\alpha-70A(\frac{y^3}{3}-\frac{y^4}{2}+\frac{y^5}{5})Cos\alpha \right]+G_1y+G_2$$

$$(A.11)$$

where G_1, G_2 are constants to be determined using the Dirichlet boundary Conditions. Using equation (A.11),

$$\theta_1\bigg|_{y=0} = 0, \rightarrow 0 = G_2$$

$$\theta_1\bigg|_{y=1} = 0, \rightarrow 0 = \frac{Re}{1680}\left[\{\frac{(9RePrA-70)}{3}+\frac{(140-34RePrA)}{4}-14+RePrA(7 \right.$$
$$\left. -2+\frac{1}{2})\}Sin\alpha-70A(\frac{1}{3}-\frac{1}{2}+\frac{1}{5})Cos\alpha \right]+G_1$$

$$\rightarrow \quad G_1 = \frac{Re}{1680}\left[\{\frac{(70-9RePrA)}{3} - \frac{(140-34RePrA)}{4} + 14-RePrA(7\right.$$

$$\left.-2+\tfrac{1}{2})\}Sin\alpha+70A(\frac{1}{3} - \frac{1}{2} + \frac{1}{5})Cos\alpha\right]$$

$$= \frac{Re}{1680}\left[(\frac{7}{3}Sin\alpha + \frac{7A}{3} Cos\alpha)\right]$$

$$G_1 = \frac{Re}{720}(Sin\alpha + ACos\alpha)$$

On substituting G_1 and G_2 into equation (A.11),

$$\frac{\theta_1}{RePrA} = \frac{Re}{1680}\left[\{\frac{(9RePrA-70)}{3} y^3+ \frac{(140-34RePrA)}{4} y^4-14y^5+RePrA(7y^5\right.$$

$$\left.-2y^7+\frac{y^8}{2})\}Sin\alpha- \frac{7A}{3}(10y^3-15y^4+6y^5)Cos\alpha\right]$$

$$+ \frac{Re}{720}(Sin\alpha + ACos\alpha)y$$

On simplifying,

$$\frac{\theta_1}{RePrA} = \frac{Re}{20160}\left[\{28y+(36RePrA-280)y^3+(420-102RePrA)y^4-168y^5\right.$$

$$\left.+RePrA(84y^5-24y^7+6y^8)\}Sin\alpha+28A(y-10y^3+15y^4\right.$$

$$\left.-6y^5)Cos\alpha\right]$$

$$\theta_1 = \frac{PrARe^2}{20160}\left[\{28y+(36RePrA-280)y^3+(420-102RePrA)y^4-168y^5+RePrA(84y^5\right.$$

$$\left.-24y^7+6y^8)\}Sin\alpha+28A(y-10y^3+15y^4-6y^5) Cos\alpha\right] \quad (A.12)$$

A3 Solution for Second-order Equations

Having found the expressions for ψ_0, θ_0, ψ_1, θ_1, proceed to substitute into equations (5.9a) and (5.9b) to find expressions for ψ_2, θ_2 respectively.

From equation (5.9a) $\dfrac{1}{Re} \nabla^4 \psi_2 = - \dfrac{\partial \theta_1}{\partial y} \sin\alpha$

Expanding the LHS gives

$$\frac{1}{Re}\left(\frac{\partial^4 \psi_2}{\partial x^4} + \frac{2\partial^4 \psi_2}{\partial x \partial y^2} + \frac{\partial^4 \psi_2}{\partial y^4}\right) = - \frac{\partial \theta_1}{\partial y} \sin\alpha$$

Since $\dfrac{\partial^4 \psi_2}{\partial x^4} = \dfrac{\partial^4 \psi_2}{\partial x^2 \partial^2} = 0$, the above equation reduces to

$$\frac{1}{Re} \frac{\partial^4 \psi_2}{\partial y^4} = - \frac{\partial \theta_1}{\partial y} \sin\alpha$$

Also, since ψ_2 and θ_1 depend on y only, then express the above equation in total derivative forms.

$$\therefore \frac{1}{Re} \frac{d^4 \psi_2}{dy^4} = - \frac{\partial \theta_1}{dy} \sin\alpha$$

$$\rightarrow + \frac{1}{Re} \frac{d^4 \psi_2}{dy^4} = - \frac{APrRe^2}{20160}\left[\{28+(108RePrA-840)y^2+(1680-408RePrA)y^3\right.$$
$$-840y^4+RePrA(420y^4-168y^6+48y^7)\}\sin\alpha$$
$$\left.+28A(1-30y^2+60y^3-30y^4)\cos\alpha\}\right]\sin\alpha$$

$$+ \frac{1}{Re} \frac{d^3 \psi_2}{dy^3} = - \frac{APrRe^2}{20160}\left[\{28y +(36RePrA-280)y^3+(420-102RePrA)y^4\right.$$
$$-168y^5+RePrA(84y^5-24y^7+6y^8)\}\sin\alpha$$
$$\left.+28A(y-10y^3+15y^4-6y^5)\cos\alpha\right]\sin\alpha + E_1$$

$$\rightarrow \quad \frac{1}{Re} \frac{d^2\psi_2}{dy^2} = -\frac{APrRe^2}{20160}\left[\{14y^2+(9RePrA-70)y^4+\frac{(420-102RePrA)y^5}{5}\right.$$

$$-28y^6+RePrA(14y^6-3y^8+\frac{2}{3}y^9)\}Sin^2\alpha$$

$$\left.+14A(\frac{y^2}{2}-\frac{10y^4}{4}+3y^5-y^6)Sin2\alpha\right]+E_1 \ y \ + \ E_2$$

$$\frac{1}{Re}\frac{d\psi_2}{dy} = -\frac{APrRe^2}{20160}\left[\{\frac{14y^3}{3}+\frac{(9RePrA-70)y^5}{5}+\frac{(420-102RePrA)y^6}{30}\right.$$

$$-4y^7+RePrA(2y^7-\frac{y^9}{3}+\frac{y^{10}}{15})\}Sin^2\alpha$$

$$\left.+14A(\frac{y^3}{6}-\frac{y^5}{2}+\frac{y^6}{2}-\frac{y^7}{7})Sin2\alpha\right]$$

$$+\frac{E_1y^2}{2}+E_2y+E_3 \ \ldots\ldots\ldots\ldots(A.13a)$$

$$\rightarrow \quad \frac{\psi_2}{Re} = -\frac{APrRe^2}{20160}\left[\{\frac{7}{6}y^4+\frac{(9RePrA-70)y^6}{30}+\frac{(420-102RePrA)y^7}{210}-\frac{y^8}{2}\right.$$

$$+RePrA(\frac{y^8}{4}-\frac{y^{10}}{30}+\frac{y^{11}}{165})\}Sin^2\alpha+14A(\frac{y^4}{24}-\frac{y^6}{12}$$

$$\left.+\frac{y^7}{14}-\frac{y^8}{56})Sin2\alpha\right]+\frac{E_1y^3}{6}+\frac{E_2y^2}{2}+E_3y+E_4 \quad (A.13b)$$

Where E_1, E_2, E_3 and E_4 are constants of integration to be determined from the B.C. For No-slip conditions (Neumann B.C.) at the rigid walls, using equation (A.13a) yields,

$$\frac{d\psi_2}{dy}\bigg|_{y=0} = 0, \rightarrow E_3 = 0$$

$$\frac{d\psi_2}{dy}\bigg|_{y=1} = 0,$$

$$\rightarrow \quad \dot{0} = -\frac{APrRe^2}{20160}\left[\{\frac{14}{3} + \frac{(9RePrA-70)}{5} + \frac{(420-102RePrA)}{30} - 4+RePrA(2-\frac{1}{3} + \frac{1}{15})\}Sin^2\alpha+14A(\frac{1}{6} - \frac{1}{2} + \frac{1}{2} - \frac{1}{7})Sin2\alpha\right]\frac{E_1}{2} + E_2 \quad (A.14)$$

From the Dirichlet Boundary conditions, using equation (A.13b),

$$\psi_2\Big|_{y=0} = 0, \rightarrow E_4 = 0$$

$$\psi_2\Big|_{y=1} = 0, \rightarrow 0 = -\frac{APrRe^2}{20160}\left[\{\frac{7}{6} + \frac{(9RePrA-70)}{30} + \frac{(420-102RePrA)}{210} - \frac{1}{2}\right.$$

$$\left. +RePrA(\frac{1}{4} - \frac{1}{30} + \frac{1}{165})\}Sin^2\alpha+14A(\frac{1}{24} - \frac{1}{12} + \frac{1}{14} - \frac{1}{56})Sin2\alpha\right]\frac{E_1}{6} + \frac{E_2}{2} \quad (A.15)$$

Equation (A.15) reduces to:

$$-\frac{APrRe^2}{20160}\left[\{\frac{2}{3} + \frac{2RePrA}{15}\}Sin^2\alpha + \frac{A}{3} Sin2\alpha\right] + \frac{E_1}{2} + E_2 = 0 \dots\dots(A.15a)$$

Also equation (A.13a) reduces to:

$$-\frac{APrRe^2}{20160}\left[\{\frac{2}{3} + \frac{57RePrA}{770}\}Sin^2\alpha + \frac{A}{3} Sin2\alpha\right] + \frac{E_1}{3} + E_2 = 0 \dots\dots(A.15b)$$

Equation (A.15a) from (A.15b) gives,

$$-\frac{APrRe^2}{20160}\left[\frac{137RePrA}{2310}Sin^2\alpha\right] + \frac{E_1}{6} = 0$$

$$\rightarrow \quad E_1 = \frac{APrRe^2}{20160}\left(\frac{274RePrA\ Sin^2\alpha}{770}\right)$$

From (A.15a) E_2 becomes

$$E_2 = \frac{APrRe^2}{20160}\left[\{\frac{2}{3} + \frac{2RePrA}{15}\}Sin^2\alpha + \frac{A}{3}Sin2\alpha\right] - \frac{APrRe^2}{20160}\left(\frac{137RePrA\ Sin^2\alpha}{770}\right)$$

$$E_2 = \frac{APrRe^2}{20160}\left[\{\frac{2}{3} - \frac{103RePrA}{2310}\}Sin^2\alpha + \frac{A}{3}\ Sin2\alpha\right]$$

Substitute E_1, E_2, E_3, E_4 into equation (A.13b)

$$\frac{\psi_2}{Re} = -\frac{APrRe^2}{20160}\left[\{\frac{7y^4}{6} + \frac{(9RePrA-70)y^6}{30} + \frac{(420-102RePrA)y^7}{210} - \frac{y^8}{2} + RePrA(\frac{y^8}{4}\right.$$

$$\left. - \frac{y^{10}}{30} + \frac{y^{11}}{165})\}Sin^2\alpha + 14A(\frac{y^4}{24} - \frac{y^6}{12} + \frac{y^7}{14} - \frac{y^8}{56})Sin2\alpha\right]$$

$$+ \frac{APrRe^2}{20160}\left(\frac{137RePrA\ Sin^2\alpha}{2310}\right)y^3 + \frac{APrRe^2}{20160}\left[\{\frac{1}{3} - \frac{103RePrA}{4620}\}Sin^2\alpha\right.$$

$$\left. + \frac{A}{6}\ Sin2\alpha\right]y^2$$

$$\rightarrow \quad \frac{\psi_2}{Re} = \frac{APrRe^2}{20160}\left[\{(\frac{1}{3} - \frac{103RePrA}{4620})y^2 + (\frac{137RePrA}{2310})y^3 - \frac{7y^4}{6} - \frac{(9RePrA-70)y^6}{30}\right.$$

$$- \frac{(420-102RePrA)y^7}{210} + \frac{y^8}{2} - RePrA(\frac{y^8}{4} - \frac{y^{10}}{30} + \frac{y^{11}}{165})\}Sin^2\alpha$$

$$\left. + \{\frac{Ay^2}{6} - 14A(\frac{y^4}{24} - \frac{y^6}{12} + \frac{y^7}{14} - \frac{y^8}{56})\}Sin2\alpha\right]$$

$$\rightarrow \quad \psi_2 = \frac{APrRe^3}{20160}\left[\{(\frac{1}{3} - \frac{103RePrA}{4620})y^2 + (\frac{137RePrAy^3}{2310} - \frac{7y^4}{6} - \frac{(9RePrA-70)y^6}{30}\right.$$

$$\left. - \frac{(420-102RePrA)y^7}{210} + \frac{y^8}{2} - RePrA(\frac{y^8}{4} - \frac{y^{10}}{30} + \frac{y^{11}}{165})\}Sin^2\alpha\right]$$

$$+ \frac{A}{12}(\frac{y^2}{6} - \frac{7y^4}{12} + \frac{7y^6}{6} - y^7 + \frac{y^8}{4})Sin2\alpha$$

$$\therefore \quad \psi_2 = \frac{APrRe^3}{20160}\left[\{(\frac{1}{3} - \frac{103RePrA}{4620})y^2 + (\frac{137RePrA}{2310})y^3 - \frac{7y^4}{6} - \frac{(9RePrA-70)y^6}{30} \right.$$

$$- \frac{(420-102RePrA)y^7}{210} + \frac{y^8}{2} - RePrA(\frac{y^8}{4} - \frac{y^{10}}{30}$$

$$\left. + \frac{y^{11}}{165})\}Sin^2\alpha + \frac{\Lambda}{12}(2y^2-7y^4+14y^6-12y^7+3y^8)Sin2\alpha\right]$$

$$(A.16)$$

Now substitute ψ_2 into equation (5.9b) given by

$$A\frac{\partial\psi_2}{\partial y} = \frac{1}{RePr}\nabla^2\theta_2$$

$$\rightarrow \quad \frac{1}{ARePr}\frac{d^2\theta_2}{dy^2} = \frac{d\psi_2}{dy}$$

$$\rightarrow \quad \frac{1}{APrRe}\frac{d\theta_2}{dy} = \frac{APrRe^3}{20160}\left[\{(\frac{1}{3} - \frac{103RePrA}{4620})y^2 + \frac{137RePrAy^3}{2310} - \frac{7y^4}{6}\right.$$

$$- \frac{(9RePrA-70)y^6}{30} - \frac{(420-102RePrA)y^7}{210}$$

$$+ \frac{y^8}{2} - RePrA(\frac{y^8}{4} - \frac{y^{10}}{30} + \frac{y^{11}}{165})\}Sin^2\alpha$$

$$\left. + \frac{A}{12}(2y^2-7y^4+14y^6-12y^7+3y^8)Sin2\alpha\right]+F_1$$

$$\rightarrow \frac{\theta_2}{APrRe} = \frac{APrRe^3}{20160}\left[\{(\frac{1}{3} - \frac{103RePrA}{4620})\frac{y^3}{3} + \frac{137RePrAy^4}{9240} - \frac{7y^5}{30} - \frac{(9RePrA-70)y^7}{210}\right.$$

$$- \frac{(420-102RePrA)y^8}{1680} + \frac{y^9}{18} \quad - \quad RePrA(\frac{y^9}{36}$$

$$- \frac{y^{11}}{330} + \frac{y^{12}}{1980})\}Sin^2\alpha + \frac{A}{12}(\frac{2y^3}{3} - \frac{7y^5}{5} + 2y^7 - \frac{3y^8}{2}$$

$$\left. + \frac{y^9}{3})Sin2\alpha\right] + F_1y + F_2 \quad \ldots\ldots\ldots\ldots(A.17)$$

where F_1 and F_2 can be determined from the boundary conditions.

From the Dirichlet Boundary conditions, using equation (A.17), yields,

$$\theta_2\Big|_{y=0} = 0, \; \rightarrow \; F_2 = 0$$

$$\theta_2\Big|_{y=1} = 0, \; \rightarrow \; 0 = \frac{APrRe^3}{20160}\left[\{(\frac{1}{9} - \frac{103RePrA}{13860}) + \frac{137RePrA}{9240} - \frac{7}{30}\right.$$

$$- \frac{(9RePrA-70)}{210} - \frac{(420-102RePrA)}{1680}$$

$$+ \frac{1}{18} - RePrA(\frac{1}{36} - \frac{1}{330} + \frac{1}{1980})\}Sin^2\alpha$$

$$+ \frac{A}{12}(\frac{2}{3} - \frac{7}{5} + 2 - \frac{3}{2} + \frac{1}{3})Sin2\alpha\Big] + F_1$$

$$\rightarrow \quad F_1 = - \frac{APrRe^3}{20160}\left[\{\frac{1}{60}\}Sin^2\alpha + \frac{A}{120}Sin2\alpha\right]$$

$$\rightarrow \quad F_1 = - \frac{APrRe^3}{20160}(\frac{1}{60}Sin^2\alpha + \frac{A}{120}Sin2\alpha)$$

Now substitute F_1 and F_2 into equation (A.17) to obtain

$$\frac{\theta_2}{APrRe} = \frac{APrRe^3}{20160}\left[\{(\frac{1}{9} - \frac{103RePrA}{13860})y^3 + \frac{137RePrAy^4}{9240} - \frac{7y^5}{30} - \frac{(9RePrA-70)y^7}{210}\right.$$

$$- \frac{(420-102RePrA)y^8}{1680} + \frac{y^9}{18} - RePrA(\frac{y^9}{36} - \frac{y^{11}}{330} + \frac{y^{12}}{1980})\}Sin^2\alpha$$

$$+ \frac{A}{360}(20y^3 - 42y^5 + 60y^7 - 45y^8 + 10y^9)Sin2\alpha\Big] - \frac{APrRe^3}{20160}(\frac{Sin^2\alpha}{60}$$

$$+ \frac{A}{120}Sin2\alpha)y$$

$$
= \frac{APrRe^3}{20160} \Bigg[\Big\{ \frac{(1540-103RePrA)y^3}{13860} + \frac{137RePrAy^4}{9240} - \frac{7y^5}{30} + \frac{(9RePrA-70)y^7}{210}
$$

$$
- \frac{(420-102RePrA)y^8}{1680} + \frac{y^9}{18} - \frac{RePrA}{1980}(55y^9
$$

$$
- 6y^{11}+y^{12}) \Big\} Sin^2\alpha + \frac{A}{360}(20y^3-42y^5
$$

$$
+ 60y^7-45y^8+10y^9)Sin2\alpha - (\frac{Sin^2\alpha}{60}
$$

$$
+ \frac{A}{120} Sin2\alpha)y \Bigg]
$$

$$
\rightarrow \quad \theta_2 = \frac{A^2Pr^2Re^4}{20160} \Bigg[\Big\{ -\frac{y}{60} + \frac{(1540-103RePrA)y^3}{13860} + \frac{137RePrAy^4}{9240} - \frac{7y^5}{30} - \frac{(9RePrA-70)y^7}{210}
$$

$$
- \frac{(420-102RePrA)y^8}{1680} + \frac{y^9}{18} - \frac{RePrA}{1980}(55y^9-6y^{11}+y^{12}) \Big\} Sin^2\alpha
$$

$$
+ \frac{A}{360}(-3y+20y^3-42y^5+60y^7-45y^8+10y^9)Sin2\alpha \Bigg] \dots (A.18)
$$

A4. Solution for Third-order Equations

Substitute θ_2 into equation (5.10a) and replace the partial derivatives

by their total counterparts.

From (5.10a) $\quad \frac{1}{Re} \nabla^4\psi_3 = \frac{\partial\theta_2}{\partial y} Sin\alpha$

$$
\rightarrow \quad \frac{1}{Re} \frac{d^4\psi_3}{dy^4} = -\frac{d\theta_2}{dy} Sin\alpha
$$

Integrating,

$$
\frac{1}{Re} \cdot \frac{d^3\psi_3}{dy^3} = -\frac{A^2Pr^2Re^4}{20160} \Bigg[\Big\{ -\frac{y}{60} + \frac{(1540-103RePrA)y^3}{13860} + \frac{137RePrAy^4}{9240} - \frac{7y^5}{30}
$$

$$
- \frac{(9RePrA-70)y^7}{210} - \frac{(420-102RePrA)y^8}{1680} + \frac{y^9}{18}
$$

$$
- \frac{RePrA}{1980}(55y^9-6y^{11}+y^{12}) \Big\} Sin^3\alpha + \frac{A}{360}(-3y+20y^3
$$

$$
- 42y^5+60y^7-45y^8+10y^9)Sin2\alpha \, Sin\alpha \Bigg] + H_1
$$

$$\frac{1}{Re}\frac{d^2\psi_3}{dy^2} = -\frac{A^2Pr^2Re^4}{20160}\left[\left\{\frac{-y^2}{120} + \frac{(1540-103RePrA)y^4}{13860x4} + \frac{137RePrAy^5}{9240x5}\right.\right.$$

$$-\frac{7y^6}{180} - \frac{(9RePrA-70)y^8}{1680} - \frac{(420-102RePrA)y^9}{1680x9}$$

$$+\frac{y^{10}}{180} - \frac{RePrA}{1980}\left(\frac{11y^{10}}{2} - \frac{y^{12}}{2} + \frac{y^{13}}{13}\right)\Big\}Sin^3\alpha$$

$$+\frac{\Lambda}{360}\left(-\frac{3y^2}{2} + 5y^4 - 7y^6 + \frac{15y^8}{2} - 5y^9\right.$$

$$\left.\left. - y^{10}\right)Sin2\alpha\ Sin\alpha\right] + H_1y + H_2$$

$$\frac{1}{Re}\frac{d\psi_3}{dy} = -\frac{A^2Pr^2Re^4}{20160}\left[\left\{\frac{-y^3}{360} + \frac{(1540-103RePrA)y^5}{13860x20} + \frac{137RePrAy^6}{9240x30} - \frac{y^7}{180}\right.\right.$$

$$-\frac{(9RePrA-70)y^9}{1680x9} - \frac{(420-102RePrA)y^{10}}{1680x90} + \frac{y^{11}}{1980}$$

$$-\frac{RePrA}{1980}\left(\frac{y^{11}}{2} - \frac{y^{13}}{26} + \frac{y^{14}}{182}\right)\Big\}Sin^3\alpha + \frac{A}{360}\left(\frac{-y^3}{2}\right.$$

$$\left. + y^5 - y^7 + \frac{5y^9}{6} - \frac{y^{10}}{2} + \frac{y^{11}}{11}\right)Sin2\alpha\ Sin\alpha\Bigg] + \frac{H_1y^2}{2}$$

$$+ H_2y + H_3 \dots\dots\dots\dots\dots\dots(\Lambda.19a)$$

$$\therefore \frac{\psi_3}{Re} = \frac{-A^2Pr^2Re^4}{20160}\left[\left\{\frac{y^4}{1440} + \frac{(1540-103RePrA)y^6}{13860x120} + \frac{137RePrAy^7}{9240x210} - \frac{y^8}{1440}\right.\right.$$

$$-\frac{(9RePrA-70)y^{10}}{1680x90} - \frac{(420-102RePrA)y^{11}}{1680x990}$$

$$+\frac{y^{12}}{1980x12} - \frac{RePrA}{1980}\left(\frac{y^{12}}{24} - \frac{y^{14}}{364} + \frac{y^{15}}{2730}\right)\Big\}Sin^3\alpha$$

$$+\frac{\Lambda}{360}\left(\frac{-y^4}{8} + \frac{y^6}{6} - \frac{y^8}{8} + \frac{y^{10}}{12} - \frac{y^{11}}{22} + \frac{y^{12}}{132}\right)Sin2\alpha Sin\alpha\Bigg]$$

$$+\frac{H_1y^3}{6} + \frac{H_2y^2}{2} + H_3y + H_4 \dots\dots\dots\dots(\Lambda.19b)$$

where H_1, H_2, H_3, H_4 are constants of integration.

For no-slip conditions (Neumann B.C.) at the rigid boundaries, using equation $(A.19a)$, gives

$$\frac{d\psi_3}{dy}\bigg|_{y=0} = 0, \rightarrow H_3 = 0$$

$$\frac{d\psi_3}{dy}\bigg|_{y=1} = 0, \rightarrow 0 = \frac{-A^2Pr^2Re^4}{20160}\left[\frac{-1}{360} + \frac{(1540-103RePrA)}{277200} + \frac{137RePrA}{277200}\right.$$

$$-\frac{1}{180} - \frac{(9RePrA-70)}{15120} - \frac{(420-120RePrA}{151200}$$

$$+\frac{1}{1980} - \frac{RePrA}{1980}(\frac{1}{2} - \frac{1}{26} + \frac{1}{182})Sin^3\alpha$$

$$+\frac{A}{360}(-\frac{1}{2} +1-1+\frac{5}{6} - \frac{1}{2}$$

$$\left.+\frac{1}{11}) Sin2\alpha Sin\alpha\right] + \frac{H_1}{2} + H_2$$

The above equation reduces to

$$\frac{-A^2Pr^2Re^4}{20160}\left[(-\frac{1}{2376} - \frac{61}{1801800} RePrA)Sin^3\alpha - \frac{ASin^2\alpha Cos\alpha}{2376}\right]$$

$$+ \frac{H_1}{2} + H_2 = 0 \dots\dots\dots\dots\dots(A.20a)$$

From the Dirichlet Boundary Conditions, using equation $(A.19b)$ gives

$$\psi_3\bigg|_{y=0} = 0, \rightarrow H_4 = 0.$$

$$\psi_3\bigg|_{y=1} = 0.$$

$$\rightarrow 0 = -\frac{A^2Pr^2Re^4}{20160}\left[\{-\frac{1}{1440} + \frac{(1540-103RePrA)}{13860 \times 120} + \frac{137RePrA}{9240 \times 210} - \frac{1}{1440}\right.$$

$$-\frac{(9RePrA-70)}{1680 \times 90} - \frac{(420-102RePrA)}{1680 \times 990} + \frac{1}{1980 \times 12} - \frac{RePrA}{1980}(\frac{1}{24}$$

$$\left.-\frac{1}{364} + \frac{1}{2730})\}Sin^3\alpha + \frac{A}{360}(-\frac{1}{8} + \frac{1}{6} - \frac{1}{8} + \frac{1}{12} - \frac{1}{22}\right.$$

$$\left.+ \frac{1}{132})Sin2\alpha\ Sin\alpha\right] + \frac{H_1}{6} + \frac{H_2}{2}$$

$$\rightarrow -\frac{A^2Pr^2Re^4}{20160}\left[\{-\frac{1}{5940} - \frac{6641RePrA}{34927200}\}Sin^3\alpha - \frac{ASin2\alpha Sin\alpha}{23760}\right] + \frac{H_1}{6} + \frac{H_2}{2} = 0$$

$$\therefore -\frac{A^2Pr^2Re^4}{20160}\left[-2(\frac{1}{5940} + \frac{6641RePrA}{34927200})Sin^3\alpha - \frac{2ASin^2\alpha Cos\alpha}{11880}\right] + \frac{H_1}{3}$$

$$+ H_2 = 0 \quad (A.20b)$$

If we substract $(A.20b)$ from $(A.20a)$ to give,

$$-\frac{A^2Pr^2Re^4}{20160}\left[\{2(\frac{1}{5940} + \frac{6641RePrA}{34927200})-(\frac{1}{2376} + \frac{61RePrA}{1801800})\}Sin^3\alpha\right.$$

$$\left.+ A(\frac{2}{11880} - \frac{1}{2376})Sin^2\alpha Cos\alpha\right] + \frac{H_1}{6} = 0$$

$$\rightarrow H_1 = \frac{6A^2Pr^2Re^4}{20160}\left[\{(\frac{1}{2970} + \frac{6641RePrA}{17463600})-(\frac{1}{2376} + \frac{61RePrA}{1801800})\}Sin^3\alpha\right.$$

$$\left.+ A(\frac{1}{5940} - \frac{1}{2376})Sin^2\alpha Cos\alpha\right]$$

$$= \frac{A^2Pr^2Re^4}{20160}\left[\{\frac{1}{495} + \frac{6641RePrA}{2910600})-(\frac{1}{396} + \frac{61RePrA}{300300})\}Sin^3\alpha\right.$$

$$\left.+ A(\frac{1}{990} - \frac{1}{396})Sin^2\alpha\ Cos\alpha\right]$$

$$H_1 = \frac{A^2Pr^2Re^4}{20160}\left[(-\frac{1}{1980} + \frac{18167457RePrA}{874053180000})Sin^3\alpha - \frac{A}{660}Sin^2\alpha Cos\alpha\right] \cdot$$

Substitute into equation (Λ.20a) and solve for H_2,

$$H_2 = \frac{A^2Pr^2Re^4}{20160}\left[-(\frac{1}{2376} + \frac{61RePrA}{1801800})Sin^3\alpha - \frac{A}{2376}Sin^2\alpha Cos\alpha\right]$$

$$- \frac{A^2Pr^2Re^4}{20160}\left[(\frac{1}{3960} + \frac{18167457RePrA}{1748106360000})Sin^3\alpha - \frac{A}{1320}Sin^2\alpha\, Cos\alpha\right]$$

$$H_2 = \frac{A^2Pr^2Re^4}{20160}\left[(\frac{1}{1485} + \frac{61RePrA}{1801800} + \frac{18167457RePrA}{1748106360000})Sin^3\alpha\right.$$

$$\left. + \frac{A}{2970}Sin^2\alpha\, Cos\alpha)\right]$$

Substitute for H_1, H_2, H_3, H_4 into equation (Λ.19b) to obtain

$$\psi_3 = -\frac{A^2Pr^2Re^5}{20160}\left[\{\frac{-y^4}{1440} + \frac{(1540-103RePrA)y^6}{13860 \times 120} + \frac{137RePrAy^7}{9240 \times 210} - \frac{y^8}{1440}\right.$$

$$- \frac{(9RePrA-70)y^{10}}{1680\times90} - \frac{(420-102RePrA)y^{11}}{1680\times990} + \frac{y^{12}}{1980\times12} - \frac{RePrA}{1980}(\frac{y^{12}}{24}$$

$$\left. - \frac{y^{14}}{364} + \frac{y^{15}}{2730})\}Sin^3\alpha\, Cos\alpha\right]+\frac{A}{360}(\frac{-y^4}{4}+\frac{y^6}{3}-\frac{y^8}{4}+\frac{y^{10}}{6} - \frac{y^{11}}{11}+\frac{y^{12}}{66})Sin^2\alpha\, Cos\alpha$$

$$+ \frac{A^2Pr^2Re^5}{20160}\left[(\frac{18167457PrePrA}{874053180000x6} - \frac{1}{11880})Sin^3\alpha - \frac{A}{3960}Sin^2\alpha Cos\alpha\right]y^3$$

$$+ \frac{A^2Pr^2Re^5}{20160}\left[-\{\frac{1}{2970} + RePrA(\frac{61}{1801800x2} + \frac{18167457}{1748106360000x2})\}Sin^3\alpha\right.$$

$$\left. + \frac{A}{5940}Sin^2\alpha\, Cos\alpha\right]\quad(\Lambda.21)$$

Proceeding to substitute ψ_3 into equation ($5.10b$) yields the
expression for θ_3 by successive integration and application of the

Dirichlet Boundary conditions. However, the complexity of equation (A.21) demonstrates the complex nature of the computation. Hence, the contributions of θ_3, ψ_3 which are temperature and streamfunction perturbations respectively, can be neglected. The analysis henceforth is restricted to the solutions of the zero, first and second order equations.

Substituting ψ_0, ψ_1, ψ_2 into equation (5.3) yields the expression for ψ. Thus,

$$\psi = (3y^2-2y^3)+Ar\frac{Re}{1680}\left[\{(9RePrA-70)y^2+(140-34RePrA)y^3-70y^4RePrA(35y^4\right.$$
$$\left.-14y^6+4y^7)Sin\alpha-70A(y^2-2y^3+y^4)Cos\alpha\}\right]$$

$$+Ar^2\left\{\frac{APrRe^3}{20160}\left[\{(\frac{1}{3}-\frac{103RePrA}{4620})y^2+\frac{137RePrAy^3}{2310}-\frac{7y^4}{6}-\frac{(9RePrA-70)y^6}{30}\right.\right.$$
$$-\frac{(420-102RePrA)y^7}{210}+\frac{y^8}{2}-RePrA(\frac{y^8}{4}-\frac{y^{10}}{30}+\frac{y^{11}}{165})\}Sin^2\alpha$$
$$\left.\left.+\frac{A}{12}(2y^2-7y^4+14y^6-12y^7+3y^8)Sin2\alpha\right]\right\}$$

Differentiating the above equation w.r.t.y yields the longitudinal velocity distribtuion across the channel.

$$\therefore \frac{d\psi}{dy} = 6y(1-y)+Ar\frac{Re}{1680}\left[\{(18RePrA-140)y+(420-102RePrA)y^2-280y^3\right.$$
$$\left.+RePrA(140y^3-84y^5+28y^6)\}Sin\alpha-140A(y-3y^2+2y^3)Cos\alpha\right]\}$$

$$+Ar^2\left\{\frac{APrRe^3}{20160}\left[\{(\frac{2}{3}-\frac{103RePrA}{2310})y+\frac{137RePrAy^2}{770}-\frac{14y^3}{3}\right.\right.$$

$$- \frac{(9RePrA-70)y^5}{5} - \frac{(140-34RePrA)y^6}{10} + 4y^7 - RePrA(2y^7 - \frac{y^9}{3} + \frac{y^{10}}{15})\}Sin^2\alpha$$

$$+ \frac{A}{12}(4y-28y^3 + 84y^5 - 84y^6 + 24y^7) \; Sin2\alpha \Bigg]$$

By Definition, the Longitudinal velocity u is given by $u = \frac{d\psi}{dy}$.

$$\therefore u = 6y(1-y) + Ar\frac{Re}{1680}\Bigg[\{(18RePrA-140)y+(420-102RePrA)y^2-280y^3$$

$$+ RePrA(140y^3-84y^5+28y^6)\}Sin\alpha - 140A(y-3y^2+2y^3)Cos\alpha \Bigg]$$

$$+ Ar^2\frac{APrRe^3}{20160}\Bigg[\{(\frac{2}{3} - \frac{103RePrA}{2310})y+\frac{137RePrAy^2}{770} - \frac{14y^3}{3} - \frac{(9RePrA-70)y^5}{5}$$

$$- \frac{(140 - 34RePrA)y^6}{10} + 4y^7 - RePrA(2y^7 - \frac{y^9}{3} + \frac{y^{10}}{15})\})Sin^2\alpha$$

$$+ \frac{A}{12}(4y - 28y^3+84y^5 - 84y^6 + 24y^7) \; Sin2\alpha \Bigg] \quad \dots(A.22)$$

A5. Determination of Wall Friction Factors

Since the fluid under consideration is Newtonian, the wall shear stress τ_ω, admits the representation $\tau_\omega = \mu \left.\frac{dU}{dY}\right|_{wall}$

The coefficient of friction C_f is defined by:

$$C_f = \frac{2\tau_\omega}{\rho_m V^2_{mean}}$$

$$\therefore C_f = \frac{2\mu \left.\frac{dU}{dY}\right|_{wall}}{\rho_m V^2_{mean}} \qquad V_{mean} = \text{mean velocity at cross-section.}$$

Introduce the usual normalising coordinates for V_{mean} and Y. Thus,

$$v_{mean} = \frac{V_{mean}}{U_m}$$

$$y = \frac{Y}{b}$$

$$\rightarrow \quad C_f = \frac{2\mu \frac{U_m}{b} \left.\frac{du}{dy}\right|_{wall}}{\rho_m U_m^2 \, v_{mean}^2} = \frac{2\mu \left.\frac{du}{dy}\right|_{wall}}{\rho_m U_m \cdot b \, v_{mean}^2}$$

$$\rightarrow \quad C_f = \frac{2 \left.\frac{du}{dy}\right|_{wall}}{(\frac{\rho_m U_m b}{\mu}) v_{mean}^2} \quad \text{where} \quad \frac{\rho_m U_m b}{\mu} \quad \text{can be recognised as the Reynolds number Re}$$

$$\therefore \quad C_f = \frac{2 \left.\frac{du}{dy}\right|_{wall}}{Re \, v_{mean}^2} \quad \dots\dots\dots\dots\dots\dots\dots\dots\dots\dots\dots\dots\dots\dots (A.23)$$

Since the rigid boundaries are kept at different but constant temperatures, the values of C_f differ for each wall. Therefore, consider each wall separately.

A5.1. Cold wall:

Differentiate equation (A.27) w.r.t.y to obtain

$$\frac{du}{dy} = 6(1-2y) + Ar\frac{Re}{1680}\left[\{18RePrA-140)+(840-204RePrA)y-840y^2\right.$$

$$+RePrA(420y^2-420y^4+168y^5)\}Sin\alpha-140A(1-6y+6y^2)Cos\alpha\right]$$

$$+Ar^2\frac{APrRe^3}{20160}\left[\{(\frac{2}{3}-\frac{103RePrA}{2310})+\frac{274RePrAy}{770}-14y^2\right.$$

$$-(9RePrA-70)y^4-\frac{(420-102RePrA)}{5}y^5+28y^6-RePrA(14y^6$$

$$-3y^8+\frac{2}{3}y^9)\}Sin^2\alpha+\frac{A}{12}(4-84y^2+420y^4-504y^5+168y^6)Sin2\alpha\right]$$

$$(A.24)$$

A5.2 <u>The Mean Velocity, V_{mean}</u>

$$v_{mean} = \frac{\int_0^1 udy}{\int_0^1 dy} = \int_0^1 udy \quad \text{since} \int_0^1 dy = 1.0.$$

substituting for u, yields

$$v_{mean} = 6\int_0^1 (y-y^2)dy+\frac{ArRe}{1680}\int_0^1\left[\{(18RePrA-140)y+(420-102RePrA)y^2\right.$$

$$-280y^3+RePrA(140y^3-84y^5+28y^6)\}Sin\alpha$$

$$-140A(y-3y^2+2y^3)Cos\alpha\right]dy$$

$$+ \frac{Ar^2 APrRe^3}{20160} \int_0^1 \left[\{ (\frac{2}{3} - \frac{103RePrA}{2310})y + \frac{137RePrAy^2}{770} - \frac{14y^3}{3} - \frac{(9RePrA-70)y^5}{5} \right.$$

$$- \frac{(140-34RePrA)y^6}{10} + 4y^7 - RePrA(2y^7 - \frac{y^9}{3} + \frac{y^{10}}{15}) \}Sin^2\alpha + \frac{A}{12}(4y-28y^3$$

$$\left. +84y^5-84y^6+24y^7) \; Sin2\alpha \right] dy$$

$$= 6\left[\frac{y^2}{2} - \frac{y^3}{3} \right]_0^1 + \frac{ArRe}{1680} \left[\{ (9RePrA-70)y^2 + (140-34RePrA)y^3 - 70y^4 + RePrA(35y^4 \right.$$

$$\left. - 14y^6 + 4y^7) \}Sin\alpha - 140A(\frac{y^2}{2} - y^3 + \frac{y^4}{2})Cos\alpha \right]_0^1$$

$$+ \frac{Ar^2 APrRe^3}{20160} \left[\{ (\frac{1}{3} - \frac{103RePrA}{4620})y^2 + \frac{137RePrAy^3}{2310} - \frac{7y^4}{6} - \frac{(9RePrA-70)y^6}{30} \right.$$

$$- \frac{(140-34RePrA)y^7}{70} + \frac{y^8}{2} - RePrA(\frac{y^8}{4} - \frac{y^{10}}{30} + \frac{y^{11}}{165}) \}Sin^2\alpha + \frac{A}{12}(2y^2-7y^4$$

$$\left. + 14y^6 - 12y^7 + 3y^8)Sin2\alpha \right]_0^1$$

$$= 1 + \frac{ArRe}{1680} \left[\{ 9RePrA-70 + 140-34RePrA-70+RePrA(35-14+4) \}Sin\alpha \right.$$

$$\left. -140A(\frac{1}{2} - 1 + \frac{1}{2})Cos\alpha \right]$$

$$+ \frac{Ar^2 APrRe^3}{20160} \left[\{ \frac{1}{3} - \frac{103RePrA}{4620} + \frac{137RePrA}{2310} - \frac{7}{6} - \frac{(9RePrA-70)}{30} - \frac{(140-34RePrA)}{70} \right.$$

$$\left. + \frac{1}{2} - RePrA(\frac{1}{4} - \frac{1}{30} + \frac{1}{165}) \}Sin^2\alpha + \frac{A}{12}(2-7+14-12+3)Sin2\alpha \right]$$

$$= 1 + 0$$

$$v_{mean} = \underline{\underline{1.0}}$$

The mean temperature merely reduces to

$\theta_m = \int_0^1 u\theta dy$ which can be approximated by the expression

$\sum_{j=1}^{N1} uj\theta j\Delta y.$

At the cold wall, y=0.

Substituting this into (A.24), gives

$$\frac{du}{dy}\bigg|_{y=0} = 6 + Ar\left[\frac{Re}{1680}\{(18RePrA-140)Sin\alpha-140ACos\alpha\}\right]$$

$$+ Ar^2\left[\frac{APrRe^3}{20160}\{(\frac{2}{3} - \frac{103RePrA}{2310})Sin^2\alpha + \frac{A}{3} Sin2\alpha\}\right]$$

Hence the cold wall friction factor C_{fcold} is given by

$$C_{fcold} = \frac{2}{Re}\{6+Ar\left[\frac{Re}{1680}\{(18RePrA-140)Sin\alpha-140ACos\alpha\}\right]$$

$$+Ar^2\left[\frac{APrRe^3}{20160}\{(\frac{2}{3} - \frac{103RePrA}{2310})Sin^2\alpha+ \frac{A}{3}Sin2\alpha\}\right]\} \quad ...(A.25)$$

A5.3. Hot wall

At the hot wall, y = 1. Substituting this into equation (A.24) gives,

$$\frac{du}{dy}\bigg|_{y=1} = -6+Ar\left\{\frac{Re}{1680}\left[\{18RePrA-140+840-204RePrA-840+420RePrA\right.\right.$$
$$\left.\left.+168RePrA\}Sin\ \alpha\right]\right\}$$

$$+A^2\left\{\frac{APrRe^3}{20160}\left[\{\frac{2}{3} - \frac{103RePrA}{2310} + \frac{274RePrA}{770} - 14-9RePrA+70-84\right.\right.$$
$$\left.\left.+\frac{102RePrA}{5} + 28-\frac{35RePrA}{3}\}Sin^2\alpha +\frac{A}{12}\ (4-84+420\right.\right.$$
$$\left.\left.-504+168)Sin2\alpha\right]\right\}$$

Simplify to obtain,

$$\frac{du}{dy}\bigg|_{y=1} - 6+Ar\left[\frac{Re}{1680}\{-(140+18RePrA)Sin\alpha-140ACos\alpha\}\right]$$

$$+ Ar^2\left[\frac{APrRe^3}{20160}\{(\frac{2}{3} + \frac{103RePrA}{2310})Sin^2\alpha + \frac{A}{3}\ Sin2\alpha\}\right]$$

Hence the hot wall friction factor is given by

$$C_{f_{hot}} = \frac{2}{Re}\{-6-Ar\left[\frac{Re}{1680}\{(140+18RePrA)Sin\alpha+140ACos\alpha\}\right]$$

$$+ Ar^2\left[\frac{APrRe^3}{20160}\{(\frac{2}{3} + \frac{103RePrA}{2310})Sin^2\alpha+ \frac{A}{3}\ Sin2\alpha\}\right] \quad \ldots\ldots\ldots(\Lambda.26)$$

NOTE: The absolute values of the friction factors $C_{f_{cold}}$ and $C_{f_{Hot}}$ are of

physical significance. They are measures of wall velocity gradients

(vorticities at the walls) for a given set of parameters.

If $\frac{du}{dy}\bigg|_{y=0} = \frac{du}{dy}\bigg|_{y=1} = 0$, then these are the conditions for separated

flows at the cold and hot walls respectively. When this occurs, the Navier stokes equations no longer hold.

However since spearation is most likely to occur earlier at the cold wall, the requirement for separation there is considered in the next section.

A5.4 Criterion for separation at the cold wall

From the foregoing analysis it appears that separation may occur at the cold rigid boundary. For separation to occur, the normal velocity gradient must vanish at such boundary. That is,

$$\frac{\partial u}{\partial y}\bigg|_{y=0} = 0$$

$$\therefore \quad C_{fcold} = \frac{2}{Re}\left[6+ \frac{Ar}{1680}\{(18RePrA-140)Sin\alpha-140ACos\alpha)\}\right.$$

$$\left. +Ar^2\{\frac{APrRe^3}{20160}\left[(\frac{2}{3} - \frac{103RePrA}{2310})Sin^2\alpha+ \frac{A}{3} Sin2\alpha\}\right]\right]$$

If $C_{fcold} = 0$, then,

$$A^2\left[\frac{APrRe^3}{20160}\{(\frac{2}{3} - \frac{103PrReA}{2310})Sin^2\alpha+ \frac{A}{3}Sin2\alpha\}\right] + Ar\left[\frac{Re}{1680}\{(18RePrA-140)Sin\alpha\right.$$

$$\left. -140ACos\alpha\}\right] + 6 = 0 \quad ...(A.26a)$$

The above equation is clearly a quadratic in Ar, the Archimedes number. The equation can be reduced to the form,

$$a \, Ar^2 + b \, Ar + c = 0$$

where $a = \dfrac{APrRe^3}{20160} \left[\left(\dfrac{2}{3} - \dfrac{103RePrA}{2310} \right) Sin^2\alpha + \dfrac{A}{3} Sin2\alpha \right]$

$b = \dfrac{Re}{1680} \left[(18RePrA-140)Sin\alpha - 140ACos\alpha \right]$

$c = 6.0$

By completing the square, the roots of the quadratic can be obtained from the following formula

$$Ar = \dfrac{-b \pm \sqrt{b^2-4a\,C}}{2a} \qquad \dots\dots\dots\dots\dots(A.26b)$$

The values of Ar thus obtained are the critical Archimedes numbers at which separation ensues. By inspection the above relation does not hold for the horizontal position for which $\alpha = 0^o$. For the horizontal case, the condition for separation is determined by substituting $\alpha = 0^o$ directly into equation (A.26a) to give

$$Ar_c = \dfrac{72}{A}$$

For non-zero inclinations, $0^o < \alpha < 90^o$, equation (A.26b) is valid. From numerical solution, for $Ar > 0.5$, separation is noticed near the vertical position. Thus the acceptable root of equation (A.26b) is

$$Ar_c = \dfrac{-b - \sqrt{b^2 - 4ac}}{2a} \qquad \dots\dots\dots\dots\dots\dots\dots\dots\dots(A.26\,c)$$

A5.5 Determination of Nusselt numbers based on the normal Temp. Gradient

Substitute θ_0, θ_1 and θ_2 into the equation (4.4) to obtain the expression for θ.

Thus,

$$\theta = y - \frac{RePrA}{2}(y - 2y^3 + y^4)$$

$$+ Ar\{\frac{APrRe^2}{20160}\left[\{28y + (36RePrA - 280)y^3 + (420 - 102RePrA)y^4 - 168y^5\right.$$

$$+ RePrA(84y^5 - 24y^7 + 6y^8)\}Sin\alpha + 28A(y - 10y^3 + 15y^4 - 6y^5)Cos\alpha$$

$$+ Ar^2\{\frac{A^2Pr^2Re^4}{20160}\left[\frac{-y}{60} + \frac{(1540 - 103RePrA)y^3}{13860} + \frac{137RePrAy^4}{9240} - \frac{7y^5}{30}\right.$$

$$- \frac{(9RePrA - 70)y^7}{210} - \frac{(420 - 102RePrA)y^8}{1680} + \frac{y^9}{18}$$

$$- \frac{RePrA}{1980}(55y^9 - 6y^{11} + y^{12})\}Sin^2\alpha + \frac{A}{360}(-3y + 20y^3$$

$$- 42y^5 + 60y^7 - 45y^8 + 10y^9)Sin2\alpha\left.\right] \} \quad \ldots\ldots\ldots(A.27)$$

Equation (A.27) represents the temperature distribtuion across the channel. Differentiate (A.27) w.r.t.y.

$$\frac{d\theta}{dy} = 1 - RePrA(1 - 6y^2 + 4y^3)$$

$$+ Ar\{\frac{APrRe^2}{20160}\left[\{28 + (108RePrA - 840)y^2 + (1680 - 408RePrA)y^3 - 840y^4\right.$$

$$+ RePrA(420y^4 - 168y^6 + 48y^7)\}Sin\alpha + 28A(1 - 30y^2$$

$$+ 60y^3 - 30y^4)Cos\alpha\left.\right] \}$$

$$+ Ar^2 \left\{ \frac{A^2 Pr^2 Re^4}{20160} \left[\left\{ -\frac{1}{60} + \frac{(1540-103RePrA)y^2}{4620} + \frac{137RePrAy^3}{2310} - \frac{7y^4}{6} - \frac{(9RePrA-70)y^6}{30} \right. \right. \right.$$

$$\left. - \frac{(420-102RePrA)y^7}{210} + \frac{y^8}{2} - \frac{RePrA}{1980}(495y^8 - 66y^{10} + 12y^{11}) \right\} Sin^2\alpha$$

$$\left. \left. + \frac{A}{360}(-3+60y^2-210y^4+420y^6-360y^7+90y^8) \; Sin2\alpha \right] \right\} \quad (A.28)$$

At $y = 1$, the value of $\frac{d\theta}{dy}$ is given by

$$\left. \frac{d\theta}{dy} \right|_{y=1} = 1 - \frac{RePrA}{2}(1-6+4)$$

$$+ Ar\frac{APrRe^2}{20160} \left[\{28+108RePrA-840+1680-408RePrA-840+RePrA(420 \right.$$

$$\left. -168+48)\}Sin\alpha + 28A(1-30+60-30)Cos\alpha \right] \}$$

$$+ Ar^2 \left\{ \frac{A^2Pr^2Re^4}{20160} \left[\left\{ \frac{-1}{60} + \frac{(1540-103RePrA)}{4620} + \frac{137RePrA}{2310} - \frac{7}{6} \right. \right. \right.$$

$$\left. - \frac{(9RePrA-70)}{30} - \frac{(420-102RePrA)}{210} + \frac{1}{2} \right.$$

$$\left. - \frac{RePrA}{1980}(495-66+12) \right\}Sin^2\alpha + \frac{A}{360}(-3+60-210$$

$$\left. \left. +420-360+90)Sin2\alpha \right] \right\}$$

On simplication,

$$\left. \frac{d\theta}{dy} \right|_{y=1} = 1 + \frac{RePrA}{2} + Ar\left[\frac{APrRe^2}{20160}\{28Sin\alpha+28ACos\alpha\} \right] + Ar^2\left[\frac{A^2Pr^2Re^4}{20160}\{(-\frac{1}{60} \right.$$

$$\left. - \frac{RePrA}{385})Sin^2\alpha - \frac{A}{120} \; Sin2\alpha\} \right]$$

Since $Ar \triangleq \dfrac{Gr}{Re^2}$ substitution in the above equation yields,

i.e.

$$\frac{d\theta}{dy}\bigg|_{y=1} = 1 + \frac{RePrA}{2.} + \frac{Gr}{Re^2}\left[\frac{APrRe^2}{20160}\{28(Sin\alpha+ACos\alpha)\}\right]$$
$$- \frac{Gr^2}{Re^4}\left[\frac{A^2Pr^2Re^4}{20160}\{(\frac{1}{60} + \frac{RePrA}{385})Sin^2\alpha + \frac{A}{120}Sin2\alpha\}\right] \quad (A.29)$$

Although the normal temperature gradient at the hot wall is of primary importance, it is also of interest to evaluate the normal temperature gradient at the cold wall.

At the cold wall, $y = 0$. Substituting this into equation (A.28) yields

$$\frac{d\theta}{dy}\bigg|_{y=0} = 1 - \frac{RePrA}{2} + Ar\left[\frac{APrRe^2}{20160}\{28Sin\alpha+28ACos\alpha\}\right]$$
$$+ Ar^2\left[\frac{A^2Pr^2Re^4}{20160}\{-\frac{1}{60}Sin^2\alpha- \frac{A}{120}Sin2\alpha\}\right].$$

Again

$$- \frac{d\theta}{dy}\bigg|_{y=0} = -1 + \frac{RePrA}{2} - \frac{Gr}{Re^2}\left[\frac{APrRe^2}{20160}\{28(Sin\alpha+ACos\alpha)\}\right]$$
$$+ \frac{Gr^2}{Re^4}\left[\frac{A^2Pr^2Re^4}{20160}\{\frac{(2Sin^2\alpha + ASin2\alpha)}{120}\}\right] \quad (A.30)$$

The aim of this analysis is to determine the heat transfer coefficient based on the characteristic linear dimension and the temperature difference between the hot and cold walls. Since the flow is laminar, it can be assumed that near the rigid boundaries, where the fluid

is substantially slowed down, the mode of heat transfer is essentially by conduction. Also, assume that this heat transfer is predominant in the direction of higher temperature gradient, that is in the direction normal to the rigid boundaries.

In general, if Q = Heat transfer per unit area

h = Heat transfer coefficient per unit area per unit temperature difference,

Then $Q = h(T_h - T_c)$ ....(A.31)

If k_f is the Thermal Conductivity of the fluid, then by Fourier's Law of heat conduction in one dimension,

$$Q = -\left(+k_f \frac{\partial T}{\partial n}\right)\Big|_{Y=b} = +k_f \frac{\partial T}{\partial Y}\Big|_{Y=b}$$

since at the hot wall $\frac{\partial T}{\partial n} = -\frac{\partial T}{\partial y}$ and n is the outward normal to the wall

i.e. $Q = +k_f \frac{\partial T}{\partial Y}\Big|_{Y=b}$ ....(A.32)

Equating (A.31) and (A.32), gives,

$$h(T_h - T_c) = +k_f \frac{\partial T}{\partial Y}\Big|_{Y=b}$$

Again, introduce the normalisation variables, i.e. $\theta = \frac{(T-T_c)}{(T_h-T_c)}$; $y = \frac{Y}{b}$, to obtain $h(T_h - T_c) = +k_f \frac{(T_h-T_c)}{b} \frac{d\theta}{dy}\Big|_{y=1}$

$$\rightarrow \quad h = +\frac{k_f}{b} \frac{\partial \theta}{\partial y}\Big|_{y=1}$$

$$\therefore \quad \frac{hb}{k_f} = +\frac{\partial \theta}{\partial y}\Big|_{y=1}$$

But $\dfrac{hb}{k_f} \triangleq Nu$, the Nusselt Number.

Since θ is y-dependent only, then $\dfrac{\partial \theta}{\partial y} = \dfrac{d\theta}{dy}$, and for the hot wall

$$\rightarrow \quad Nu_H = + \left.\dfrac{d\theta}{dy}\right|_{y=1} \quad \dots\dots\dots\dots\dots\dots\dots\dots\dots\dots\dots(A.33)$$

Equation (A.33) represents the hot wall Nusselt Number.

Substituting $\left.\dfrac{d\theta}{dy}\right|_{y=1}$ from equation (A.29), equation (A.33) becomes,

$$Nu_H = 1 + \dfrac{RePrA}{2} + \dfrac{Gr}{Re^2}\left[\dfrac{APrRe^2}{20160}\{28(Sin\alpha+ACos\alpha)\}\right]$$

$$- \dfrac{G_r^2}{Re^4}\left[\dfrac{A^2Pr^2Re^4}{20160}\{(\dfrac{1}{60} + \dfrac{RePrA}{385})\ Sin^2\alpha + \dfrac{A}{120}\ Sin2\alpha\}\right] \quad (A.34)$$

Similarly, for the cold wall $Nu_c = \left.\dfrac{d\theta}{dy}\right|_{y=0}$

$$\rightarrow \quad Nu_c = 1 - \dfrac{RePrA}{2} + \dfrac{Gr}{Re^2}\left[\dfrac{APrRe^2}{20160}\{28(Sin\alpha+ACos\alpha)\}\right]$$

$$- \dfrac{G_r^2}{Re^4}\left[\dfrac{A^2Pr^2Re^4}{20160}\{\dfrac{(2Sin^2\alpha + A\ Sin2\alpha)}{120}\}\right] \quad \dots\dots\dots(A.33)$$

A6 Determination of the mean Nusselt Number

It is customary in most heat transfer problems to specify the convection conductance h in terms of the difference between the Bulk temperature and the wall temperature

$$\theta_B = \dfrac{\int_0^1 u\theta dy}{v_{mean}}.$$

The mean hot wall and cold wall Nusselt numbers are therefore respectively,

$$Nu_{BH} = \frac{(\frac{d\theta}{dy}\Big|_{y=1})}{(\theta_{hw} - \theta_B)} \qquad (A.36)$$

$$Nu_{BC} = \frac{(\frac{d\theta}{dy}\Big|_{y=0})}{(\theta_{cw} - \theta_B)} \qquad (A.37)$$

A7. Validity of Solution

For the perturbation solution to be valid, the dimensionless longitudinal temperature gradient A must be independent of the power series expansion parameter, Ar and the angle of inclination, α to the horizontal. Clearly, the basic temperature distribution, $\theta_o = y(1 - \frac{RePrA}{2})$ satisfies the above requirements. For realistic temperature distribution across the channel, the values of θ_o must always be positive. Thus, 0<RePrA<2. For small rates of heating considered, A could be quite small for fully developed flows. Consequently, the range of modified Peclet numbers used is given by

$$0.088 \leq RePrA \leq 0.350.$$

A8   Correlations by three-dimensional power laws

The primary objective of this analysis is to investigate the existence, if any, of optimum angles of inclination to the horizontal for which the heat transfer and non-dimensional bulk temperature are maximum. The investigation has yielded results which predict the existence of such optimum inclinations. It is therefore proposed that these maximum heat transfer parameters and their corresponding optimum inclinations (in radians) be properly correlated by a set of three dimensional power Laws.

Thus for the mean hot wall Nusselt Number,

$$Nu_{BH} = C(Ar)^{\lambda_1} (\alpha_{o_{PT}})^{\lambda_2} \quad \dots\dots\dots\dots\dots\dots\dots\dots\dots\dots (A.38)$$

and for the dimensionless bulk temperature,

$$\theta_B = C_1 (Ar)^{n_3} (\alpha_{o_{PT}})^{n_4} \quad \dots\dots\dots\dots\dots\dots\dots\dots\dots (A.39)$$

where C, C_1 are proportionality constants and n_1, n_2, n_3, n_4 are exponents to be determined.

These equations will be considered separately, starting with (A.39)

A. $\theta_B = C_1 (Ar)^{n_3} (\alpha_{o_{PT}})^{n_4}$

The table below depicts extracts of appropriate values of θ_B and α_{OPT} from figure 5.12.

TABLE A.1. MAXIMUM BULK TEMPERATURES

Ar	θ_B	α_{OPT}	
		Degrees	Radians
0.0313	0.455	30.00	$\frac{\pi}{6}$
0.080	0.477	37.50	$\frac{5\pi}{24}$
0.125	0.486	45.00	$\frac{\pi}{4}$
0.222	0.499	52.50	$\frac{7\pi}{24}$

Equation (A.39) can be linearised by taking the logarithm to base 10 of each side. Thus,

$$\log_{10} \theta_B = \log_{10} C_1 + n_3 \log_{10} Ar + n_4 \log_{10} \alpha_{OPT}$$

Writing $\log_{10} \theta_B$ as z, $\log_{10} C_1$ as C_0, $\log_{10} Ar$ as x and $\log_{10} \alpha_{OPT}$ as y,

then,

$$z = C_0 + n_3 x + n_4 y \quad \dots\dots\dots\dots\dots\dots\dots\dots\dots(A.40)$$

Equation (A.40) represents the equation of a surface defined by points in the preceeding table. Since there are three constants to be evaluated, three equations are adequate:

(i)   For Ar = 0.0313

$$z = \log_{10} 0.455 \quad = \; - 0.342$$

$$x = \log_{10} 0.0313 \quad = \; - 1.504$$

$$y = \log_{10} \frac{\pi}{6} \qquad = \; - 0.280$$

Hence the corresponding equation is

$$0.342 = 1.504 \, n_3 + 0.280 n_4 - C_0 \quad \dots\dots\dots\dots\dots(A.41)$$

(ii)   For Ar = 0.125

$$z = \log_{10} 0.486 \quad = -0.313$$

$$x = \log_{10} 0.125 \quad = -0.903$$

$$y = \log_{10} \frac{\pi}{4} \quad = -0.104$$

Hence the corresponding equation is

$$0.313 = 0.903 n_3 + 0.104 n_4 - C_o \quad \dots \dots \dots \dots \dots (A.42)$$

(iii)   For Ar = 0.222

$$z = \log_{10} 0.499 \quad = -0.302$$

$$x = \log_{10} 0.222 \quad = -0.654$$

$$y = \log_{10} \frac{7\pi}{24} \quad = -0.037$$

Hence the corresponding equation is

$$0.302 = 0.654 n_3 + 0.037 n_4 - C_o \quad \dots \dots \dots \dots \dots (A.43)$$

The solution to these simultaneous equations yield

$$n_3 = -0.00286 = -0.003$$

$$n_4 = +0.175$$

$$C_o = -0.2974, \quad \rightarrow \quad C_1 = 0.504$$

Hence the three-dimensional power Law for θ_B and α_{OPT} is

$$\theta_B = 0.504 \,(Ar)^{-0.003} (\alpha_{OPT})^{0.175} \quad \dots \dots \dots \dots \dots (A.44)$$

$$0.0313 \leqslant Ar \leqslant 0.222$$

$$\frac{\pi}{6} \leqslant \alpha_{OPT} \leqslant \frac{7\pi}{24}$$

If we cross check for Ar = 0.080, the above correlation yields

$$\theta_B = 0.473.$$

The error involved is 0.477-0.473 = 0.004. This is an error of about 0.8%. The correlation   therefore appears to be satisfactory.

B. The following power Law is for the mean hot-wall Nusselt number. Again, the following table depicts extracts from figure 5.13.

TABLE A.2. MAXIMUM NUSSELT NUMBERS AT HOT WALL

Ar	Nu_{BH}	α_{OPT}	
		Degrees	Radians
0.0313	2.1650	$30^{\circ}.00^{\circ}$	$\frac{\pi}{6}$
0.080	2.1275	37.50°	$\frac{5\pi}{24}$
0.125	2.1225	45.0	$\frac{\pi}{4}$
0.222	2.1375	54.0°	$\frac{3\pi}{10}$

Equation (A.38) can be linearised as before to yield

$$z_1 = C_o' + \lambda_1 x_1 + \lambda_2 y_1 \quad \dots \dots \dots \dots (A.45)$$

where $C_o' = \log_{10} C$; $z_1 = \log_{10} Nu_{BH}$; $x_1 = \log_{10} Ar$; $y_1 = \log_{10} \alpha_{OPT}$

Since α_{OPT} is the same as before, $y_1 = y$ in equations (A.41), (A.42) and (A.42). Also $x_1 = x$ in these equations.

(i)   For Ar = 0.0313

$$z_1 = \log_{10} Nu_{BH} = 0.3360$$

The corresponding equation is

$$0.3360 = C_o^1 - 1.504 \lambda_1 - 0.280 \lambda_2 \quad \dots \dots \dots (A.46)$$

(ii)   <u>For Ar = 0.125</u>

$$Z_1 = \log_{10} Nu_{BH} = 0.3270$$

$$\rightarrow 0.3270 = C_o' - 0.903\lambda_1 - 0.104\lambda_2 \qquad (A.47)$$

(iii)   <u>For Ar = 0.222</u>

$$Z_1 = \log_{10} Nu_{BH} = 0.3290$$

$$\rightarrow 0.3290 = C_o' - 0.654\lambda_1 - 0.124\lambda_2 \qquad (A.48)$$

Solving the above equations simultaneously gives

$$\lambda_1 = 0.005$$

$$\lambda_2 = 0.038$$

$$C_o' = 0.3275, \rightarrow C = 2.120.$$

Hence the three-dimensional power Law is

$$Nu_{BH} = 2.120 \, (Ar)^{0.005} \, (\alpha_{OPT})^{-0.038} \qquad (A.49)$$

provided that, $0.0313 \leqslant Ar \leqslant 0.222$ $150 \leqslant Re \leqslant 400$

$$\frac{\pi}{6} \leqslant \alpha_{OPT} \leqslant \frac{3\pi}{10} \qquad \text{where} \left\{ \begin{array}{c} \\ 0 \leqslant Gr \leqslant 5000 \end{array} \right\}$$

Cross-checking for Ar = 0.083 indicates that equation (A.47)
is satisfactory.

APPENDIX B

SAMPLE COMPUTATIONS FOR ANALYSIS OF EXPERIMENTAL RESULTS

B1   Input Mean Velocity, U_m

   If the recorded pressure drop at channel inlet is $\Delta p(N/m^2)$, γ^o, the angle of inclination of the manometer, it can be shown that for air, the corresponding induced mean velocity is given by

$$U_m = 1.3\sqrt{\Delta PSin\gamma} \quad (m/s)$$

From the calibration curves in fig. 7.1, for a setting of the fan variable transformer at 5.0 m/s, the equivalent mean input velocity for the second power input run is estimated to be 0.189 m/s.

B2   Reynolds number, Re

$$U_m = 0.189 \text{ m/s}$$

$$b = 0.12 \text{ m}$$

$$\nu = 1.703 \times 10^{-5} \text{ m}^2/s$$

$$\therefore Re = \frac{U_m b}{\nu}$$

$$= \frac{0.189 \frac{m}{s} \times 0.12 \text{ m}}{1.703 \times 10^{-5} \frac{m^2}{s}}$$

Simplication yields

$$Re = 1331.76$$

B3   <u>Modified Grashof number, Gr_m</u>

The estimated longitudinal hot wall temperature gradient A^* is given by

$$A^* = \frac{1}{M} \sum_{i=1}^{M} \frac{\left[T_h \Big|_{i+1} - T_h \Big|_{i} \right]}{\Delta x}$$

where M = number of stations along channel.

ΔX = Distance between two consecutive stations.

From table 6.12 , substituting for T_h in the above equation yields

$$A^* = 1.230^{\circ}K/m.$$

$$\beta = 3.3090 \times 10^{-3}/^{\circ}K$$

$$g = 9.81 \ m/s^2$$

But $Gr_m = \dfrac{\beta g A^* b^4}{\nu^2}$

Substituting the above values in the equation yields

$$Gr_m = 28,547.90$$

B4   <u>Modified Archimedes number, Ar_m</u>

The parameter which represents the combined convective phenomena is the Archimedes number given by,

$$Ar_m = \frac{Gr_m}{Re^2}$$

$$= \frac{28547.90}{(1331.76)^2}$$

$$\therefore Ar_m = 0.0161$$

B5   Evaluation of Local and Mean Nusselt numbers

The local Nusselt number which is based on the normal temperature
gradient at the wall is obtained from the following expression.

$$Nu_{i,N+1} = (7\theta_{i,N+1} - 8\theta_{i,N} + \theta_{i,N-1})/(6\Delta y\theta_{i,N+1}) \qquad (B.1)$$

Consider the case of $\alpha = 0^{\circ}$. From table 6.13, for station 5,
the experimental temperatures are:

$$T_{5,N+1} = 54.0^{\circ}C$$
$$T_{5,N} = 33.0^{\circ}C$$
$$T_{5,N-1} = 31.5^{\circ}C$$
$$\Delta y = 0.2$$
$$T_{\infty} = 29.2^{\circ}C$$

The non-dimensional equivalent temperatures are

$$\theta_{5,N+1} = \frac{(T_{5,N+1} - T_{\infty})}{RePr\ A^{*}b}$$

$$\theta_{5,N} = \frac{(T_{5,N} - T_{\infty})}{RePr\ A^{*}b}$$

$$\theta_{5,N-1} = \frac{(T_{5,N-1} - T_{\infty})}{RePr\ A^{*}b}$$

Substituting these into equation (B1) yields

$$Nu_{5,N+1} = \frac{[7T_{5,N+1} - 8T_{5,N} + T_{5,N-1}]}{[6\Delta y(T_{5,N+1} - T_{\infty})]}$$

Substituting for Δy, $T_{5,N+1}$, $T_{5,N}$, $T_{5,N-1}$ and T_∞ and simplifying yields

$$Nu_{5,N+1} = 4.889$$

The average hot wall Nusselt number is that obtained for the three experimental stations.

B6   Local and Mean Stanton numbers

The local Stanton number is obtained from $\dfrac{Nu_x}{RePr}$.

Thus for $Nu_{5,N+1} = 4.889$

$$Re = 1331.76$$

$$Pr = 0.704$$

$$St_{5,N+1} = \frac{4.889}{1331.76 \times 0.704}$$
$$= 0.521 \times 10^{-2}$$

The average Stanton number is that obtained for the three experimental stations.

B7   Local and Mean Friction Factors

The local friction factor is given by

$$f_{i,N+1} = \frac{2}{Reu_{mi}^2} (u_{i,N-1} - 4\,u_{i,N})/2\Delta y$$

Since we have dimensional velocities in the experimental results, the above expression will be transformed to contain dimensional velocities.

$$U_m u_{mi} = U_{mi}$$

$$\therefore \quad u_{m_i} = \frac{U_{mi}}{U_m}$$

$$u_{i,N} = \frac{U_{i,N}}{U_m}$$

$$u_{i,N-1} = \frac{U_{i,N-1}}{U_m}$$

Substitution into the expression for $f_{i,N+1}$ gives

$$f_{i,N+1} = \frac{U_m}{Re\ U_{mi}^2 \Delta y} \cdot \left[U_{i,N-1} - 4\ U_{i,N} \right]$$

For station 5 from table 6.13

$$f_{5,N+1} = \frac{U_m}{Re\ U_{mi}^2\ \Delta y} \left[U_{5,N-1} - 4U_{5,N} \right]$$

where $U_m = 0.189$ m/s

$U_{m5} = 0.198$ m/s

$U_{5,N-1} = 0.405$ m/s

$U_{5,N} = 0.210$ m/s

$Re = 1331.75$

Substitution of these velocities yields $f_{5,N+1} = 0.864 \times 10^{-2}$

The mean value is computed from the those of the three stations.

APPENDIX C

PUBLICATIONS

C1. The paper presented here was based on an aspect of the problem investigated in this thesis. The paper was jointly prepared by Professor V.A. Akinsete and F.L. Bello-Ochende. The paper was accepted for presentation in the V Congresso Brasileiro De Engenharia Mecanica by the Editorial Counsel of the V COBEM - V Braz. Cong. of Mech. Eng. at an International Conference held in Brazil from 12th to 15th December 1979. A photocopy of the acceptance notice is attached.

The title of the thesis is:

" Combined Free and Forced Laminar Convection In Inclined Rectangular Channels Heated From Below and Cooled From Above."

The Authors are:

(a) Professor V.A. Akinsete
Head, Mech. Eng. Department,
Lagos UNiversity,
Lagos, Nigeria.

(b) F.L. Bello-Ochende
Graduate Student,
Mech. Eng. Department,
Lagos University,
Lagos, Nigeria.

C2. A research paper based on the subject of this thesis was jointly presented by Professor V.A. Akinsete, the thesis Adviser and F.L. Bello-Ochende at a Faculty of Engineering Seminar on the 23rd of January, 1979 at the Faculty of Engineering, Lagos University. Comments and constructive criticisms by Seminar attendants contributed substantially to improvements in the thesis.

COMBINED FREE AND FORCED LAMINAR CONVECTION IN
INCLINED RECTANGULAR CHANNELS HEATED FROM BELOW
AND COOLED FROM ABOVE

V.A. AKINSETE[*] and F.L. BELLO-OCHENDE[+]

DEPARTMENT OF MECHANICAL ENGINEERING, LAGOS UNIVERSITY,
LAGOS, NIGERIA.

Abstract - Steady state numerical results for the solution to the
non-linear thermal problem of combined free and forced laminar convection
in inclined rectangular channels with constant but unequal surface
temperatures are presented for an incompressible, viscous fluid whose
Prandtl number, Pr = 0.73. Fluid properties are assumed constant, except
for density variations with temperature. Maximum values exist for the
mean hotwall friction factor, Nusselt and Stanton numbers when the inclina-
tion to the horizontal lies between 30° and 60° for a given Archimedes
number, Ar. Also, for any given inclination, a unique solution exists
when Ar = 0.50.

NOMENCLATURE

Ar,   Archimedes number Gr/Re^2

b,   height of Rectangular channel

Cp,   specific heat at constant pressure

f,   friction factor, $2\tau_w/\rho_m u_m^2$

f_{mh} mean friction factor at hot wall

g,   gravitational acceleration

Gr,   Grashof number, $g\beta (T_h - T_c) b^3/v^2$

*   Professor, Department of Mechanical Engineering, Lagos University,

+   Graduate Student, Department of Mechanical Engineering Lagos
     University.

COBEM 79

V CONGRESSO BRASILEIRO DE ENGENHARIA MECÂNICA

12 a 15 Dezembro 1979   **Campinas - SP.- Brasil**

Promoção

ABCM - Associação Brasileira de Ciências Mecânicas
CNPq - Conselho Nacional de Desenvolvimento Científico e Tecnológico
UNICAMP - Universidade Estadual de Campinas

The Editorial Counsel of the V COBEM - V Braz. Cong. of Mech. Eng. decided to classify your paper according to the following:

Title: Combined free and forced laminar convection in
          inclined rectangular channels heated from below
Author(s): and cooled from above

          V. A. Akinsete

Paper to be

☐ Published in the Proceedings

☒ Presented in Technical Session and published in the Proceedings.

in the form of:

☐ Research Paper

☒ Technical Paper

To assure the publication of the paper in the Congress   Proceedings at least one of the authors should register till the 15th of October.

Enclosed please find informations and the registration forms. We are looking forward to meet you.

Yours faithfully

h_x,   local heat transfer coefficient at hot wall

K_f,   thermal conductivity of fluid

M, N,   number of divisions in X and Y - directions respectively.

Nu_x,   local hotwall Nusselt number

Nu_{mh},   means hotwall Nusselt number

Pe,   Peclet number, RePr

Pr,   Prandtl number, λ/ν

P_x,   local dimensional pressure

p_x,   local non-dimensional pressure $P_x/\frac{1}{2}\rho_m u_m^2$

Re,   Reynolds number, $U_m b/\nu$

St_x,   local hotwall Stanton number $h_x/\rho_m C_p U_m$

St_{mh},   mean hotwall Stanton number

T.,   local dimensional temperature

U,V,   dimensional velocity components in X and Y - directions resp.

u,v,   non-dimensional velocity components, $(U,V)/U_m$

X,Y,   Rectangular cartesian coordinate axes

x,y,   Non-dimensional distances, (X,Y)/b

X_L,   dimensional channel length

x_L,   non-dimensional channel length

$\Delta x, \Delta y$,   dimensionless grid sizes in x - and y directions respectively,

               (x/M, y/N)

Greek Symbols

α,   angle of inclination to the horizontal

β,   volumetric coefficient of expansion with temperature

θ,   dimensionless temperature difference, $\dfrac{T - Tc}{(T_h - T_c)}$

ϕ,   Dummy variable

c,   iteration convergence criterion

λ,   thermal diffusivity of fluid

μ,   Coefficient of dynamic viscosity

ν,   Coefficient of Kinematic viscosity $\dfrac{\mu}{\rho_m}$

ρ,   local density of fluid

ρ_m,   mean fluid density

τ,   shear stress

ψ,   dimensionless stream function

ω,   dimensionless vorticity, $-\nabla^2\psi$

∇^2,   dimensionless Laplacian operator in rectangular

coordinates, $\left(\dfrac{\partial^2}{\partial x^2} + \dfrac{\partial^2}{\partial y^2}\right)$

∇^4,   Laplacian of Laplacian in rectangular coordinates,

$$\left(\frac{\partial^2}{\partial x^2} + \frac{\partial^2}{\partial y^2}\right)\left(\frac{\partial^2}{\partial x^2} + \frac{\partial^2}{\partial y^2}\right)$$

Subscripts:

c,   cold wall value

h,   hot wall value

mh,   mean value at hot wall

w,   wall value

i,j,   location of a grid point in x -   and y -   directions resp.

Super Script.

k,   iteration counter

4

1. INTRODUCTION

When in non-isothermal flow density variations which arise as a result of temperature gradients are sufficiently large to produce bouyant forces in a gravitational field, the buoyant force terms must be retained in the governing equations of Navier-Stokes. The relative magnitudes of the forced and free convection effects are obtained by normalising the partial differential equations which describe the flow and by examining the relative magnitudes of such parameters as the Reynolds, Grashof and Prandtl numbers. Of particular significance in the case of combined free and forced laminar convection in rectangular channels, is the orientation of the gravitational field. The purpose of this paper is therefore to present the heat and flow results for combined free and forced laminar convection in inclined rectangular channels with constant but unequal surface temperatures for $Pr= 0.73$.

The combined effect of the mutually interacting fields can be represented by an emergent parameter, $\frac{Gr}{Re^2}$, in the non-dimensional form of the vorticity transport equation. The existence of optimum inclinations, if any, at which heat transfer rate is maximum is of considerable importance in some areas of application. For example, in flat-plate Solar collectors, convection must necessarily occur in an oriented gravitational field.

Numerical studies of fully developed combined free and forced laminar convection in inclined rectangular channels under the thermal boundary conditions of axially uniform wall heat-flux has been reported by Ou et all [1].

The improved formulation used by these authors redefined the Reynolds and Rayleigh numbers in terms of the angle of inclination to the horizontal. Because of the introdution of these modified non-dimensional parameters, their formulation failed to recover the horizontal case as a limiting orientation. Cheng and Hwang [2] presented numerical results for fully developed combined free and forced laminar convection in horizontal rectangular channels under the thermal boundary conditions of axially uniform wall heat-flux and preipherally uniform wall temperature, while Cheng and Hong [3] reported a numerical study using a combination of boundary vorticity and the line iterative methods to determine free convection effects on fully developed laminar upward flow in inclined tubes with the angle of inclination appearing expicitly in their formulation. Iqbal and Stachiewcz [4] obtained theoretical results of variable density effects on fully developed combined free and forced laminar convection in inclined tubes. Also Iqbal and Stachiewcz [4] reported the study of the same phenomenon in clined tubes and showed that for a given set of non-dimensional parameters, their exists a particular tube inclination that produces a maximum heat transfer rate. The work of Ozoe et al [5],though on pure natural convection, showed that a critical angle exists at which the heat transfer is a maximum.

In all the foregoing references the formulations, except the first, have the orientation of the gravitational field appearing explicity. However, they all have the same thermal boundary conditions and their analyses are restricted to only the fully developed regimes. In the presen work, a steady - state analysis is carried out numerically for the two-dimensional problem.

6

No general assumptions of fully developed régimes are made except that at remote distances from the channel entrance, the hydrodynamic and thermal fields are assumed not to vary with distance. In solving the problem, the pressure gradient terms are eliminated by cross-differentiation of the momentum equations. The combined momentum and energy equations are then normalized following Mori and Uchida [6]. The voriticity transport equation is derived from the combined momentum equation with the angle of inclination appearing explicity in the formulation. The vorticity transport and energy equations are discretized following Dennis [7]. These equations are solved simultaneously using the boundary vorticity method and the five-point Gauss-seidal iterative procedure for the prescribed inhomogeneous thermal boundary conditions. For computational convenience, the inlet conditions are those of uniform velocity and temperature equal to that of the cooled surface.

2. MATHEMATICAL FORMULATION OF THE PROBLEM

In formulating the problem, it is assumed, a priori, that the channel aspect ratio is large and its width is several times the magnitude of its height so that the lateral end effects are negligible when a longitudinal section, far-removed from the vertical bounding sides, is taken. For moderate temperature gradients, the problem reduces to a two-dimensional one. The channel can therefore be regarded as an open domain bounded by two parallel surfaces kept at constant but unequal temperatures.

7.

When the temperature difference between the surface is appreciable, buoyant forces are generated and the resulting secondary flow is super-imposed on the pure forced convection. The mutual interation of the hydrodynamic and thermal fields in an oriented gravitational field is investigated by making the following simplifying assumptions to reduce the mathematical complexity of the governing equations.

(a) The thermophysical properties are constant, except for the density variations with temperature (Boussinesq approximation).

(b) The flow is upward, steady, laminar and incompressible.

(c) Viscous dissipation is negligible.

(d) There is no internal heat generation.

In addition, the final combined momentum equations, is recast in terms of the vorticity function, ω, in order to avoid the use of the biharmonic equation, in ψ and to employ the recently developed Boundary Vorticity Method.

The governing equations in rectangular cartesian coordinate system are:

Continuity:

$$\frac{\partial U}{\partial X} + \frac{\partial V}{\partial Y} = 0 \quad .. \quad .. \quad .. \quad .. \quad .. \quad .. \quad .. \tag{1}$$

Momentum (or Navier - Stokes) Equation in X- and Y- directions respectively:

$$\frac{U\partial U}{\partial X} + \frac{V\partial U}{\partial Y} = -\frac{1}{\rho_m}\frac{\partial P}{\partial X} + \nu\nabla^2 U + g\beta(T - T_c)\sin\alpha \quad .. \tag{2}$$

$$\frac{U\partial V}{\partial X} + \frac{V\partial V}{\partial Y} = -\frac{1}{\rho_m}\frac{\partial P}{\partial Y} + \nu\nabla^2 V - g\beta(T - T_c)\cos\alpha \quad .. \tag{3}$$

8

Energy Equation:

$$\frac{U\partial T}{\partial X} + \frac{V\partial T}{\partial Y} = \lambda \nabla^2 T \quad .. \quad .. \quad .. \quad .. \quad .. \quad .. \tag{4}$$

Equation of State (Boussineq approximation):

$$\rho = \rho_m \left[1 - \beta (T - Tc) \right] .. \quad .. \quad .. \quad .. \tag{5}$$

Boundary Conditions:

(a) Thermal Boundary Conditions:-

(i) At entrance, $T = Tc$, for $X = 0$, $0 < Y < b$

(ii) At exit, $\frac{\partial T}{\partial X} = 0$, for $X = X_L$, $0 < Y < b$

(iii) At the cold wall, $T = T_c$, for $Y = 0$ and all X

(iv) At the Hot wall, $T = T_h$, for $Y = b$ and all X

(b) Hydrodynamic Boundary Conditions:-

(i) At entrance, $U = U_m$ (Uniform flow) for

$X = 0$ and $0 < Y < b$

(ii) At exit, $\frac{\partial U}{\partial X} = \frac{\partial V}{\partial X} = 0$ (fully developed

flow) for $X = X_L$, $0 < Y < b$

(iii) At the Rigid boundaries, $U = V = 0$

(No-Slip Condition) for all X.

The pressure gradient terms in the momentum equations can be eliminated
by cross - differentation of equations (2) and (3) to yield the following
equations:

$$V\frac{\partial}{\partial Y}\left[\frac{\partial U}{\partial Y} - \frac{\partial V}{\partial X}\right] + U\frac{\partial}{\partial X}\left[\frac{\partial U}{\partial Y} - \frac{\partial V}{\partial X}\right] = \nu \left[\frac{\partial^2}{\partial X^2}\left[\frac{\partial U}{\partial Y} - \frac{\partial V}{\partial X}\right] + \frac{\partial^2}{\partial Y^2}\left[\frac{\partial U}{\partial Y} - \frac{\partial V}{\partial X}\right]\right]$$

$$+ g\beta \left[\frac{\partial T}{\partial Y} \sin\alpha + \frac{\partial T}{\partial X} \cos\alpha \right] \quad ... \tag{6}$$

ע

The above equation and the energy equation can be reduced to their non-dimensional forms using the following transformation coordinates.

$$U = U_\text{m} u$$

$$V = U_\text{m} v$$

$$Y = by$$

$$X = bx$$

$$\theta = \frac{T - Tc}{Th - Tc}$$

$$\omega = \frac{\partial v}{\partial x} - \frac{\partial u}{\partial y} = -\nabla^2 \psi$$

where u, v and ψ are connected by the relations

$$u = \frac{\partial \psi}{\partial y}$$

$$v = -\frac{\partial \psi}{\partial x}$$

The non-dimensional forms of the governing equations are:

(a) Continuity:

$$\frac{\partial u}{\partial x} + \frac{\partial u}{\partial y} = 0 \quad .. \quad .. \quad .. \quad .. \quad .. \quad .. \tag{7}$$

(b) Vorticity Transport:

$$\frac{u \partial \omega}{\partial x} + \frac{v \partial \omega}{\partial y} = \frac{1}{Re} \nabla^2 \omega - \frac{Gr}{Re^2} \left(\frac{\partial \theta}{\partial y} \sin\alpha + \frac{\partial \theta}{\partial x} \cos\alpha \right) \tag{8}$$

(c) Energy Transport:

$$\frac{u \partial \theta}{\partial x} + \frac{v \partial \theta}{\partial y} = \frac{1}{RePr} \nabla^2 \theta \quad .. \quad .. \quad .. \quad .. \tag{9}$$

The normalized forms of the boundary conditions are

A. Thermal boundary conditons

$$\theta \Big|_{\substack{x = 0 \\ 0 \le y < 1.0}} = \theta \Big|_{\substack{y = 0 \\ 0 \le x \le x_L}} = \frac{\partial \theta}{\partial x} \Big|_{\substack{x = x_L \\ 0 < y < 1}} = 0; \quad \theta \Big|_{\substack{y = 1 \\ 0 \le x \le x_L}} = 1.0$$

10

B.   Hydrodynamic boundary conditions:

(i) $u\Big|_{\substack{x=0 \\ 0<y<+1.0}} = +1.0$ (uniform flow at entrance)

$v\Big|_{\substack{x=0 \\ 0<y<+1.0}} = 0$

(ii) $u\Big|_{\substack{y=0 \\ 0\leq x\leq x_L}} = v\Big|_{\substack{y=0 \\ 0\leq x\leq x_L}} = \Psi\Big|_{\substack{y=0= \\ 0\leq x\leq x_L}} = 0$

But $\omega\Big|_{\substack{y=0 \\ 0\leq x\leq x_L}} \neq 0$ (No - slip condition)

(iii) $u\Big|_{\substack{y=+1.0 \\ 0\leq x\leq x_L}} = v\Big|_{\substack{y=+1.0 \\ 0\leq x\leq x_L}} = 0$

$\Psi\Big|_{\substack{y=+1.0 \\ 0\leq x\leq x_L}} = +1.0$

But $\omega\Big|_{\substack{y=+1.0 \\ 0\leq x\leq x_L}} \neq 0$ (No - slip condition)

(iv) $\dfrac{\partial\Psi}{\partial x}\Big|_{\substack{x=x_L \\ 0<y<+1.0}} = \dfrac{\partial\omega}{\partial x}\Big|_{\substack{x=x_L \\ 0<y<+1.0}} = 0$ (Condition for fully developed hydrodynamic regime)

3. ANALYSIS OF NUMERICAL METHOD

Considering the fact that in some regions of the flow field the secondary effects may aid or oppose the forced flow, the method suggested by Spalding and Greenspan [8] may be used in discretizing the non-linear terms in the governing equations for constant coefficients. As usual, the non-convective components in the equations are discretized using the central-difference approximation. The finite-difference analogs of the governing equations are:

(a) Energy transport Equation:

$$\theta_{i,j} = \frac{\left[\frac{1}{RePr}\left(\theta_{i,j+1} + \theta_{i,j-1}\right)\Big/(\Delta y)^2 + \left(\theta_{i+1,j} + \theta_{i-1,j}\right)\Big/(\Delta x)^2 + \left(u_{i,j}\,\theta_{i-1,j}\right)\Big/\Delta x + v_{i,j}\left(A_2\theta_{i,j-1} \; A_1\theta_{i,j+1}\right)\Big/\Delta y\right]}{\left[\frac{u_{i,j}}{\Delta x} + \frac{(A_2-A_1)v_{i,j}}{\Delta y} + \frac{2}{RePr}\left(\frac{1}{(\Delta x)^2} + \frac{1}{(\Delta y)^2}\right)\right]} \qquad \dots (10)$$

where $i = 2,3, \dots M$
$j = 2,3, \dots N$

and $\left.\begin{array}{l} A_1 = +1.0 \\ A_2 = 0.0 \end{array}\right\} v_{i,j} < 0$

$\left.\begin{array}{l} A_1 = 0.0 \\ A_2 = 1.0 \end{array}\right\} v_{i,j} > 0$

12

(b)　Vorticity Transport Equation:

$$\omega_{i,j} = \frac{\left[\begin{array}{l} \frac{1}{Re}\left(\omega_{i+1,j} + \omega_{i-1,j}\right)\Big/(\Delta x)^2 + \left(\omega_{i,j+1} + \omega_{i,j-1}\right)\Big/(\Delta y)^2 \\[2mm] +\left(u_{i,j}\omega_{i-1,j}\right)\Big/\Delta x + v_{i,j}\left(A_3\omega_{i,j-1} - A_4\omega_{i,j+1}\right)\Big/\Delta y \\[2mm] -\frac{Gr}{Re^2}\left[\left\{A_4\left(\theta_{i,j+1} - \theta_{i,j}\right) + A_3\left(\theta_{i,j} - \theta_{i,j-1}\right)\right\}\frac{Sin\alpha}{\Delta y} \right. \\[2mm] \left. + (\theta_{i,j} - \theta_{i-1,j})\frac{Cos\alpha}{\Delta x}\right] \end{array}\right]}{\left[\dfrac{u_{i,j}}{\Delta x} + \dfrac{(A_3-A_4)v_{i,j}}{\Delta y} + \dfrac{2}{Re}\left(\dfrac{1}{(\Delta x)^2} + \dfrac{1}{(\Delta y)^2}\right)\right]} \qquad (11)$$

where　$i = 2, 3, \dots M$　　　and　　$\left.\begin{array}{l} A_3 = 0.0 \\ A_4 = +1.0 \end{array}\right\}$　$v_{i,j} < 0$

$j = 2, 3, \dots N$　　　　　$\left.\begin{array}{l} A_3 = +1.0 \\ A_4 = 0.0 \end{array}\right\}$　$v_{i,j} > 0$

The stream function is obtained from the finite – difference analog of the Poisson equation, $\omega = -\nabla^2 \psi$.

(c)　Stream function Equation:

$$\psi_{i,j} = \frac{\left[\omega_{i,j} + \left(\psi_{i,j+1} + \psi_{i,j-1}\right)\Big/(\Delta y)^2 + \left(\psi_{i+1,j} + \psi_{i-1,j}\right)\Big/(\Delta x)^2\right]}{2\left[\dfrac{1}{(\Delta x)^2} + \dfrac{1}{(\Delta y)^2}\right]} \qquad (12)$$

where $i = 2,3, \dots M$

$j = 3,4, \dots N-1$

13

The near - boundary values are approximated as follows:

$$\psi_{1,2} = (\psi_{1,3} + 3\psi_{1,1})/4 \quad \ldots \ldots \ldots \quad (13)$$

$$\psi_{1,N} = (\psi_{1,N-1} + 3\psi_{1,N+1})/4 \ldots \ldots \ldots \ldots \quad (14)$$

where $i = 2,3, \ldots M$

The velocity components are given by :

$$u_{1,j} = (\psi_{1,j+1} - \psi_{1,j-1})/2\Delta y \ldots \ldots \ldots \ldots \quad (15)$$

$$v_{1,j} = -(\psi_{i+1,j} - \psi_{i-1,j})/2\Delta x \ldots \ldots \ldots \ldots \quad (16)$$

where $i = 2,3, \ldots M$

$$j = 2,3, \ldots N$$

The boundary vorticities are given by

$$\omega_{1,1} = (u_{1,3} - 4u_{1,2}) / 2\Delta y \quad \ldots \ldots \ldots \ldots \ldots \quad (17)$$

$$\omega_{1,N+1} = (4u_{1,N} - u_{1,N-1}) / 2\Delta y \quad \ldots \ldots \ldots \ldots \ldots \quad (18)$$

where $i = 2,3, \ldots M, M+1$

At the channel exit, the following less restrictive computational outflow boundary conditions are invoked.

$$\theta_{M+1,j} = \theta_{M,j} \ldots \ldots \ldots \ldots \ldots \ldots \ldots \ldots (18a)$$

$$\omega_{M+1,j} = \omega_{M,j} \ldots \ldots \ldots \ldots \ldots \ldots \ldots \ldots (18b)$$

$$\psi_{M+1,j} = \psi_{M,j} \ldots \ldots \ldots \ldots \ldots \ldots \ldots \ldots (18c)$$

where $j = 2, 3, \ldots N$

(d) Treatment of Numerical singularity at $(x=0, y=0)$; $(x=0, y=1.0)$: The streamfunction, velocity components and temperature values present no problem since they have been specified. Therefore the geometric singularity affects the vorticity only since it depends on derivatives of some space variables. To evaluate the vorticities at these singular points, the no-slip wall condition

14

can be applied for a first-order formulation using Taylor

series expansion for the stream function.

Thus at $x = 0$, $y = 0$:

$$\omega_{1,1} = -2(\psi_{1,2} - \psi_{1,1}) / (\Delta y)^2 \quad . \quad . \quad . \quad (19a)$$

at $x = 0$, $y = 1.0$:

$$\omega_{1,N+1} = - (\psi_{1,N} - \psi_{1,N+1}) / (\Delta y)^2 . \quad . \quad (19b)$$

$\omega_{1,1}$ and $\omega_{1,N+1}$ are approximated as above when they enter into computations for evaluating vorticities at neighbouring points.

4. GENERAL COMPUTATIONAL PROCEDURE

The coupled vorticity transport and energy equations are solved simultaneously using the Gauss-Seidel iterative procedure. The type of intergration step involves the following nested iterative processes.

1. θ, u, v, ψ are initialized for all interior, inlet and outlet grid points. Using the initial values of u and v, the boundary vorticities are computed from equations (17) and (18). Thereafter the following quantities are evaluated in the order given using the most recently computed values of other quantities.

2. θ at interior points from equation (10) and on the outflow boundary from equation (18a).

3. ω at interior points from equation (11) and on the outflow boundary from (18b).

4. ψ at interior points from equations (12), (13), (14) and on the outflow boundary from (18c).

5. u, v, are finally computed for all interior points and outflow boundaries from equations (15) and (16) respectively.

6. Using the values of u,v, obtained in step 5 as fresh initial values, new boundary vorticities are computed using equations (17) and (18).

7. The above steps, starting from step 2, are repeated until convergence is achieved.

The convergence criterion used in the computation is the same for all variables. This is so in order to compare the rates of convergence of the fields.

$$\epsilon = \Sigma \left| \phi^{k+1} - \phi^k_{i,j} \right| < 10^{-3}$$

$$\text{where} \quad i = 2,3, \ldots M$$

$$j = 2,3 \ldots N$$

5. FLOW AND HEAT TRANSFER RESULTS

The local and mean hotwall flow and heat transfer coefficients are based on the normal velocity and temperature gradients respectively.

$$f_x = \frac{2}{Re} \left. \frac{\partial u}{\partial n} \right|_w \quad ; \quad f_{mh} = \frac{1}{x_L} \int_o^{x_L} f_x dx$$

$$Nu_x = - \left. \frac{\partial \theta}{\partial n} \right|_w \quad ; \quad Nu_{mh} = \frac{1}{x_L} \int_o^{x_L} Nu_x dx$$

$$St_x = \frac{Nu_x}{RePr} \quad ; \quad St_{mh} = \frac{Nu_{mh}}{RePr}$$

Since three independent parameters are involved in the present problem, a complete parametric study is not practical, hence only representative cases for air (Pr= 0.73) are given to illustrate the inclination angle or body-force orientation effects. Also, since the flow must be forced, the free convection is regarded as a perturbation superposed on the forced flow. The parameter which represents the mutual interaction of the free and forced convection effects is $\frac{Gr}{Re^2}$, the Archimedes number.

6. DISCUSSION OF NUMERICAL RESULTS

Figures 2 and 3 respectively show the influence of the angle of inclination on the velocity and temperature fields. At the channel axis of symmetry, the local velocity is practically insensitive to changes in inclination. A possible explanation could be that at this point, the aiding and opposing effects of free convection counter-balance each other. Near the hot plate the local velocity is high while it is low near the cold plate. This is anticipated since energy is added to the fluid at the hot plate and extracted near the cold plate. Figure 3 shows that the mean temperatures generally increase with increasing inclination.

Figure 4 shows the variation of the local Nusselt numbers with channel length for a given Archimedes number with the angle of inclination as parameter. It is found that the local Nusselt number decreases asymptotically ot its fully developed value. This is anticipated since the temperature distribution within the channel increases with its length; hence the decrease in the normal temperature gradient along the channel.

Using Ar as parameter, the variations of the mean Nusselt number, friction numbers and friction factor with channel orientation are presented in figures 5, 6, and 7 respectively. Of particular interest, is the variation of the mean Nusselt number with the angle of inclination. A number of important observations can be made in Fig. 5. At $\alpha = 15^{\circ}$, the Nusselt number is the same for all non-variable Archimedes numbers. At $\alpha = 30^{\circ}$ and $\alpha = 60^{\circ}$, there is a certain angle at which the mean Nusselt number is a maximum for a given Ar. The mean Nusselt number varies with Ar while the corresponding critical angle increases with Ar. For a given Ar, this variation of the mean Nusselt number with is similar to that obtained by Oroa et al [4] for the variation of the mean Nusselt number with the angle of inclination for natural convection in an inclined channel heated isothermally from below and similarly cooled from above.

assume land mass to surface, the and critical modes the following

can be made.

1. The mean Nussalt number is independent of the non-zero Archimed...
    numbers when the angle of inclination to the horizontal is 1...

2. For a given non-zero Archimedes number, the critical angle at which
    the mean Nussalt number and friction factors are maximum lie between
    30° and 60°.

3. A unique solution to the thermal problem exists for a given
    inclination only when the Archimedes number, $Ar = 0.50$.

4. The results of Ozoe et al [5], which have been confirmed experimental
    by the authors, lend support to the validity of the present solution
    and the conclusions arrived at.

REFERENCES

1. JENN - WUU OU, K.C. CHENG and RAN-CHAU LIN, combined free forced laminar convection in inclined rectangular channels, Int. J. Heat Mass Transfer, 19, 277 - 283 (1976).

2. K. C. CHENG and GUANG-JYH HWANG, Numerical Solution of combined free and forced laminar convection in horizontal rectangular channels, J. Heat Transfer, 59 - 66 (1959).

3. K. C. CHENG and S. W. HONG, Effects of tube inclination on laminar convection in uniformly heated tubes for flat plate solar collector, Solar Energy, 13, 363 - 371 (1972).

4. M. IQBAL and J. W. STACHIEWICZ, Variable density effects in combined free and forced convection in inclined tubes, Int. J. Heat Mass Transfer, 10, 1625 - 1629 (1967); also, Influence of orientation on combined free and forced laminar convection heat transfer, J. Heat Transfer, 100 - 116 (Feb. 1966).

5. HIROYUKI OZOE, HAYATOSHI SAYAMA and STUART W. CHURCHILL, Natural convection in inclined square channel, Int. J. Heat Mass Transfer, 17, 401 - 406 (1974).

6. YASUO MORI and YUTAKA UCHIDA, Forced convective heat transfer between horizontal parallel plates, Int. J. Heat Mass Transfer, 9, 803 - 817 (1966).

7. S. C. R. DENNIS, Numerical solution of vorticity transport equation, Proc. of Third Int. Conference on Numerical Methods in Fluid Mechanics 19, Vol. 11, 120 - 121 (July, 1972).
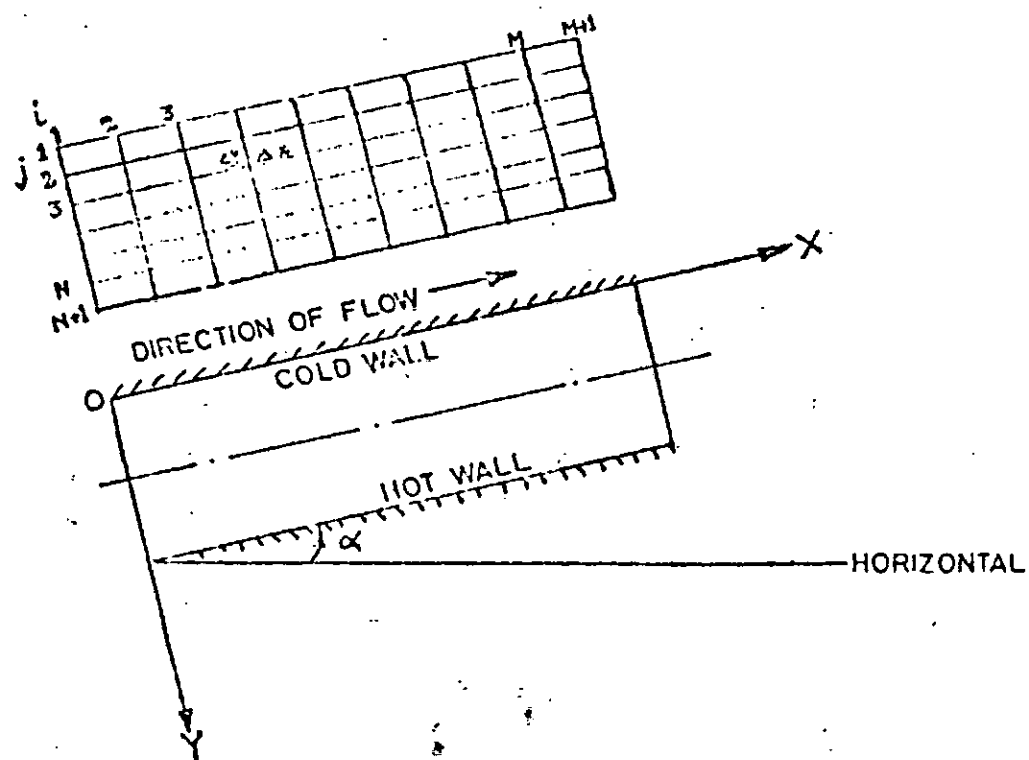
CAPTIONS FOR FIG RES
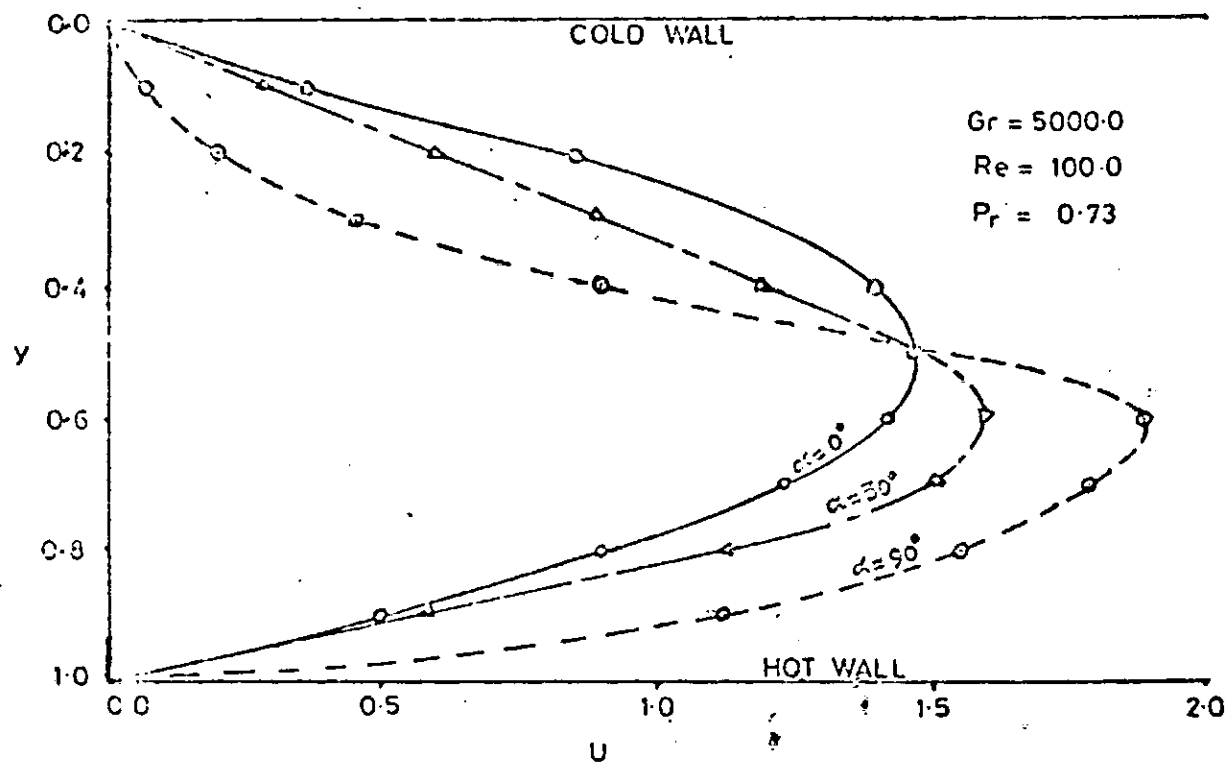
1. Physical Model, Coordinate System and Numerical grid.

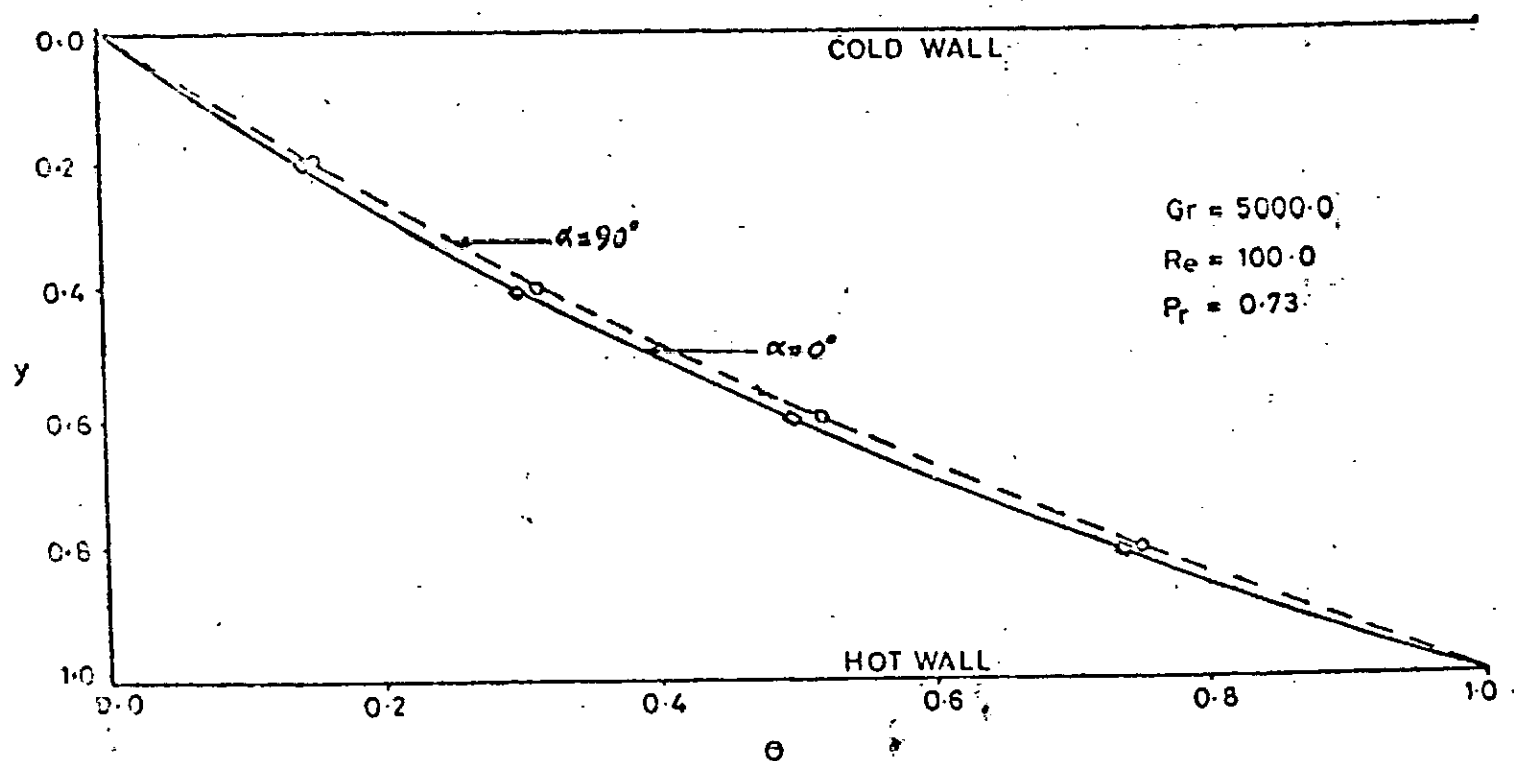2. Influence of channel orientation on dimensionless longitudinal velocity profiles.

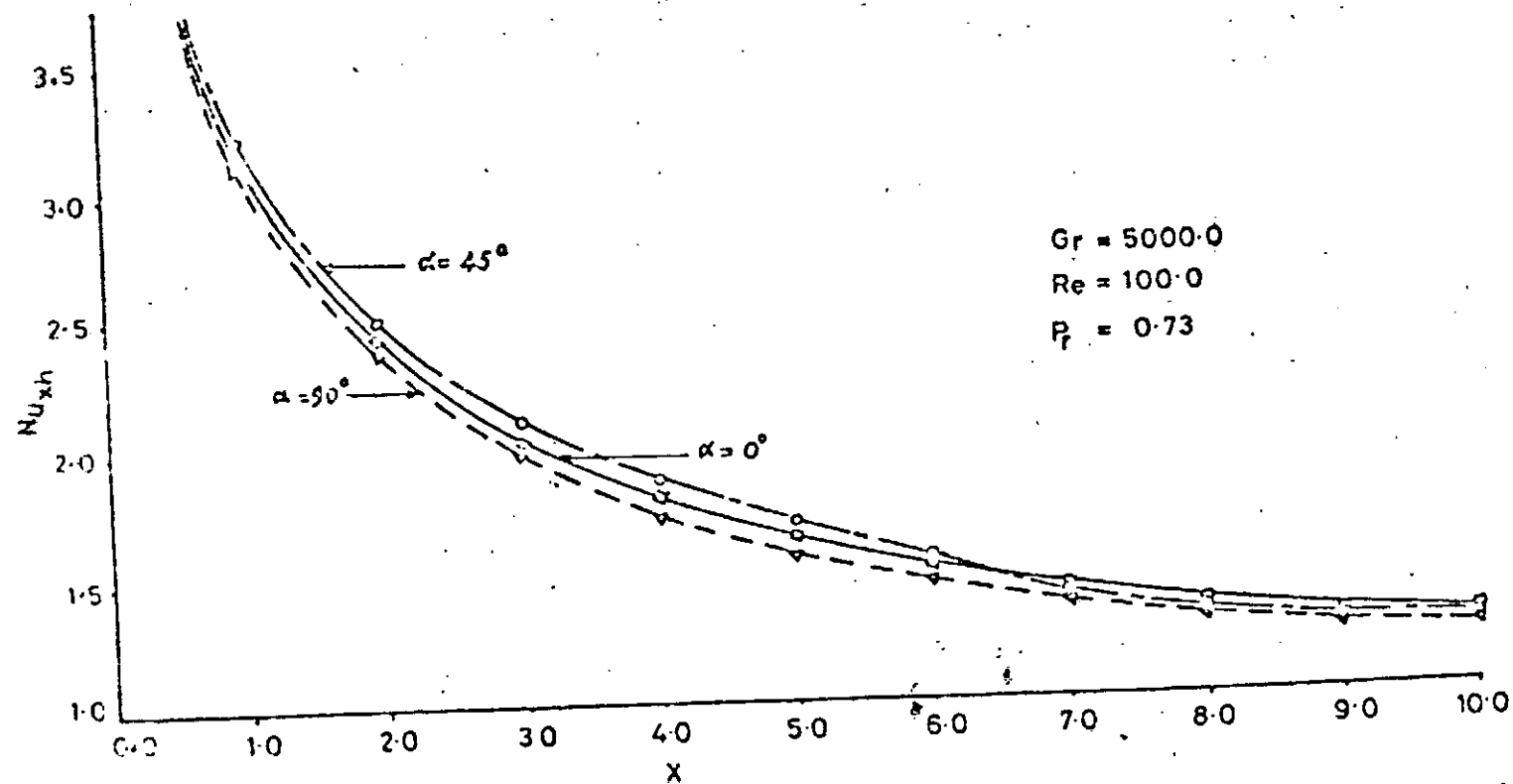3. Influence of channel orientation on dimensionless temperature Profiles.

4. Variation of the local Nusselt number with dimensionless longitudinal distance, with α as parameter.

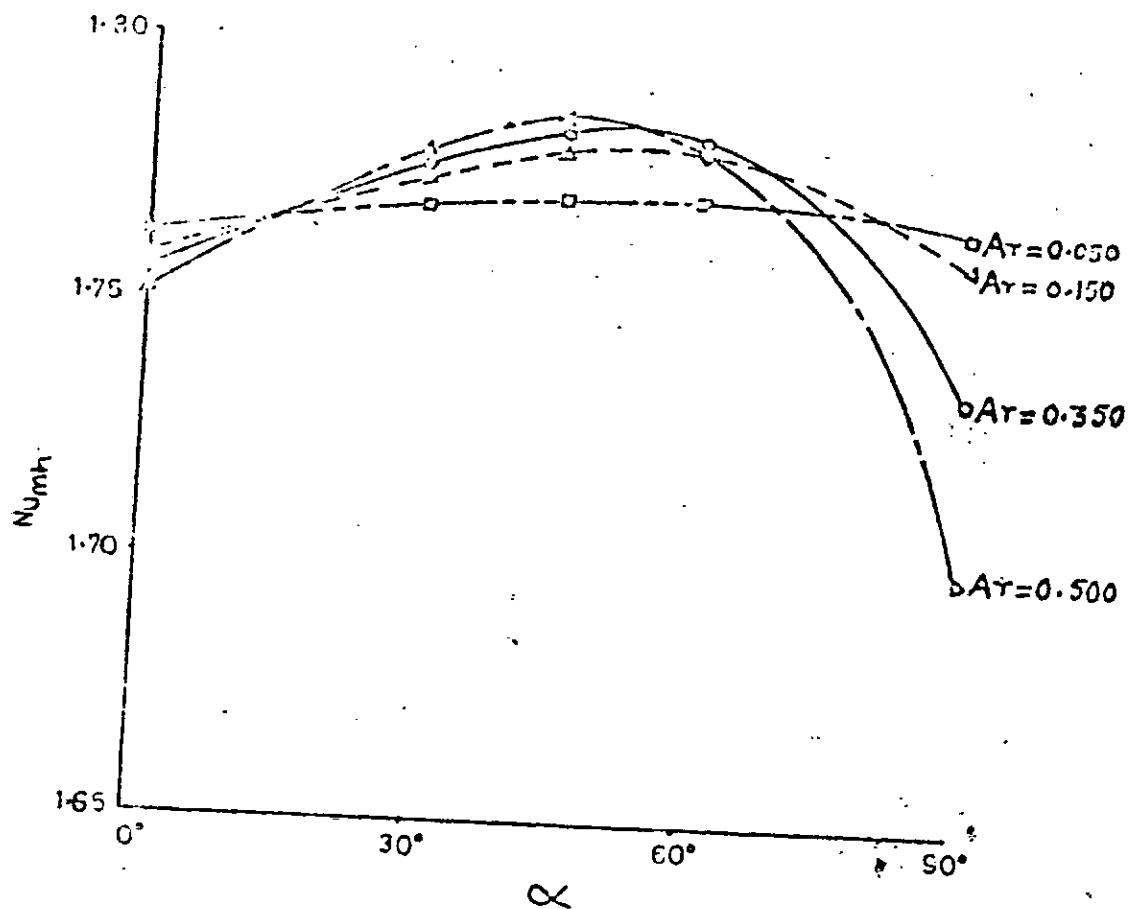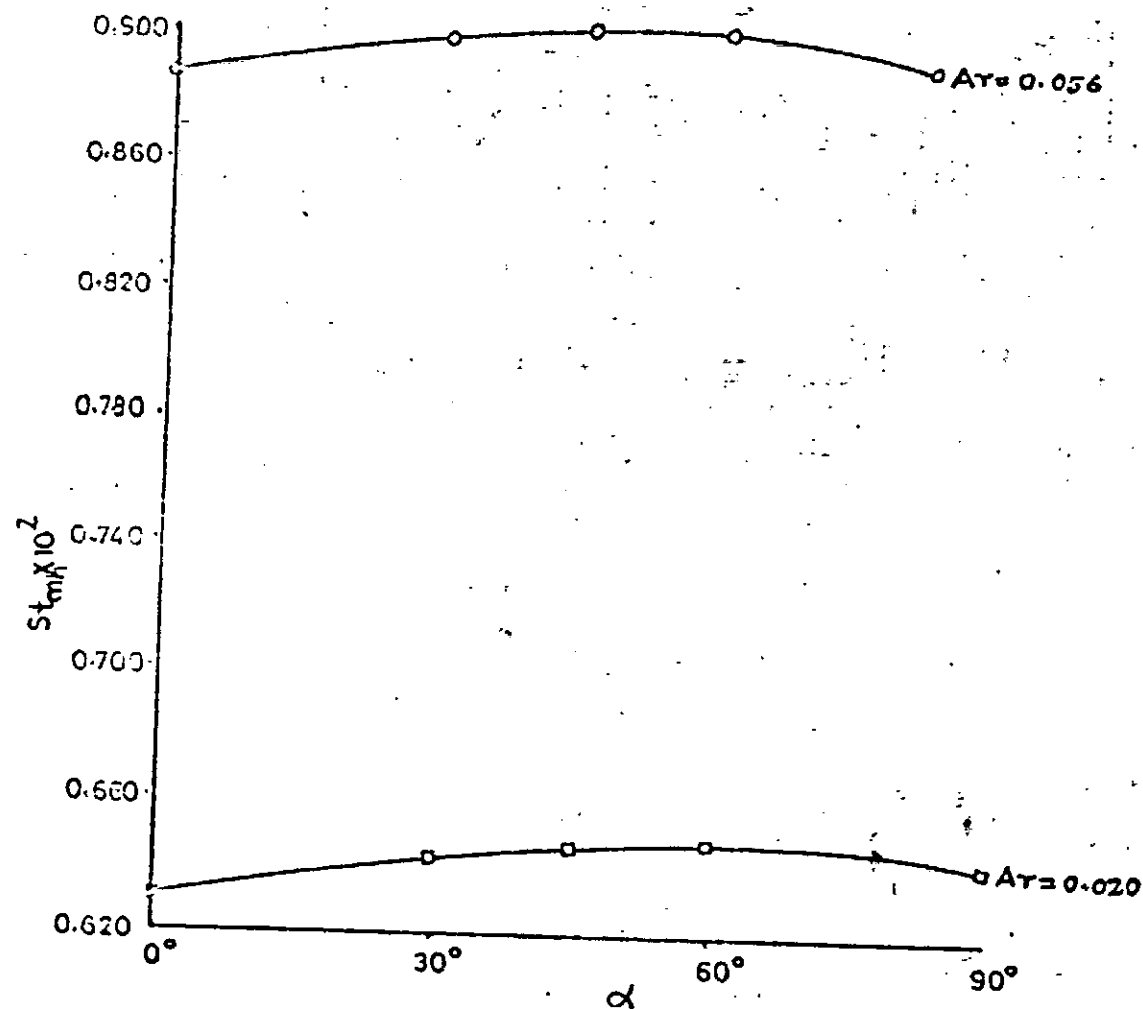5. Influence of channel orientation on the mean Nusselt number with Ar as parameter for Pr = 0.73.
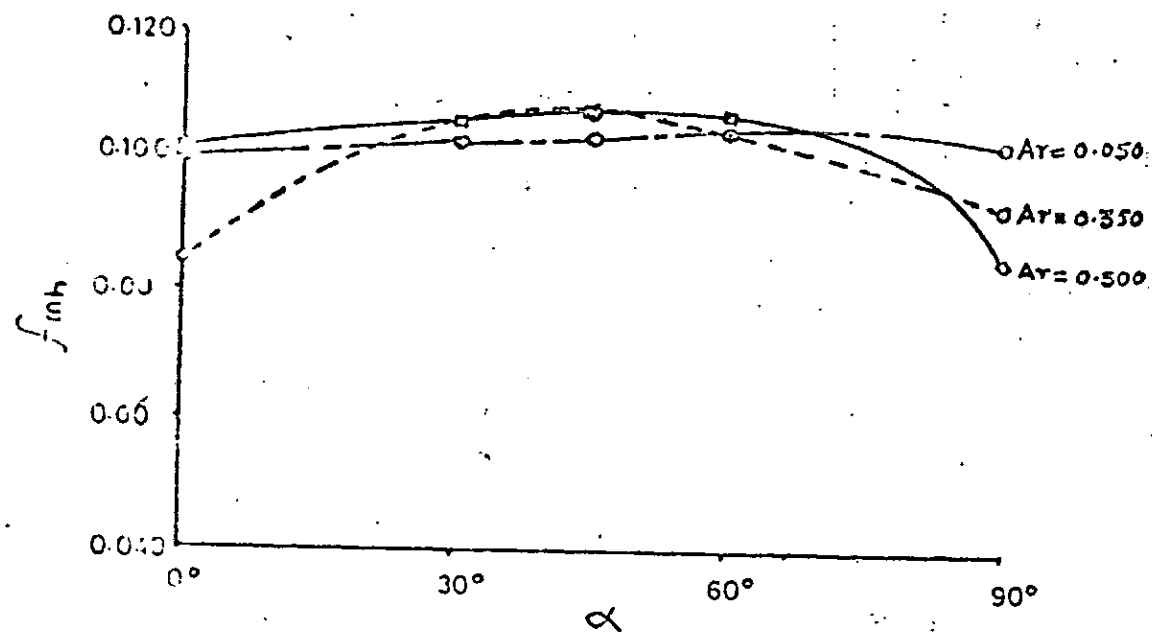
6. Variation of the mean Stanton number with α for Pr = 0.73.

7. Influence of channel orientation on the mean friction factor with Ar as parameter for Pr = 0.73.

8. Variation of mean Nusselt number with Ar, with α as parameter for Pr = 0.73.

9. Variation of mean friction factor with Ar, with α as parameter for Pr = 0.73.

Fig. 1. Physical model, coordinate system and Numerical grid.

Fig. 2. Influence of channel orientation on
dimensionless longitudinal velocity profiles.

Fig.3. Influence of channel orientation on dimensionless temperature profiles.

Fig.4. Variation of the local Nusselt number with dimensionless longitudinal distance, with α as parameter.

Fig. 5. Influence of channel orientation on the mean Nusselt number with Ar as parameter for $P_r = 0.73$

Fig.6. Variation of the mean Stanton number
with α for $p_r \doteqdot 0.73$

Fig.7. Influence of channel orientation on the
mean friction factor with Ar as parámeter
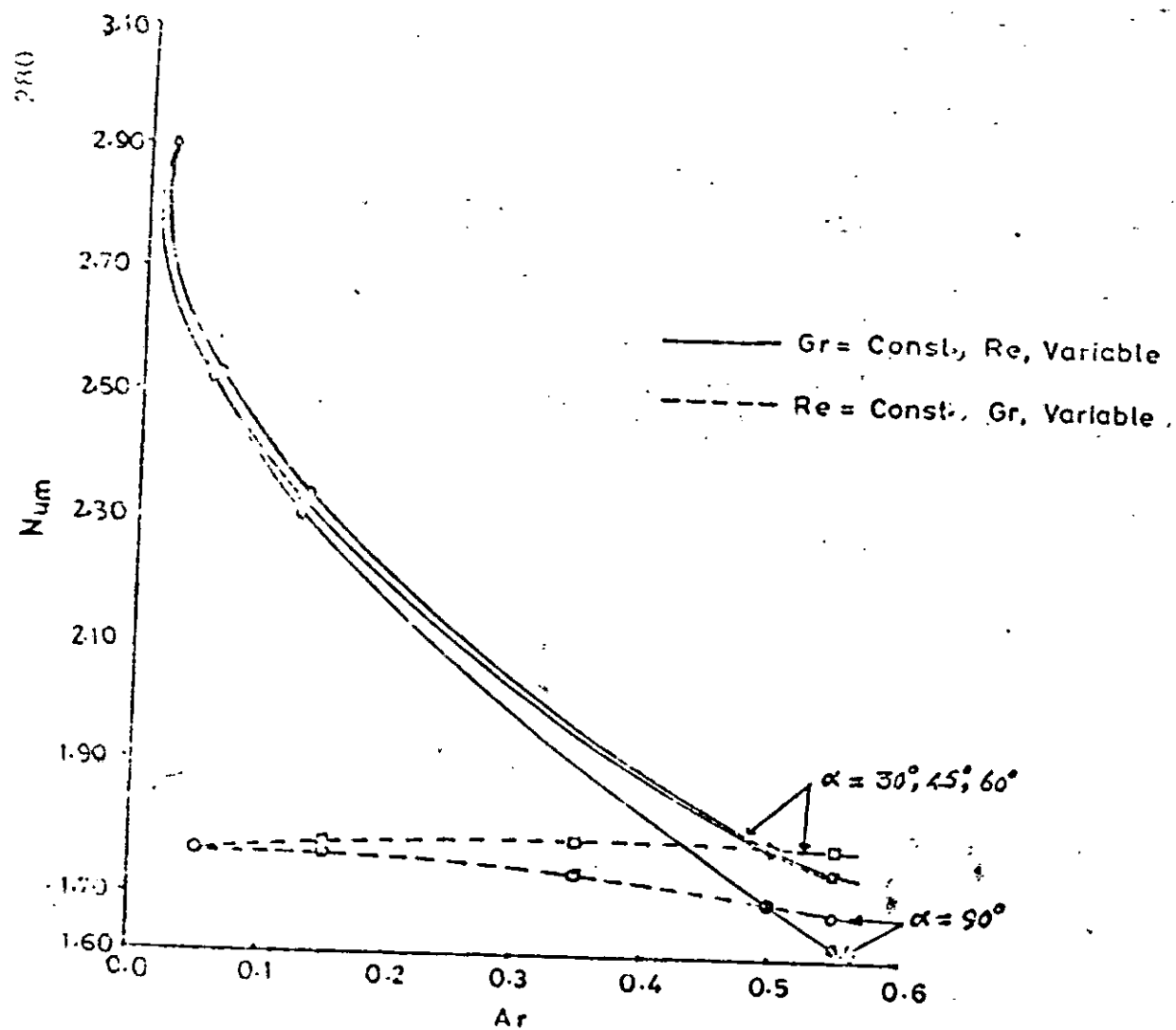for $p_r = 0.73$

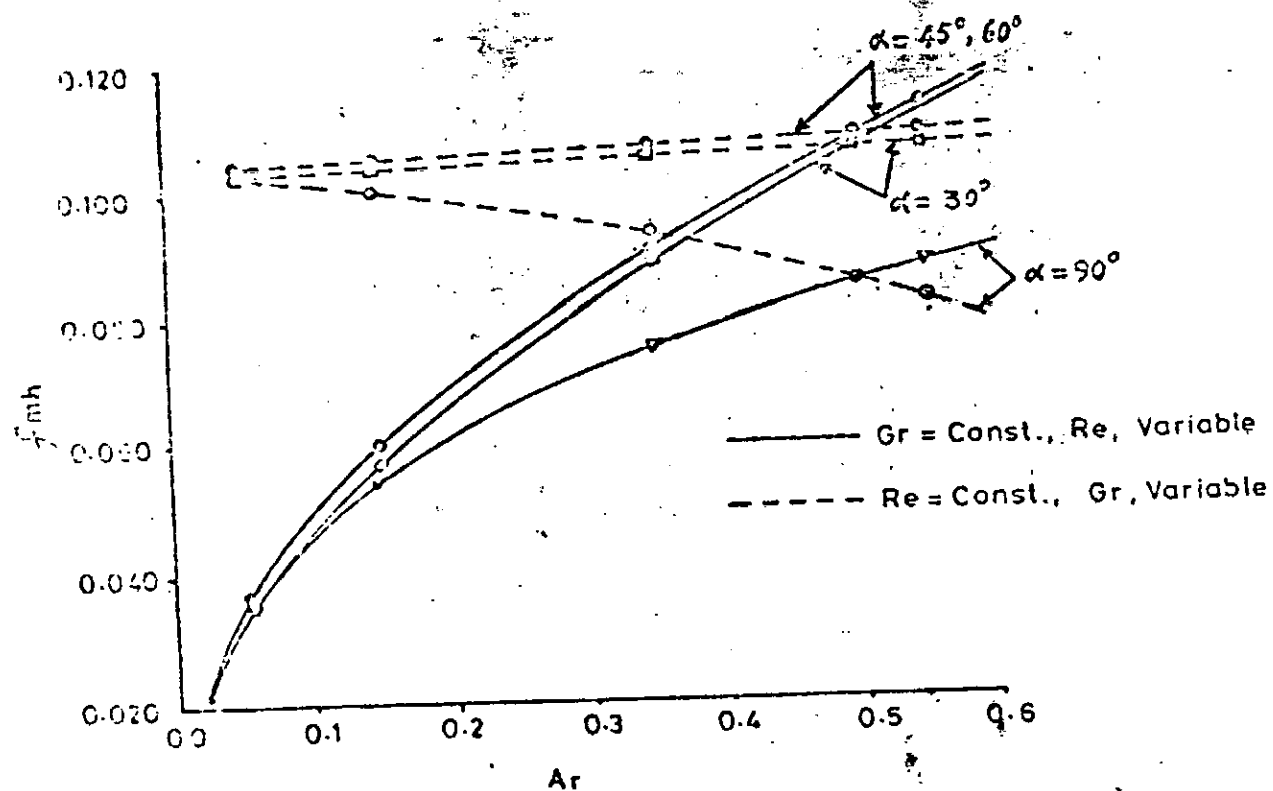Fig. 8. Variation of mean Nusselt number with Ar, with α as parameter for $P_r = 0.73$.

Fig.9. Variation of mean friction factor with Ar, with α as parameter for $p_r = 0.73$.